

ALMA MATER STUDIORUM - UNIVERSITÀ DI BOLOGNA

FACOLTA' DI INGEGNERIA
CORSO DI LAUREA IN INGEGNERIA CIVILE

*Dipartimento di Ingegneria delle strutture.
dei Trasporti, delle Acque, del Rilevamento, del Territorio
(D.I.S.T.A.R.T.)*

TESI DI LAUREA
in
Calcolo Automatico delle Strutture

**Monitoraggio delle condizioni strutturali
del Rio Dell – Hwy 101/Painter Street Overpass
attraverso l'utilizzo di dati dinamici**

CANDIDATO:
Luciana Balsamo

RELATORE:
Prof. Francesco Ubertini

CORRELATORE:
Prof. Raimondo Betti

Anno Accademico 2008/2009
Sessione III

*Computers are incredibly fast,
accurate and stupid.*

*Human beings are incredibly slow,
inaccurate and brilliant.*

*Together they are
powerful beyond imagination.*

– Albert Einstein

Table of Contents

1. INTRODUCTION	Pag. 1
2. REVIEW OF PREVIOUS STUDIES	Pag. 8
2.1 Introduction	Pag. 9
2.2 The Geometrical Characteristics of the Bridge	Pag. 10
2.3 Dynamic Characteristics of the Bridge	Pag. 11
2.4 Soil-Structure Interaction	Pag. 26
2.5 Structural Identification through OKID	Pag. 32
3. SYSTEM IDENTIFICATION VIA OKID/ERA	Pag. 34
3.1 Introduction	Pag. 35
3.1.1 <i>The Historical Path of OKID/ERA Algorithm</i>	<i>Pag. 37</i>
3.2 Basic Formulation	Pag. 38
3.2.1 <i>Input-Output Relations</i>	<i>Pag. 37</i>
3.2.2 <i>Observer/Kalman filter Identification</i>	<i>Pag. 41</i>
3.2.3 <i>Eigensystem Realization Algorithm</i>	<i>Pag. 43</i>
3.2.4 <i>Refining the Identified State-Space Model</i>	<i>Pag. 45</i>
3.2.5 <i>Recovering the Dynamics of the System from the Realized State-Space Model</i>	<i>Pag. 49</i>

3.3	Numerical Results	Pag. 51
3.3.1	<i>Trinidad Offshore (November 8, 1980)</i>	<i>Pag. 54</i>
3.3.1.1	Discussion of the Results	Pag. 57
3.3.2	<i>Rio Dell Earthquake: Discussion of the Results</i>	<i>Pag. 72</i>
3.3.3	<i>Petrolia Earthquake: Discussion of the Results</i>	<i>Pag. 86</i>
4.	FINITE ELEMENT MODEL	Pag. 100
4.1	Introduction	Pag. 101
4.2	Formulation of the Displacement-Based Finite Element Method	Pag. 103
4.2.1	<i>General Derivation of Finite Element Equilibrium Equations</i>	<i>Pag. 105</i>
4.2.1.1	The Principle of Virtual Displacements	Pag. 107
4.2.1.2	Finite Element Equations	Pag. 109
4.2.2	<i>Finite Element Formulation for Euler Beams</i>	<i>Pag. 112</i>
4.2.3	<i>Finite Element Formulation for Plates and Shells</i>	<i>Pag. 115</i>
4.2.3.1	Kirchhoff Plate	Pag. 116
4.2.3.2	Reissner-Mindlin Plate	Pag. 119

4.2.4	<i>Modal Analysis</i>	<i>Pag. 120</i>
4.2.4.1	Verification Example: Modal Analysis of a Beam via STRAUS7 and SAP2000	Pag. 122
4.3	Finite Element Models	Pag. 125
4.3.1	<i>First Model: the Beam Model</i>	<i>Pag. 125</i>
4.3.2	<i>Second Model: the Grid Model</i>	<i>Pag. 129</i>
4.3.3	<i>Third Model: Shell Model</i>	<i>Pag. 142</i>
4.3.3.1	The Shell Element in SAP2000	Pag. 142
4.3.3.2	Thick-Shell Elements Model	Pag. 145
4.3.3.3	Thin-Shell Elements Model	Pag.149
4.4	Model Calibration	Pag. 155
4.4.1	<i>Genetic Algorithm (GA)</i>	<i>Pag. 155</i>
4.4.2	<i>The Code Used in the Optimization Process</i>	<i>Pag. 157</i>
4.4.2.1	Tournament Selection with a Shifting Technique	Pag. 159
4.4.2.2	Single Point and Uniform Crossover	Pag. 159
4.4.2.3	Jump and Creep Mutation	Pag. 160
5.	CONCLUSIONS	Pag. 161
	BIBLIOGRAPHY	Pag. 164
	APPENDIX	Pag. 167

1

INTRODUCTION

Sommario

Il problema del monitoraggio delle condizioni strutturali di sistemi quali quelli pontuali è divenuto ormai un tema centrale nel campo dell'ingegneria civile. Per questo, negli ultimi decenni, si sono sviluppati sempre più metodi aventi come obiettivo quello del controllo dello stato della struttura. Molto sviluppati, in questo senso, sono quelli che si avvalgono di dati dinamici, registrati ad esempio da strumenti quali gli accelerometri. Questi metodi permettono l'osservazione dello stato strutturale del sistema oggetto d'analisi e nel contempo possono fornire informazioni utili per il rinvenimento di danno, generatosi, ad esempio, a seguito di un evento sismico importante. Nel presente lavoro è stata compiuta l'analisi strutturale del Rio Dell – Hwy 101/Painter Street Overpass.

Il Painter Street Overpass è collocato presso Rio Dell, nella California del Nord (Figure 1.1). Si tratta di un ponte a due campate, con impalcato a cassone in cemento armato precompresso. La geometria è complicata da un'inclinazione pari a 38.9 gradi dell'asse trasversale dell'impalcato rispetto a quello longitudinale. Il ponte è stato munito di accelerometri nel 1977 ad opera del Dipartimento dei Sottosuoli e della Geologia della California. In figura 1.2 è mostrata la disposizione di tali strumenti.

Il metodo di monitoraggio qui proposto si sviluppa in cinque passaggi. Essenzialmente, la vera e propria fase di monitoraggio si esplica solo al quinto passo, mentre i primi quattro possono considerarsi stadi necessari alla creazione di strumenti indispensabili per la finale individuazione del danno.

The use of dynamic data aimed to structurally identify systems such as bridges has become a well known non-destructive method able to provide evaluation of the condition of the structure. The subject of the present work is the Rio Dell - Highway 101/Painter Street Overpass, California. The approach presented herein is thought to offer an almost immediate estimation of whether or not the bridge under consideration has suffered some damage and, possibly, the location of the damage.

The Painter Street Overpass is located near Rio Dell, in Northern California (Figure 1.1). It is a continuous, two span, cast-in-place, pre-stressed post-tension, concrete, box-girder bridge. The geometry is complicated by a 38.9 degrees skew of the bent with respect to the deck longitudinal axis. The bridge was instrumented in 1977 by the California Division of Mines and Geology. Figure 1.2 shows the location of the accelerometers.

The health condition monitoring method here proposed is developed in five stages. Essentially, the proper monitoring phase is only the fifth one, while the first four can be considered as the necessary steps that have to be taken in order to create the indispensable tools required for the final damage detection.

First Phase: Review of Previous Studies

The review of previous studies enables to have some granted information on the structure, resulting as a starting point for the development of the actual work. At this stage, one should not seek any detail in particular. Any data gained should be accurately analyzed, since they could offer some hints such as indications on how to model the system, or suggestions on the boundary conditions to employ.

Second Phase: Structural Identification through OKID Algorithm

In this part, special attention is devoted in identifying the dynamic characteristics of the bridge. An Observer/Kalman filter Identification (OKID) algorithm is applied using the recorded time histories available at the Center of Engineering Strong Motion Data website. This stage is essential to define the modal characteristics that will be some of the thresholds of the calibration of the mechanical model that will be built in the following step.

Third Phase: Linear Finite Element Model of the Bridge

It consists in developing a *linear* finite element model of the bridge. This part is crucial in the development of the future steps. It is required to the finite element model to be the most accurate as possible, in order to constitute a reliable tool on which perform the future damage detection. A number of finite element models are created with an increasing level of detail. Once the modal characteristics and the response of the model cannot be improved any further, the model has to be calibrated. In this study a genetic algorithm is applied. The calibration thresholds are the modal frequencies identified in the previous step, and the acceleration time histories available for the Painter Street Overpass.

Fourth Phase: Non-Linear Finite Element Model

The previously generated FE model is extended to the nonlinear range. By progressively increasing the load in the three space directions, the most stressed zones of the system are individuated. In these areas the elastic limit can be overcome, but this may not necessarily imply damage is occurred. On the contrary, it may only mean that the system has a non-linear behavior. Therefore, introducing non-linear elements in the most stressed regions will lead to handle with a model that will resemble more likely the actual response of the bridge. The simulated time histories of the response from the nonlinear model represent a new set of data that are used in the next phase to test rapid response evaluation tools.

Fifth Phase: Damage Detection

This phase is herein presented to utterly describe the approach. Nonetheless, the phase explained below has not been tested, since the Painter Street Overpass had not suffered any damage at the time of the research.

The “amplified” ground motion time histories are fed through the high-fidelity bridge model developed, and the predicted response of the bridge at the various sensor locations on the superstructure is estimated. If the predicted response of the model matches the simulated response from Phase IV at all of the sensor locations, it will be indication that no damage has occurred in the bridge. If, instead, the previously identified model provides structural responses that do not match the ones from Phase IV, then this will serve as a caution that damage might have occurred somewhere in the bridge. Since the nonlinear response data are simulated through the model developed in Phase IV, different damage levels will be investigated and a sensitivity analysis on the damage intensity level should be performed.

Another indicator of potential damage could consist in the relative displacements between critical sensor locations. Using the nonlinear model from Phase IV, time histories of the structural displacements at different sensor

locations and their relative magnitude will be determined. A displacement between two recording stations that is close to or beyond a certain threshold will be an indication of potential damage between the two sensor locations and an in-depth damage assessment at that specified location will be necessary. This indicator can also be obtained in a relatively short time after the occurrence of the earthquake and can be run concurrently at the first approach.

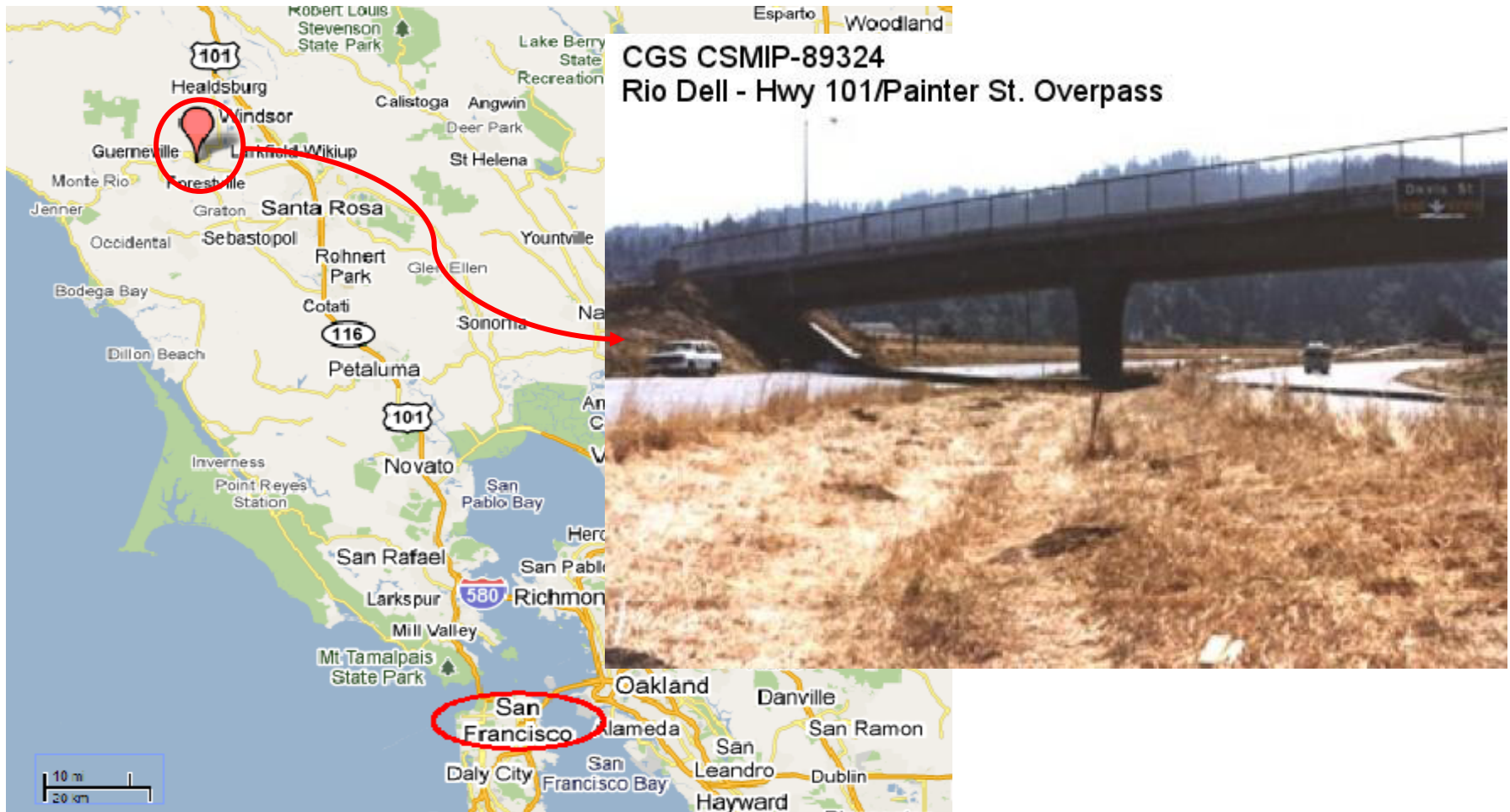


Figure 1.1: Geographical Location and View of Rio Dell-Hwy 101/Painter Street Overpass

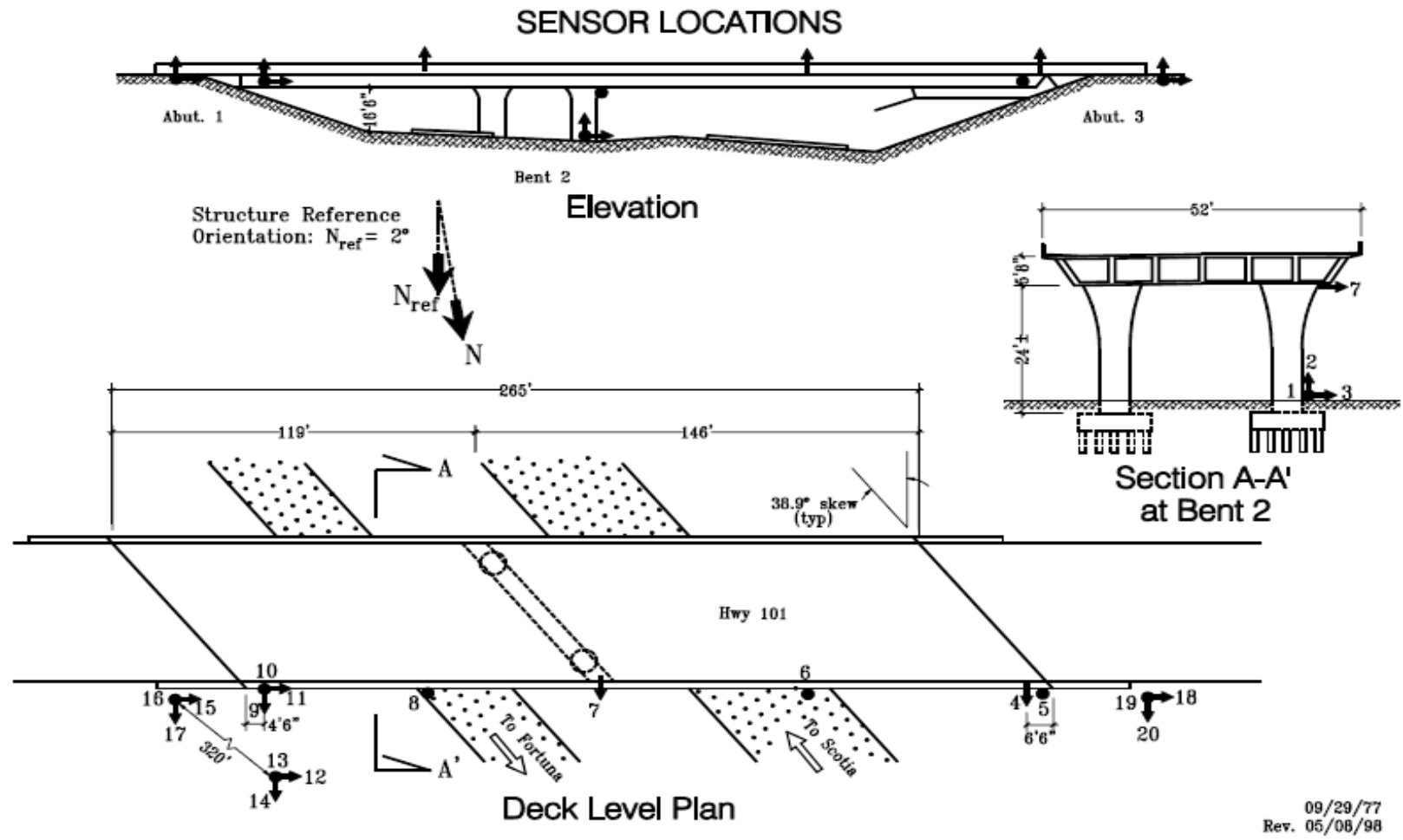


Figure 1.2: Sensors Location on Painter Street Overpass

2

REVIEW OF PREVIOUS STUDIES

Sommario

Il capitolo che segue è frutto della ricerca bibliografica di studi precedentemente compiuti, aventi come oggetto il Rio Dell Overpass. Una volta reperito la maggior quantità di materiale possibile sull'argomento, è possibile analizzarlo e cogliere spunti di approfondimento. In particolare, nel seguito verranno analizzate le caratteristiche geometriche della struttura, il comportamento dinamico desunto dai dati ambientali registrati dagli accelerometri di cui il ponte è stato munito dal 1977 ad opera del Dipartimento dei Sottosuoli e della Geologia della California, l'interazione terreno-struttura ed infine verrà introdotto il problema dell'identificazione strutturale per mezzo dell'algoritmo OKID/ERA, sebbene nella letteratura scientifica sia difficile trovare pubblicazioni a riguardo. Infatti, l'algoritmo menzionato è stato creato per applicazioni nel campo dell'ingegneria aeronautica e solo ultimamente è stato introdotto nel campo dell'ingegneria civile.

2.1 Introduction

As mentioned in the previous chapter, the Rio Dell Overpass was instrumented in 1977 by the California Division of Mines and Geology with twenty accelerometers (Figure 1.2). Eighteen accelerometers were located on the north edge of the bridge, while the remaining three sensors were put on the embankment in order to measure free field accelerations. However, the position of the channels give some problems for the determination of the characteristics of the system. Since the bent is skewed, the deck torsional deformations are not negligible. Nonetheless, the torsional contribute to the deformation cannot be caught only by means of the consideration of the recorded accelerations. It results apparent the necessity of the finite element model for a detailed structural identification of the Rio Dell Overpass.

Moreover, despite the fact that the bridge was instrumented thirty three years ago, accelerograms of only three earthquake events are available at the Center of Engineering Strong Motion Data (CESMD) website. Therefore, maybe these are some of the reasons why there are not many papers published on the Painter Street Overpass subject. Nevertheless, the researches available offer very helpful hints for structural identification through both OKID algorithm and finite elements model.

Essentially, the literature available on the subject of the Painter Street Overpass is focused on the characteristics of the bridge derived from the acceleration time histories analysis. The soil-structure interaction is another issue accurately described in many papers.

The literature on the use of the OKID/ERA algorithm for the structural identification is less ordinary. In fact, this is one of the first research in which this tool is exploited for structural purposes. The OKID/ERA algorithm was born in the mechanical engineering field, and only recently, for an intuition of Professor Betti and Professor Longman, has begun to be successfully tested in the civil engineering field.

2.2 The Geometrical Characteristics of the Bridge

Identified as CSMIP Station No. 89324, the US 101/ Painter Street Overpass is located in Rio Dell, California. The Rio Dell overpass is a two span bridge crossing Highway 101 at Painter Street, 265 feet long. The bridge is a monolithic, cast in place, prestressed concrete, multi-cell box girder road deck with end diaphragm abutments and a two columns bent. Both the abutment and bent foundations are supported on piles. The behavior is complicated by a 38.9 degrees skew between the centerline of the bent and the centerline of Highway 101 passing. The bent spans 38 feet measured along the centerline of the skewed cross sections and is monolithically connected top and bottom to the footings and superstructure respectively. The columns are approximately 20 feet in height. The abutments have been constructed on top fill material to provide appropriate vertical clearance over Highway 101 below. The west abutment rests on a neoprene bearing strip which is part of a designed thermal expansion joint. All of the foundations are supported on driven 45 ton concrete friction piles.

2.3 Dynamic Characteristics of the Bridge

Due to the records of the seismic events that interested the bridge since the Trinidad Earthquake in 1980, it is possible to examine the dynamic behavior of the bridge by means of the analysis of the aforementioned records. The following analysis are inspired by some papers published by Prof. Romstad, from the California University.

The first analysis performed consists in calculating and plotting the power spectral density functions for individual earthquakes for each sensor. Figures 2.1 show the results. From the observation of all figures 2.1, it can be inferred that earthquakes tend to show a spike at 3.3 – 3.6 Hz, indicating an active natural mode with significant participation of all of the sensors. Other spikes tend to be concentrated at about 2.3, 4.2-4.4, 5.5 and 6.8 Hz. Nonetheless, only figures 2.1b and 2.1c show clearly dominating spikes; in particular, for sensor 6 two natural frequencies can be identified at 3.37 and 5.45 Hz, while for sensor 8 the dominating frequencies correspond to the values of 3.42, 4.40 and 6.98 Hz. However, it should be important to analyze the contribute to the modal characteristics of sensors 9 and 11, since they are the only sensors that measure transversal and longitudinal accelerations respectively. Anyway, observation of figures 2.1d and 2.1f demonstrates that the measurements recorded from these channels are quite invalidated by the noise. Therefore, only the modal frequencies at 3.42-3.52 Hz and at 4.20 Hz can be considered reasonable, since the frequency content of the other channels show this values too. Summarizing, from this initial analysis, four modal frequencies can be identified: the first is in the range from 3.2 to 3.6 Hz, and is supposed to have both longitudinal and vertical and transverse contributes, since all of the channels have a peak corresponding to this value; then, the modal frequency of about 4.3 Hz is identified by both vertical and transverse channels; follow the modal frequencies at 5.5 and 7 Hz, both identified through sensors that measure vertical accelerations.

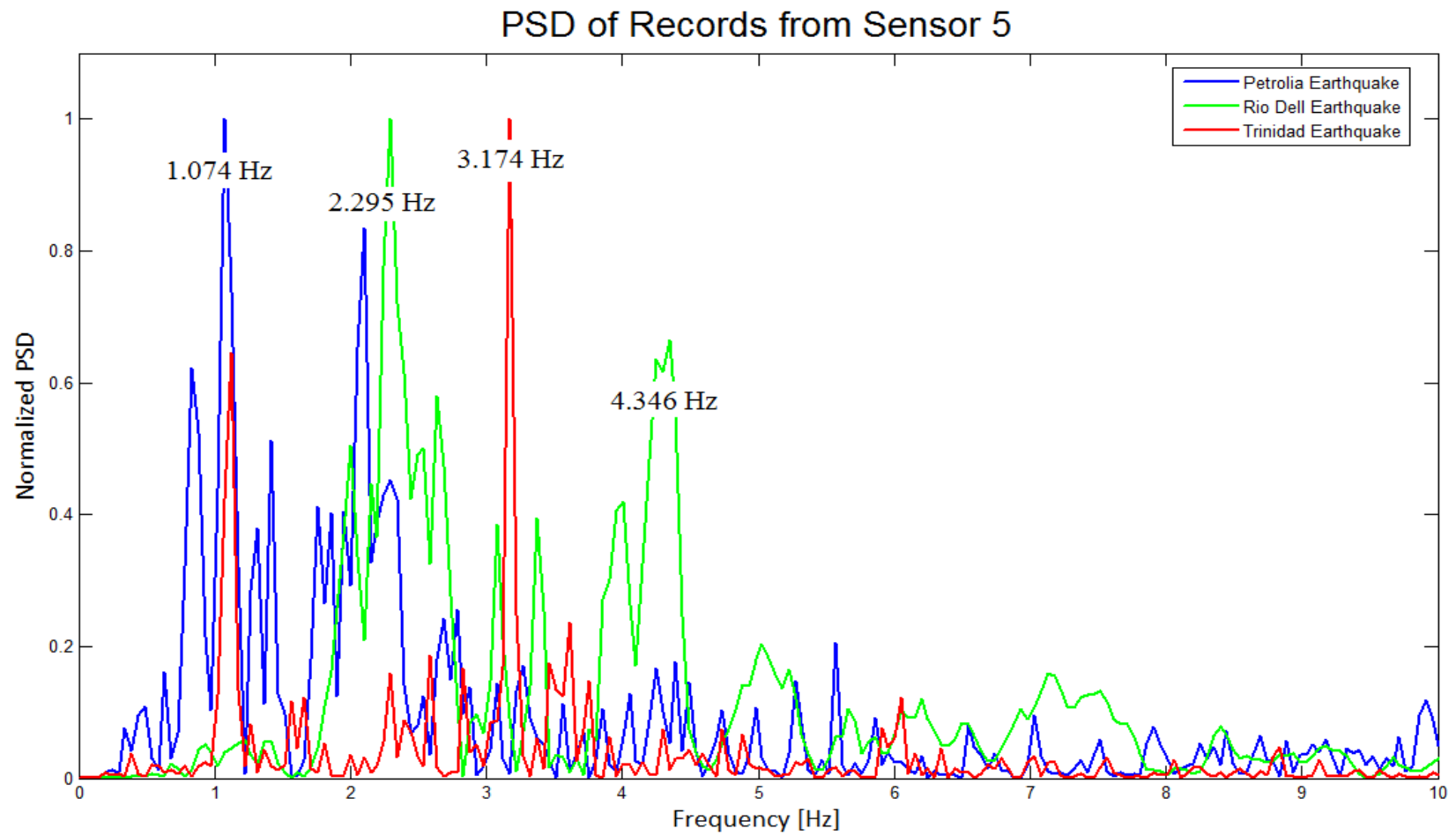


Figure. 2.1a: Sensor 5 PSD for Trinidad Rio Dell Earthquake and Petrolia Earthquake

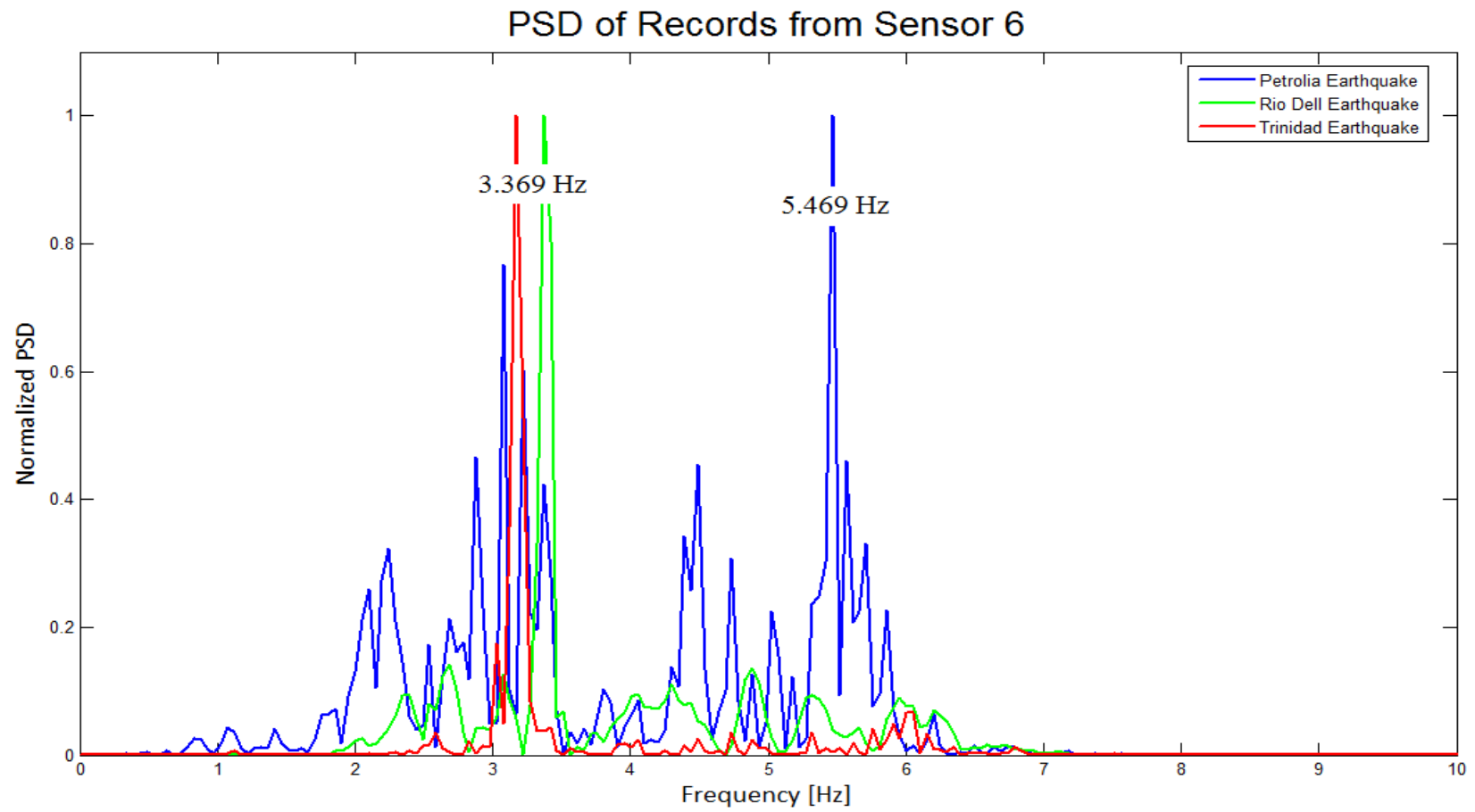


Figure 2.1b: Sensor 6 PSD for Trinidad Rio Dell Earthquake and Petrolia Earthquake

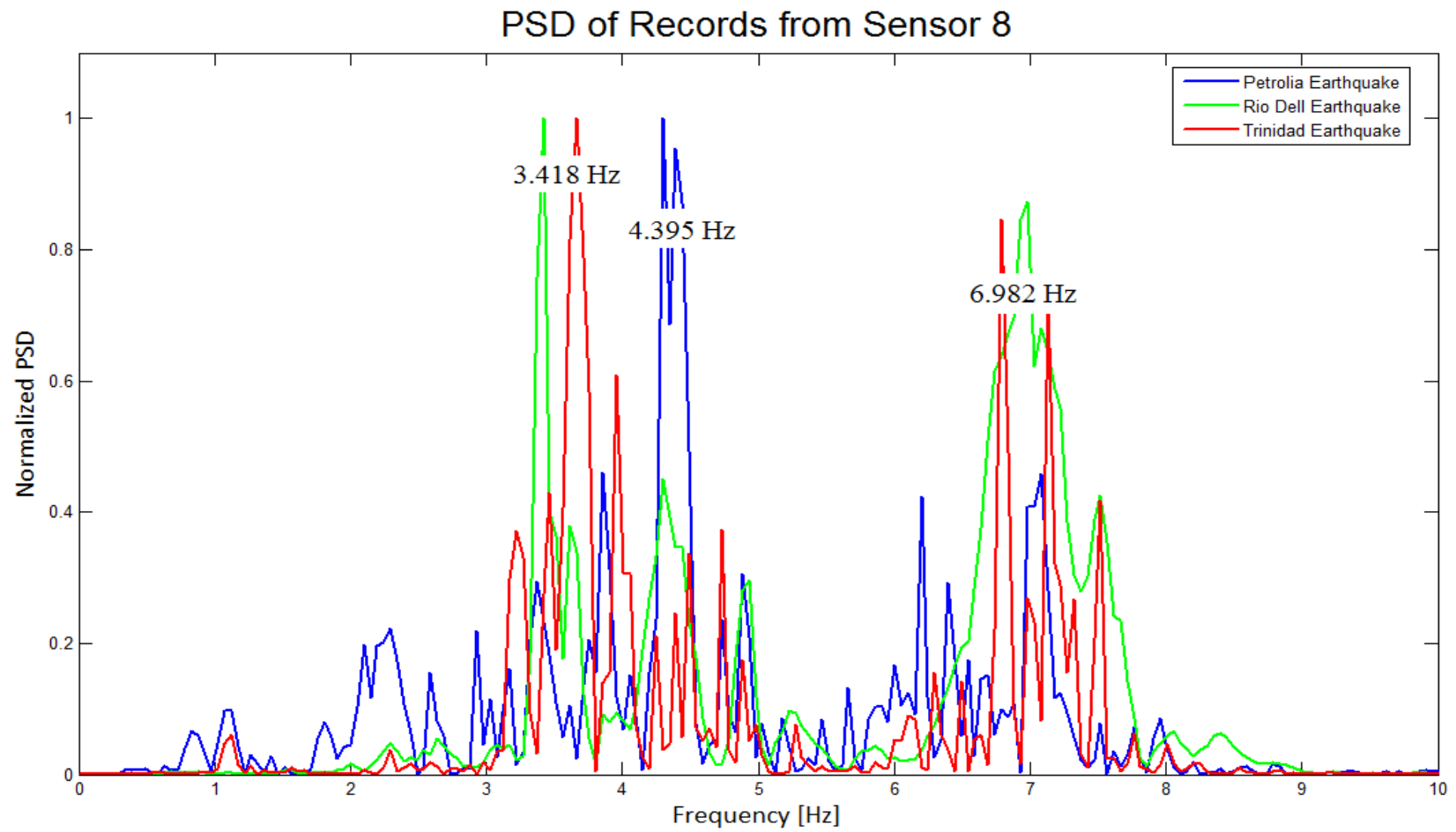


Figure 2.1c: Sensor 8 PSD for Trinidad Rio Dell Earthquake and Petrolia Earthquake

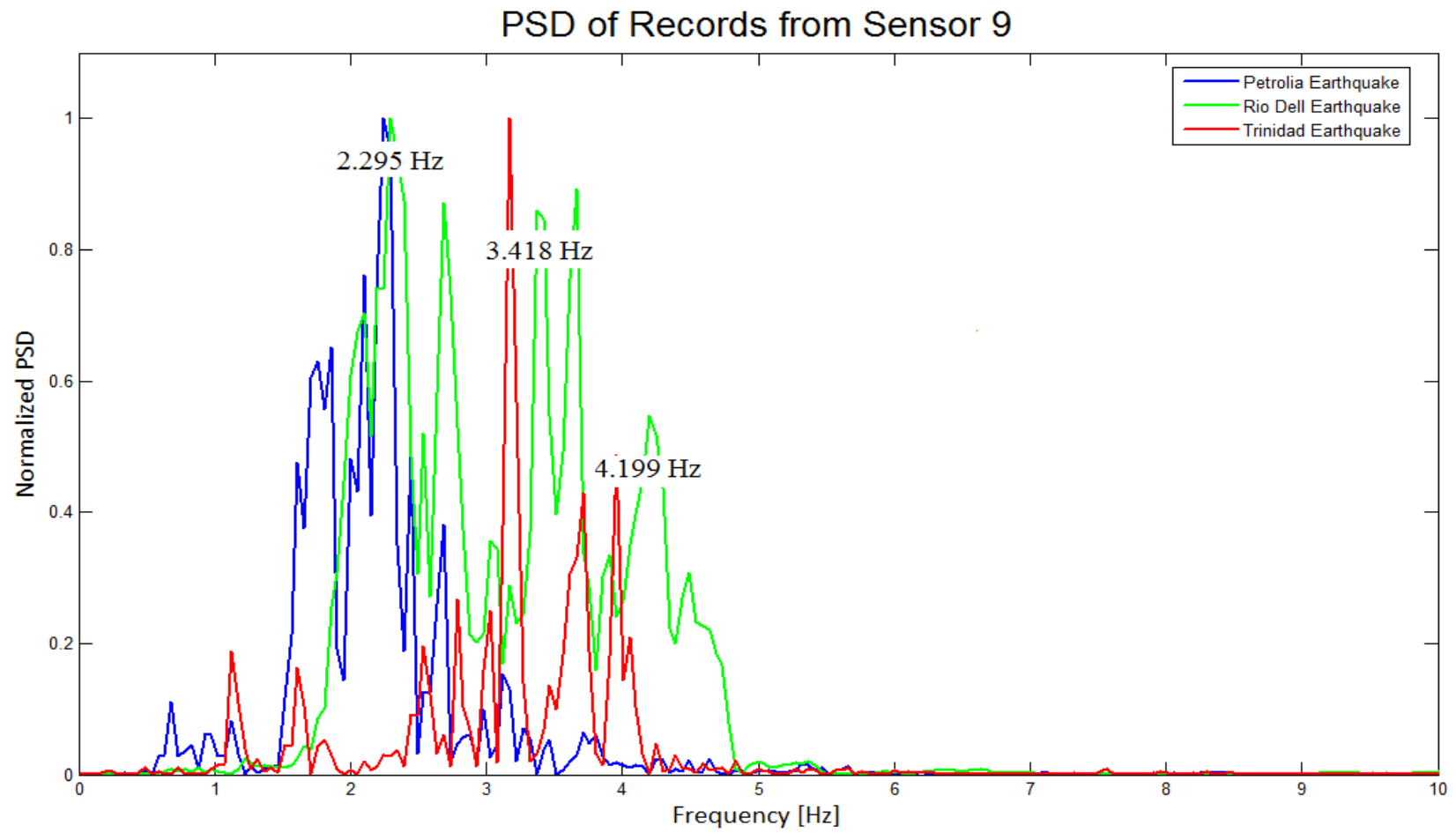


Figure. 2.1d Sensor 9 PSD for Trinidad Rio Dell Earthquake and Petrolia Earthquake

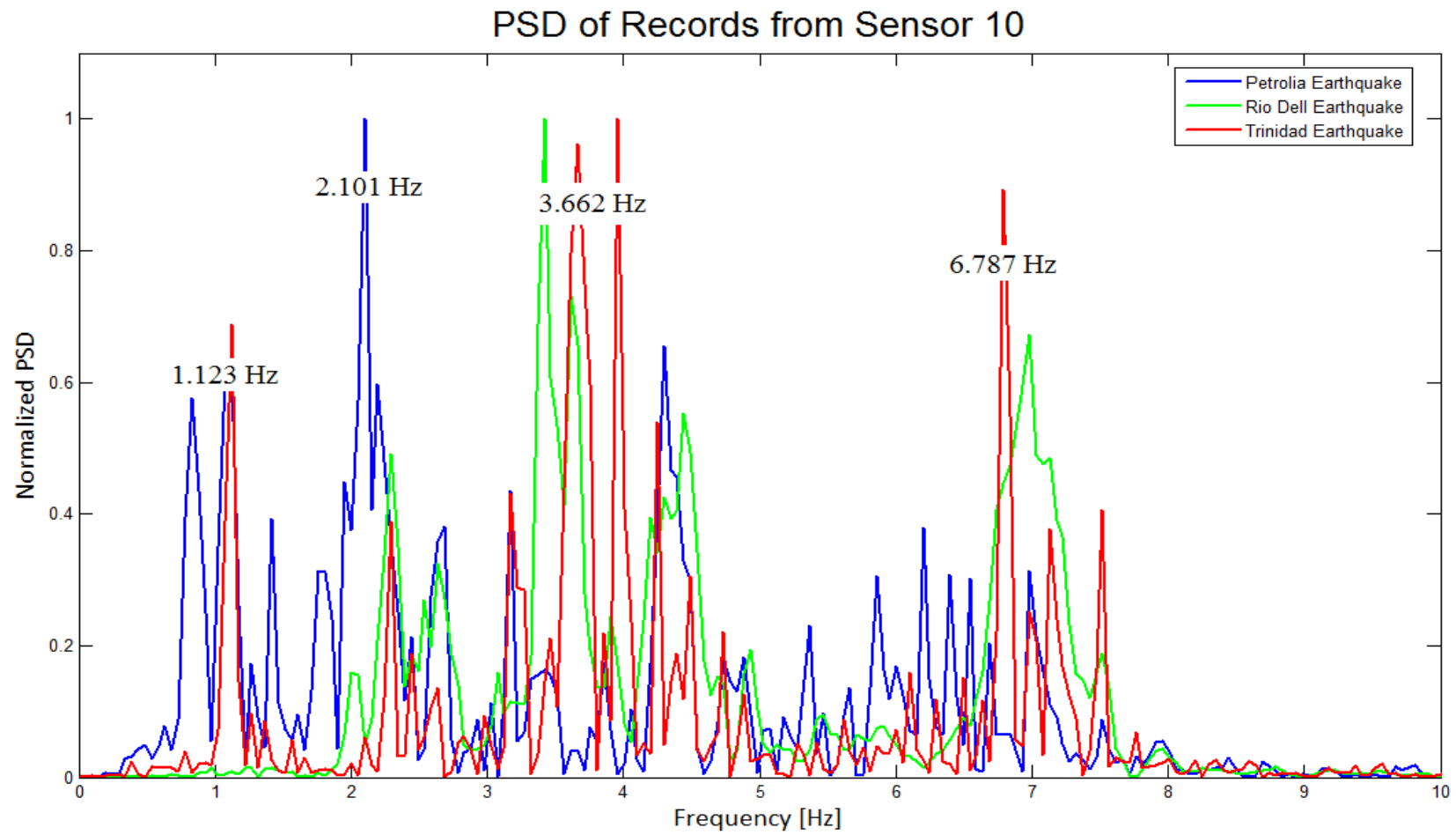


Figure 2.1e: Sensor 10 PSD for Trinidad Rio Dell Earthquake and Petrolia Earthquake

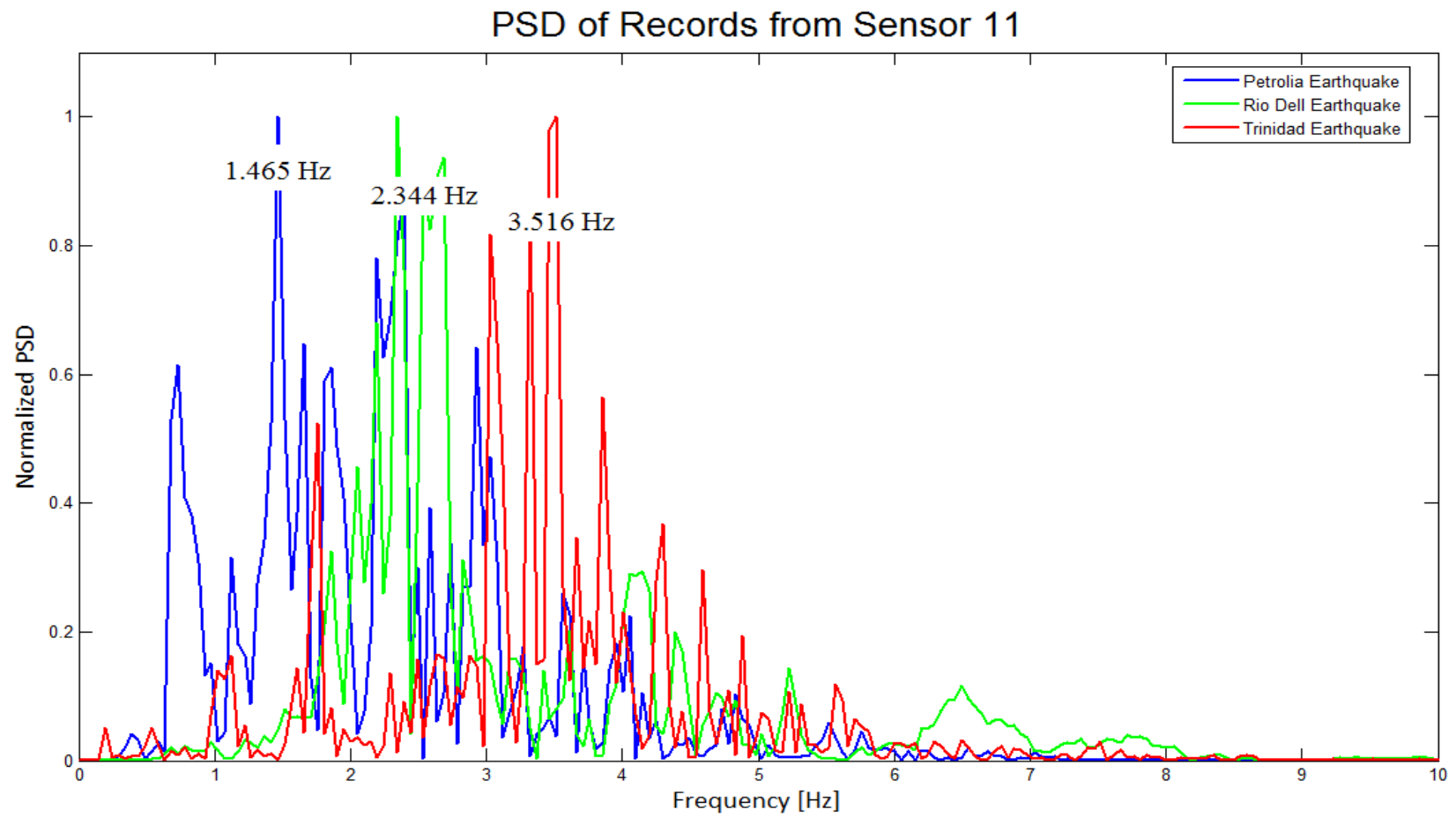


Figure 2.1f: Sensor 11 PSD for Trinidad Rio Dell Earthquake and Petrolia Earthquake

Another analysis is performed on the Fourier transforms of the time histories recorded from channels that measure accelerations at the base of the pier (1, 2, 3), in free field (12, 13, 14), at the top of the east abutment (15, 16, 17) and on the bridge deck above the same abutment (9, 10, 11). First of all, the average value of the records between the Trinidad and Petrolia earthquakes is computed. Then, the Fourier transforms of the resulting time histories are calculated, grouping the plots depending on the direction of the measured motions. Then, three plots are obtained: the first representing the frequency content of the longitudinal accelerations, from channels 1, 11, 12 and 15; the second presenting the vertical accelerations, from sensors 2, 10, 13 and 16; the last showing the transverse behavior, from accelerometers 3, 9, 14 and 17. Results are presented in figures 2.2.

Analysis of figures 2.2 demonstrates a minor soil-structure interaction in the area of the pier. In fact, free field and base of the pier motions are similar. On the other hand, the interaction soil-structure is considerable in the area of the embankment, as can be inferred from the differences between the free field and the top of abutment motion. Lastly, the similarity of the motions on top of the fill with the motions on the bridge deck could imply that the embankment fill moves with the bridge deck.

The trend identified via Fourier Transforms is found again by comparing the acceleration amplitude of the channels, plotted in figures 2.3. The maximum longitudinal accelerations on the abutment fill and on the structure are essentially the same as the free field motion for all earthquakes, possibly indicating the bridge is moving as a rigid body with the ground in the longitudinal direction. Practically, the same behavior is observed in the vertical direction. On the contrary, in the transverse direction the abutment and deck accelerations are amplified compared to the free field ones.

These observations offer valuable information on how to model the boundary conditions of the finite element system. In fact, the soil-structure interaction between the base of the pier and the soil can be modeled through fixed

restraints, since the two systems move together as a rigid body. On the other hand, the area through which the deck approaches the abutment does not need any special representation, for the two systems move as rigid body as well. On the contrary, the soil-structure interaction needs to be well understood and then modeled at the abutment level. As will be deeply clarified in the following paragraph, the best model for this connection is represented by a set of springs, whose stiffness choice constitutes a crucial step to obtain a model with realistic response.

Other interesting information on the dynamic behavior of skewed bridges can be found in a paper of Eng. Shamsabadi and Eng. Kapuskar. The research of the two engineers is focused on the determination of the response of skewed bridges to seismic inputs as a function of skew angle. Their results have obtained by exciting three-dimensional model of two-span box girder bridges with a skew angle varying from 0 to 60 degrees with non-linear time histories. It is observed that skewed bridges are affected by strong rotations with respect to the vertical axis during the seismic event, while present an irreversible transverse displacement after the shaking is terminated. On the contrary, the bridge with zero skew angle do not show this behavior. Moreover it is observed that, for particularly intense ground motions, the deck could experience the unseat at the abutments. The engineers clarify that what causes the severe deck rotations is a non uniform passive soil wedge behind the abutment wall, that results in asymmetric soil reactions of the wall itself. What deserves to be underlined is that the response changes as the direction of the applied motions vary. Therefore, it is important to be provided of earthquake time histories with more than one component and different records in order to completely identify the dynamic behavior of a skewed bridge.

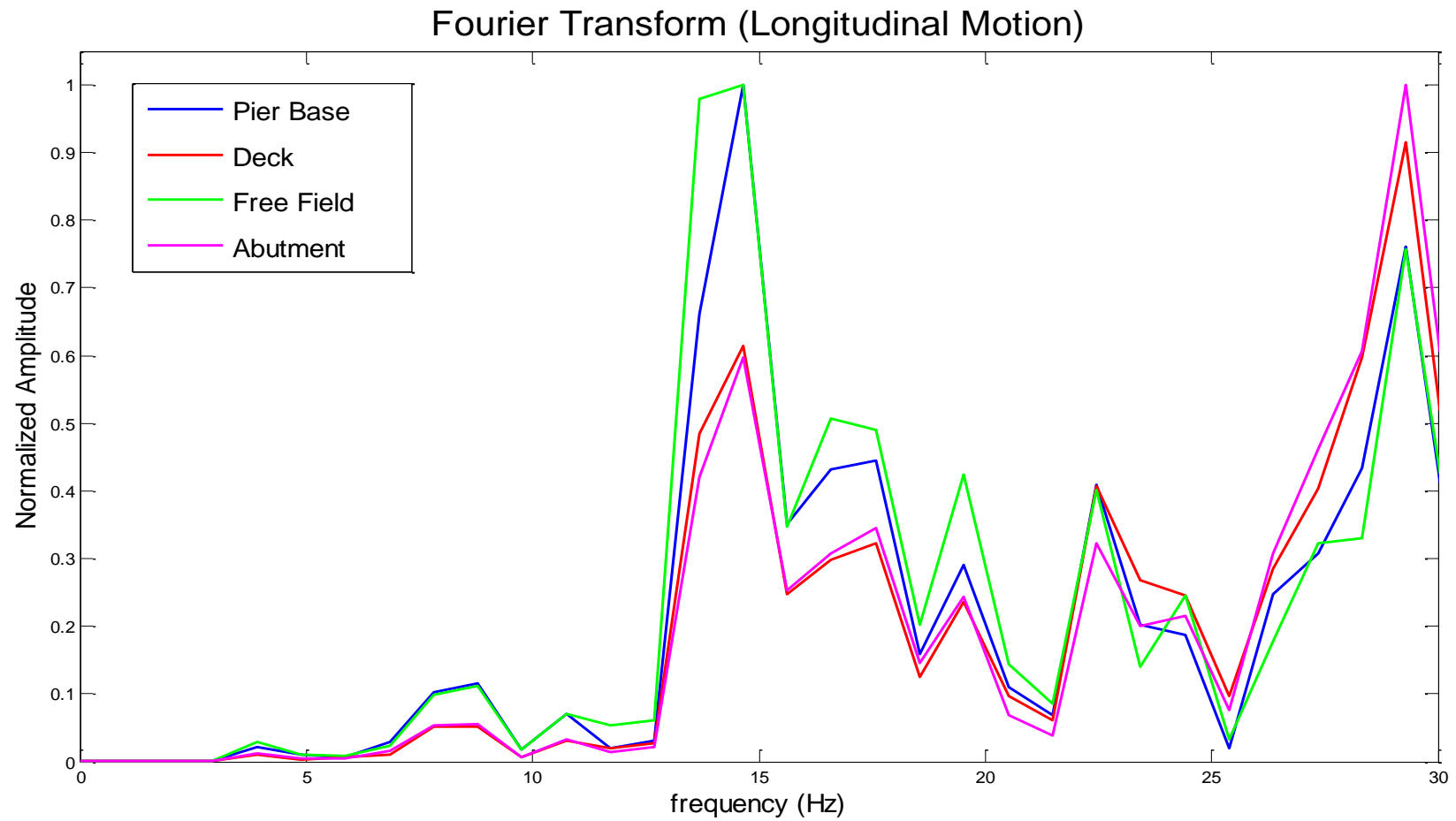


Figure 2.2a: Average Fourier Amplitude for Sensors 1 (Base of Pier), 11 (Deck), 12 (Free field) and 15 (West Abutment)

Fourier Transform (Vertical Motion)

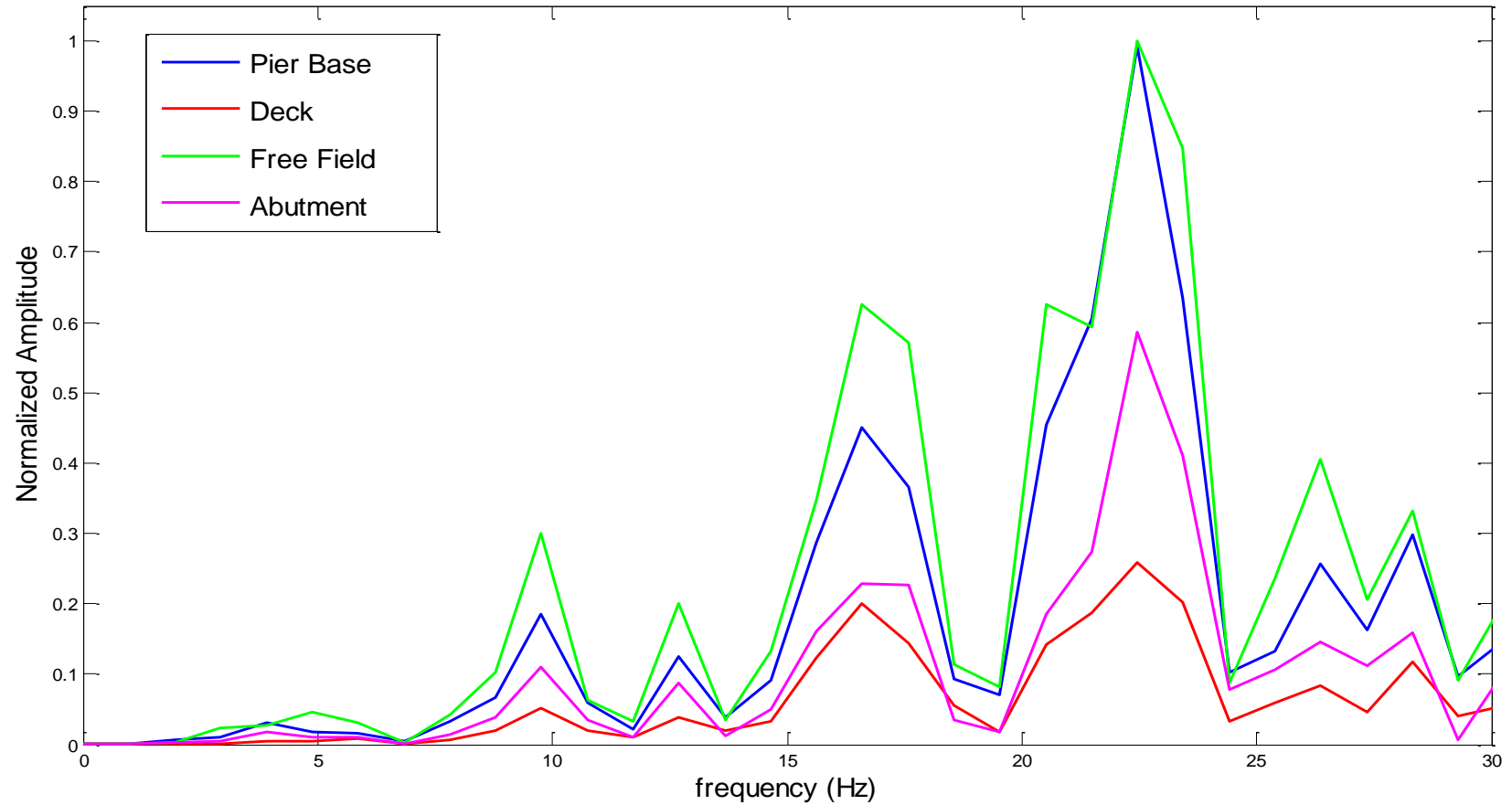


Figure 2.2b: Average Fourier Amplitude for Sensors 2 (Base of Pier), 10(Deck), 13 (Free field) and 16 (West Abutment)

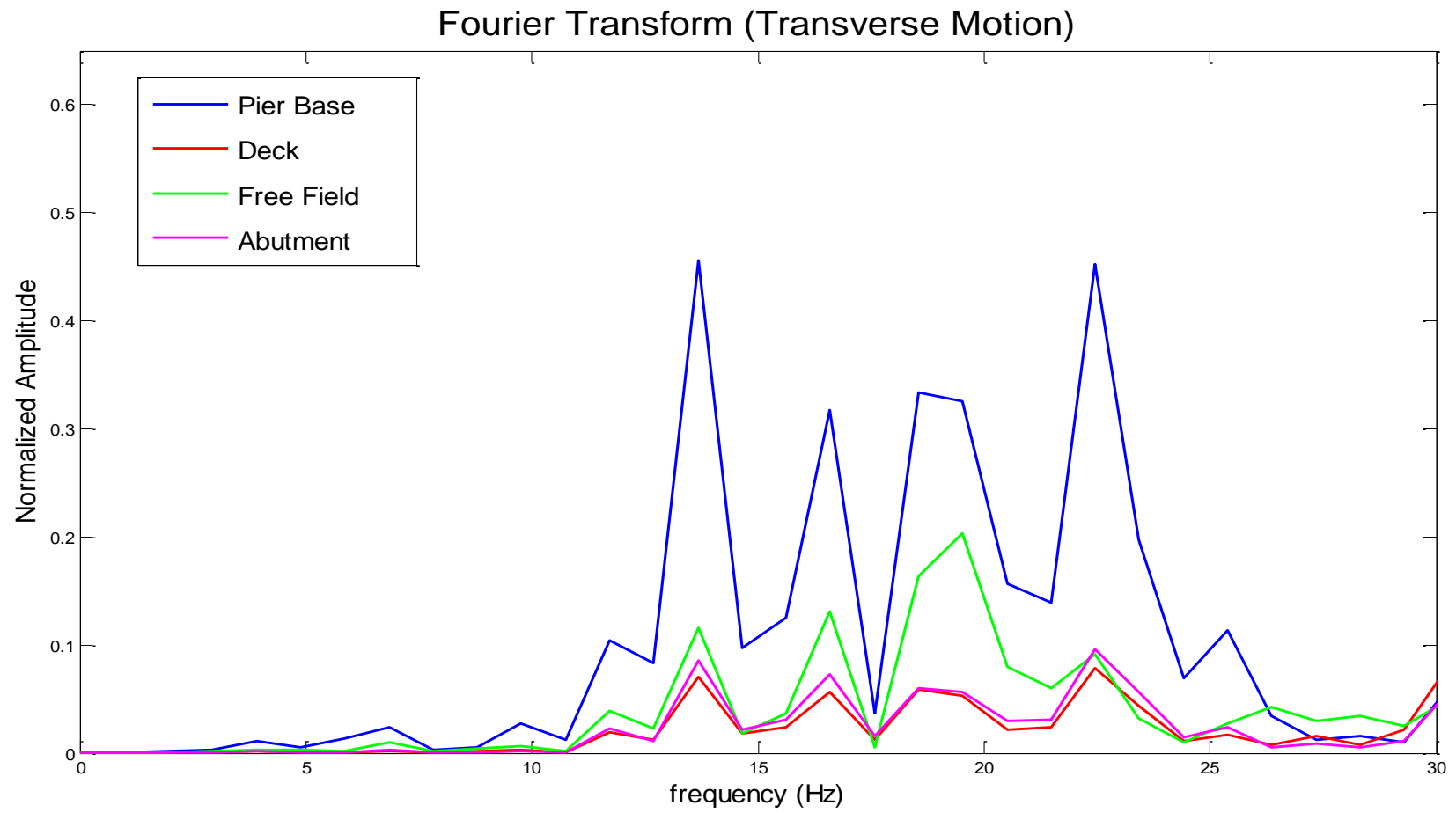


Figure 2.2c: Average Fourier Amplitude for Sensors 3 (Base of Pier), 9 (Deck), 14 (Free field) and 17 (West Abutment)

Time Histories of Longitudinal Motions (channels 11, 12 and 15)

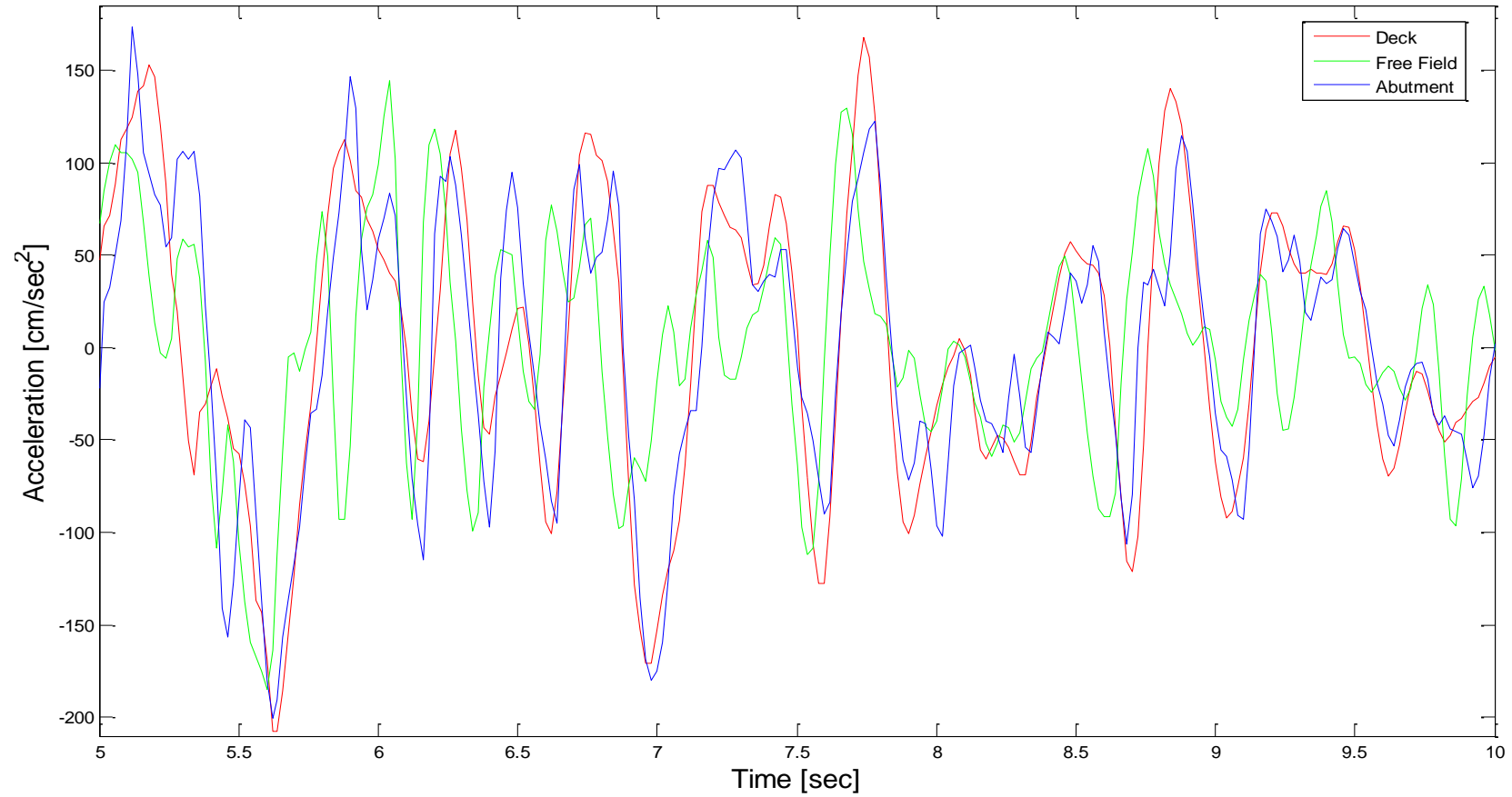


Figure 2.3a: Average Acceleration Amplitude for Sensors 11(Deck), 12 (Free field) and 15 (West Abutment)

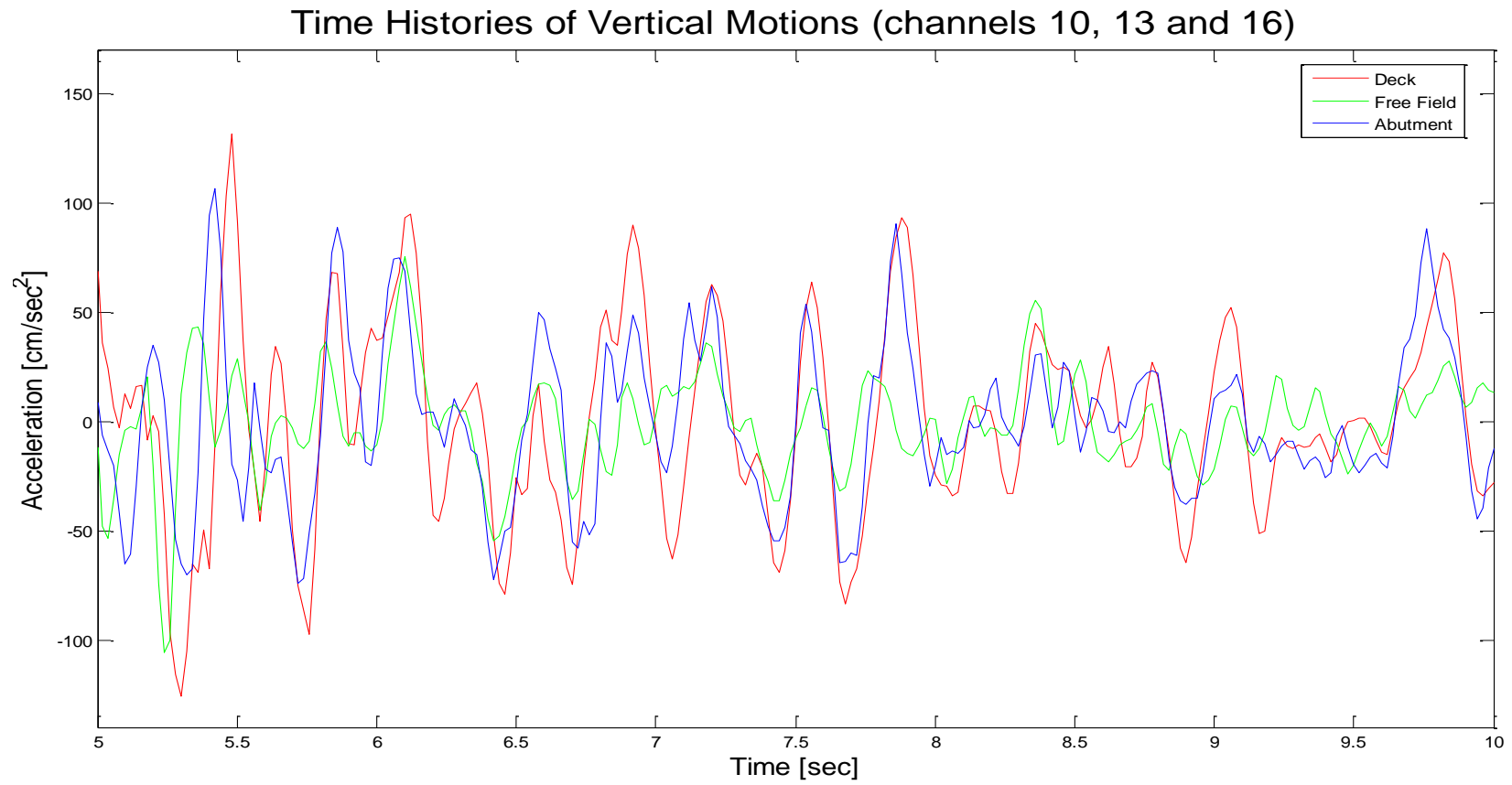


Figure 2.3b: Average Acceleration Amplitude for Sensors 10(Deck), 13 (Free field) and 16 (West Abutment)

Time Histories of Transverse Motions (channels 9, 14 and 17)

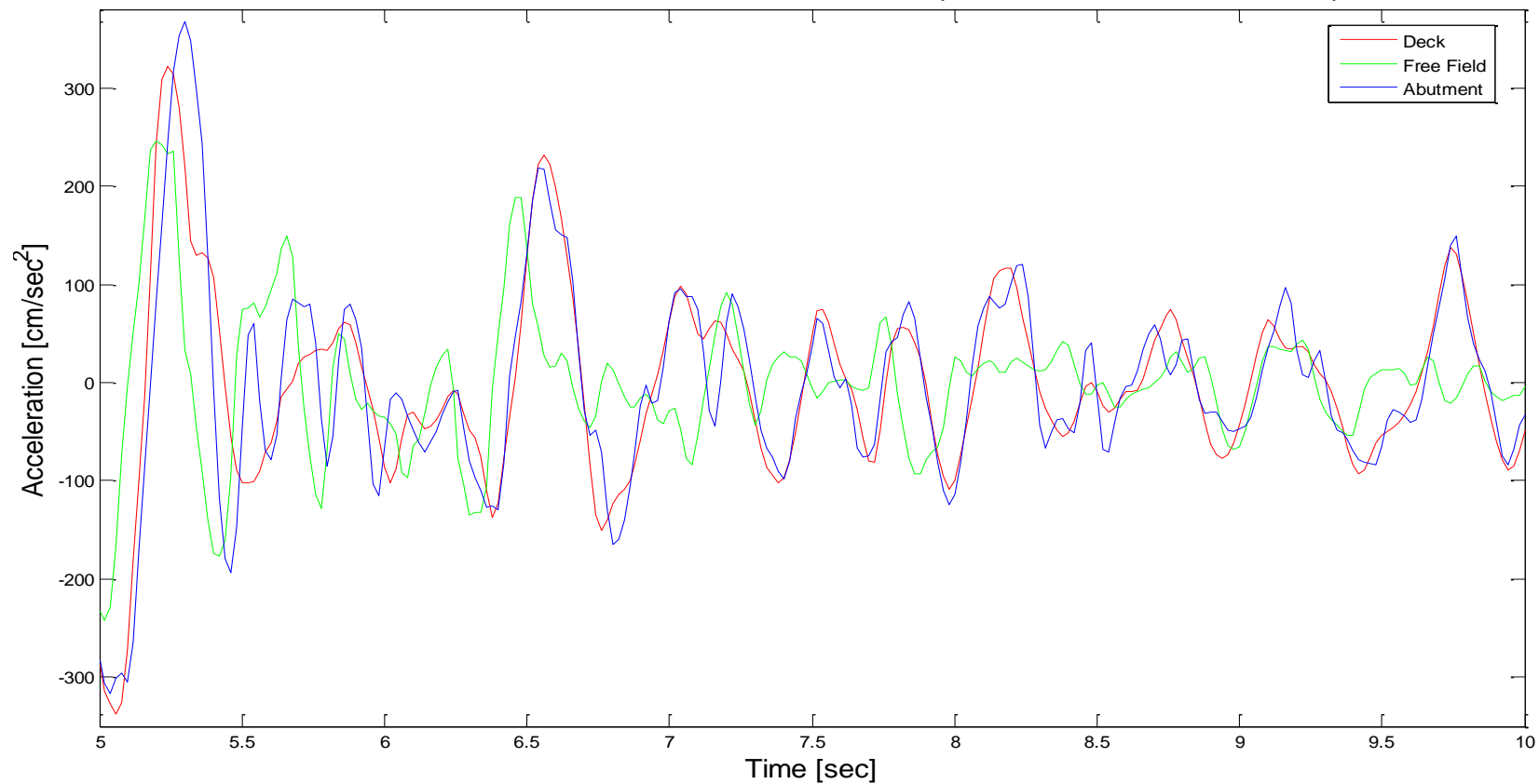


Figure 2.3c: Average Acceleration Amplitude for Sensors 9(Deck), 14 (Free field) and 17 (West Abutment)

2.4 Soil-Structure Interaction

As derived in the previous paragraph, it is essential to individuate a model through which reasonably represent the soil-structure interaction at the base of the abutment. Moreover, the final aim of this study is obtaining a realistic non-linear model of the Rio Dell Painter Street Overpass. It becomes apparent that this leads to deal with large displacements theory. As displacements raise, the behavior of bridge abutments cannot be modeled as linear anymore. Studies proved that the peak accelerations recorded near and on highway overcrossing approach embankments can be more than twice the crest motion of the pile cap of the center bent. Then, the kinematic response of the embankment strongly effects the bridge response. Design procedures used by Caltrans (1989) solve the problem by means of distributed linear springs whose objective is modeling the stiffness of the embankment. Nevertheless, the Caltrans approach does not take into account neither the energy absorbed by the embankment nor the dynamic nature of the problem. Thus, this simplified approach becomes unacceptable when there is an attempt to seek more detailed results.

The solution proposed by Prof. Romstad consists of a complex system of springs reflecting soil, pile, concrete and interaction properties, as the one presented in figure 2.4. At both abutments the wingwalls are pinned with respect to moment about the vertical global Y axis. The wing wall cannot move out from the centerline of the bridge, once the joint filler is crushed to transfer the load. Nevertheless, there is not resistance to movement of the wingwall toward the longitudinal centerline of the bridge, except frictional resistance at the base of the wingwall. Moreover, the west backwall and the foundation are separated by a 1/4" neoprene bearing strip. Shear keys bound the abutment backwall in the case gross relative displacements in both transverse directions and in the skewed longitudinal direction such that the backwall cannot move into the soil.

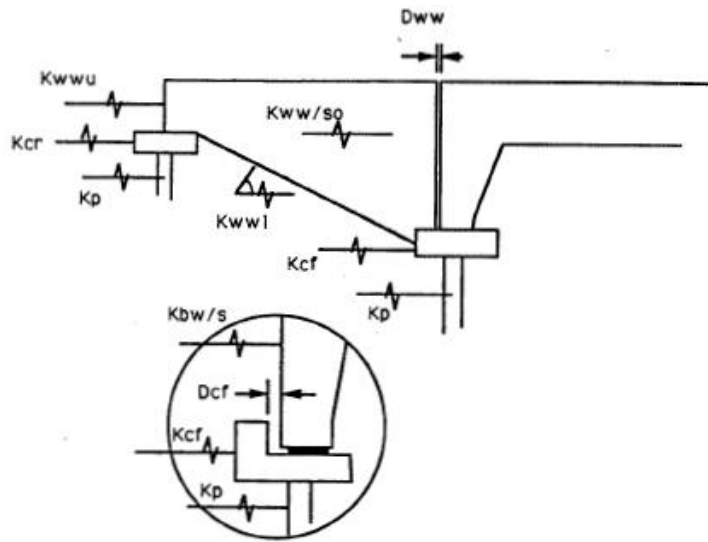


Figure 2.4a: Elevation View of Longitudinal West Abutment Resisting Elements

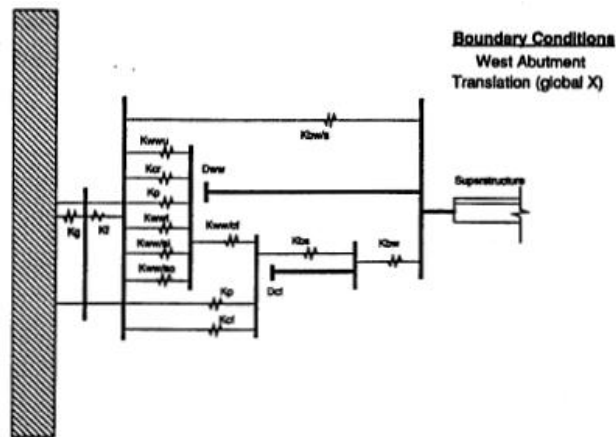


Figure 2.4b: Schematic Representation of Longitudinal West Abutment Active Spring Elements

However, this model seems to be very complex to apply and to be implemented in an FE model. Therefore, it is looked for another model. The research published by Zhang and Makris seems to achieve the purpose. The two researchers presented a study on Painter Street Overpass, providing the values of

the spring stiffness and dash-pot damping coefficients that can be used in a three dimensional finite element model in order to represent the soil-structure interaction at the end abutments. In the first phase of the method, the kinematic response of the embankments is evaluated. Through this step the shear modulus G and the damping coefficient η of the soil embankment are determined. In particular, the shear modulus of the Rio Dell Overpass embankment is set equal to 8 MPa, while the damping coefficient equals 0.5. Then, it is possible to complete the dynamic stiffness calculation. Since this second phase is the one that leads to the values of interest, the detailed calculations are presented below:

1. Computation of the dynamic stiffness of the unit-width shear wedge:

$$\hat{k}_x(\omega) = G(1 + i\eta)B_c k \frac{J_1(kz_0)Y_0[k(z_0 + H)] - J_0[k(z_0 + H)]Y_1(kz_0)}{Y_0[k(z_0 + H)]J_0(kz_0) - J_0[k(z_0 + H)]Y_0(kz_0)} \quad (2.1)$$

where

$$G = 8 \text{ MPa}$$

$$\eta = 0.5$$

$$V_s = 190 \text{ m/s}$$

$$B_c = 15.24 \text{ m}$$

$$z_0 = 3.81 \text{ m}$$

$$H = 9.6 \text{ m}$$

$$k = \frac{\omega}{V_s(1 + i\eta)}$$

$J_0(\omega)$ = Zero Order Bessel Function of the First Kind

$J_1(\omega)$ = First Order Bessel Function of the First Kind

$Y_0(\omega)$ = Zero Order Bessel Function of the Second Kind

$Y_1(\omega)$ = First Order Bessel Function of the Second Kind

2. Plot of the real and the imaginary parts of equation 2.1 as a function of frequency $f = \omega/2\pi$:

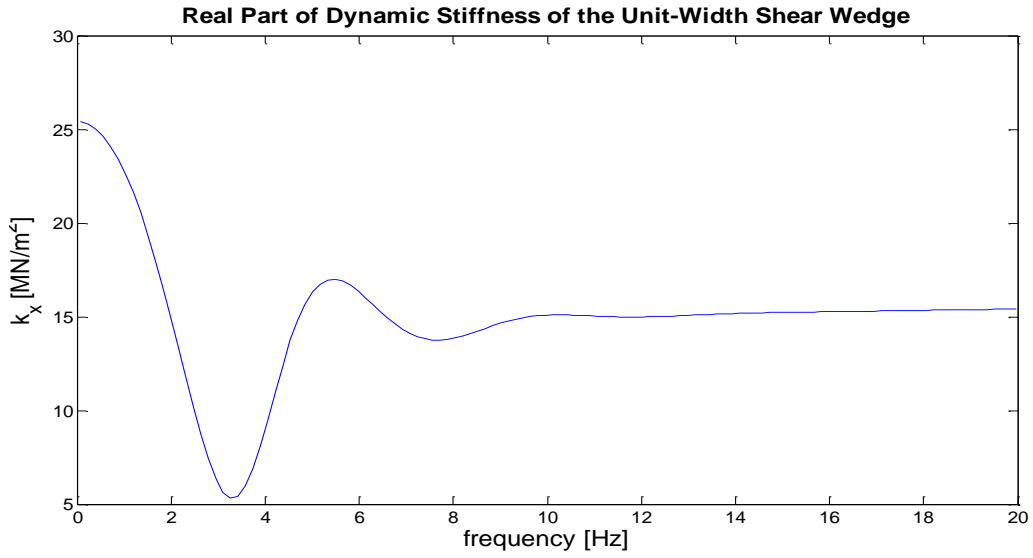


Figure 2.5: Plot of the Real Part of Equation 2.1

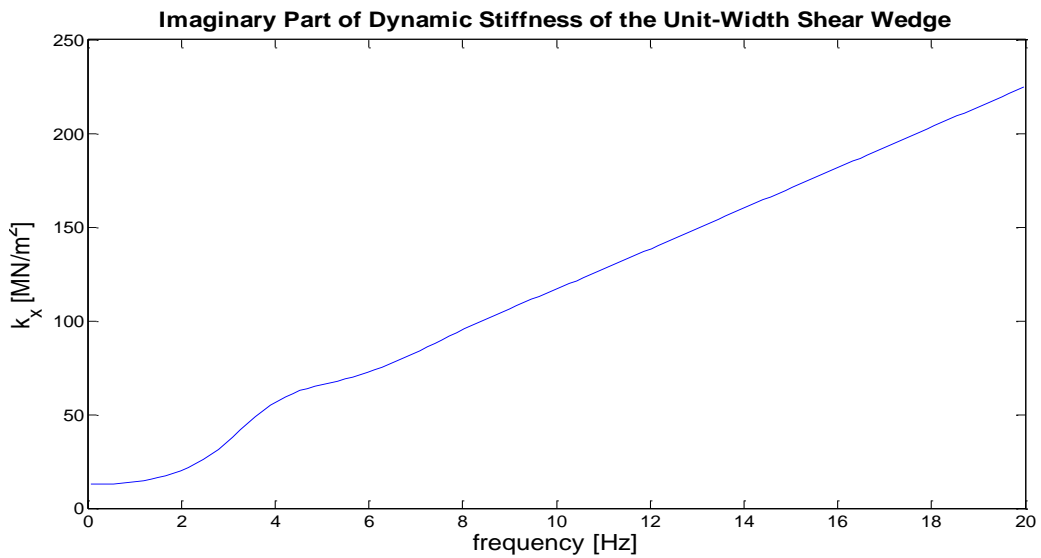


Figure 2.6: Plot of the Imaginary Part of Equation 2.1

- Selection of practical spring and dash-pot values by passing a horizontal line through the graph of the real part and inclined line through the graph of the imaginary part at locations that capture with satisfaction the low frequency behavior:

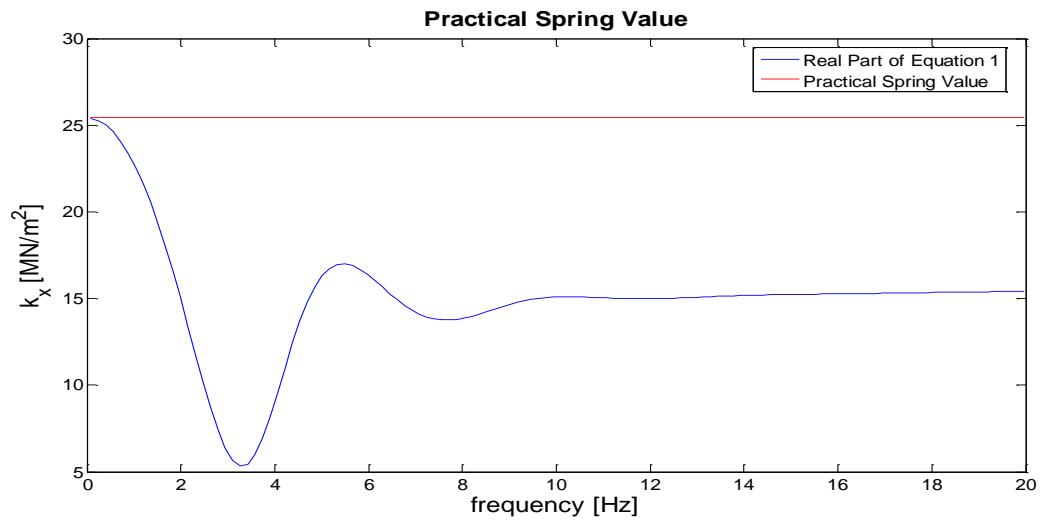


Figure 2.7: Practical Spring Value

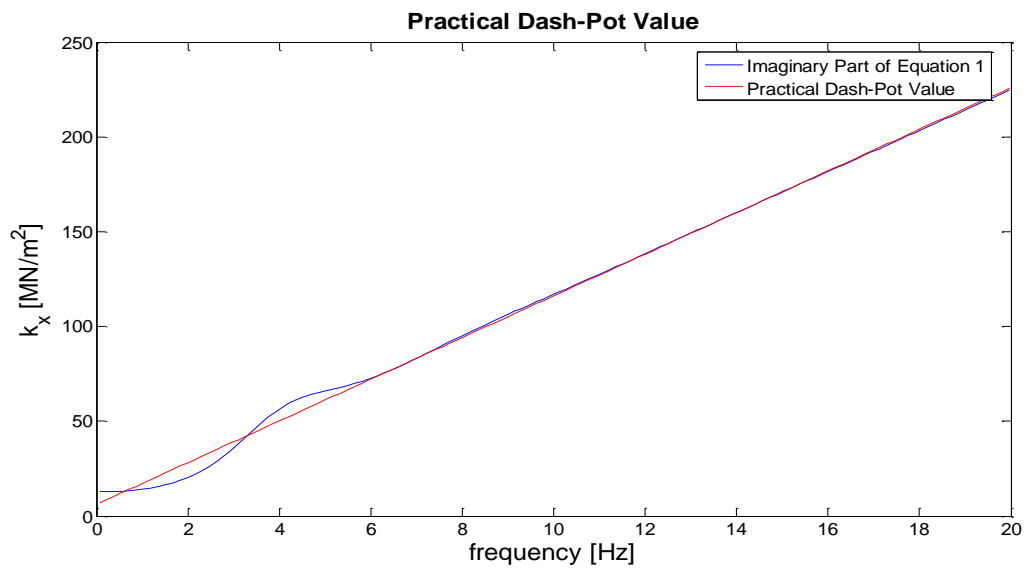


Figure 2.8: Practical Dash-Pot Value

Figures above show that the practical spring value can be taken equal to 25.413 MN/m², while the slope of the imaginary part of the unit-width shear wedge gives the practical dash-pot value of the soil embankment:

$$\zeta=10.992 \quad (2.2)$$

4. Computation of the transverse spring and dash-pot values of the embankment by multiplying the practical values with the critical length defined by equation 2.3:

$$L_c = 0.7\sqrt{S B_c H} = 5.987 \quad (2.3)$$

where

$$S = 0.5$$

$$B_c = 15.24 \text{ m}$$

$$H = 9.6 \text{ m}$$

Finally, the transverse and longitudinal values of the spring stiffness are:

$$k_x = k_y = 152.148 \text{ MN/m} = 10,425,450 \text{ lbf / ft} \quad (2.4)$$

while the transverse and longitudinal values of the dash-pot damping coefficients are:

$$\zeta_x = \zeta_y = 65.809 \quad (2.5)$$

2.5 Structural Identification through OKID

Examination of the literature demonstrates that essentially the subject is explored in the damage identification field. The most common use of the OKID tool is that where data is recorded at two different period of time, and the goal is that of establish whether the system has suffered damage in the time between the two observations. At the beginning of the development of structural health monitoring technique, the recorded time histories were used to optimize a mechanical model of the system under analysis in the two states, and then the damage was identified by comparing the differences in the two conditions. Nonetheless, because of the high level of uncertainty and complexity strictly linked to the generation of a structural model, the results were not always reasonable and reliable. Trying to fix a guideline for the Structural Health Monitoring, the dynamics committee of ASCEE formed a Task group on the subject in 1999. One of the solution the task group considered was that of obtaining a state-space realization from the measured signals. Moreover, in order to solve the state-space model in discrete time, the Eigensystem Realization Algorithm with a Kalman Observer (ERA-OKID) was used. As will be completely clear in next chapter, this is the starting point for the structural identification of the system through the OKID Algorithm. The damage identification strategy then developed by the task follows by extracting flexibility matrices from the matrices realization, computing the change in flexibility from the undamaged to the damaged state, reducing the subset of potentially damaged elements by examination of the change in flexibility and finally, quantifying the damage using the identified damaged flexibility. The technique finds its power in the simplicity of application. However, the exigency of disposing of many channel represents an important limitation of the method. Moreover, the technique was tested on relatively simple systems. Finally, this method represents a valid

tool to identify damage when occurred, and it is not the case of the Painter Street Overpass.

The last mention technique was used to solve the so called benchmark problem. Starting from the proposed solutions of the ASCEE task group, a team of researchers, led by Prof. Betti and Prof. Lus, introduced a new approach in the structural identification and damage detection theory. The method is divided into two stages: the first consists in identifying a state-space model, by using the recorded data, through the OKID/ERA algorithm, and then optimizing it through a non-linear optimization approach. The second step leads to the identification of the second order dynamic model characteristics from the previously realized state-space model. Through the identification of the main dynamic model parameters, as mass, stiffness and damping, a set of information of the undamaged system can be organized. The variation of such values could mean the system has suffered damage. The intriguing advantage of this approach is the use of only the available input-output measurement data, without the need neither of manipulating them, nor of imposing any limitation on the kind of damping by which the system is subjected.

3

SYSTEM IDENTIFICATION VIA OKID\ERA

Sommario

Di seguito è presentata una metodologia per l'identificazione di modelli che descrivono lo stato di un sistema strutturale attraverso l'utilizzo di time histories registrate delle accelerazioni al suolo e sulla struttura stessa registrate durante eventi sismici.

Da tali modelli possono essere facilmente ricavati i parametri modali della struttura, quali le frequenze, i rapporti di smorzamento e le forme modali. Tale approccio d'identificazione si basa sull'utilizzo dell'Eigensystem Realization Algorithm (ERA), complementato dall'algoritmo Observer/Kalman filter Identification (OKID). Per l'ottenimento dei risultati finali, si attua un'ottimizzazione tramite la minimizzazione dell'errore tra la risposta dedotta computazionalmente e quella misurata. L'analisi dei risultati porta a concludere che la metodologia qui proposta è efficace nell'identificare le caratteristiche strutturali del sistema, sebbene si debba riconoscere che tali risultati potrebbero essere migliorati avendo ad esempio a disposizione time histories più lunghe o accelerogrammi registrati anche sulla sponda sud del ponte.

Fin dall'inizio della sua introduzione, molti utenti hanno trovato questo metodo efficace in numerose applicazioni pratiche nel contesto del controllo delle vibrazioni di strutture flessibili in campo aerospaziale e meccanico. La teoria, dunque, è stata originariamente coniata appositamente per questo tipo di sistemi, tuttavia la formulazione matematica si basa su ipotesi facilmente applicabili a qualsiasi tipo di struttura.

3.1 Introduction

In the field of identification of structures, the common practice is to create an analytical model and to update it by using static and dynamic testing. The initial finite element model is calibrated by comparing the numerical eigendata (natural frequencies and mode shapes) with the eigendata acquired from the model tests. Approaches based on frequency response functions and fast Fourier transforms are still dominant in the model updating philosophy. The aim of experimental modal analysis is to retrieve the system's modal characteristics, such as the natural frequencies, mode shapes, etc. from experimental data. However, such experiments generally require a large number of actuators and sensors to pick up most of the modal data. An alternative approach to determine an appropriate structural model is to use input-output relations, as the one developed in the present work.

The time histories available at the Center of Engineering Strong Motion Data (CESMD) are necessary to the Observer/Kalman filter Identification (OKID) algorithm to compute the Markov parameters of the system. The quality of the estimated state of the system by a designed observer depends on the accuracy of not only the assumed system model, but also the assumed system and measurement noise characteristics. Information of both the system and the noise characteristics are embedded in the above mentioned Markov parameters. For a lightly damped system, the number of system Markov parameters needed to be solved for becomes exceedingly large. It is known that not all the system Markov parameters are independent. By invoking the Cayley-Hamilton theorem we know that every Markov parameter can be expressed as a linear combination of a finite number of "independent" system Markov parameters where the unknown coefficients of the linear combination are those of the system characteristic equation. The key issue is how to reduce the number of unknowns without having to pose this problem as a non-linear parameter estimation problem. It is possible

to compress the original set of system Markov parameters into another set of parameters where the details of the compression is explained via a special matrix, which is precisely an observer gain described previously.

The observer Markov parameters are then used by the Eigensystem Realization Algorithm (ERA) to realize the discrete time first order system matrices. Then, via a non-linear optimization algorithm, the output error between the measured and detected response is minimized. Finally, the physical characteristics of the structure are recovered by means of a technique discussed by Lus (2001) and De Angelis (2002).

For my purposes I have used one of the latest version of the function OKID/ERA/non-linear optimization algorithms written in the Matlab programming language. Essentially, the user provides a set (or multiple sets) of input-output data, together with such information as the number of inputs, the number of outputs, sampling interval, etc., the function will return an identified state-space model, associated observer gain and physical characteristics of the model.

3.1.1 The Historical Path of OKID/ERA Algorithm

During the last three decades, there has been a vast number of studies and algorithms concerning the construction of state space representations in the time-domain for linear dynamical systems, beginning with the works of Gilbert and Kalman. One of the first result obtained in this field was about ‘minimal realizations’, indicating ‘a model with the smallest state-space dimension among system realized that has the same input-output relations within a specified degree of accuracy...’. It was shown by Ho and Kalman, that the minimum representation problem was equivalent to the problem of identifying the sequence of real matrices, known as the Markov parameters, which represent the unit pulse responses of a linear dynamical system. Following a time-domain formulation and incorporating results from control theory, Juang and Pappa proposed an Eigensystem Realization Algorithm (ERA) for modal parameter identification and model reduction of linear dynamical systems, which extends the Ho-Kalman algorithm and creates a minimal realization that mimics the output history of the system when it is subjected to unit pulse inputs. Later, this algorithm was refined to better handle the effects of noise and structural non-linearities, and the ERA with data correlations (ERA/DC) was proposed. When general input data such as an earthquake-induced ground motion is used, difficulties in retrieving the system Markov parameters can arise related to problem dimensionality and numerical conditioning. Among the algorithms proposed to overcome these difficulties, the Observer/Kalman filter IDentification (OKID) algorithm introduces an asymptotically stable observer which increases the stability of the system and reduces the computation time, improving the performance even when the noise and slight non-linearities are present. This technique has proven to be quite successful in the aerospace community in the identification of complex, high-dimensional space craft structures.

3.2 Basic Formulation

3.2.1 Input-Output relations

The dynamic behavior of an N degrees of freedom linear structural system can be represented by the second-order differential equation:

$$\mathbf{M}\ddot{\mathbf{q}}(t) + \mathbf{L}\dot{\mathbf{q}}(t) + \mathbf{K}\mathbf{q}(t) = \mathbf{B}\mathbf{u}(t) \quad (3.1)$$

where $\mathbf{q} \in \mathbb{R}^N$ is the structural displacement vector in a fixed system of reference. The matrices \mathbf{M} , \mathbf{L} and \mathbf{K} , all $\mathbb{R}^{N \times N}$, are the mass, damping and stiffness matrices, respectively, while $\mathbf{B} \in \mathbb{R}^{N \times r}$ indicates the continuous time input matrix, in fact, the vector $\mathbf{u}(t)$ is assumed to contain r external excitations applied to the system. When the input is represented by a seismic excitation, the components of $\mathbf{q}(t)$ correspond to nodal displacements with respect to a system of reference whose origin is at the base of the structure and moves together with the base. The external forcing term $\mathbf{B}\mathbf{u}(t)$ can now be replaced by $-\mathbf{M}\mathbf{I}_{N \times 1}\ddot{x}_g(t)$, with $\mathbf{I}_{N \times 1}$ being the unitary vector and $\ddot{x}_g(t)$ the ground acceleration at the time t .

The same structural system of equation (3.1) can also be represented as a system of first-order differential equation in state-space form, setting $\dot{\mathbf{v}}(t) = \mathbf{q}(t)$:

$$\begin{cases} \mathbf{M}\dot{\mathbf{v}}(t) + \mathbf{L}\mathbf{v}(t) + \mathbf{K}\mathbf{q}(t) = \mathbf{B}\mathbf{u}(t) \\ \mathbf{v}(t) = \dot{\mathbf{q}}(t) \end{cases} \quad (3.2)$$

Let assume that one is provided of only m output time histories of the response, then, it is possible to introduce a new vector $\mathbf{y}(t)$, containing the measurements available (generally $m \neq N$).

Finally, it is possible to form the following system:

$$\begin{cases} \begin{bmatrix} \dot{\mathbf{q}}(t) \\ \dot{\mathbf{v}}(t) \end{bmatrix} = \begin{bmatrix} 0 & 1 \\ -\frac{\mathbf{K}}{\mathbf{M}} & -\frac{\mathbf{L}}{\mathbf{M}} \end{bmatrix} \begin{bmatrix} \mathbf{q}(t) \\ \mathbf{v}(t) \end{bmatrix} + \begin{bmatrix} 0 \\ \frac{\mathbf{B}}{\mathbf{M}} \end{bmatrix} \\ \mathbf{y}(t) = \begin{bmatrix} (\Psi_p \mathbf{q}(t))^T & (\Psi_v \dot{\mathbf{q}}(t))^T & (\Psi_a \ddot{\mathbf{q}}(t))^T \end{bmatrix}^T \end{cases} \quad (3.3)$$

$$\begin{cases} \dot{\mathbf{x}}(t) = \mathbf{A} \mathbf{x}(t) + \mathbf{B} \mathbf{u}(t) \\ \mathbf{y}(t) = \mathbf{C} \mathbf{x}(t) + \mathbf{D} \mathbf{u}(t) \end{cases} \quad (3.4)$$

$$\begin{cases} \mathbf{y}(t) = \mathbf{C} \mathbf{x}(t) + \mathbf{D} \mathbf{u}(t) \end{cases} \quad (3.5)$$

where \mathbf{x} is the n -dimensional state vector, and \mathbf{y} is the m -dimensional output vector, where n is $2N$. The matrices $\mathbf{A} \in \mathbb{R}^{n \times n}$, $\mathbf{B} \in \mathbb{R}^{n \times r}$, $\mathbf{C} \in \mathbb{R}^{m \times n}$ and $\mathbf{D} \in \mathbb{R}^{m \times r}$ represent the time invariant system matrices. Since we receive measurements of input and output as sets of discrete data, it is convenient to work in the discrete time domain so that equation (3.4) and (3.5) can be expressed as difference equations in the following form:

$$\begin{cases} \mathbf{x}(k+1) = \Phi \mathbf{x}(k) + \Gamma \mathbf{u}(k) \\ \mathbf{y}(k) = \mathbf{C} \mathbf{x}(k) + \mathbf{D} \mathbf{u}(k) \end{cases} \quad (3.6)$$

$$\begin{cases} \mathbf{y}(k) = \mathbf{C} \mathbf{x}(k) + \mathbf{D} \mathbf{u}(k) \end{cases} \quad (3.7)$$

where the integer k denotes the time step number, i.e. $\mathbf{x}(k+1) = \mathbf{x}[k(\Delta T) + \Delta T]$, with ΔT being the time step interval. Assuming the input as a unit pulse, we obtain:

$$\begin{aligned} \text{for } k=0 & \quad x_1 = 1 \\ \text{for } k=1 & \quad x_2 = \Phi x_1 = \Phi \Gamma \\ & \quad \vdots \\ \text{for } k=n-1 & \quad x_n = \Phi x_{n-1} = \Phi^{n-1} \Gamma \Rightarrow y_n = \mathbf{C} x_n = \mathbf{C} \Phi^{n-1} \Gamma \end{aligned} \quad (3.8)$$

The y_n are called *system* Markov parameters, they are the response of the system to a unit pulse. For a zero-order hold approximation and a sampling time ΔT , the

discrete time system matrices Φ and Γ can be evaluated as $\Phi = e^{A(\Delta T)}$, so that $\Gamma = \left(\int_0^{\Delta T} e^{A\sigma} d\sigma \right) B$, and the solution of equations (3.6) and (3.7) is given by the

following convolution sum:

$$x(k) = \Phi^k x(0) + \sum_{j=0}^{k-1} \Phi^{k-1-j} \Gamma u(j) \quad (3.9)$$

$$y(k) = C\Phi^k x(0) + \sum_{j=0}^{k-1} C\Phi^{k-1-j} \Gamma u(j) + D u(k) \quad (3.10)$$

For zero initial conditions, equation (3.10) can also be written in matrix form for a sequence of l consecutive time steps as:

$$\mathbf{Y}_{m \times l} = \mathbf{M}_{m \times r l} \mathbf{U}_{r l \times l} \quad (3.11)$$

where

$$\mathbf{Y}_{m \times l} = [y(0), y(1), y(2), \dots, y(l-1)] \quad (3.12)$$

$$\mathbf{M}_{m \times r l} = [D, C\Gamma, C\Phi\Gamma, \dots, C\Phi^{l-2}\Gamma] \quad (3.13)$$

$$\mathbf{U}_{r l \times l} = \begin{bmatrix} u(0) & u(1) & u(2) & \dots & u(l-1) \\ & u(0) & u(1) & \dots & u(l-2) \\ & & \ddots & & \vdots \\ & & & u(0) & u(1) \\ & & & & u(0) \end{bmatrix} \quad (3.14)$$

the matrix \mathbf{Y} is a matrix whose columns are the output vectors for the l time steps, while the matrix \mathbf{U} contains the input vectors for different time steps arranged in an upper-triangular form. The matrix \mathbf{M} contains the Markov parameters, in form of its partitions. The *system* Markov parameters form a basis for the ERA.

3.2.2 Observer/Kalman filter IDentification

The aim of this paragraph is that of explaining how to extract the *system* Markov parameters when only input-output data are available. The first attempt would be that of solving equation 3.11. However, for a multiple-input multiple-output system the solution of that system is not unique, unless one truncates the Markov parameters sequence. In addition, deciding at which order truncate that sequence is problematic as well, especially for lightly damped structures. OKID algorithm solves these issues by introducing an observer to the state space equations, so that equations 3.6 and 3.7 become:

$$\left\{ \begin{array}{l} \mathbf{x}(\mathbf{k} + 1) = \mathbf{\Phi} \mathbf{x}(\mathbf{k}) + \mathbf{\Gamma} \mathbf{u}(\mathbf{k}) + \mathbf{R} \mathbf{y}(\mathbf{k}) - \mathbf{R} \mathbf{y}(\mathbf{k}) \\ \quad = (\mathbf{\Phi} + \mathbf{R}\mathbf{C})\mathbf{x}(\mathbf{k}) + (\mathbf{\Gamma} + \mathbf{R}\mathbf{D})\mathbf{u}(\mathbf{k}) - \mathbf{R}\mathbf{y}(\mathbf{k}) \\ \quad = \hat{\mathbf{\Phi}}\mathbf{x}(\mathbf{k}) + \hat{\mathbf{\Gamma}}\mathbf{v}(\mathbf{k}) \end{array} \right. \quad (3.15)$$

$$\mathbf{y}(\mathbf{k}) = \mathbf{C} \mathbf{x}(\mathbf{k}) + \mathbf{D} \mathbf{u}(\mathbf{k}) \quad (3.16)$$

where:

$$\begin{aligned} \hat{\mathbf{\Phi}} &= (\mathbf{\Phi} + \mathbf{R}\mathbf{C}) \\ \hat{\mathbf{\Gamma}} &= [(\mathbf{\Gamma} + \mathbf{R}\mathbf{D}) \quad -\mathbf{R}] \\ \mathbf{v}(\mathbf{k}) &= \begin{bmatrix} \mathbf{u}(\mathbf{k})^T & \mathbf{y}(\mathbf{k})^T \end{bmatrix}^T \end{aligned} \quad (3.17)$$

The new matrix \mathbf{R} is chosen in order to make the system of equations 3.15 and 3.16 as stable as possible. The gained system can be considered as an observer system, therefore its Markov parameters are called *observer* Markov parameters. By choosing \mathbf{R} such that $\hat{\mathbf{\Phi}}$ is asymptotically stable, one can obtain the result $\mathbf{C} \hat{\mathbf{\Phi}}^h \hat{\mathbf{\Gamma}} \approx 0$ for $h > p$, and the input/output relation can be written as:

$$\mathbf{Y}_{m \times 1} = \hat{\mathbf{M}}_{m \times [(r+m)p+r]} \mathbf{V}_{[(r+m)p+r] \times 1} \quad (3.18)$$

The observer Markov parameters are the block partitions of the matrix $\hat{\mathbf{M}}$, and they are obtained by finding the least-squares solution of Equation 3.18 as:

$$\hat{\mathbf{M}} = \mathbf{Y} \mathbf{V}^\dagger \quad (3.19)$$

with $()^\dagger$ denoting the pseudo-inverse of a matrix. It should be noted that when both \mathbf{Y} and \mathbf{V} are polluted with noise, the least square solutions might be problematic. Moreover, since the Markov parameters of the real system are retrieved from the identified *observer* Markov parameters, any bias introduced in the initial least-squares solution might propagate and become more pronounced in the Markov parameters of the real system, leading possibly to loss of accuracy in the final identified model. Having identified the *observer* Markov parameters, the *system* Markov parameters can be retrieved using the recursive formula:

$$\mathbf{M}_k = \hat{\mathbf{M}}_k^{(1)} + \sum_{i=0}^{k-1} \hat{\mathbf{M}}_i^{(2)} \mathbf{M}_{k-i-1} + \hat{\mathbf{M}}_k^{(2)} \mathbf{D} \quad (3.20)$$

Once the *system* Markov parameters have been identified, they can be used in the ERA formulation for the identification of the dynamic structural characteristics.

3.2.3 Eigensystem Realization Algorithm

The objective now is solving the so called minimal realization problem, i.e. finding a set of minimum order discrete time matrices Φ, Γ, C, D , from the system Markov parameters identified previously.

Let us consider that r impulse tests have been performed on a system with m outputs. Let us denote with $\mathbf{y}^j(k)$ a new vector, of dimension m , that represents the response of the system at time $k\Delta T$ to the unit impulse input \mathbf{u}_j at time zero. In this way, we can package the data as:

$$\mathbf{Y}(k) = [\mathbf{y}^1 \quad \mathbf{y}^2 \quad \dots \quad \mathbf{y}^r] \quad (3.21)$$

For definition given in the first paragraph of this chapter, the vector $\mathbf{Y}(k)$ represents the system Markov parameters at time $k \Delta t$. The evaluation of the matrix D is then very simple, since it is apparent that:

$$\mathbf{D} = \mathbf{Y}(0) \quad (3.22)$$

Having identified the \mathbf{D} matrix, we now look for \mathbf{C}, Φ, Γ . ERA solves the problem by means of the singular value decomposition of the Hankel matrix, an $ms \times rs$ matrix constructed by means of the system Markov parameters just identified:

$$\mathbf{H}^s(k-1) = \begin{bmatrix} \mathbf{Y}(k) & \mathbf{Y}(k+1) & \dots & \mathbf{Y}(k+s-1) \\ & \mathbf{Y}(k+2) & \dots & \mathbf{Y}(k+s) \\ \text{symm} & & \ddots & \vdots \\ & & & \mathbf{Y}[k+2(s-1)] \end{bmatrix} \quad (3.23)$$

where s is an integer that determines the size of such a matrix. The Hankel matrix is a block symmetric matrix: denoting with $\tilde{\mathbf{O}}$ the $ms \times n$ the observability matrix and with $\tilde{\mathbf{C}}$ the $n \times rs$ controllability matrix, the Hankel matrix can be written as:

$$\mathbf{H}(i) = \tilde{\mathbf{O}} \Phi^i \tilde{\mathbf{C}} \quad (3.24)$$

where:

$$\tilde{\mathbf{O}} = \begin{bmatrix} \mathbf{C}^T & (\mathbf{C}\Phi)^T & (\mathbf{C}\Phi^2)^T & \dots & (\mathbf{C}\Phi^{s-1})^T \end{bmatrix}^T \quad (3.25)$$

$$\tilde{\mathbf{C}} = \begin{bmatrix} \Gamma & \Phi\Gamma & \Phi^2\Gamma & \dots & \Phi^{s-1}\Gamma \end{bmatrix}^T \quad (3.26)$$

$$\mathbf{H}(i) = \begin{bmatrix} \mathbf{C}\Phi^i\Gamma & \mathbf{C}\Phi^{i+1}\Gamma & \dots & \mathbf{C}\Phi^{i+s-1}\Gamma \\ & \mathbf{C}\Phi^{i+2}\Gamma & \dots & \mathbf{C}\Phi^{i+s}\Gamma \\ \text{symm} & & \ddots & \vdots \\ & & & \mathbf{C}\Phi^{i+2(s-1)}\Gamma \end{bmatrix} \quad (3.27)$$

The rank of the Hankel matrix is equal to the dimension of the minimum realization. The singular value decomposition of the Hankel matrix can then be written as:

$$\mathbf{H}(0) = \tilde{\mathbf{O}} \tilde{\mathbf{C}} = \mathbf{U}\mathbf{\Sigma}\mathbf{\Sigma}^T = \begin{bmatrix} \mathbf{U}_1 & \mathbf{U}_2 \end{bmatrix} \begin{bmatrix} \mathbf{S} & \mathbf{0} \\ \mathbf{0} & \mathbf{0} \end{bmatrix} \begin{bmatrix} \mathbf{V}_1^T \\ \mathbf{V}_2^T \end{bmatrix} = \mathbf{U}_1 \mathbf{S} \mathbf{V}_1^T \quad (3.28)$$

where the matrices \mathbf{U} , of $ms \times ms$ dimension, and \mathbf{V} , of $rs \times rs$ dimension, are unitary matrices, while the diagonal matrix \mathbf{S} encloses exactly n singular values for a system deprived of noise. It is then clear the statement of the ERA theorem:

$$\begin{aligned}
\tilde{\mathbf{O}} &= \mathbf{U}_1 \mathbf{S}^{1/2} \\
\tilde{\mathbf{C}} &= \mathbf{S}^{1/2} \mathbf{V}_1^T \\
\mathbf{\Phi} &= \tilde{\mathbf{O}}^\dagger \mathbf{H}(1) \tilde{\mathbf{C}}^\dagger
\end{aligned} \tag{3.29}$$

where $()^\dagger$ denotes the pseudo-inverse of a matrix. The input matrix $\mathbf{\Gamma}$ can be easily determined, as it is the first block partition of $\tilde{\mathbf{C}}$, and, similarly, the output matrix \mathbf{C} is the first block partition of $\tilde{\mathbf{O}}$.

3.2.4 Refining the Identified State-Space Model

The method described in the preceding sections performs quite well for finite-dimensional system when:

- 1) the available input/output data time histories are sufficiently long;
- 2) the noise is white, of zero mean and small.

When these conditions are not satisfied, the results could be not acceptable. Moreover, measurement noise is not the only issue one has to consider. Other problems such as non-stationary and insufficient excitations, and truncation errors introduced in the ERA stage, also contribute to the errors. Therefore, it is apparent that the basic OKID/ERA methodology needs an optimization. The technique used to obtain the results of the present work is the output error minimization approach, a non-linear least squares problem based on the minimization of the following function:

$$\mathcal{F}(\boldsymbol{\rho}) = \frac{1}{2} \sum_{i=k}^L [\mathbf{y}(k, \boldsymbol{\rho}) - \bar{\mathbf{y}}(k)]^T [\mathbf{y}(k, \boldsymbol{\rho}) - \bar{\mathbf{y}}(k)] \tag{3.30}$$

where $\boldsymbol{\rho}$ contains the parameters to be optimized, the vector $\mathbf{y}(k, \boldsymbol{\rho})$ is the output vector obtained from the state-space realization at time-step k , while $\bar{\mathbf{y}}(k)$ is the

measured output at time step k , with the index k varying from an initial time t_i to a final time t_f .

In particular, the method used for the optimization of the state-space realization is the ‘Sequential Quadratic Programming’ (SQP) technique, belonging to the quasi-Newton-type methods family; such methods guarantee fast convergence provided that the initial conditions are sufficiently close to the desirable solutions. This issue is solved for the problem analyzed, since the solutions provided by the methodologies discussed previously will serve as reasonably good estimates to initiate the search.

The Taylor series expansion truncated at the second order of equation 3.30 is:

$$\mathcal{F}(\boldsymbol{\rho} + \Delta\boldsymbol{\rho}) \approx \mathcal{F}(\boldsymbol{\rho}) + \mathcal{G}(\boldsymbol{\rho})\Delta\boldsymbol{\rho} + \frac{1}{2}\Delta\boldsymbol{\rho}^T \mathcal{H}(\boldsymbol{\rho})\Delta\boldsymbol{\rho} \quad (3.31)$$

where, for i referring the i^{th} output, the following terms have been considered :

$$\begin{aligned} \mathcal{G}(\boldsymbol{\rho}) &= \frac{\partial \mathcal{F}(\boldsymbol{\rho})}{\partial \boldsymbol{\rho}} = \sum_{i=k}^L [\mathbf{y}(k, \boldsymbol{\rho}) - \bar{\mathbf{y}}(k)]^T \left[\frac{\partial \mathbf{y}(k, \boldsymbol{\rho})}{\partial \boldsymbol{\rho}} \right] \\ \mathcal{H}(\boldsymbol{\rho}) &= \frac{\partial^2 \mathcal{F}(\boldsymbol{\rho})}{\partial \boldsymbol{\rho}^2} = \sum_{k=t_i}^{t_f} \left[\frac{\partial \mathbf{y}(k, \boldsymbol{\rho})}{\partial \boldsymbol{\rho}} \right]^T \left[\frac{\partial \mathbf{y}(k, \boldsymbol{\rho})}{\partial \boldsymbol{\rho}} \right] + \boldsymbol{\Pi}(\boldsymbol{\rho}) \end{aligned} \quad (3.32)$$

$$\boldsymbol{\Pi}(\boldsymbol{\rho}) = \sum_{k=t_i}^{t_f} \left[\sum_{i=1}^m [y_i(k, \boldsymbol{\rho}) - \bar{y}_i(k)] \frac{\partial^2 y_i(k, \boldsymbol{\rho})}{\partial \boldsymbol{\rho}^2} \right] \quad (3.33)$$

It is necessary to have the Hessian at worst positive semi-definite, therefore, the contribution of only the positive eigenvalues of $\boldsymbol{\Pi}(\boldsymbol{\rho})$ to $\mathcal{H}(\boldsymbol{\rho})$ will be considered.

The SQP technique is an iterative method: in each iteration the parameters are updated via the following formula:

$$\boldsymbol{\rho}_{j+1} = \boldsymbol{\rho}_j - \mathbf{d}_j [\mathcal{H}^*(\boldsymbol{\rho}_j)]^{-1} \mathcal{G}^T(\boldsymbol{\rho}_j) \quad (3.34)$$

where j denotes the j^{th} iteration, d_j is the step size, and $\mathcal{H}^*(\boldsymbol{\rho}_j)$ and $\mathcal{G}^T(\boldsymbol{\rho}_j)$ are obtained by evaluating Equations (3.32) using the parameters $\boldsymbol{\rho}_j$. The size of the iteration step size has to be calibrated in order to avoid any instability, and to have a decrease of the objective function $\mathcal{F}(\boldsymbol{\rho})$.

An important issue is the choice of the parameters to be optimized. It can be observed that the observer Markov parameters play a crucial role in the identification of the state-space realization, and then, indirectly, to the determination of the dynamics of the system, that are the proper objectives of the whole identification. Of course, one could decide to optimize all of the variables in the discrete time state space matrices, and in that case the number of elements of $\boldsymbol{\rho}$ would be $n^2 + n \times r + m \times n$. This approach would give reliable results, but the computational effort requested will be very high for complex structures. An alternative is represented by the transformation of the state space discrete time system realization to a set of modal coordinates. Since the eigenvalues of the identified first-order system appear in complex conjugate pairs as $\tilde{\sigma}_i \pm j\tilde{\omega}_i$, with j representing the imaginary unit, the discrete time equations can be transformed into a new basis in which they can be written as $n/2$ uncoupled equations (one for each structural vibration mode) as

$$\begin{aligned}\mathbf{z}(k+1) &= \boldsymbol{\Phi}_B \mathbf{z}(k) + \boldsymbol{\Gamma}_B \mathbf{u}(k) \\ \mathbf{y}(k) &= \mathbf{C}_B \mathbf{z}(k) + \mathbf{D} \mathbf{u}(k)\end{aligned}\tag{3.35}$$

where:

$$\boldsymbol{\Phi}_B = \begin{bmatrix} \tilde{\sigma}_1 & \tilde{\omega}_1 & 0 & 0 & \cdots & 0 & 0 \\ -\tilde{\omega}_1 & \tilde{\sigma}_1 & 0 & 0 & \cdots & 0 & 0 \\ 0 & 0 & \tilde{\sigma}_2 & \tilde{\omega}_2 & \cdots & 0 & 0 \\ 0 & 0 & -\tilde{\omega}_2 & \tilde{\sigma}_2 & \cdots & 0 & 0 \\ \vdots & \vdots & \vdots & \vdots & \vdots & \vdots & \vdots \\ 0 & 0 & 0 & 0 & \cdots & \tilde{\sigma}_{n/2} & \tilde{\omega}_{n/2} \\ 0 & 0 & 0 & 0 & \cdots & -\tilde{\omega}_{n/2} & \tilde{\sigma}_{n/2} \end{bmatrix}\tag{3.36a}$$

$$\mathbf{\Gamma}_B = \begin{bmatrix} \gamma_{11,1} & \cdots & \gamma_{1r,1} \\ \gamma_{21,1} & \cdots & \gamma_{2r,1} \\ \vdots & \vdots & \vdots \\ \gamma_{11,n/2} & \cdots & \gamma_{1r,n/2} \\ \gamma_{21,n/2} & \cdots & \gamma_{2r,n/2} \end{bmatrix}, \mathbf{D} = \begin{bmatrix} \mathbf{d}_{11} & \cdots & \mathbf{d}_{1r} \\ \vdots & \vdots & \vdots \\ \mathbf{d}_{m1} & \cdots & \mathbf{d}_{mr} \end{bmatrix} \quad (3.36b)$$

$$\mathbf{C}_B = \begin{bmatrix} \mathbf{c}_{11,1} & \mathbf{c}_{12,1} & \cdots & \mathbf{c}_{11,n/2} & \mathbf{c}_{12,n/2} \\ \vdots & \vdots & \vdots & \vdots & \vdots \\ \mathbf{c}_{m1,1} & \mathbf{c}_{m2,1} & \cdots & \mathbf{c}_{m1,n/2} & \mathbf{c}_{m2,n/2} \end{bmatrix} \quad (3.36c)$$

and the state vector can now be expressed as $\mathbf{z}(k) = [\mathbf{z}_{,1}^T(k) \cdots \mathbf{z}_{,n/2}^T(k)]^T$. With this formulation, the total number of parameters is reduced to $n + n \times r + m \times n + m \times r$. The discrete time equations for each mode in the state vector can now be written separately as:

$$\begin{cases} \dot{\mathbf{z}}(t) = \mathbf{\Lambda} \mathbf{z}(t) + \boldsymbol{\phi}^{-1} \mathbf{B} \mathbf{u}(t) \\ \mathbf{y}(t) = \mathbf{C} \boldsymbol{\phi} \mathbf{z}(t) + \mathbf{D} \mathbf{u}(t) \end{cases} \quad (3.37)$$

where in $\mathbf{\Lambda}$ are embedded the continuous time eigenvalues of the identified state space model, while $\boldsymbol{\phi}$, of order $n \times n$, is the matrix of the eigenvectors corresponding to the eigenvalues of $\mathbf{\Lambda}$.

3.2.5 Recovering the dynamics of the system from the realized state-space model

Finally, it is possible to retrieve the dynamics of the system using the optimized state-space realization 3.37. Let recall the well-known eigenvalue problem:

$$\left(\lambda_i^2 \mathbf{M} + \lambda_i \mathbf{L} + \mathbf{K}\right) \psi_i = 0 \quad (3.38)$$

where λ_i represents the i^{th} complex eigenvalue $\lambda_i = \sigma_i \pm j\omega_i$, for $i = 1, 2, \dots, N$. The eigenvectors are then scaled such that:

$$\begin{bmatrix} \psi & \psi \Lambda \end{bmatrix} \begin{bmatrix} \mathbf{L} & \mathbf{M} \\ \mathbf{M} & \mathbf{0} \end{bmatrix} \begin{bmatrix} \psi \\ \psi \Lambda \end{bmatrix} = \mathbf{I} \quad (3.39)$$

$$\begin{bmatrix} \psi & \psi \Lambda \end{bmatrix} \begin{bmatrix} \mathbf{K} & \mathbf{0} \\ \mathbf{0} & -\mathbf{M} \end{bmatrix} \begin{bmatrix} \psi \\ \psi \Lambda \end{bmatrix} = -\Lambda \quad (3.40)$$

where Λ is the matrix containing the complex eigenvalues, while ψ the one of the corresponding eigenvectors. By using the assumptions presented in equations 3.39 and 3.40, the system of equations 3.4 and 3.5 becomes:

$$\begin{cases} \dot{\xi}(t) = \Lambda \xi(t) + \psi^T \mathbf{B} \mathbf{u}(t) \\ \mathbf{y}(t) = \mathbf{C}_p \psi \xi(t) \end{cases} \quad (3.41)$$

that represents the first order modal form of the equation of motion 3.1. Formulation given by equations 3.41 is a different model of the same system represented by equations 3.37: there must be a transformation matrix T that relates the two representations:

$$\begin{aligned}
T^{-1} \Lambda T &= \Lambda \\
T^{-1} \phi^{-1} B &= \Psi^T B \\
C \phi^{-1} T &= C_p \Psi
\end{aligned} \tag{3.42}$$

Once the eigenvectors matrix is determined, the evaluation of the mass, damping and stiffness matrices are retrievable from equations 3.39 and 3.40:

$$\begin{aligned}
\mathbf{M} &= (\Psi \Lambda \Psi^T)^{-1} \\
\mathbf{L} &= -\mathbf{M} \Psi \Lambda^2 \Psi^T \mathbf{M} \\
\mathbf{K} &= -(\Psi \Lambda^{-1} \Psi^T)^{-1}
\end{aligned} \tag{3.43}$$

and undamped natural frequencies and damping ratios can be finally calculated:

$$\begin{aligned}
\Omega_i &= \sqrt{\sigma_i^2 + \omega_i^2} \\
f_i &= \frac{\Omega_i}{2\pi} \\
\zeta_i &= -\cos \left[\arctan \left(\frac{\omega_i}{\sigma_i} \right) \right]
\end{aligned} \tag{3.44}$$

3.3 Numerical Results

The Painter Street Overcrossing was instrumented in 1977 by the California Division of Mines and Geology as part of the California Strong Motion Instrumentation Program. The bridge site was instrumented with twenty strong accelerometers capturing various motions on and off the bridge as shown in figure 3.1. Channels 12, 13 and 14 measure free field motions (longitudinal, vertical and transverse to the bridge axis respectively) near the bridge site. At the east end of the bridge, triaxial sets of sensors are located both on the embankment (15, 16, 17) and on the end of the bridge deck (9, 10, 11) so that relative motion between the embankment and the deck could be assessed. A triaxial set of sensors (1, 2, 3) is also located at the base of the bent's north column to aid in measuring soil-structure interaction. A transverse sensor (7) is located at the base of the deck adjacent to the center bent and vertical sensors are located at midspan of the east (8) and west (6) spans on the north side of the deck. An important issue is the absence of accelerometers at the south edge of the bridge: torsion of the bridge cannot be directly assessed.

Since the overpass was instrumented, it has been shaken by six earthquake. Of these only three set of data are available at Center of Engineering of Strong Motion Data (CESMD). Therefore, the results herein proposed are obtained by using records of Trinidad Offshore, Rio Dell earthquake and the first event of Petrolia earthquake. Table 3.1 presents the characteristics of the six earthquakes that interested the structure since 1977.

In figure 3.1 are circled in different colors the sensors whose records are used as input and output data. In particular, the sensors circled in red offer input data, while the ones circled in blue give the output data.

Event	Date	Mag. [ML]	Epic. Dist. [km]	Maximum Ground Acceleration			Maximum Bridge Acceleration		
				<i>C12</i>	<i>C13</i>	<i>C14</i>	<i>C6</i>	<i>C7</i>	<i>C8</i>
Trinidad	11/08/80	6.9	72	0.15g	0.03g	0.06g	0.34g	-	0.25g
Rio Dell	12/16/82	4.4	15	-	-	-	0.39g	0.43g	0.59g
Cape Medoncino	08/24/83	5.5	61	-	-	-	0.27g	0.22g	0.16g
Petrolia (#1)	11/21/86	5.1	32	0.46g	0.08g	0.16g	0.24g	0.26g	0.33g
Petrolia (#2)	11/21/86	5.1	26	0.15g	0.02g	0.12g	0.21g	0.36g	0.29g
Cape Medoncino	07/31/87	5.5	28	0.15g	0.04g	0.09g	-	0.34g	0.27g

Table 3.1: Characteristics of the six seismic events recorded by instrumentation located on Painter Street Overcrossing

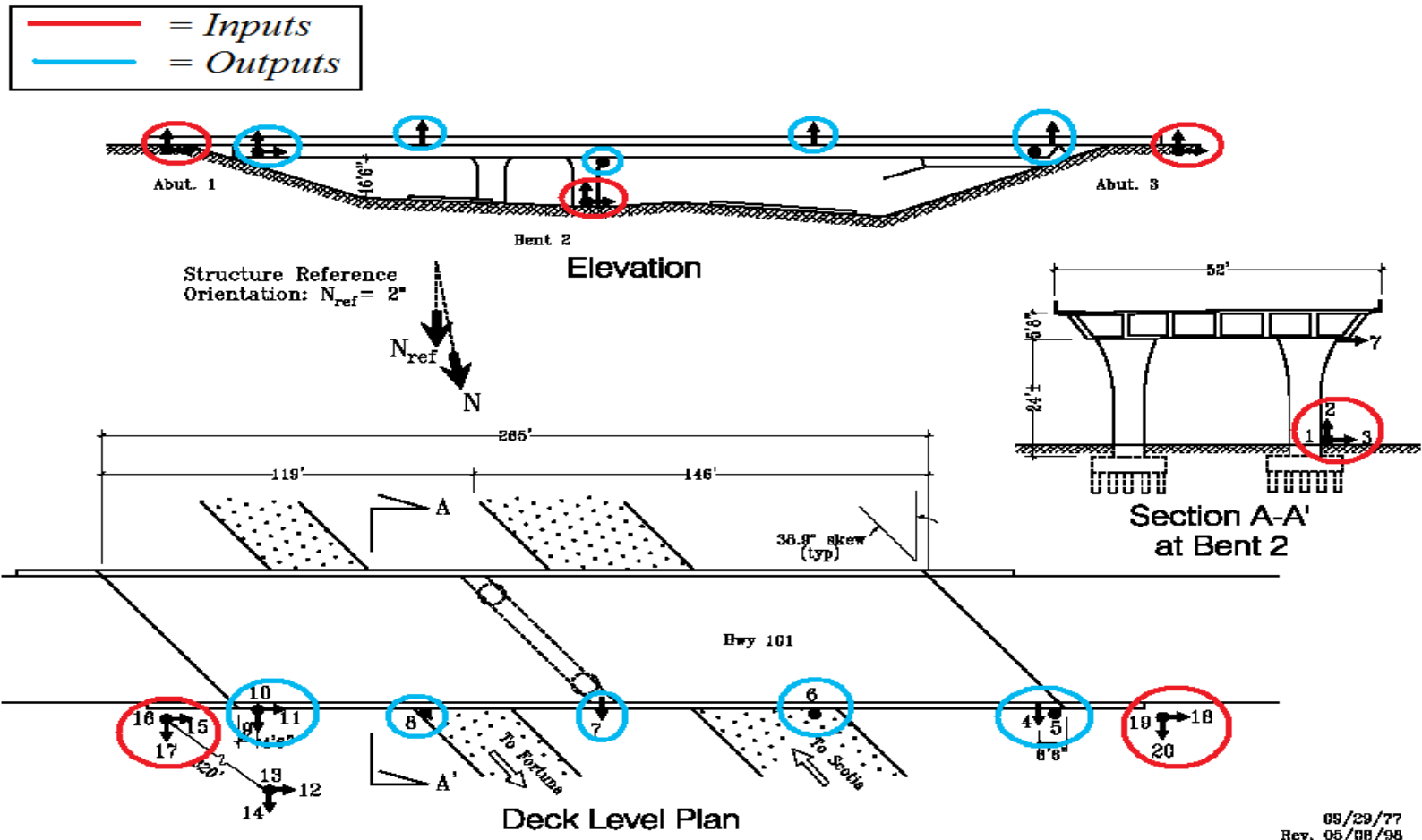


Fig. 3.1: Input and Output Sensors Location

3.3.1 Trinidad Offshore (November 8, 1980)

For this set of data records from channels 1, 2, 3, 15, 16, 17, 18, 19, 20 are used as inputs, while the ones from channels 5, 6, 8, 9, 10, 11 as outputs. The total number of data points for each record is 1104, at a sampling interval of 0.02 seconds.

As discussed, the choice of the number of *observer* Markov parameters affects the solution of the observer system, and then it is critical in the determination of the characteristics of the structure. It is important to choose the value of the number of *observer* Markov parameters (denoted as 'p' from now on) as higher as possible. The upper bound for p is given by the following demonstrable formula:

$$p_{\max} = \frac{l - r}{m + r} = 73 \quad (3.45)$$

where

r = number of inputs (9)

m = number of outputs (6)

l = number of data points (1104)

The number of *system* Markov parameters is usually set from two to four times the one of p. In the present work 'nmarkov' (number of system Markov parameters) equals four times p.

With the values of 'p' and 'nmarkov' defined, it is now possible to run the OKID/ERA via MATLAB. The program needs the asks for the definition of other parameters. The first thing one has to choose is the number of singular values of the $\mathbf{V}^*\mathbf{V}^T$ matrix to keep to compute *observer* Markov Parameters. Usually, it is chosen the number of singular values just above the sharp drop, that in this case equals 1031. Nonetheless, after many trials, it has been observed that for this set of data the most stable results are

obtained by keeping 558 singular values, whose amount is one of the first to be not negligible (Figure B.1). The next step is to choose the number of singular values of the decomposed Hankel Matrix $\mathbf{H}(0)*\mathbf{H}(0)^T$ (Figure B.2). When output observations are not contaminated by noise, the dimension of the state matrix can be clearly indicated by singular values of $\mathbf{H}(0)*\mathbf{H}(0)^T$ and so the modal parameters for the system modes can be estimated just from a realized model. However, when output measurements are disturbed by noise, the Hankel matrix has full rank and this makes it difficult to assign a certain order to an identified system model only based on the singular values distribution. Even though it is true that having a higher order identified model helps in minimizing the error between the measured data and the reconstructed responses from the identified model, this error reduction could be due to noise modes that are now included to improve the fitting between the data sets. For this reason the extraction of modal parameters corresponding to structural modes is generally complemented by a Stabilization Diagram (SD). Such a diagram, which represents the identified frequencies as a function of the model order, highlights modes whose properties do not change significantly when varying the dimension of the state vector; such modes are considered as structural modes. In order to form the SD, an observability matrix is repeatedly formulated from equation 3.29 varying the dimension of the state, which provides different pairs of state and output matrices of corresponding orders. The properties of poles in a model of a certain order are compared with those of a two order larger model and stable and unstable modes are determined on the basis of the identified frequencies, damping ratios and mode shapes. A star in the diagram represents a value for which modal shape, frequency and damping are stable; an 'f' indicates that only modal frequency is stable, while a 'v' should give stable modal shape and frequency; finally, a 'd' informs that modal frequency and damping are stable (Figure 3.1).

Therefore, the following approach is developed: a very high order is chosen; then, from the observation of the stabilization diagram the first trial is run by choosing only the frequencies that appear to be stable, i.e only frequencies denoted with either ‘star’, or ‘v’, or ‘d’ in the stabilization diagram. In the following trial the modal frequencies either with too high (greater than 10%) or too low (less than 0.1%) damping ratio are neglected. The trials continue until the system reduces to only the modal frequencies characterized by reasonable damping ratios. The last observed modal frequencies are considered the ones that identify the system dynamics.

In next pages are presented the results obtained by choosing two values for the order of the system. The first bunch of results is obtained by choosing a value of 80, the second through a value of 118. The screens of the identified system before and after the optimization are presented in Appendix B. Moreover, for each trial it is calculated the relative error between the measured and optimized output time histories. Such an error is computed as follows:

$$e_{\text{relative}} = \frac{\|y_{\text{measured}} - y_{\text{optimized}}\|}{\|y_{\text{measured}}\|} \quad (3.46)$$

3.3.1.1 Discussion on the Results

The results herein presented are only the last of many trials performed in order to retrieve the best possible combination of the parameters defined previously. In Appendix B there are two examples of the numerical results, in the present paragraph is instead given a semi-qualitative comment to the approach used for choosing the best identified model and are shown the parameters that will be used for the following applications.

The error computed with the formula 3.46 is calculated first for the entire time histories, as shown in tables 3.2 and 3.3, for a model order of 80 and 118 respectively. Then, the time histories recorded by each channel are divided into three parts (the first from 0 to 7 seconds, the second from 7.02 to 17 seconds, and the third from 17.02 to 22.08 seconds), and the relative error is computed for each one of the three pieces. This allows to consider the contribute to the error of each portion, in particular, one should be interested in the contribute given by the second piece of the time histories, the one from 7.02 to 17 seconds, for which the acceleration amplitude is the maximum. These results are presented in tables 3.4 and 3.5. As can be observed, while the global error is lower for the system of order set equal to 80, the contribute to the error given by the second part of the time histories is lower if one considers the system performed with an order of 118.

Therefore, the second set of data leads to the modal parameters that better represent the structural characteristics of the Rio Dell Overpass. It is important to note that the determined dynamics give values close to the ones expected from the analysis of the frequency content, analyzed in the second chapter. Finally, figures 3.5 and 3.7 show the modal shapes corresponding to the identified modal frequencies although the modal shapes retrieved cannot display the torsional modes. For instance, it could be assumed that the third and fourth are torsional modes, but only a finite element model may give the validation of this assumption.

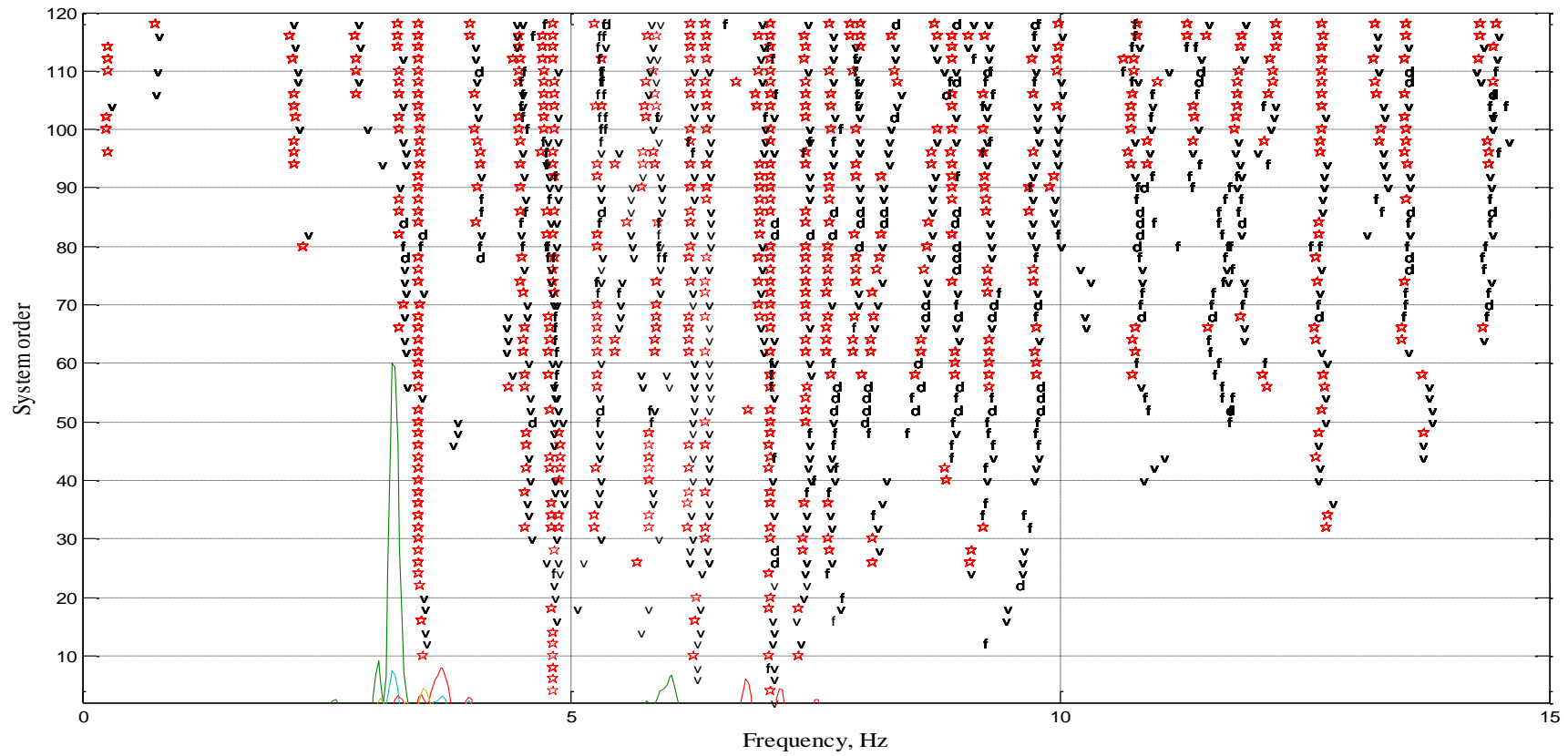


Fig. 3.2: Stabilization Diagram for a system realized with 73 Observer Markov Parameters and 558 Singular Values

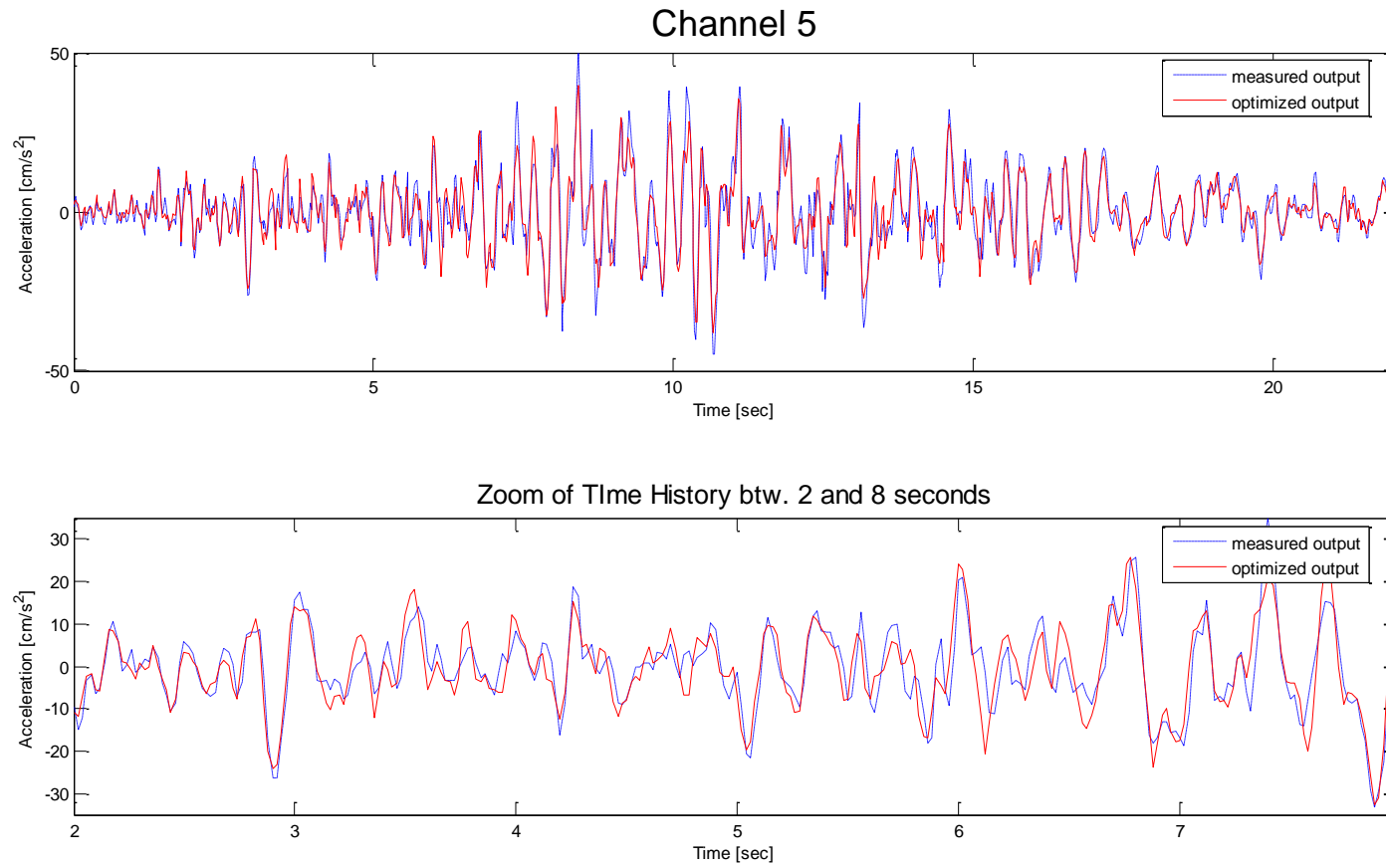


Figure 3.3a: Comparison between measured and optimized time history recorded by channel 5

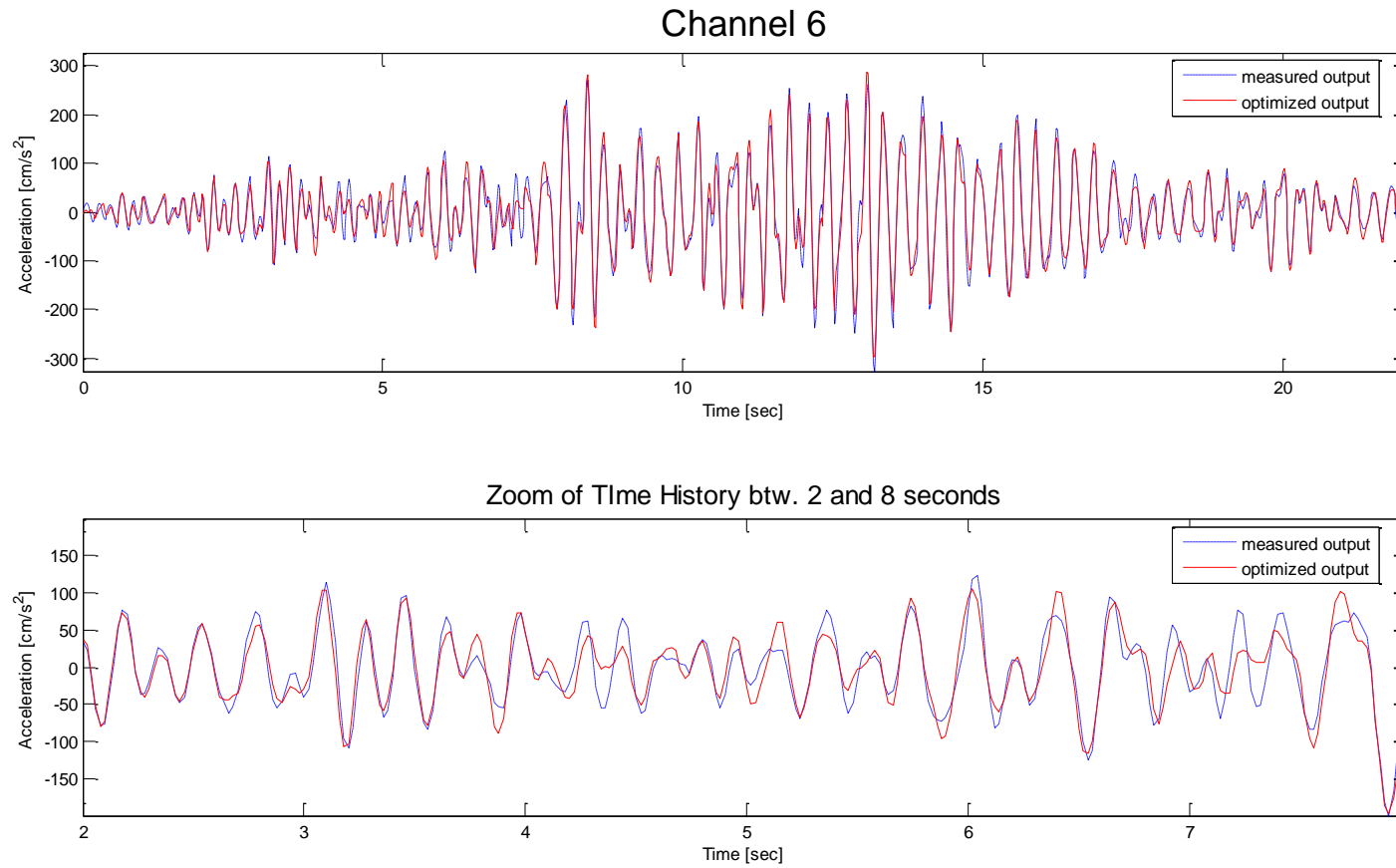


Figure 3.3b: Comparison between measured and optimized time history recorded by channel 6

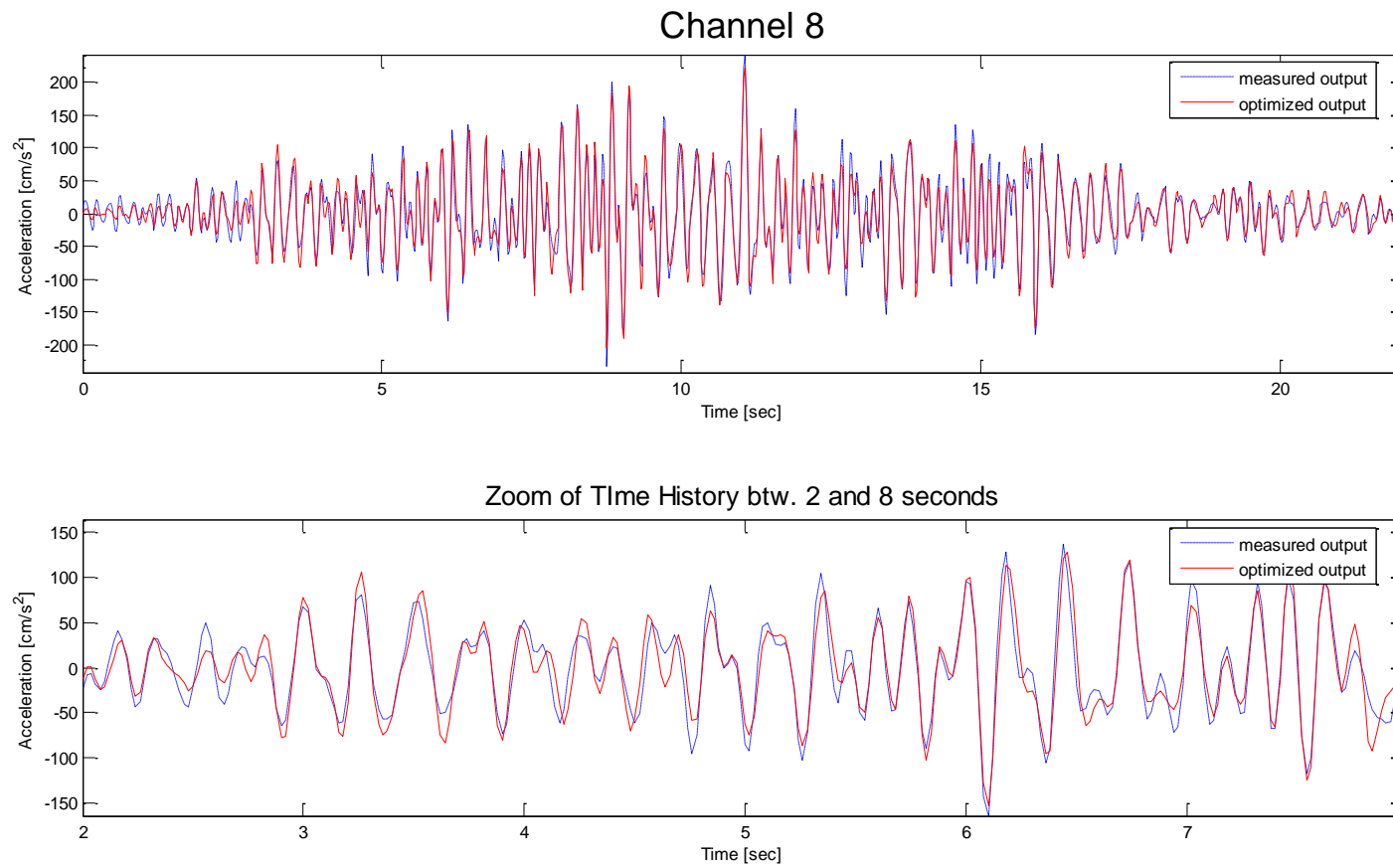


Figure 3.3c: Comparison between measured and optimized time history recorded by channel 8

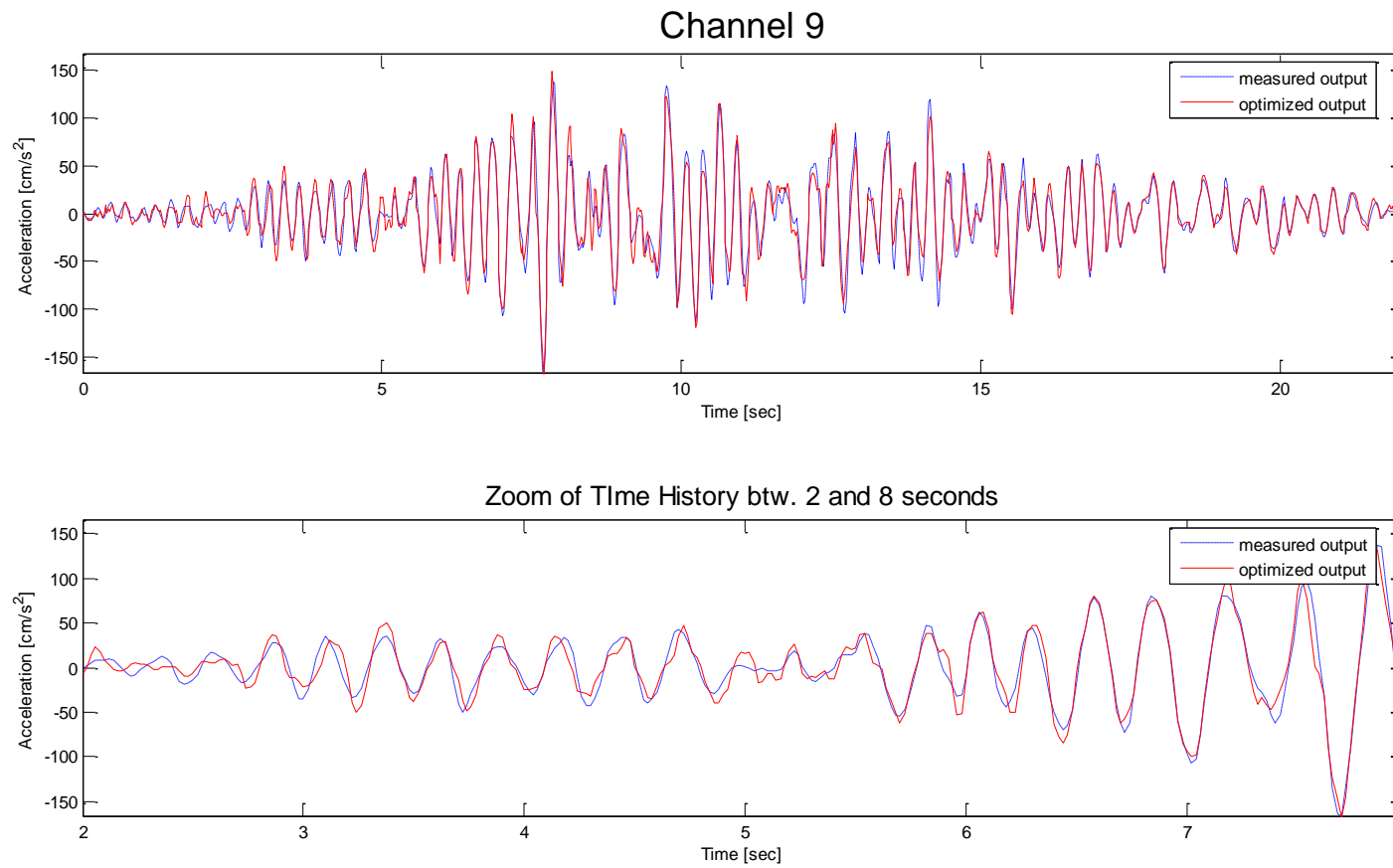


Figure 3.3d: Comparison between measured and optimized time history recorded by channel 9

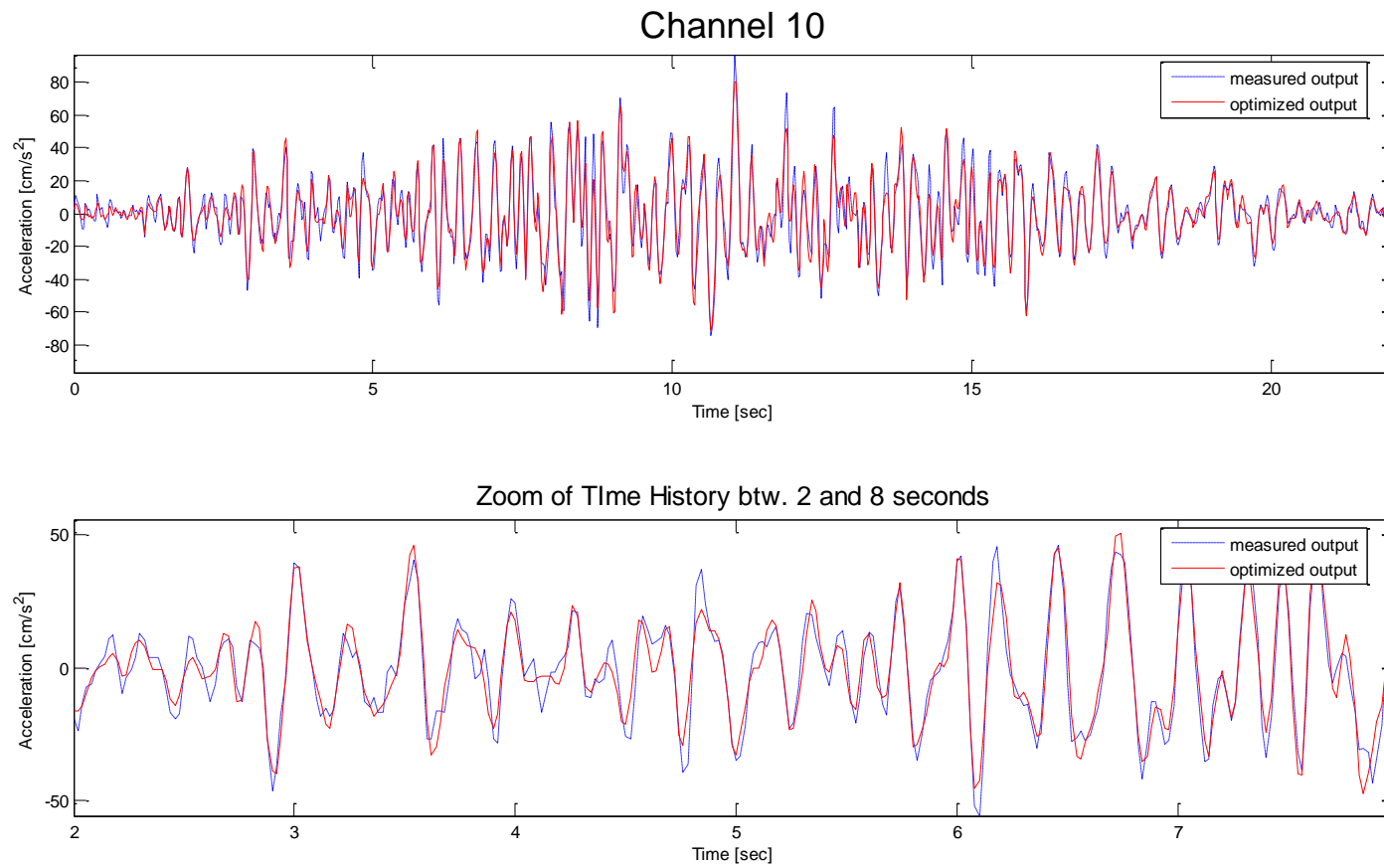


Figure 3.3e: Comparison between measured and optimized time history recorded by channel 10

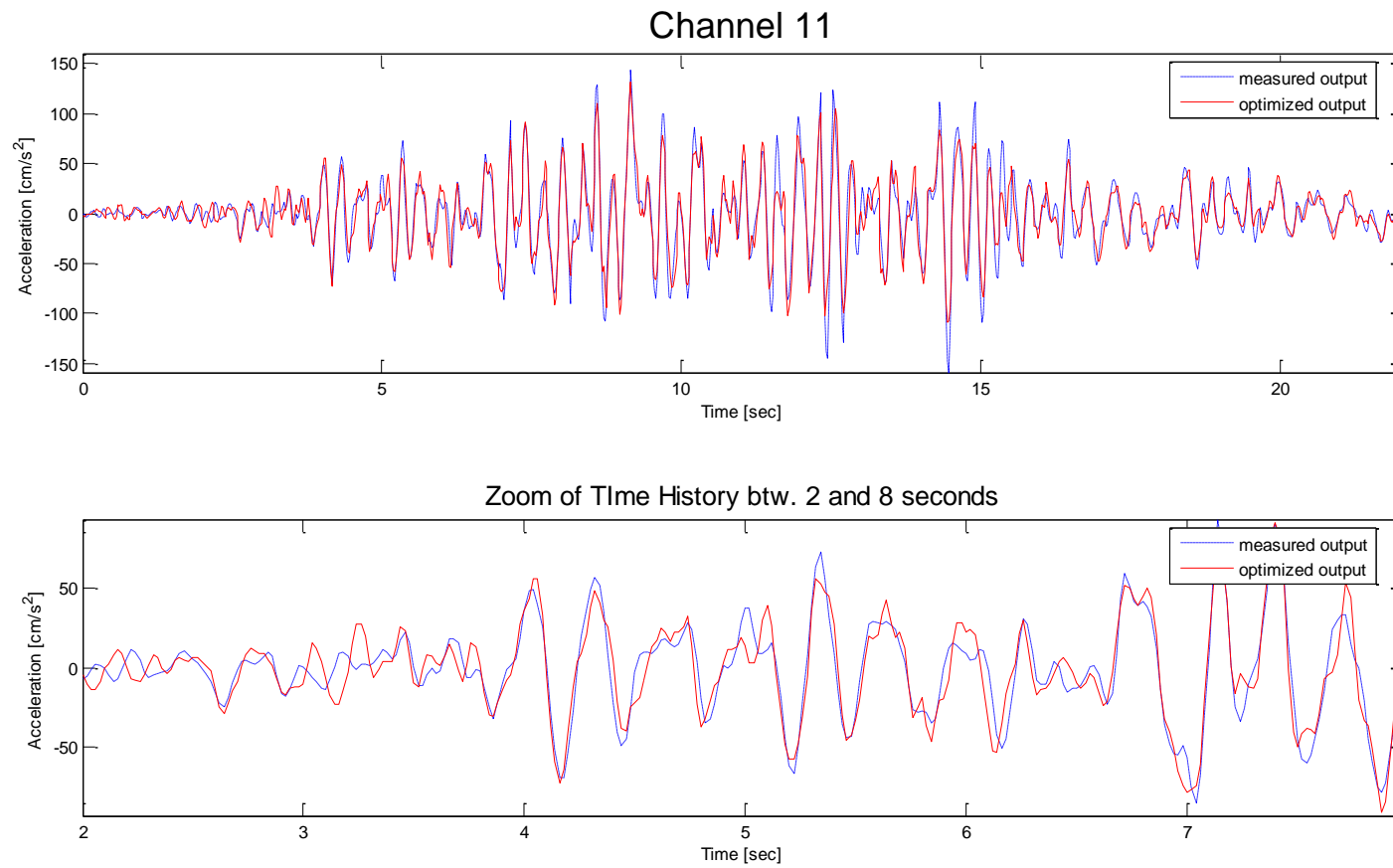


Figure 3.3f: Comparison between measured and optimized time history recorded by channel 11

Mode 1: 3.407 Hz

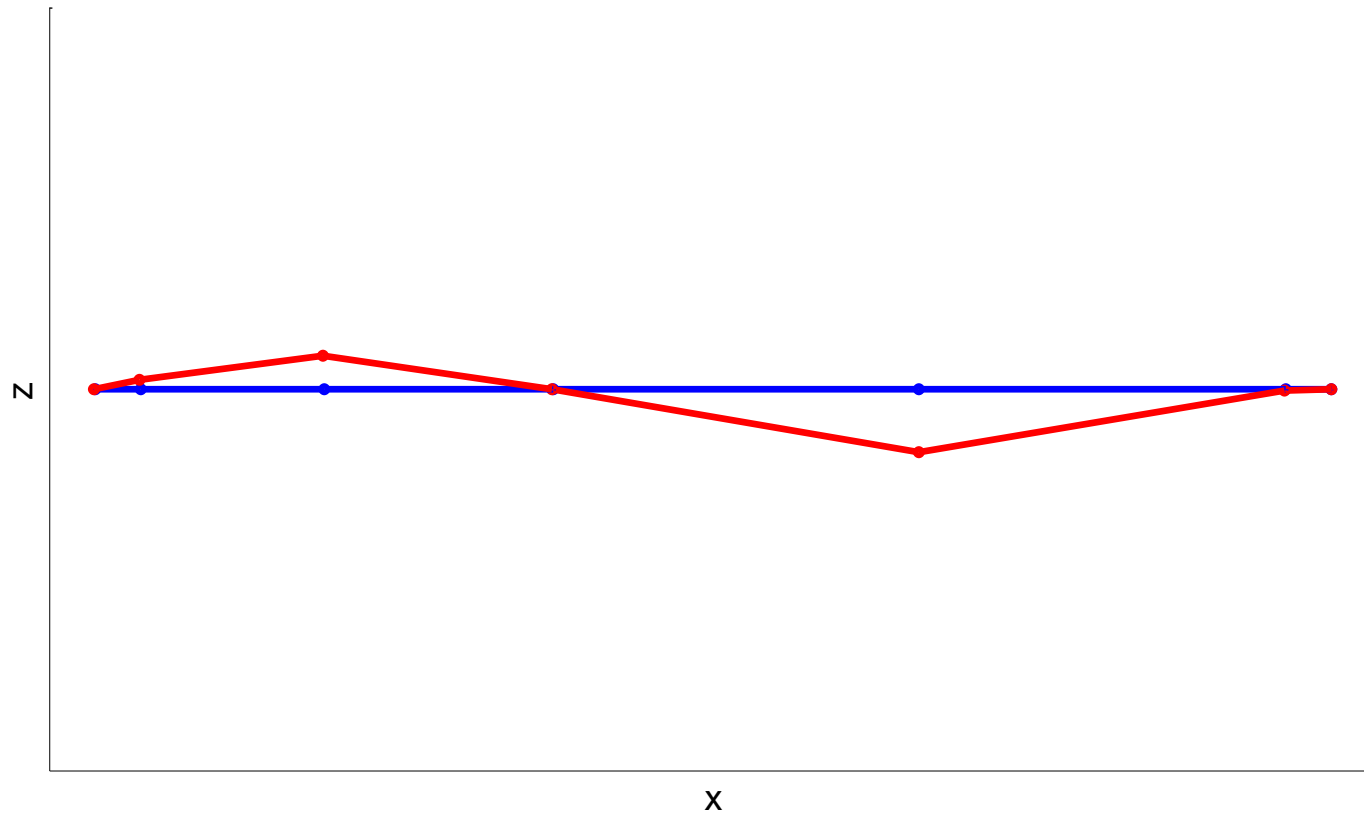


Figure 3.4a: First Identified Modal Shape

Mode 2: 4.757 Hz

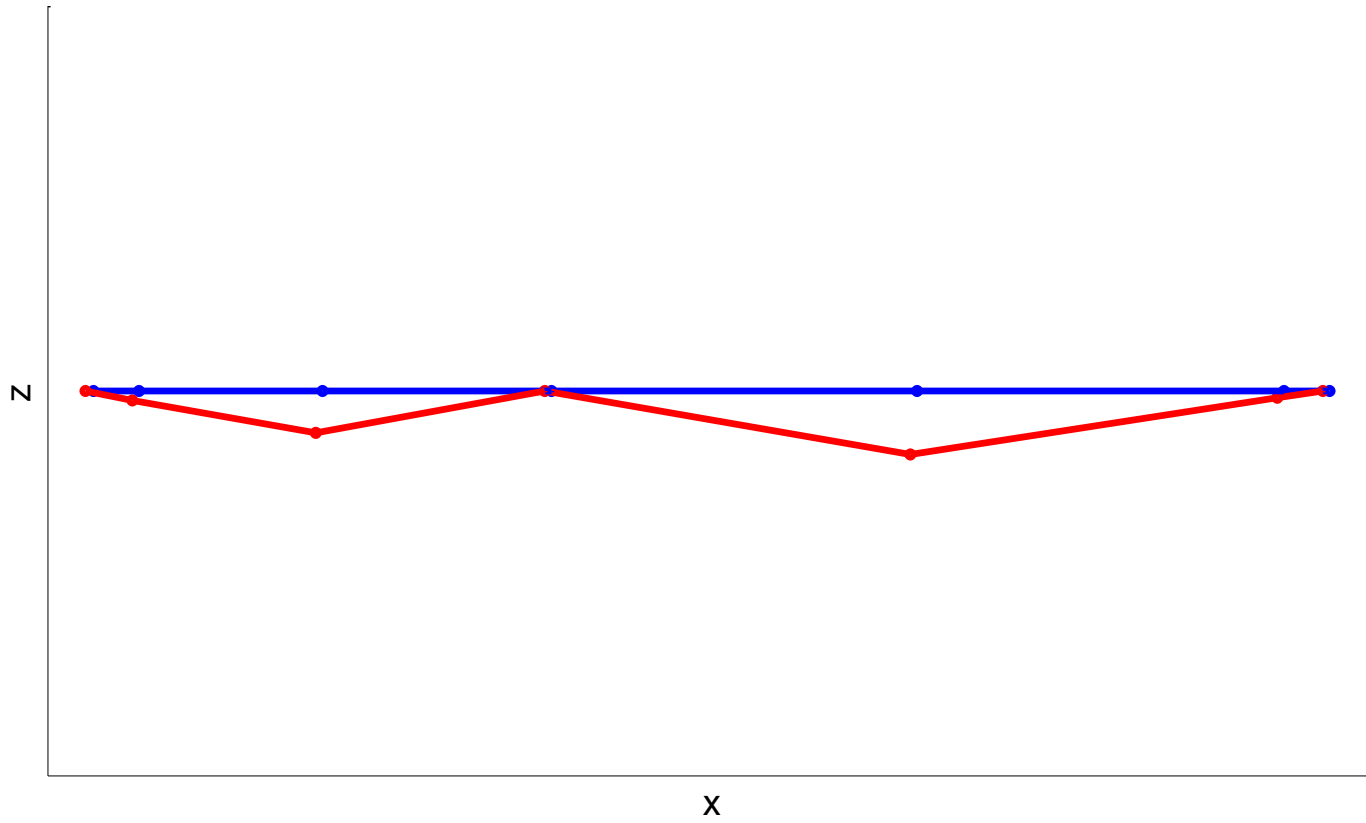


Figure 3.4b: Second Identified Modal Shape

Mode 3: 6.122 Hz

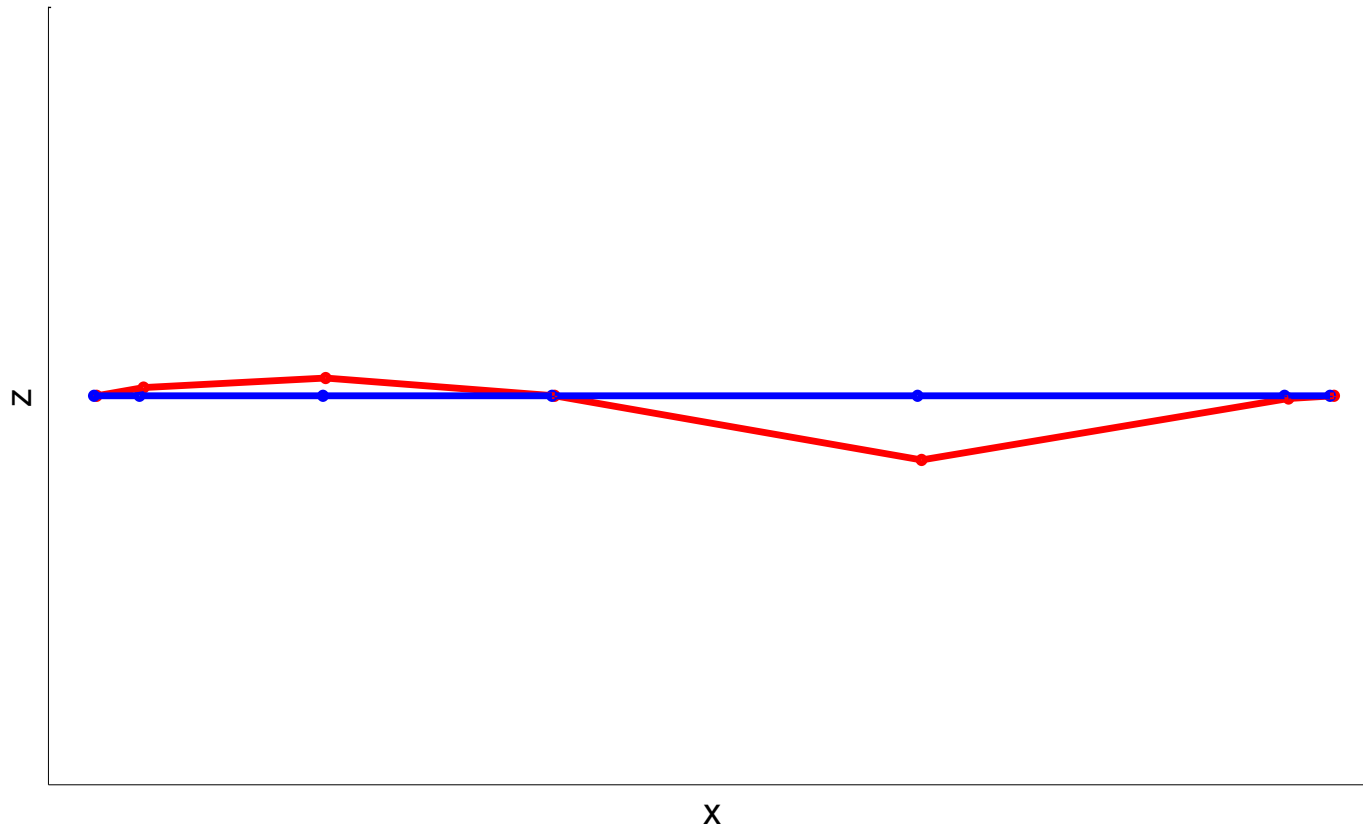


Figure 3.4c: Third Identified Modal Shape

Mode 4: 7.335 Hz

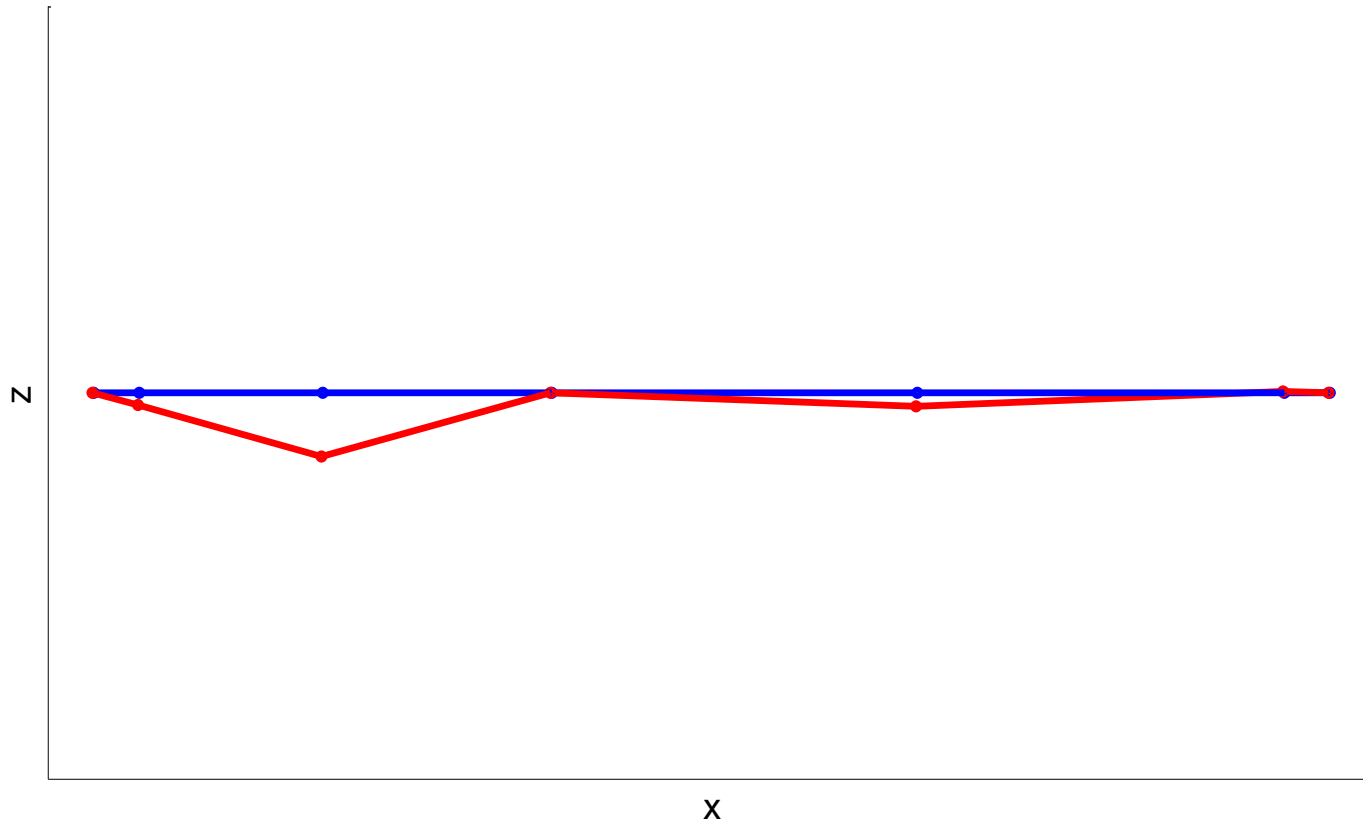


Figure 3.4c: Fourth Identified Modal Shape

<i>Trial</i>	Ch05	Ch06	Ch08	Ch09	Ch10	Ch11
1	0.47	0.38	0.35	0.26	0.33	0.30
2	0.39	0.18	0.26	0.22	0.25	0.24
3	0.30	0.13	0.18	0.17	0.22	0.18
4	0.50	0.42	0.38	0.27	0.35	0.32
5	0.43	0.17	0.29	0.25	0.28	0.29
6	0.39	0.17	0.27	0.22	0.27	0.24
7	0.38	0.15	0.26	0.20	0.25	0.23
8	0.37	0.15	0.26	0.19	0.26	0.20
9	0.43	0.24	0.36	0.33	0.31	0.30
10	0.41	0.22	0.29	0.23	0.30	0.30

Table 3.2: Error Computed on the entire time history for System Order of 80

<i>Trial</i>	Ch05	Ch06	Ch08	Ch09	Ch10	Ch11
1	0.27	0.08	0.11	0.12	0.17	0.15
2	0.30	0.09	0.11	0.12	0.18	0.17
3	0.32	0.09	0.14	0.13	0.17	0.15
4	0.34	0.13	0.19	0.16	0.23	0.21
5	0.32	0.14	0.17	0.16	0.21	0.16
6	0.34	0.14	0.23	0.17	0.24	0.17
7	0.66	0.23	0.41	0.27	0.41	0.45
8	0.43	0.15	0.26	0.20	0.26	0.20
9	0.41	0.17	0.26	0.18	0.26	0.20
10	0.45	0.18	0.26	0.20	0.27	0.21
11	0.49	0.20	0.26	0.25	0.29	0.26
12	0.41	0.21	0.26	0.27	0.30	0.35
13	0.42	0.23	0.27	0.29	0.31	0.38

Table 3.3: Error computed on the entire time history for System Order of 118

		Ch 05	Ch 06	Ch 08	Ch 09	Ch 10	Ch 11
Trial 1	ep ₁	0.54	0.59	0.35	0.32	0.37	0.35
	ep ₂	0.46	0.35	0.33	0.25	0.32	0.29
	ep ₃	0.45	0.50	0.58	0.33	0.36	0.37
Trial 2	ep ₁	0.44	0.35	0.26	0.27	0.29	0.35
	ep ₂	0.38	0.14	0.24	0.21	0.23	0.22
	ep ₃	0.42	0.27	0.45	0.30	0.3	0.29
Trial 3	ep ₁	0.38	0.24	0.21	0.24	0.27	0.26
	ep ₂	0.29	0.11	0.15	0.15	0.20	0.17
	ep ₃	0.26	0.20	0.36	0.23	0.28	0.25
Trial 4	ep ₁	0.56	0.63	0.40	0.31	0.36	0.4
	ep ₂	0.49	0.39	0.36	0.26	0.35	0.31
	ep ₃	0.54	0.52	0.6	0.37	0.36	0.35
Trial 5	ep ₁	0.54	0.35	0.32	0.28	0.31	0.36
	ep ₂	0.41	0.14	0.28	0.24	0.27	0.28
	ep ₃	0.44	0.27	0.45	0.33	0.29	0.36
Trial 6	ep ₁	0.47	0.35	0.31	0.29	0.30	0.35
	ep ₂	0.38	0.13	0.25	0.20	0.26	0.22
	ep ₃	0.39	0.25	0.44	0.28	0.28	0.31
Trial 7	ep ₁	0.45	0.30	0.29	0.28	0.29	0.29
	ep ₂	0.37	0.12	0.24	0.18	0.24	0.21
	ep ₃	0.37	0.22	0.41	0.23	0.27	0.30
Trial 8	ep ₁	0.47	0.32	0.31	0.26	0.31	0.28
	ep ₂	0.35	0.12	0.24	0.18	0.25	0.18
	ep ₃	0.31	0.23	0.36	0.22	0.26	0.24
Trial 9	ep ₁	0.54	0.38	0.38	0.37	0.34	0.45
	ep ₂	0.41	0.21	0.35	0.32	0.31	0.28
	ep ₃	0.36	0.32	0.44	0.33	0.29	0.29
Trial 10	ep ₁	0.51	0.37	0.33	0.25	0.30	0.39
	ep ₂	0.39	0.20	0.27	0.22	0.30	0.28
	ep ₃	0.38	0.30	0.43	0.24	0.29	0.28

Table 3.4: Error computed on three pieces of time history separately for a system order equal to 80

		Ch 05	Ch 06	Ch 08	Ch 09	Ch 10	Ch 11
Trial 1	ep ₁	0.36	0.16	0.13	0.16	0.20	0.21
	ep ₂	0.25	0.06	0.09	0.10	0.15	0.14
	ep ₃	0.29	0.13	0.25	0.22	0.21	0.22
Trial 2	ep ₁	0.36	0.19	0.14	0.18	0.21	0.25
	ep ₂	0.29	0.06	0.09	0.10	0.16	0.15
	ep ₃	0.37	0.14	0.26	0.20	0.24	0.25
Trial 3	ep ₁	0.43	0.18	0.16	0.18	0.19	0.20
	ep ₂	0.30	0.07	0.11	0.11	0.16	0.13
	ep ₃	0.34	0.15	0.30	0.18	0.23	0.25
Trial 4	ep ₁	0.53	0.23	0.25	0.20	0.26	0.31
	ep ₂	0.31	0.11	0.15	0.15	0.21	0.19
	ep ₃	0.32	0.22	0.38	0.20	0.29	0.28
Trial 5	ep ₁	0.37	0.25	0.24	0.18	0.25	0.24
	ep ₂	0.31	0.11	0.14	0.15	0.20	0.15
	ep ₃	0.33	0.25	0.34	0.19	0.26	0.25
Trial 6	ep ₁	0.41	0.24	0.30	0.22	0.27	0.25
	ep ₂	0.32	0.11	0.20	0.16	0.23	0.16
	ep ₃	0.36	0.23	0.38	0.18	0.26	0.23
Trial 7	ep ₁	0.76	0.42	0.55	0.38	0.46	0.50
	ep ₂	0.60	0.19	0.37	0.25	0.39	0.44
	ep ₃	0.97	0.39	0.54	0.28	0.51	0.53
Trial 8	ep ₁	0.64	0.28	0.34	0.27	0.30	0.24
	ep ₂	0.39	0.12	0.23	0.19	0.25	0.20
	ep ₃	0.42	0.24	0.39	0.20	0.25	0.25
Trial 9	ep ₁	0.54	0.31	0.33	0.20	0.29	0.23
	ep ₂	0.38	0.14	0.22	0.17	0.25	0.19
	ep ₃	0.37	0.30	0.37	0.20	0.25	0.25
Trial 10	ep ₁	0.57	0.32	0.35	0.22	0.31	0.30
	ep ₂	0.43	0.15	0.22	0.19	0.26	0.20
	ep ₃	0.38	0.31	0.37	0.20	0.24	0.28
Trial 11	ep ₁	0.51	0.36	0.33	0.35	0.31	0.37
	ep ₂	0.50	0.17	0.23	0.23	0.29	0.24
	ep ₃	0.43	0.31	0.37	0.25	0.26	0.31
Trial 12	ep ₁	0.51	0.35	0.34	0.34	0.31	0.44
	ep ₂	0.40	0.18	0.23	0.26	0.30	0.34
	ep ₃	0.36	0.31	0.38	0.26	0.29	0.36
Trial 13	ep ₁	0.54	0.40	0.37	0.37	0.33	0.48
	ep ₂	0.40	0.19	0.24	0.28	0.31	0.36
	ep ₃	0.37	0.33	0.38	0.23	0.29	0.40

Table 3.5: Error computed on three pieces of time history separately for a system order equal to 118

3.3.2 Rio Dell (December 16, 1982)

For this set of data records from channels 2, 15, 16, 17, 18, 19, 20 are used as inputs, while the ones from channels 4, 5, 6, 7, 8, 9, 10, 11 as outputs. The total number of data points for each record is 1064, at a sampling interval of 0.02 seconds.

The upper bound for p for this set of data is given by:

$$p_{\max} = \frac{l - r}{m + r} = 75 \quad (3.47)$$

where

r = number of inputs (7)

m = number of outputs (8)

l = number of data points (1064)

Also in this case the number of *system* Markov parameters is set equal to four times p . To obtain the final model it is chosen to keep 138 singular values of the matrix $\mathbf{V}*\mathbf{V}^T$ to compute *observer* Markov Parameters. Moreover, the realized model order is set equal to 80. Also for this case, the MATLAB results (only for the final experiment) are presented in appendix B with the corresponding plots.

The results obtained from this set of data may complete the identification performed with the Trinidad set of data. In fact, for the Rio Dell records, time histories from transversal sensor are available. This may allow to identify also the transverse modal shapes. Nonetheless, by running the algorithm the best results obtained so far are characterized by the relative error shown in table 3.6. For these accelerograms, the part characterized by the major amplitudes is that from 2 to 4 seconds. As can be observed from table 3.6, the values of the error are very high, imposing a high level of criticism in considering the results:

	Ch04	Ch05	Ch06	Ch07	Ch08	Ch09	Ch10	Ch11
e_{total}	0.30	0.48	0.54	0.19	0.31	0.25	0.36	0.46
$e_{0-2\ sec}$	1.50	0.89	0.64	0.89	0.54	1.58	0.68	1.08
$e_{2-4\ sec}$	0.26	0.42	0.33	0.13	0.18	0.21	0.29	0.44
$e_{4-21.28\ sec}$	0.56	0.67	0.79	0.57	0.78	0.47	0.73	0.49

Table 3.6: Relative Error for the model identified through Rio Dell Earthquake Event

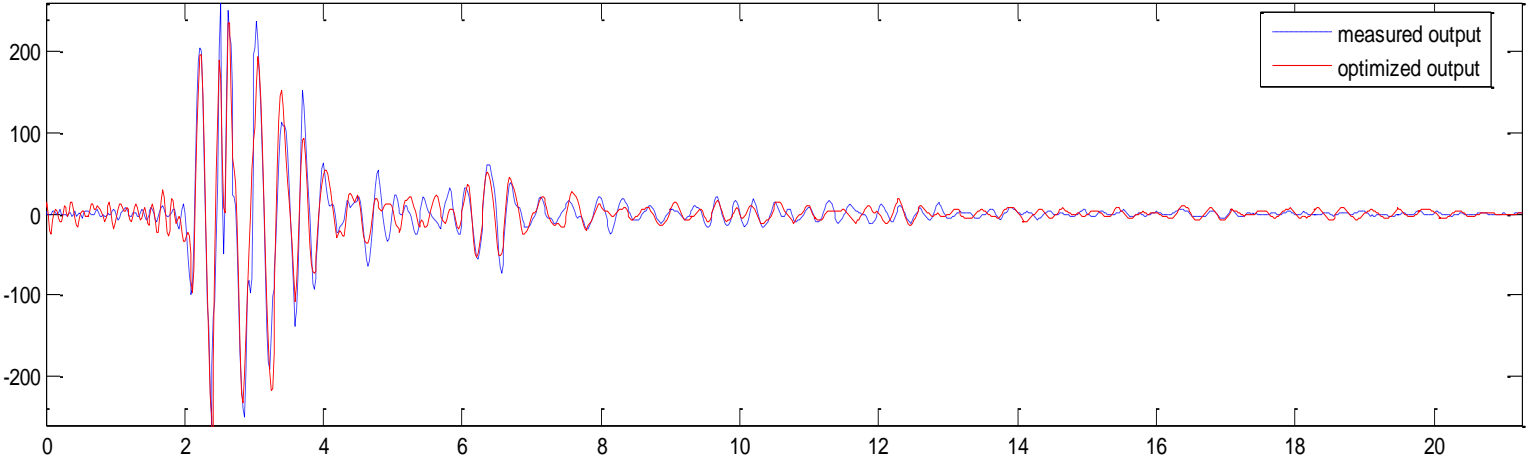
In considering these results may be helpful referring to the ones obtained with the previous set of data. Moreover, for this case, it is reasonable to analyze the plot of the modal shapes in the space, and only their vertical view. In fact, as mentioned, for these records also transversal measurements are available, although it is possible to have the motion at only two points of the north edge. Figure 3.6a plots what is supposed to be the first mode, nonetheless the shape is too complicated to be likely to represent the first natural mode of the structure. This result is considered to be strongly affected by noise and is then neglected. For what concerns the second and third frequencies, from observation of figures 3.6b and 3.6c, it can be inferred that the two represents the same mode. This conclusion can be evaluated also by comparing these values with those individuated in the initial analysis, presented in chapter 2. Finally, the last mode may represent a torsional mode, but again, it is not possible to guarantee this assumption before running a modal analysis on the three-dimensional finite element model.

In conclusion, the modal parameters individuated for this case are presented in table 3.7:

Mode	Frequency [Hz]	Period [sec]	Damping ratio
1	2.590	0.386	0.06
2	5.349	0.187	0.05
3	5.732	0.174	0.06
4	8.107	0.123	0.08

Table 3.7: Modal Parameters Identified with Rio Dell Earthquake records

Channel 4



Zoom of Time History btw. 2.02 and 8 seconds

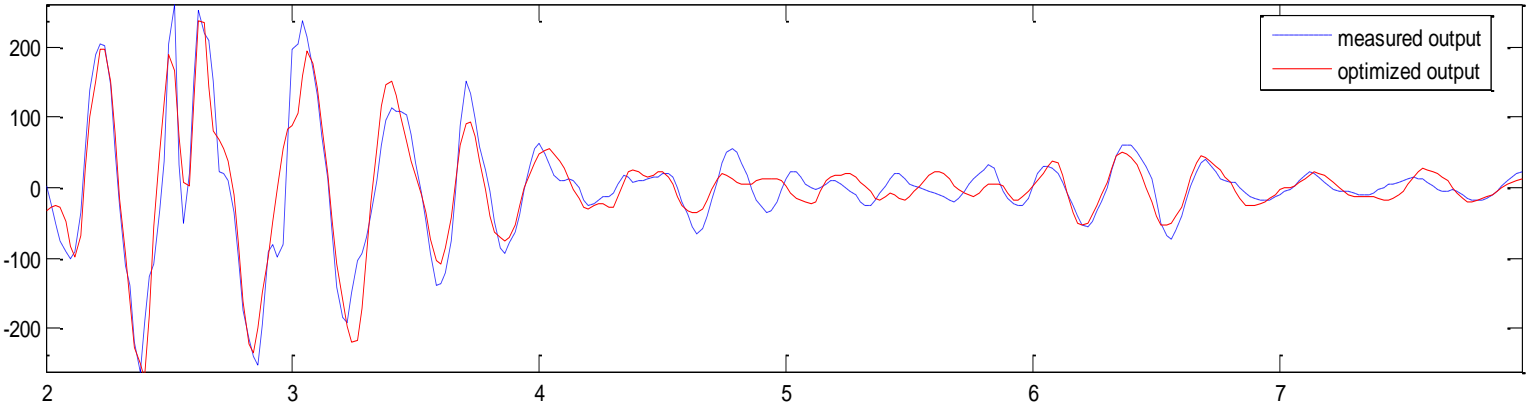
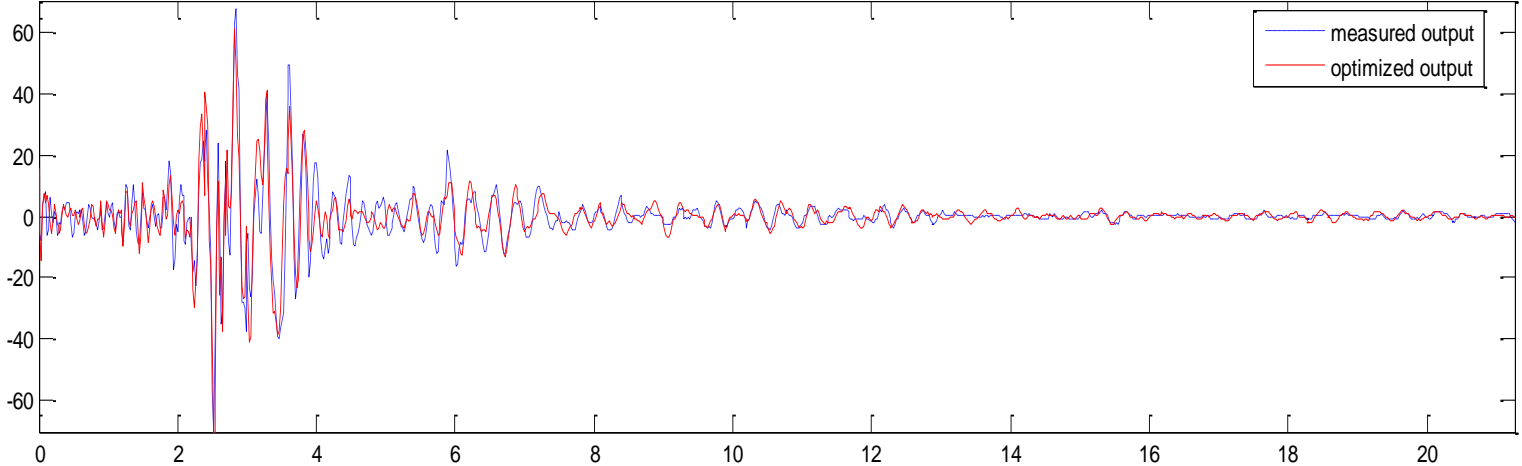


Figure 3.5a: Comparison between optimized and measured time History of channel 4

Channel 5



Zoom of Time History btw. 2.02 and 8 seconds

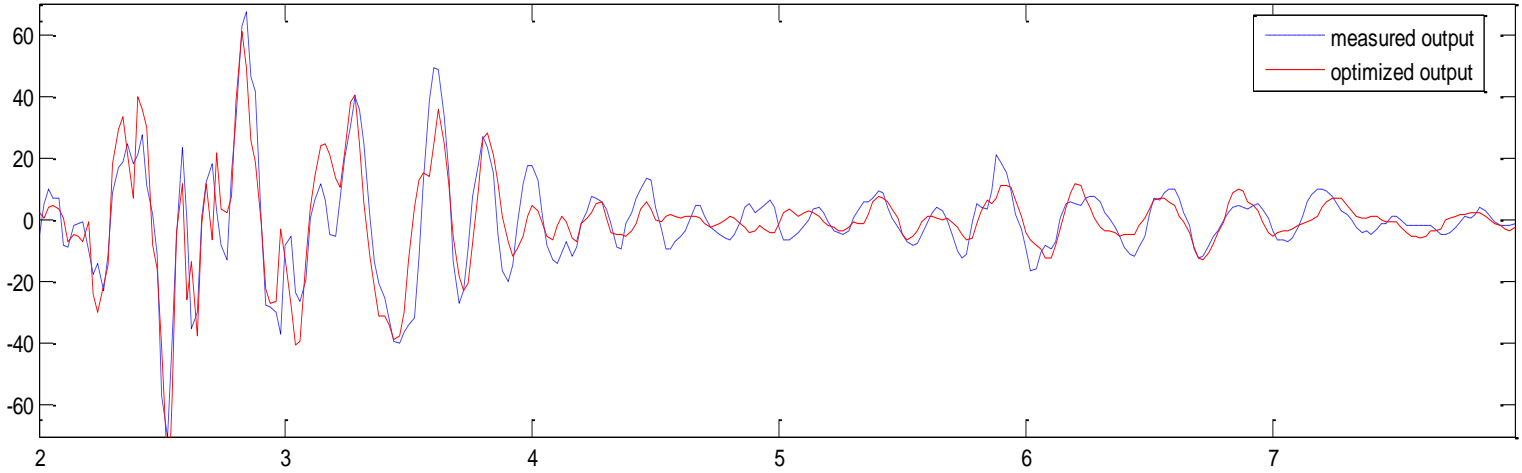
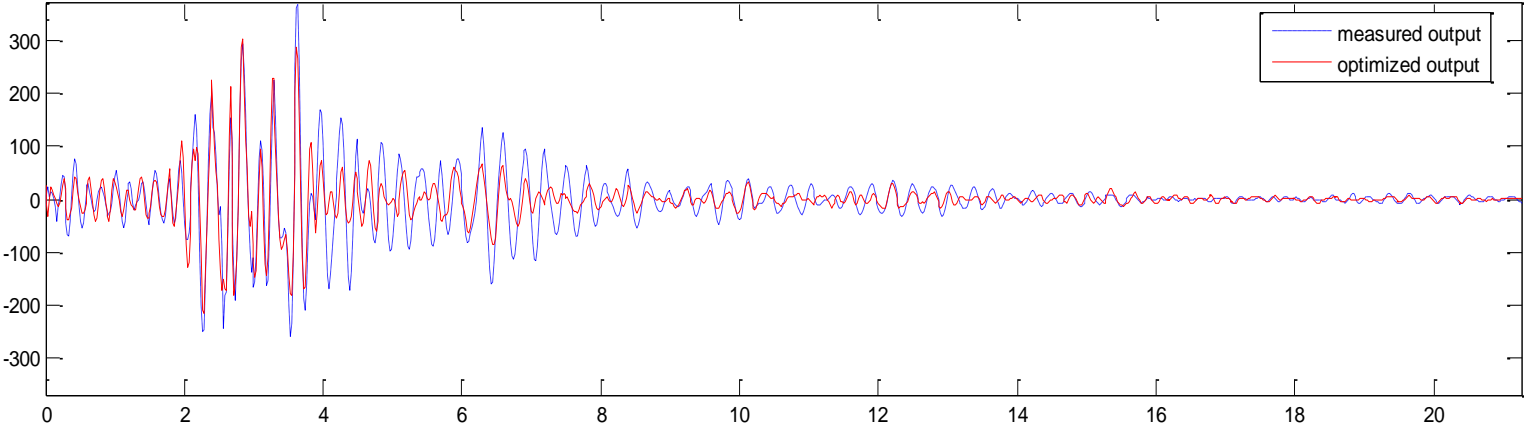


Figure 3.5b: Comparison between optimized and measured time History of channel 5

Channel 6



Zoom of Time History btw. 2.02 and 8 seconds

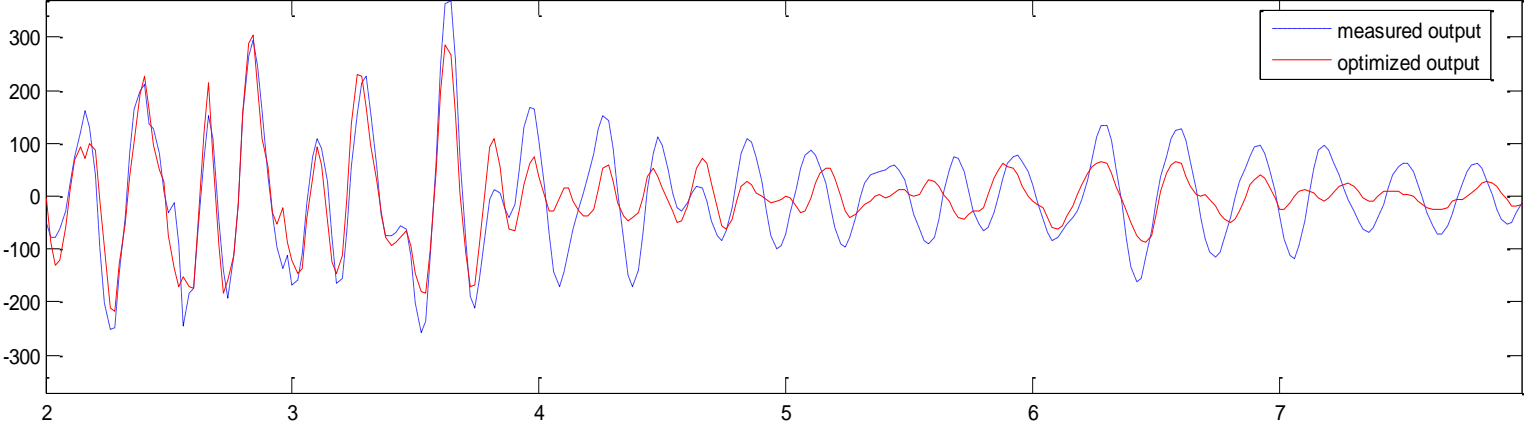


Figure 3.5c: Comparison between optimized and measured time History of channel 6

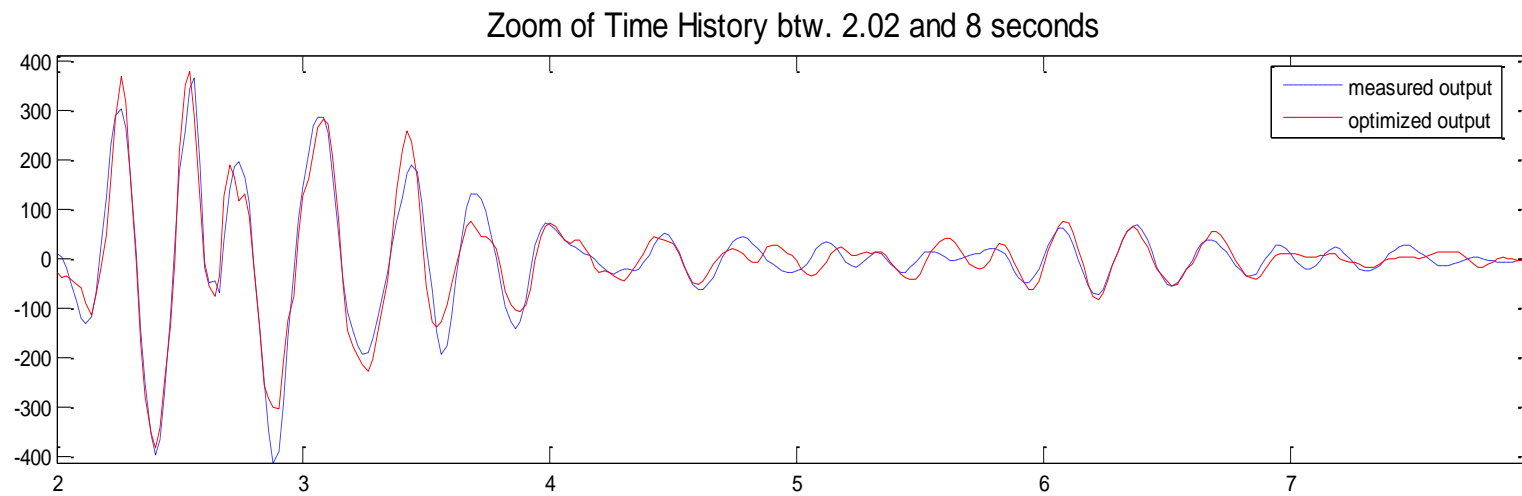
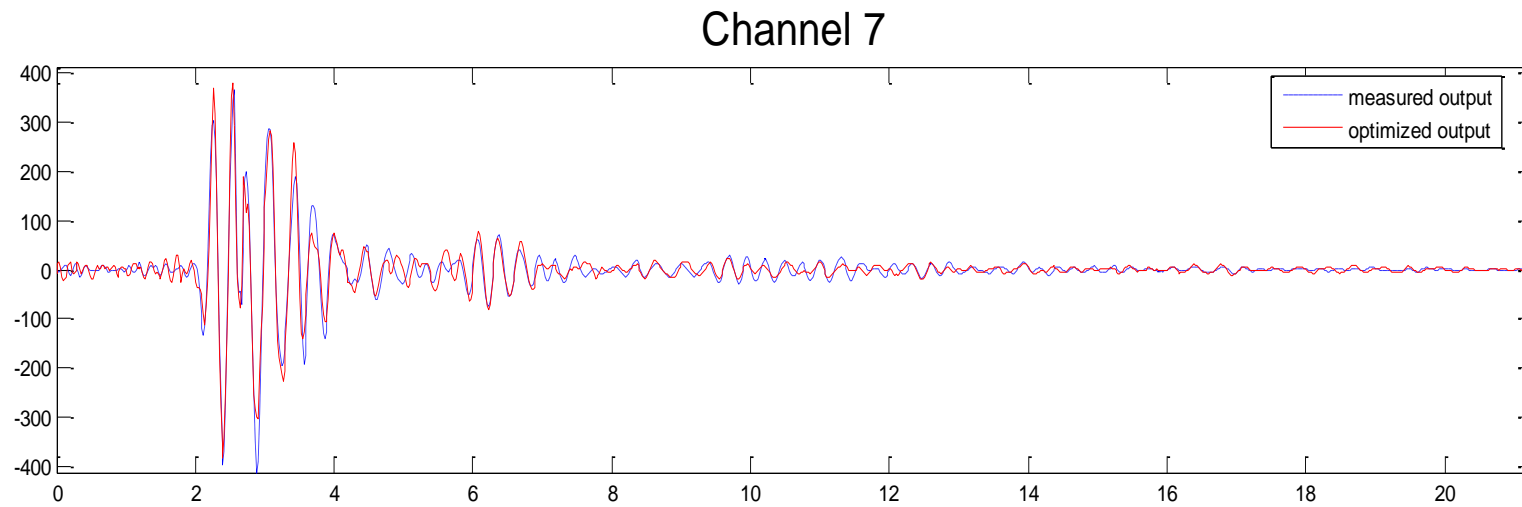


Figure 3.5d: Comparison between optimized and measured time History of channel 7

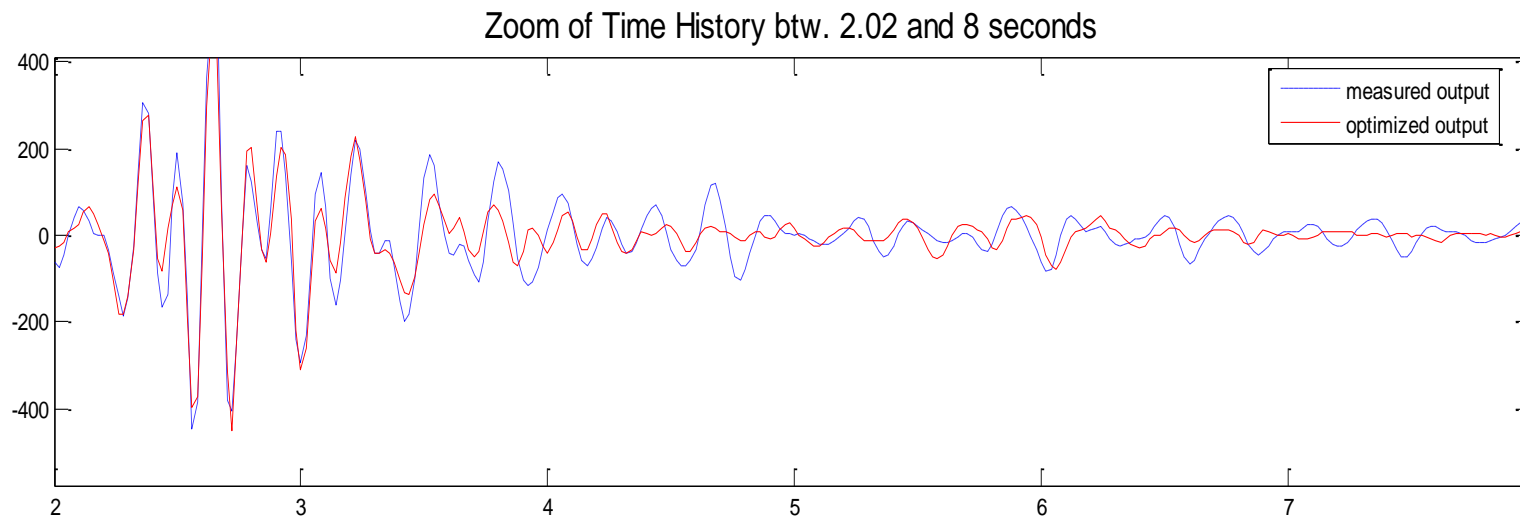
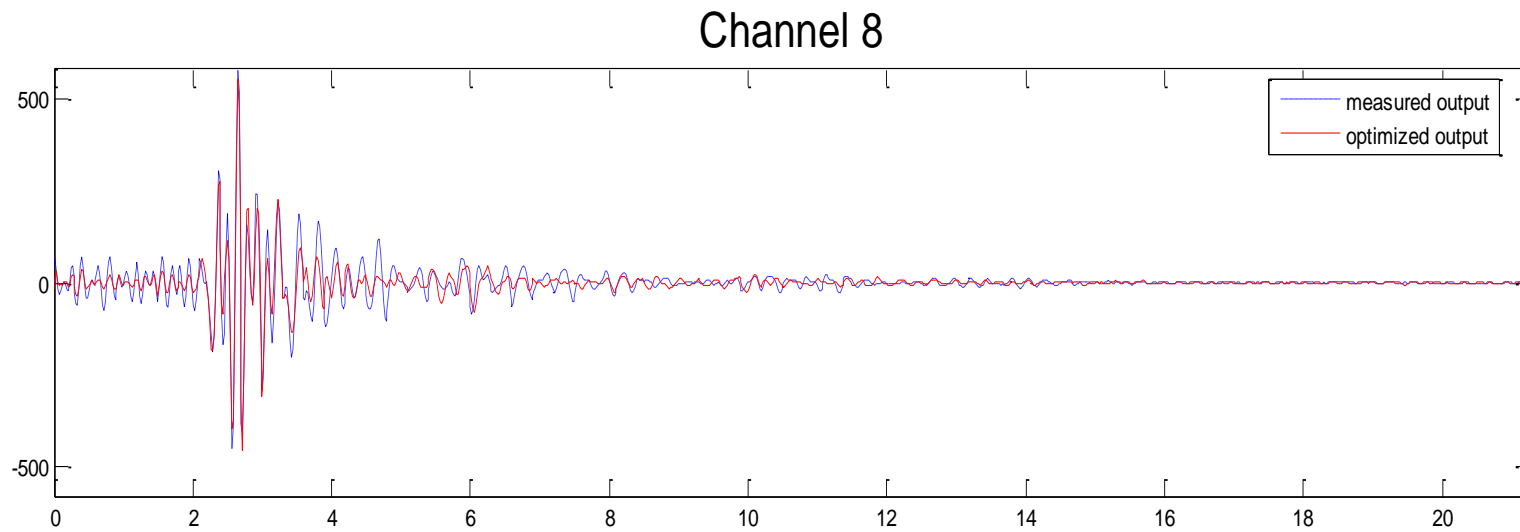
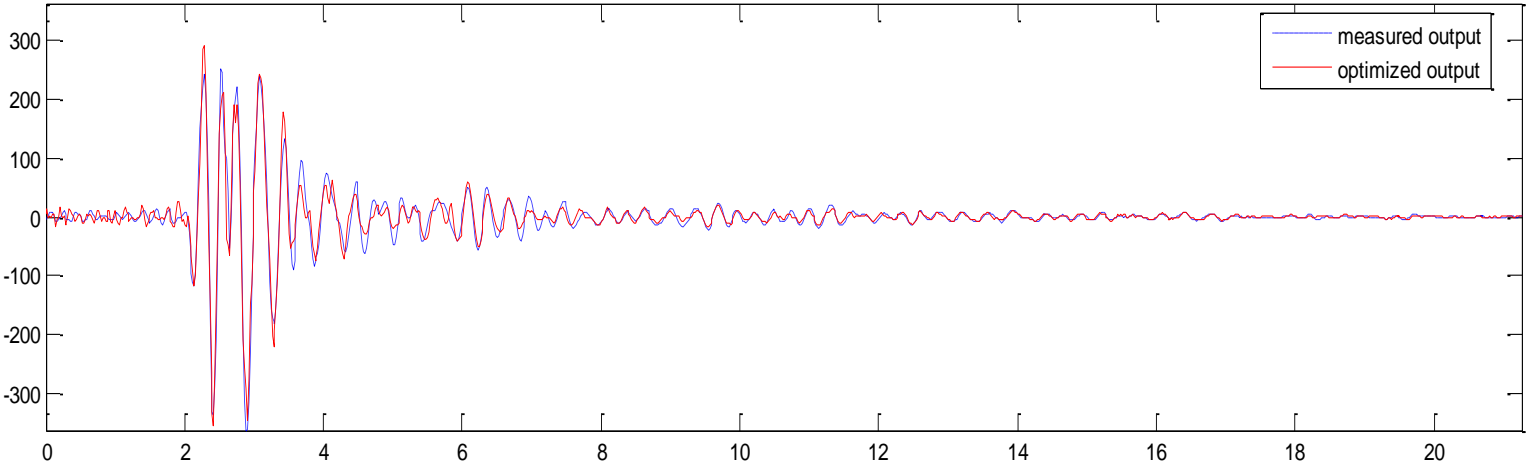


Figure 3.5e: Comparison between optimized and measured time History of channel 8

Channel 9



Zoom of Time History btw. 2.02 and 8 seconds

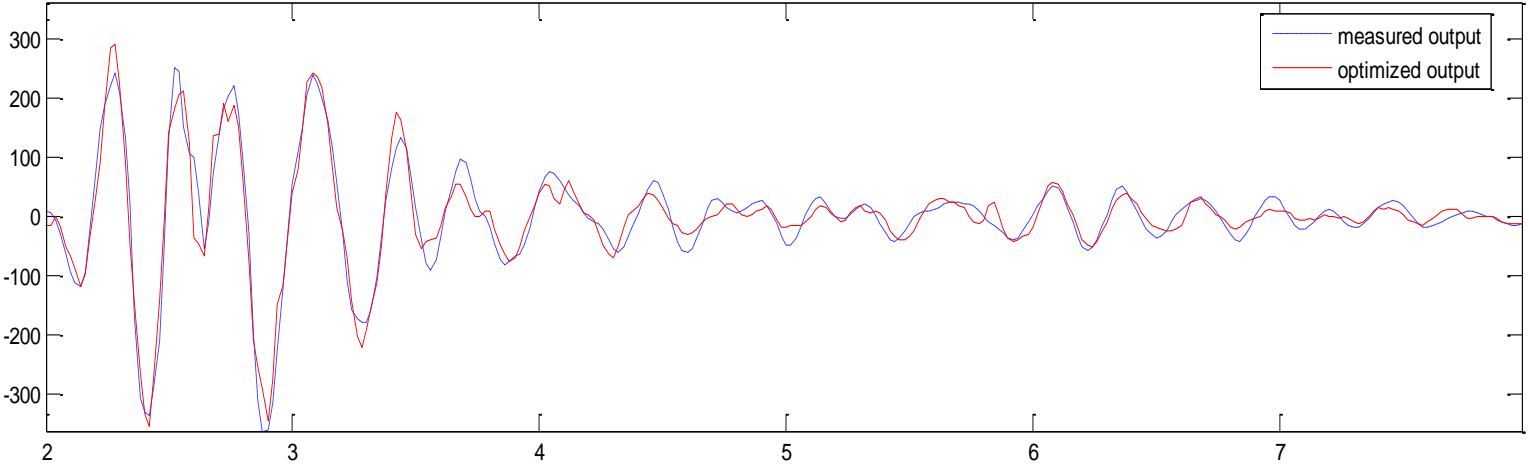
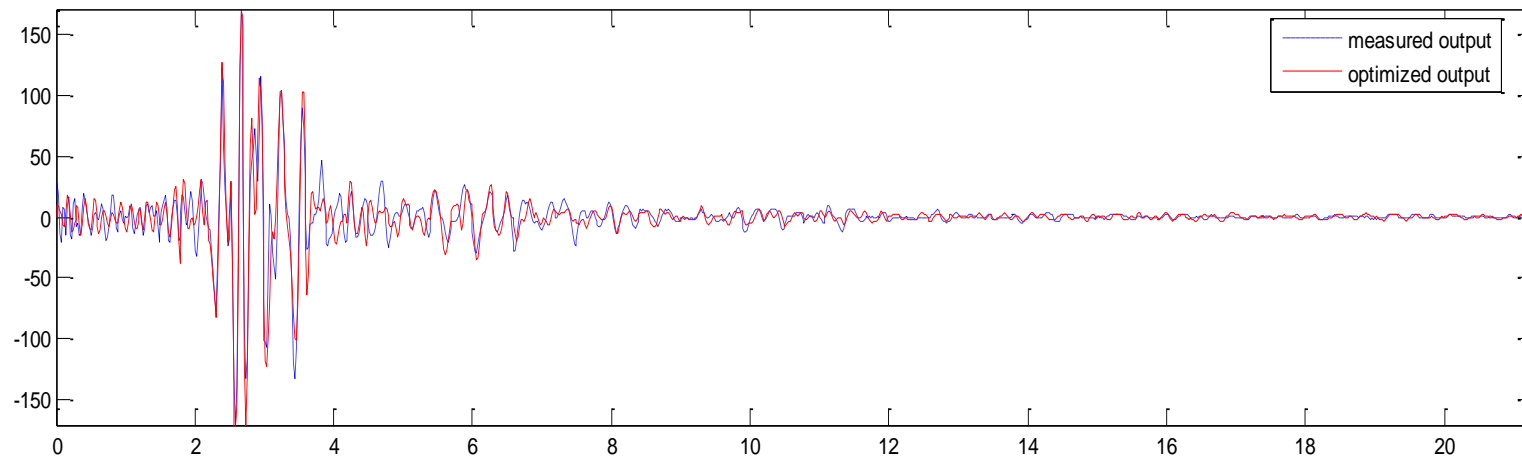


Figure 3.5f: Comparison between optimized and measured time History of channel 9

Channel 10



Zoom of Time History btw. 2.02 and 8 seconds

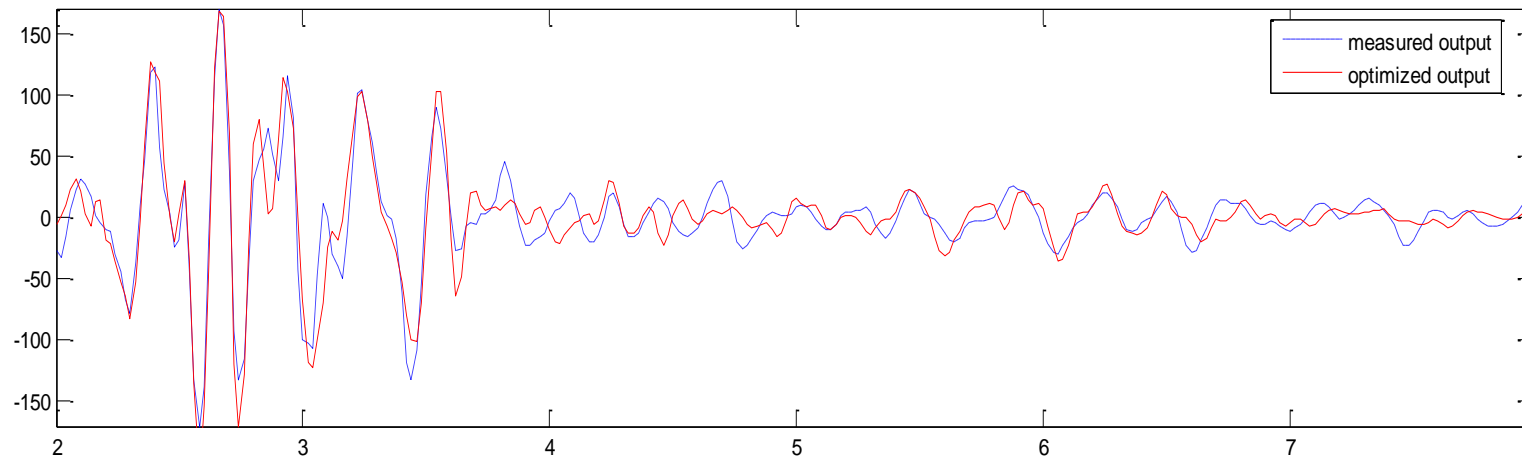
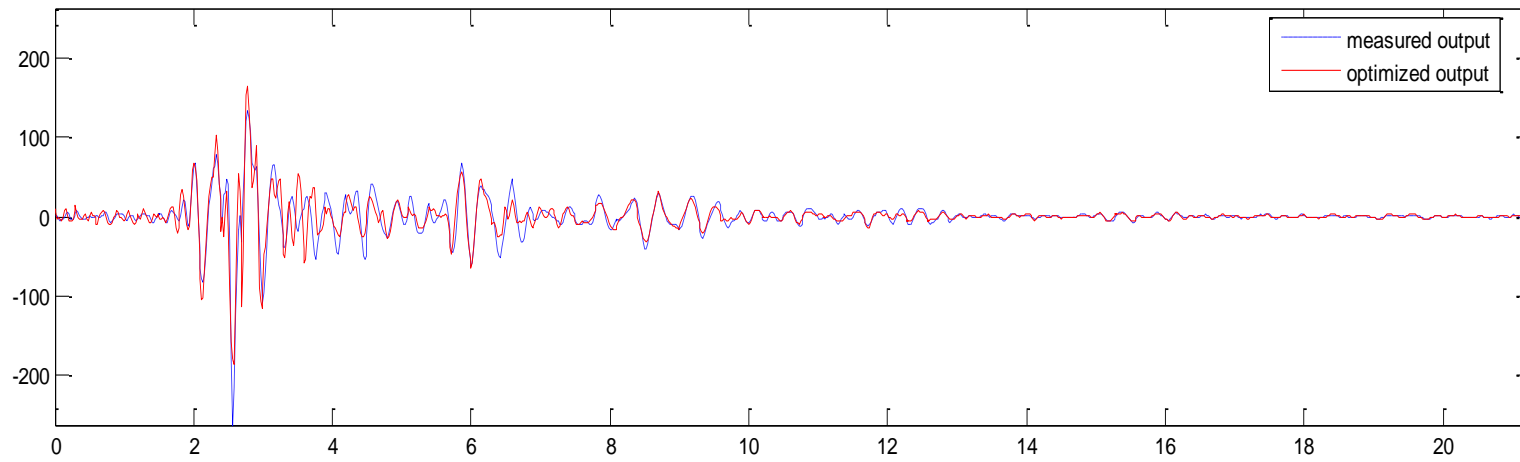


Figure 3.5g: Comparison between optimized and measured time History of channel 10

Channel 11



Zoom of Time History btw. 2.02 and 8 seconds

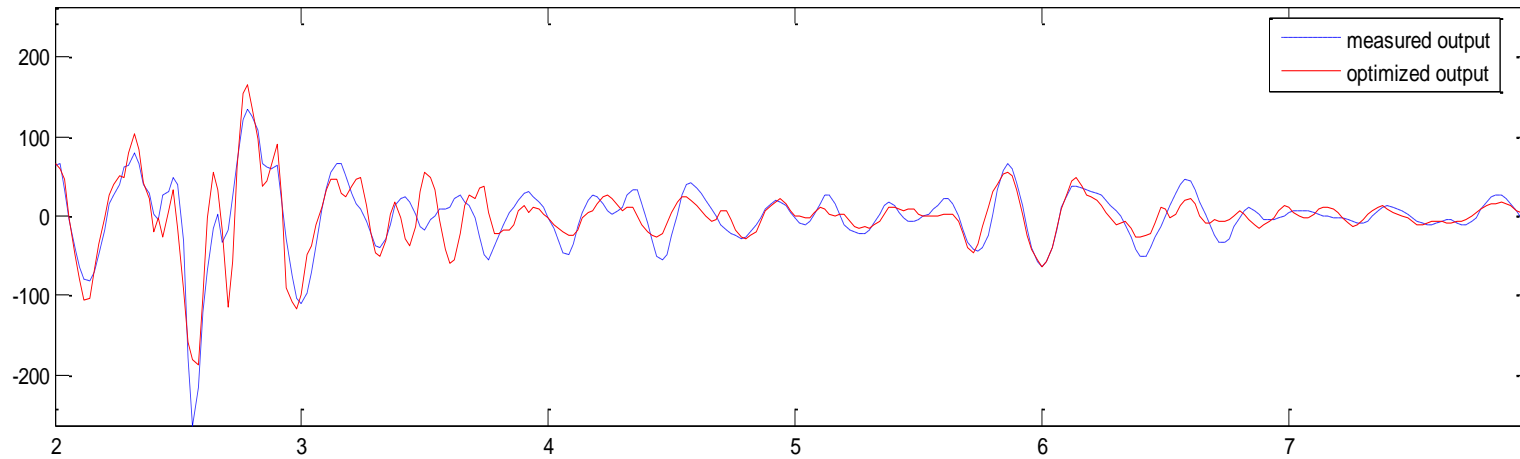


Figure 3.5h: Comparison between optimized and measured time History of channel 11

Mode 1: 2.590 Hz

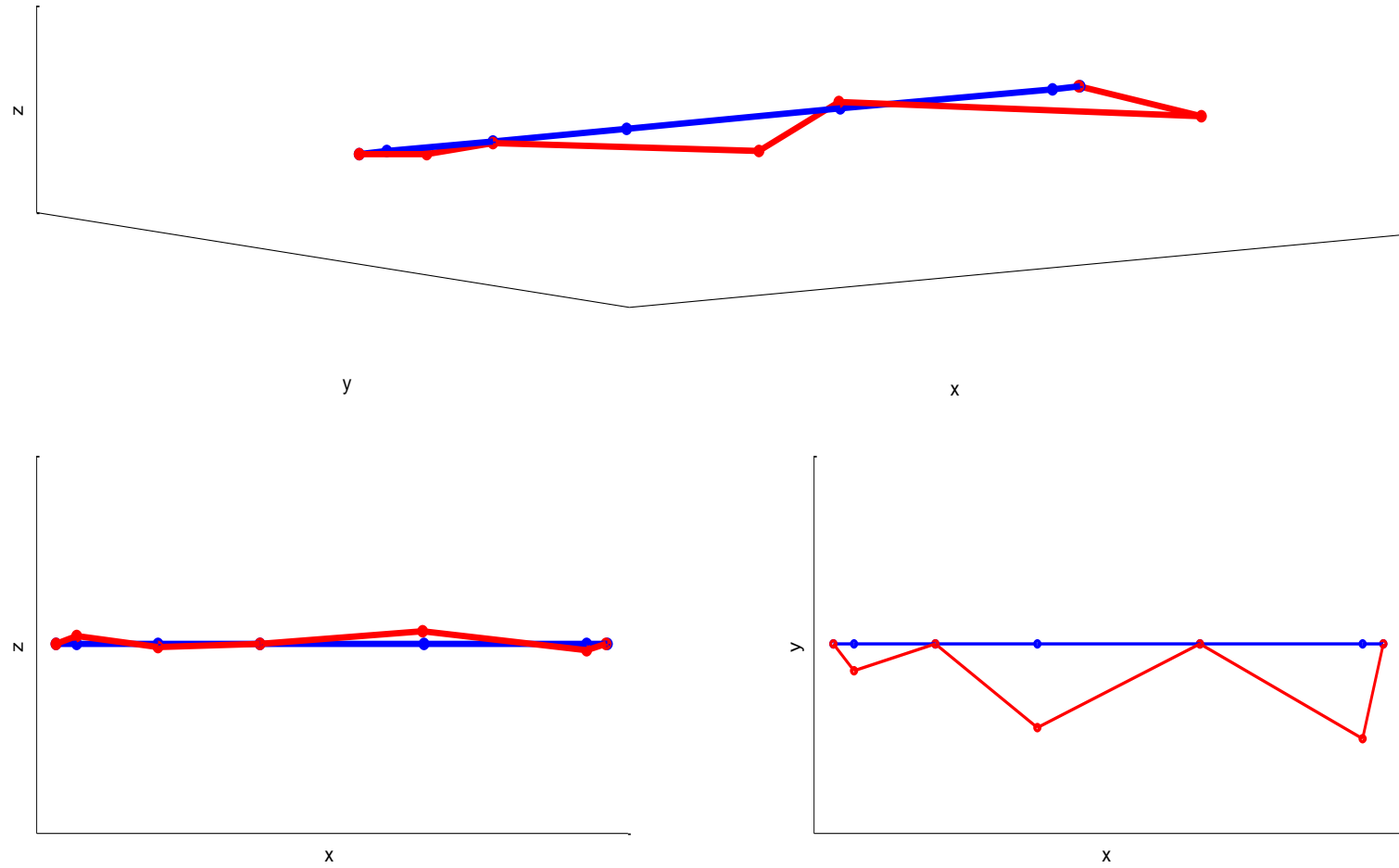


Figure 3.6a: First Identified Modal Shape

Mode 2: 5.349 Hz

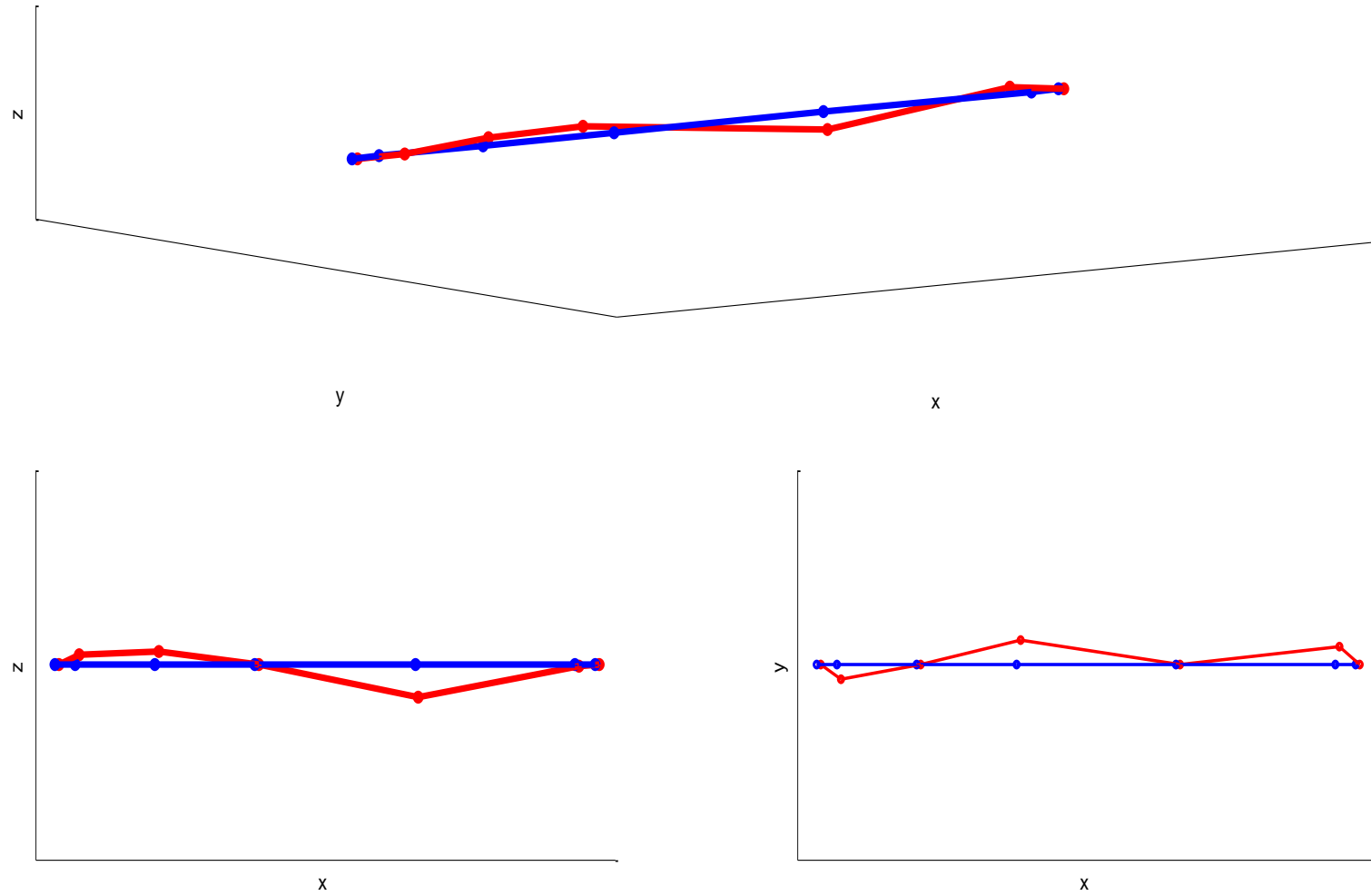


Figure 3.6b: Second Identified Modal Shape

Mode 3: 5.732 Hz

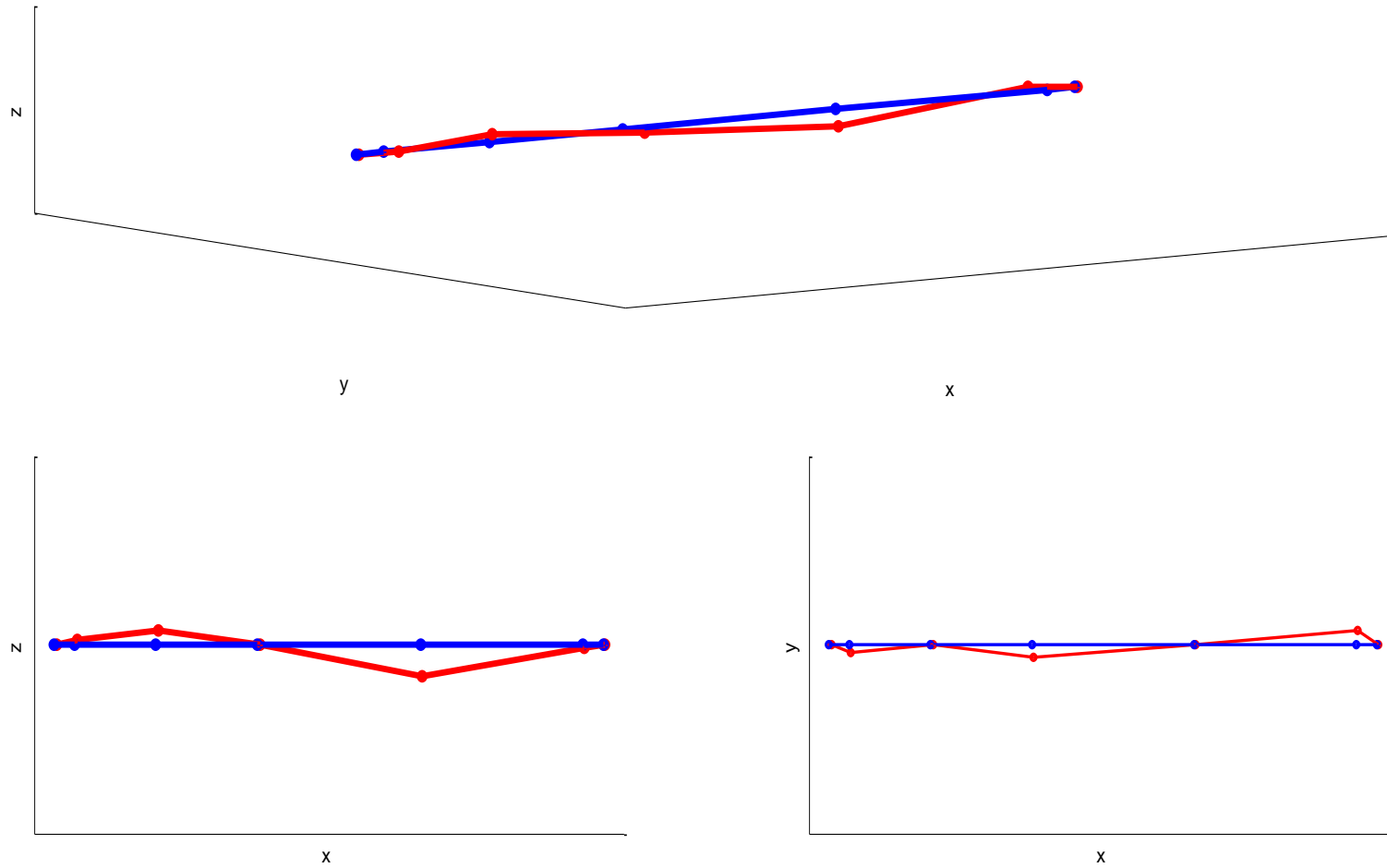


Figure 3.6c: Third Identified Modal Shape

Mode 4: 8.106 Hz

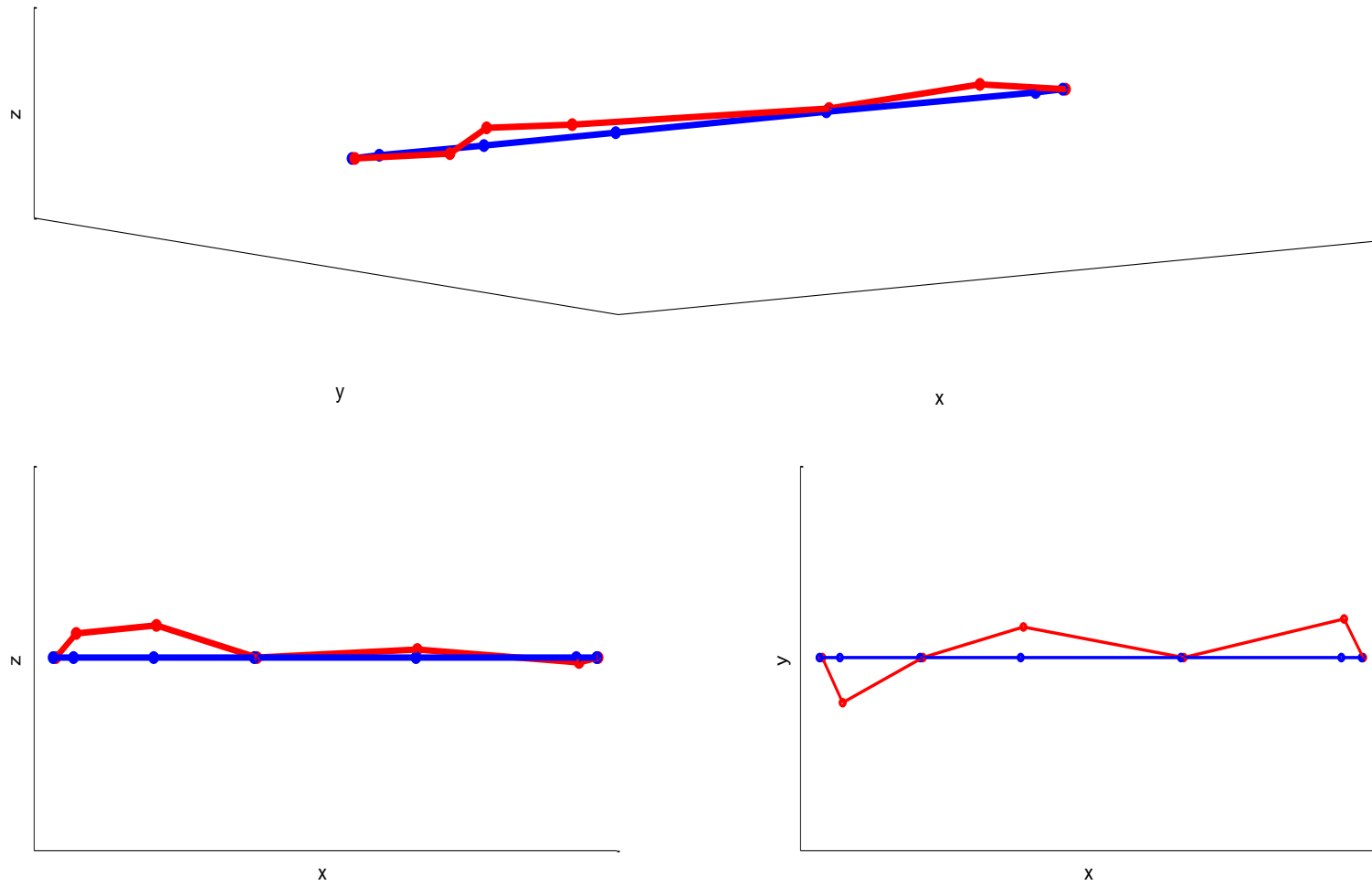


Figure 3.6d: Fourth Identified Modal Shape

3.3.3 Petrolia (April 25th, 1992)

For this set of data records from all of the channels are available: accelerations measured from channels 1, 2, 3, 15, 16, 17, 18, 19, 20 are used as inputs, while records from sensors 4, 5, 6, 7, 8, 9, 10, 11 are treated as outputs. These time histories are the longest available for the Rio Dell/Painter Street Overpass, since they are constituted by 3000 data points measured every 0.02 sec. With these values, the maximum number of observer Markov parameters is possible to compute is given by:

$$p_{\max} = \frac{l-r}{m+r} = 175 \quad (3.47)$$

where

r = number of inputs (9)

m = number of outputs (8)

l = number of data points (3000)

The best results that can be obtained with this set of data is evaluated by computing 175 Markov parameters, keeping 808 singular values from the VT*V matrix, and constituting a model of order 60. The relative errors for this trial are presented in table 3.6:

	Ch04	Ch05	Ch06	Ch07	Ch08	Ch09	Ch10	Ch11
e_{tot}	0.39	0.57	0.69	0.29	0.68	0.32	0.52	0.42
e_{0-10 s}	0.37	0.58	0.68	0.26	0.66	0.30	0.52	0.42
e_{10-30 s}	0.49	0.53	0.74	0.38	0.76	0.40	0.49	0.40
e_{30-60 s}	0.54	0.56	0.74	0.52	0.80	0.60	0.54	0.49

Table 3.6: Errors for the model identified through Petrolia Earthquake Records

It is clear as this set of data cannot give reasonable results, since the errors computed both on the entire time histories and on parts of those are too high to consider the gained values reliable. Therefore, also for this set of data it is requested an exercise of critical analysis of what evaluated.

In particular, the modal parameters gained through Petrolia Earthquake records are presented in table 3.7:

Mode	Frequency [Hz]	Period [sec]	Damping ratio
1	3.366	0.297	0.05
2	4.382	0.228	0.09
3	6.173	0.162	0.05

Table 3.7: Modal parameters identified with Petrolia Earthquake records

By comparing the findings to the those obtained with the more reliable Trinidad Earthquake set of data, it can be observed a clear resemblance between the two. Nonetheless, the modal shapes are not reasonable. The first two plots seem to represent the same natural mode, but the corresponding frequencies are supposed appreciable both for the results gained with Trinidad set of data and for those detected through the initial frequency content analysis performed on the acceleration time histories records.

In conclusion, from this set of data only the modal frequencies are retrieved, and considered as the validation of previous gains.

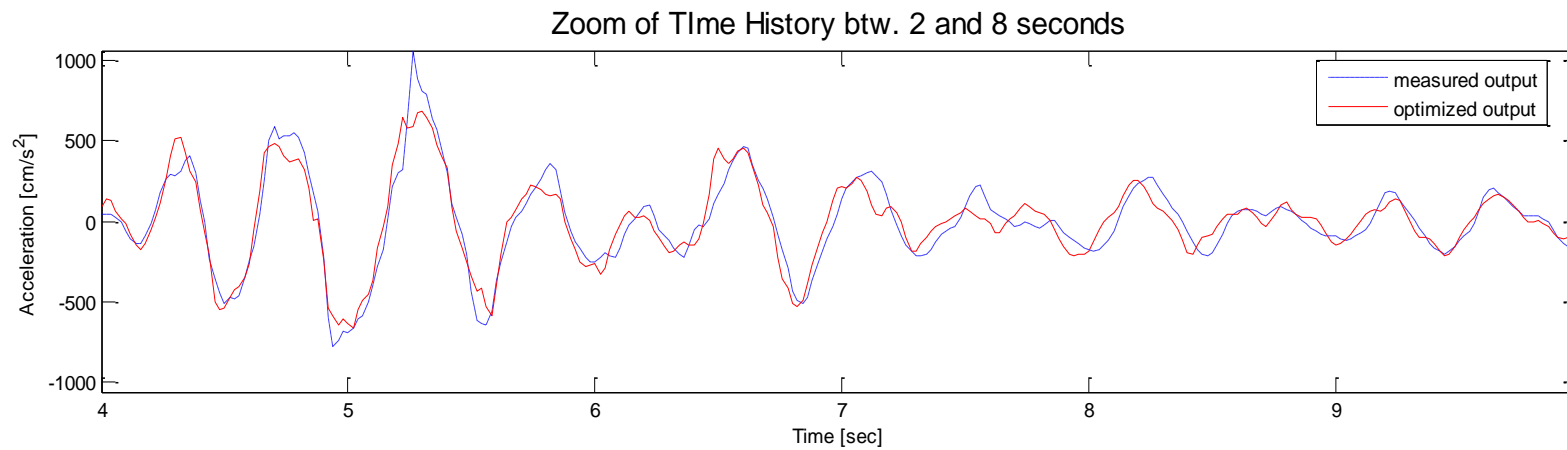
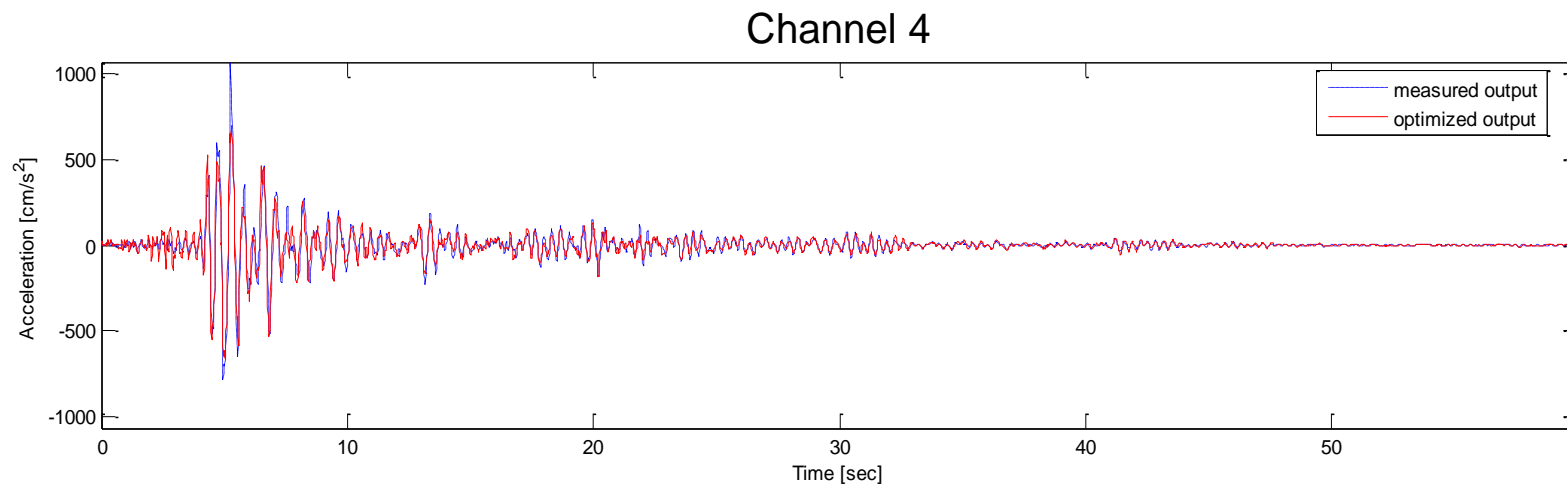


Figure 3.7a: Comparison between optimized and measured time History of channel 4

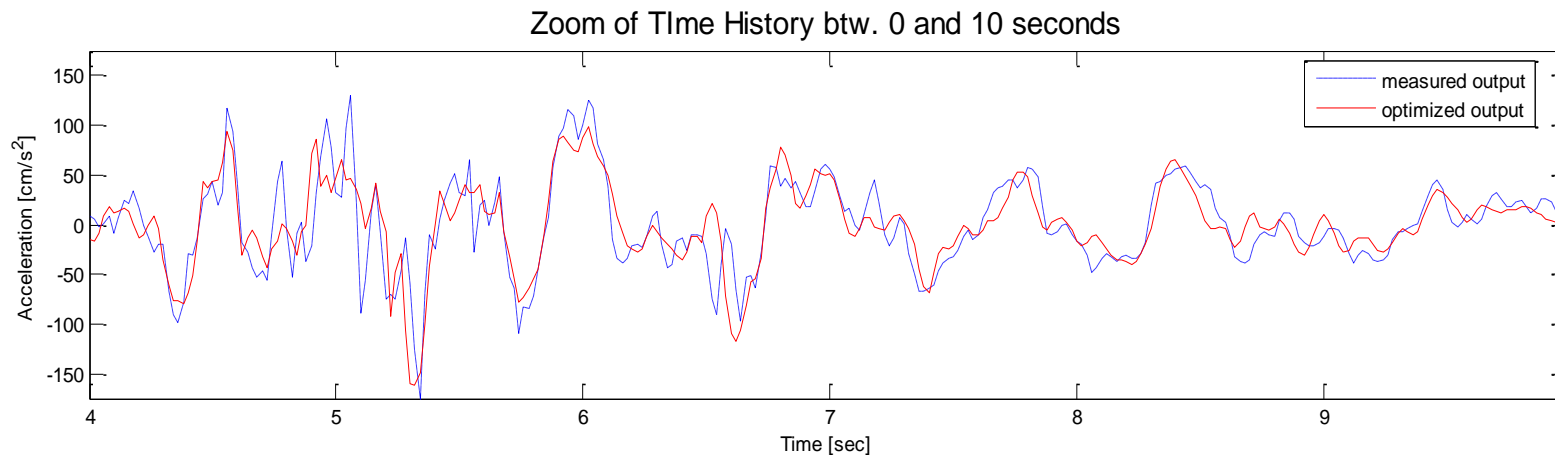
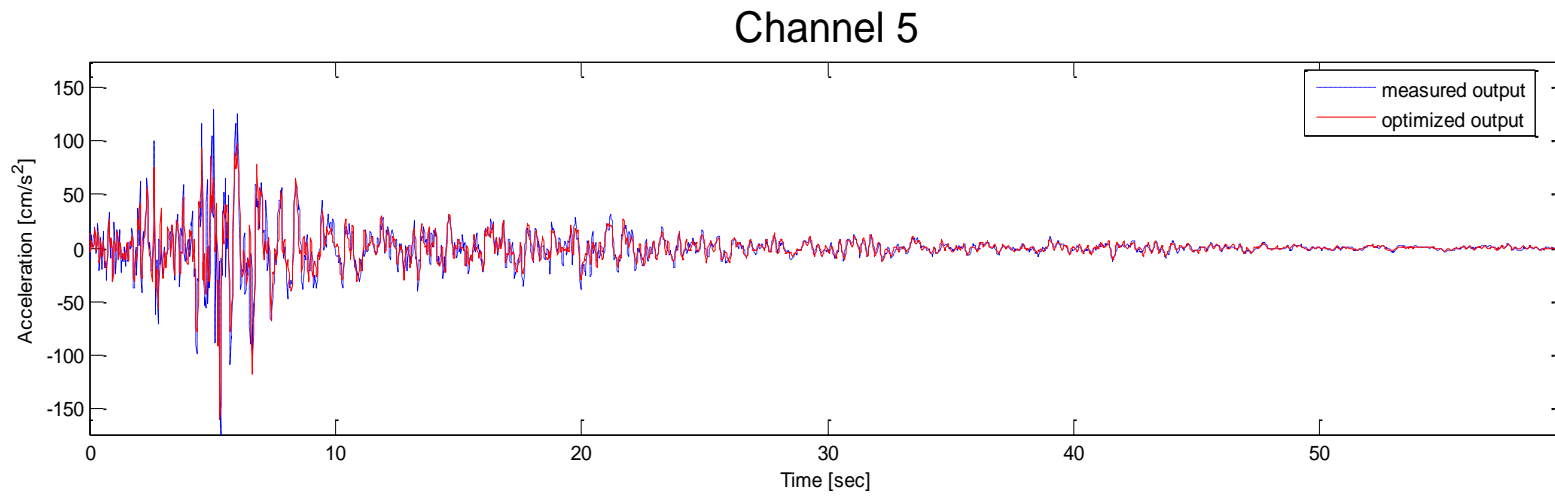


Figure 3.7b: Comparison between optimized and measured time History of channel 5

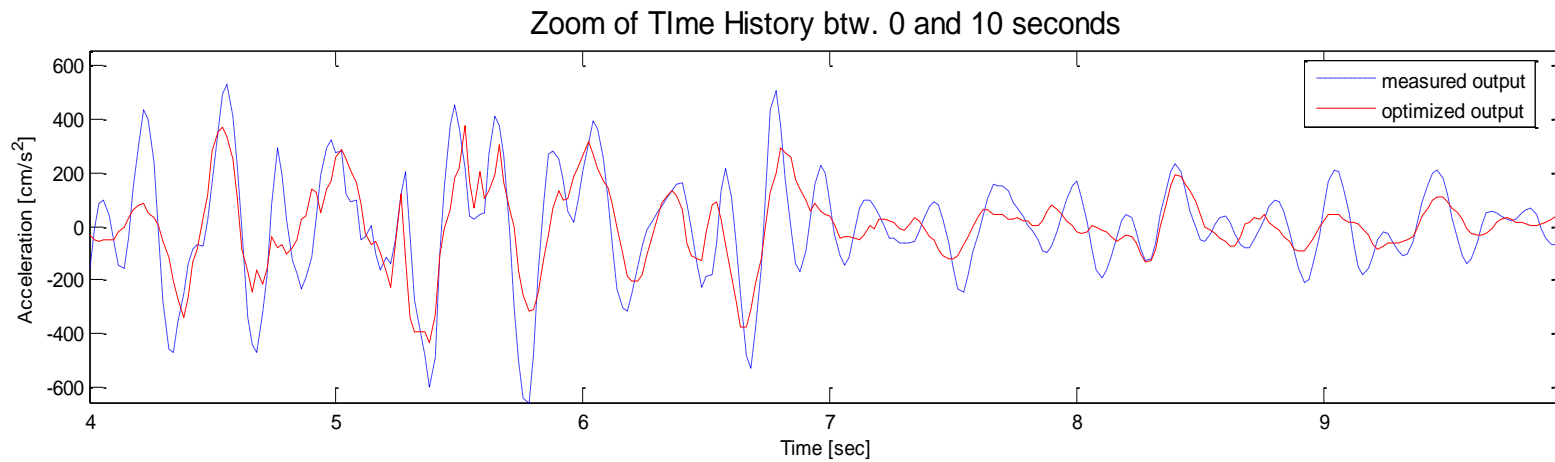
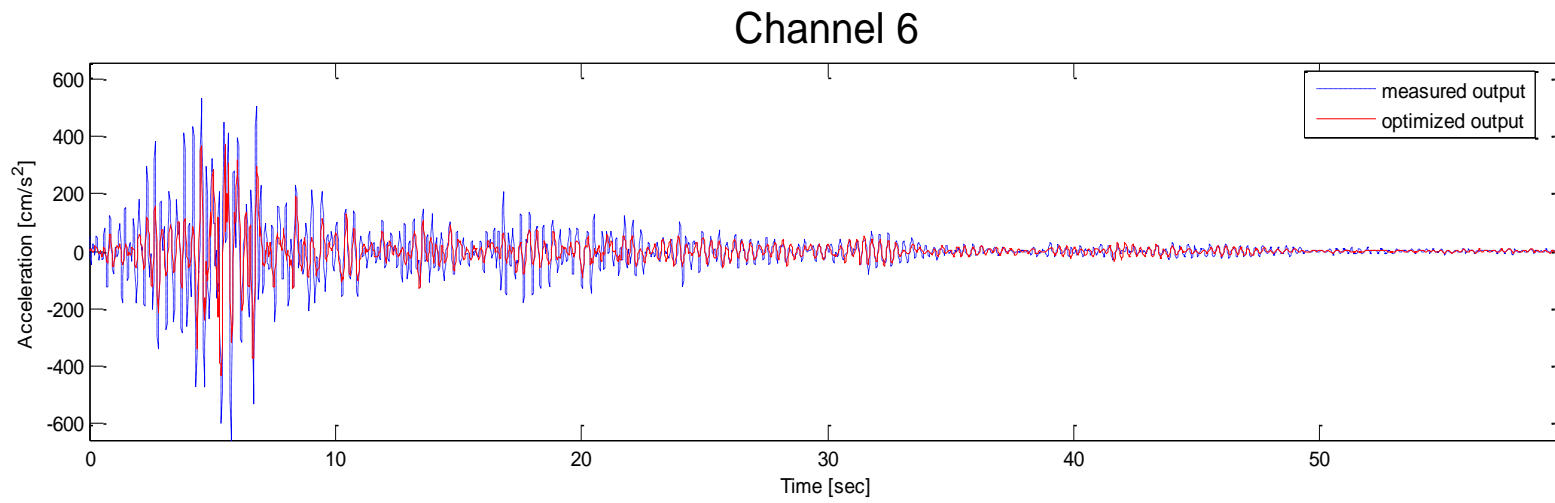


Figure 3.7c: Comparison between optimized and measured time History of channel 6

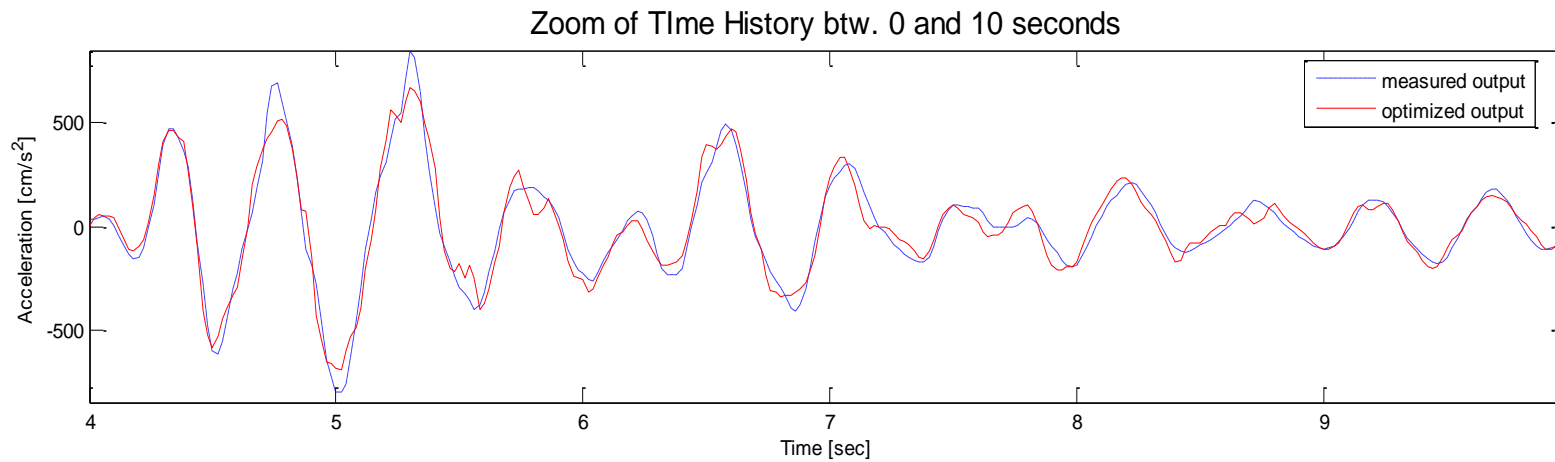
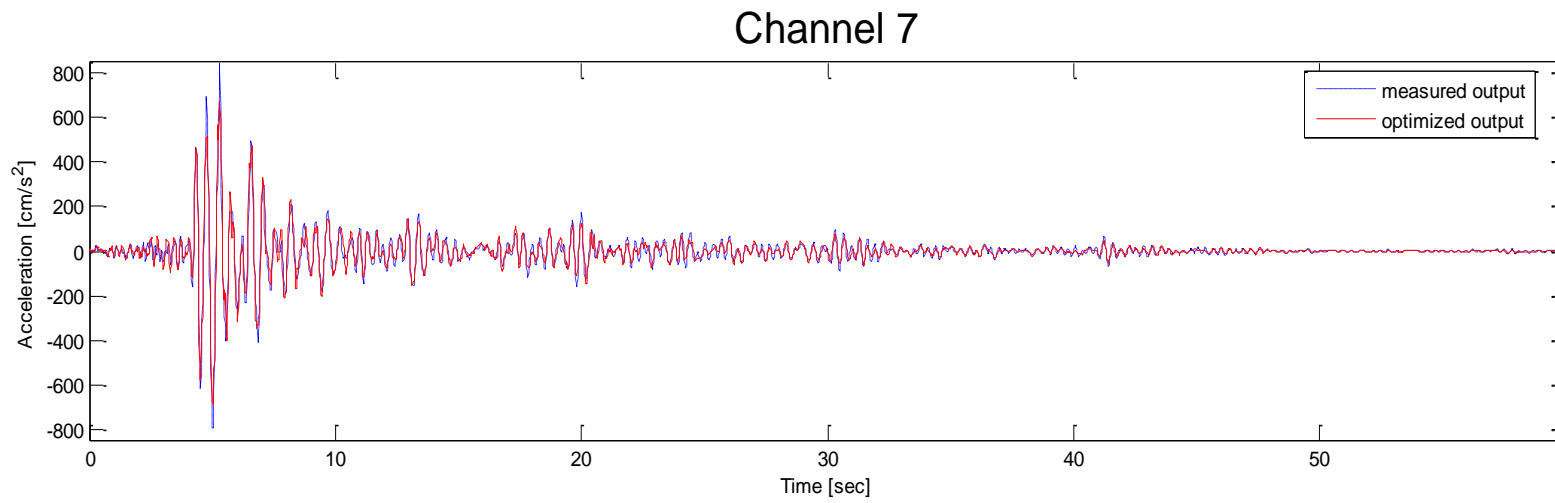


Figure 3.7d: Comparison between optimized and measured time History of channel 7

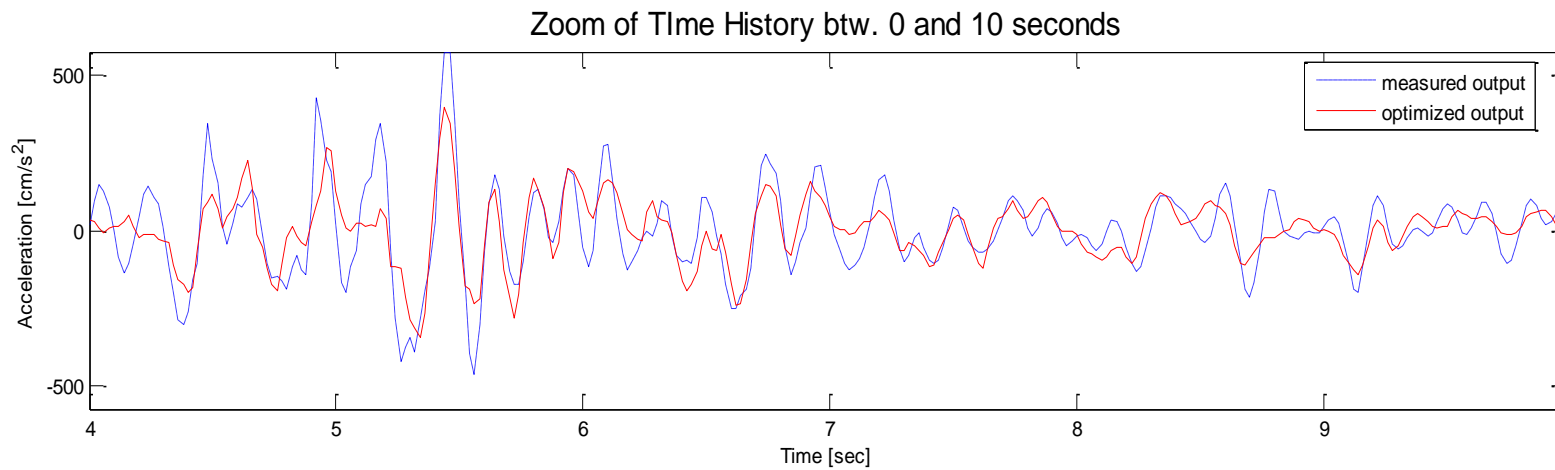
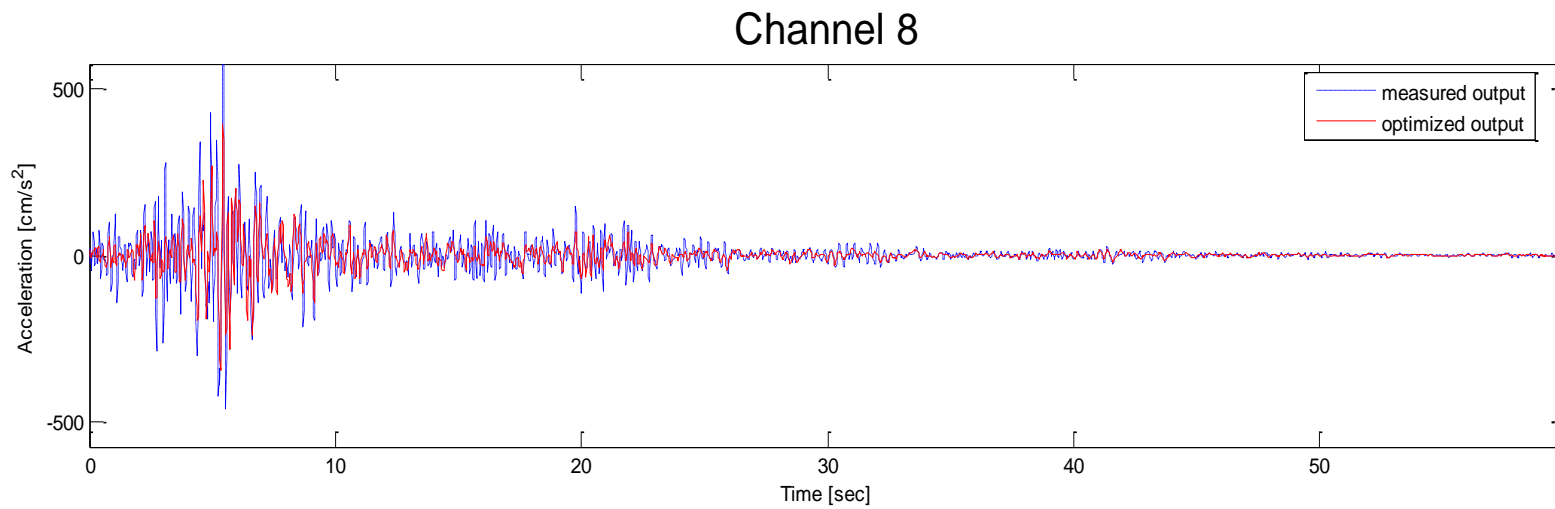


Figure 3.7e: Comparison between optimized and measured time History of channel 8

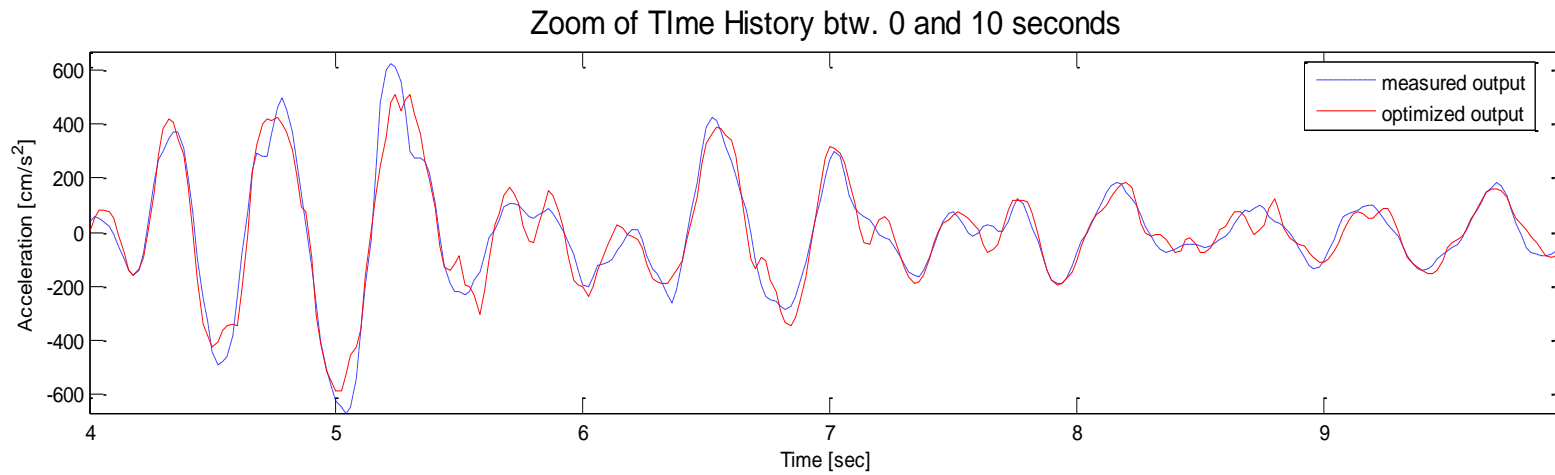
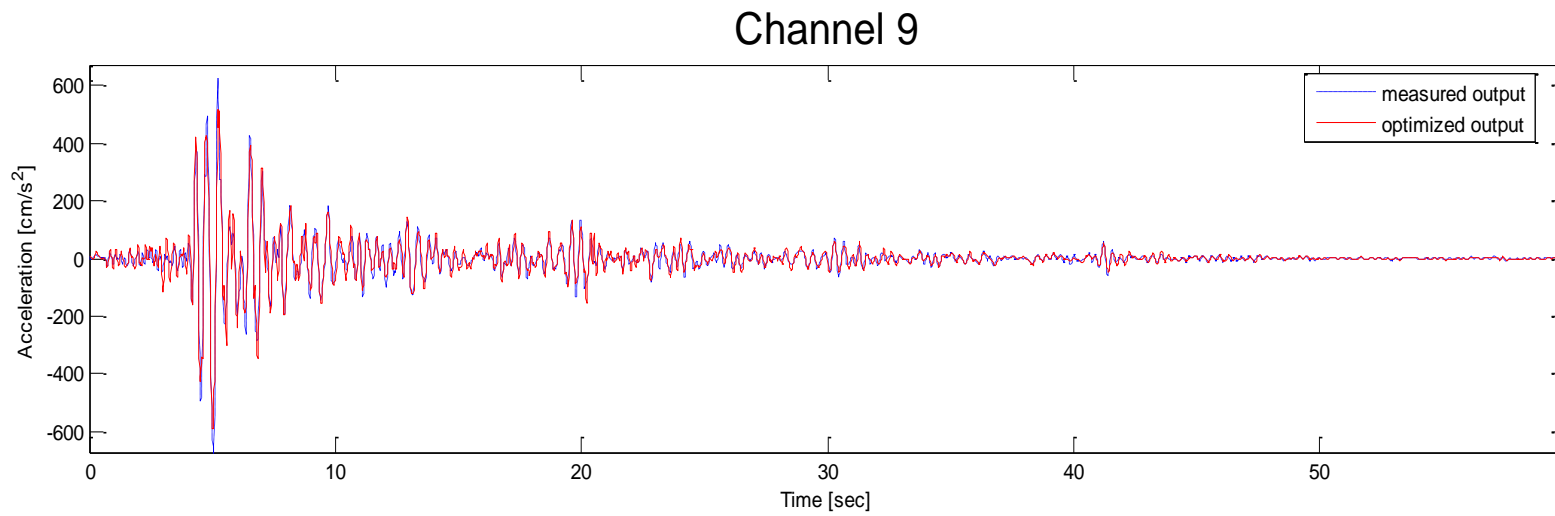


Figure 3.7f: Comparison between optimized and measured time History of channel 9

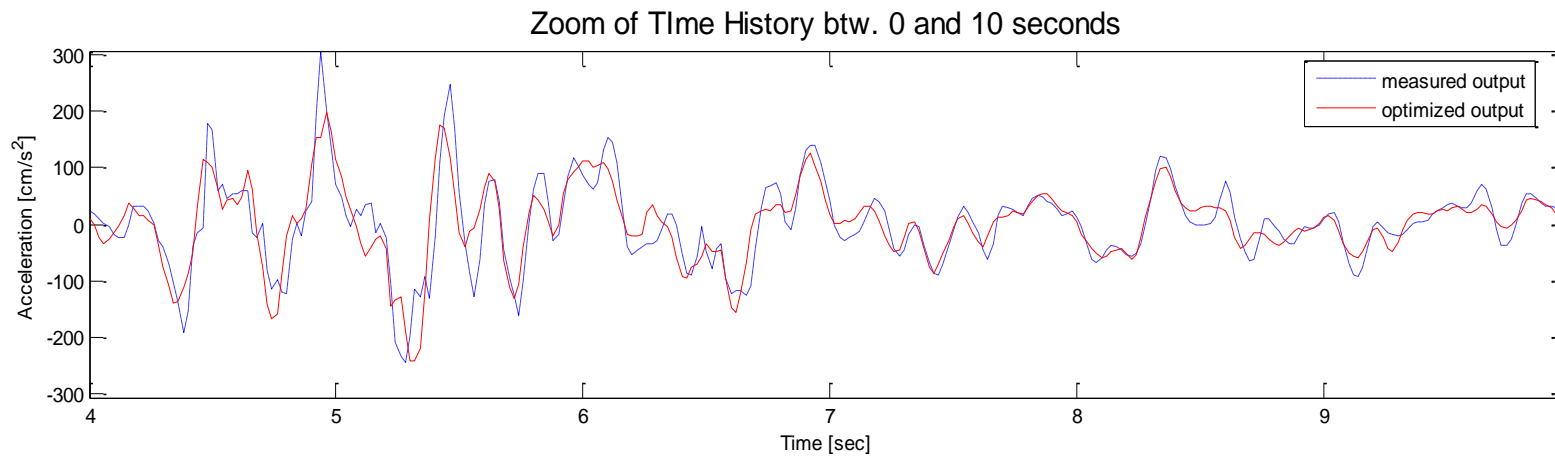
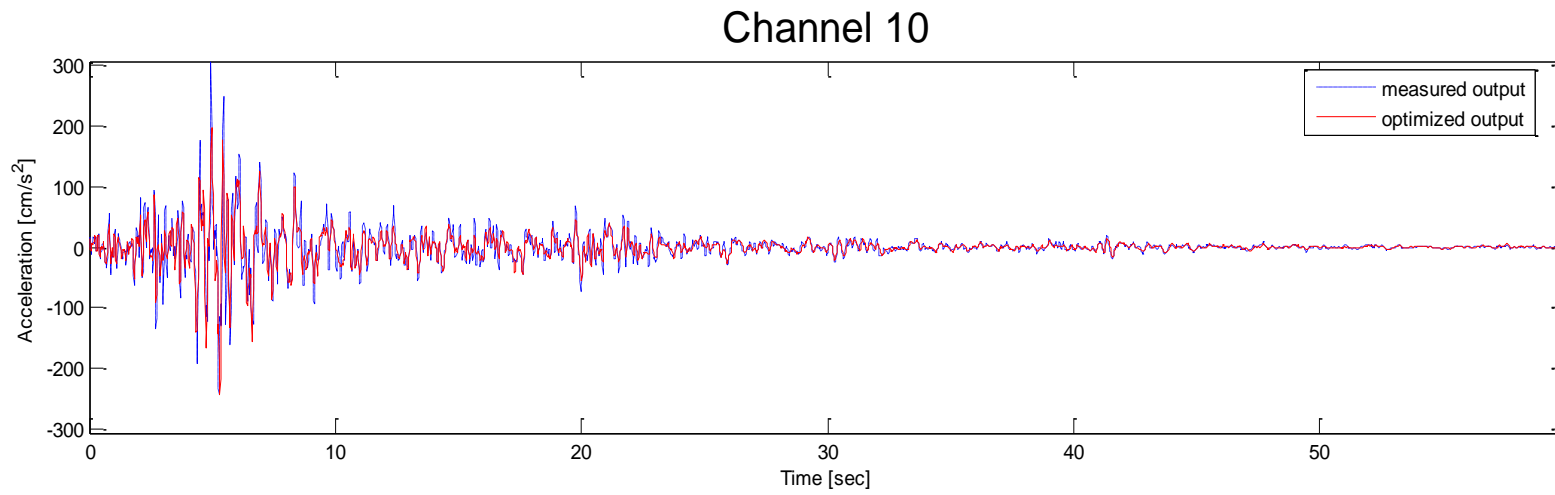


Figure 3.7g: Comparison between optimized and measured time History of channel 10

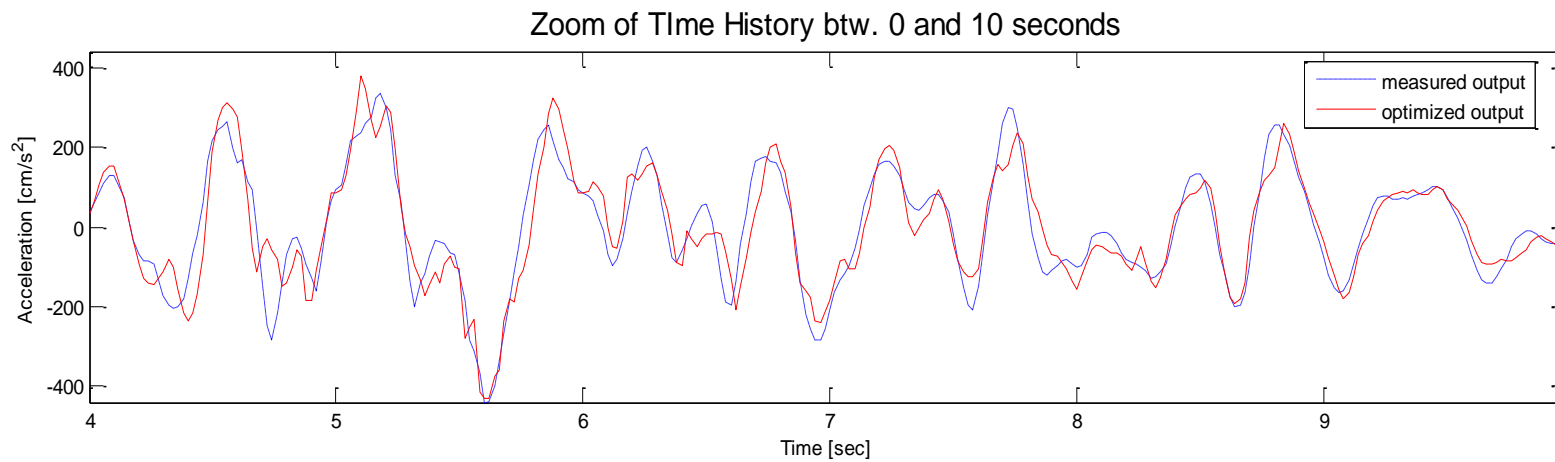
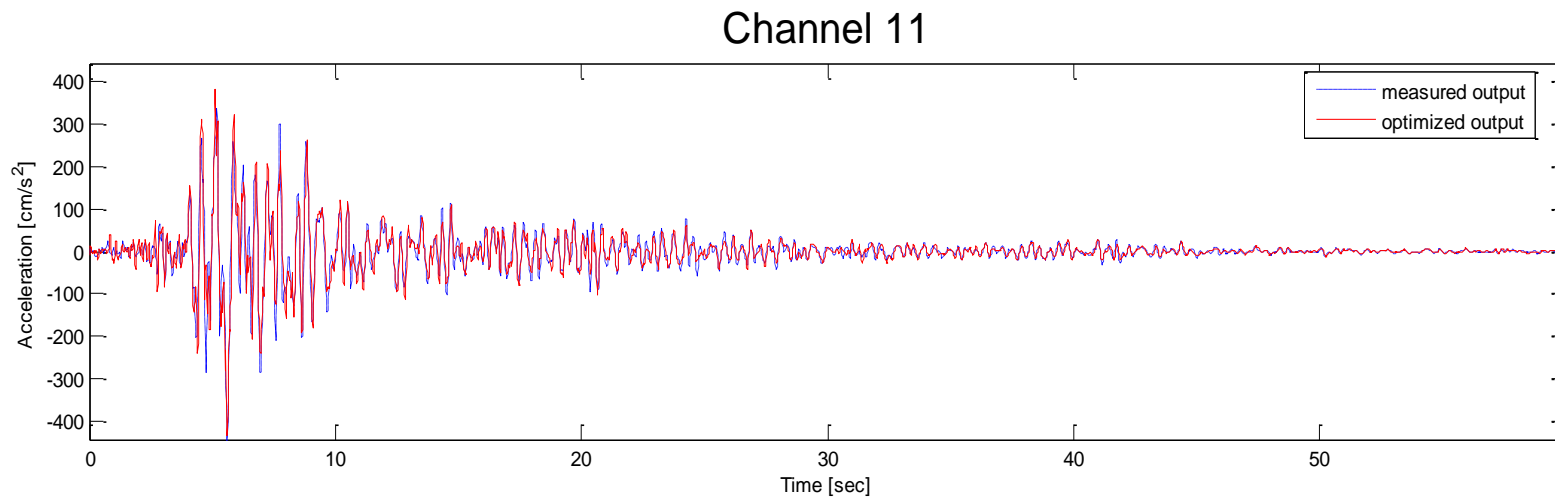


Figure 3.7h: Comparison between optimized and measured time History of channel 11

Mode 1: 3.366 Hz

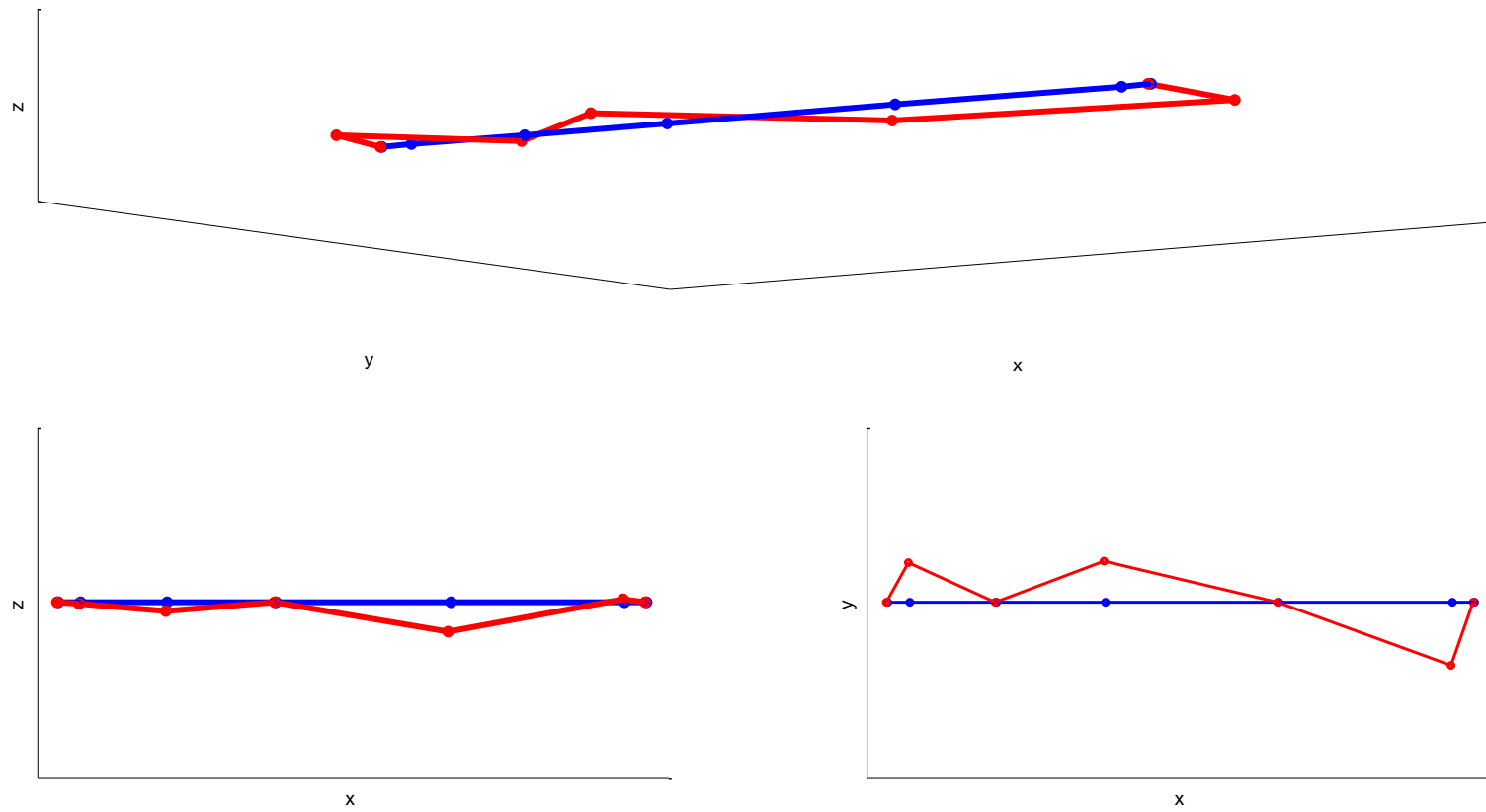


Figure 3.8a: First Identified Modal Shape

Mode 2: 4.382 Hz

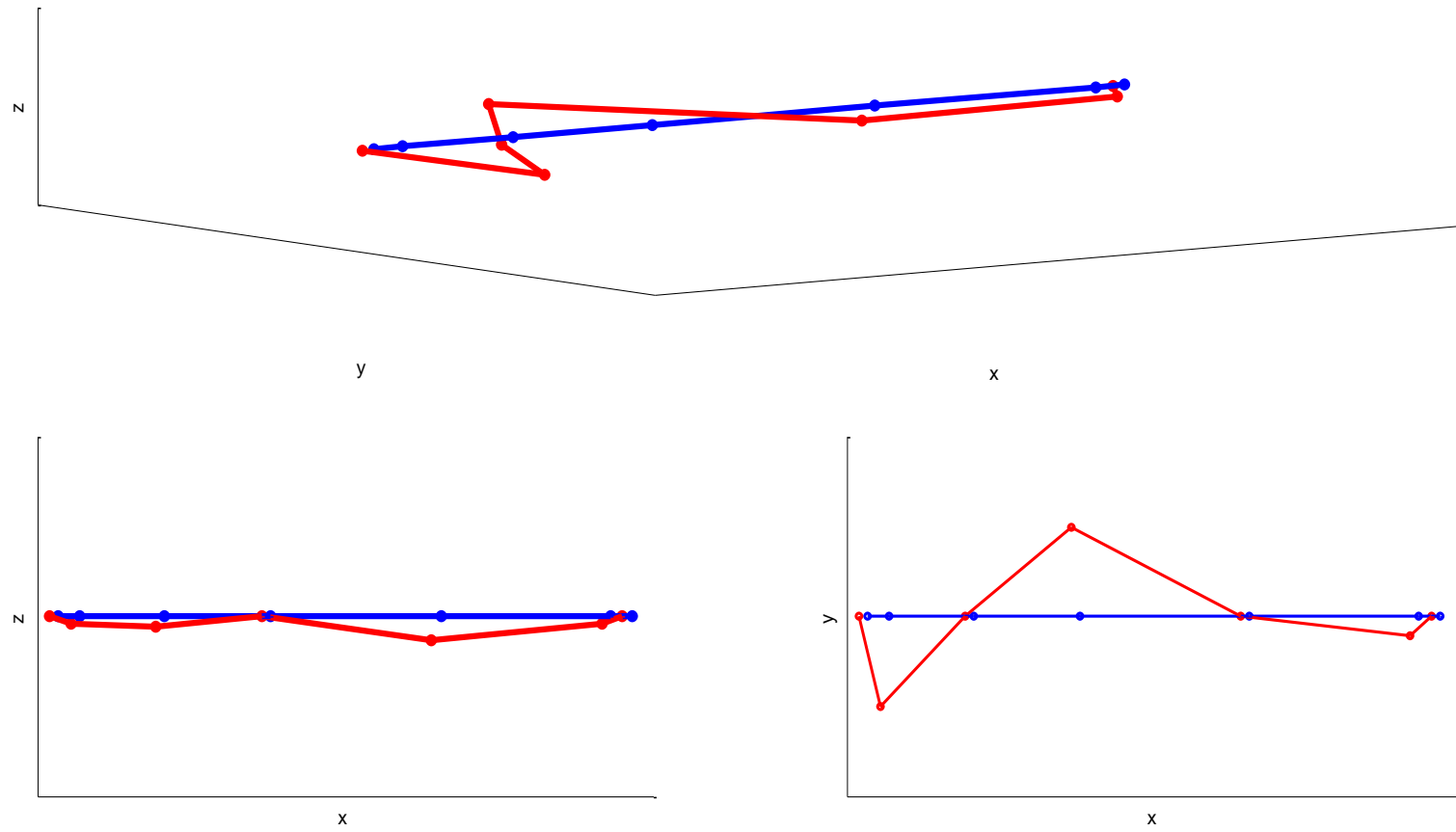


Figure 3.8b: Second Identified Modal Shape

Mode 3: 6.173 Hz

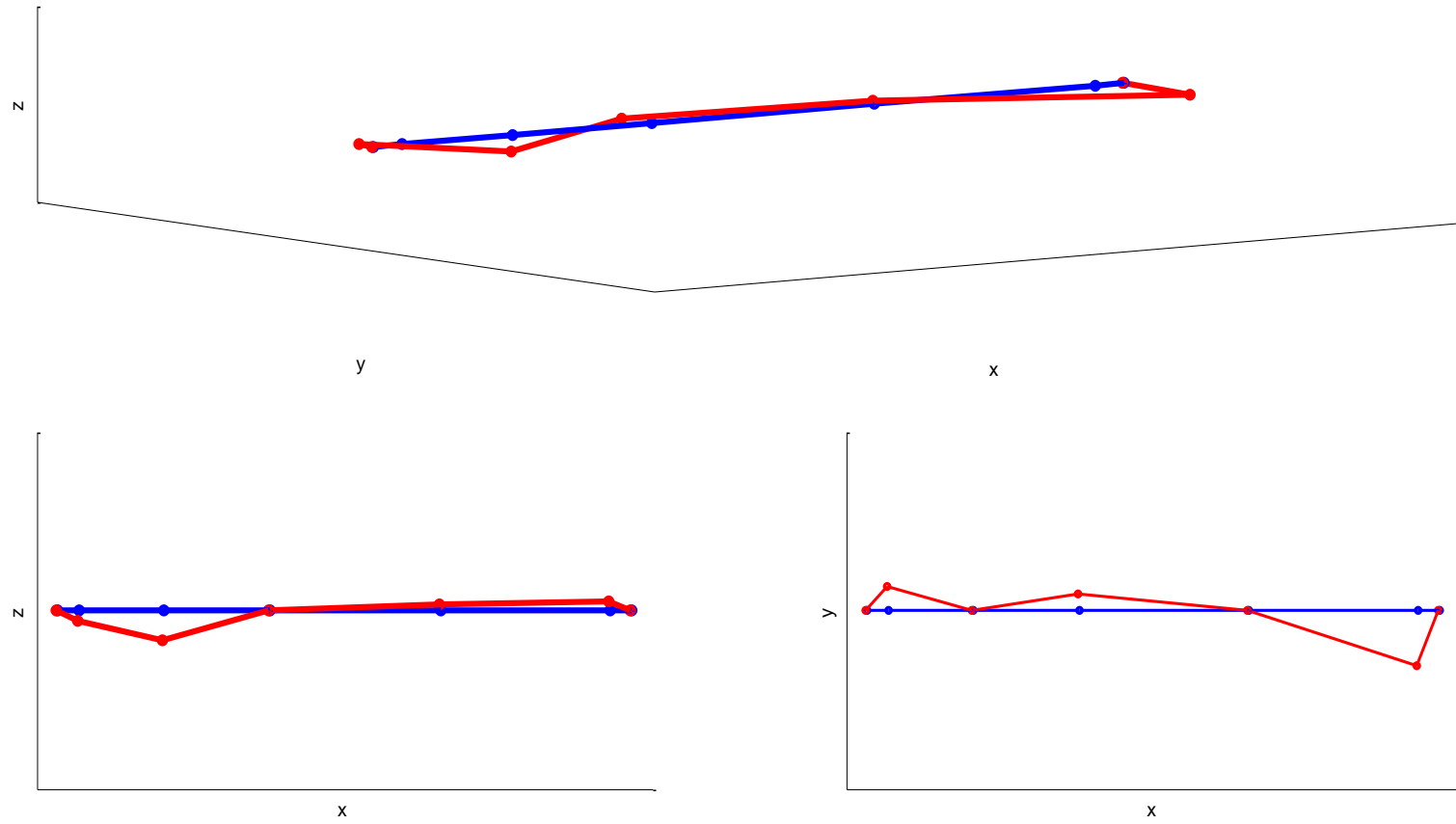


Figure 3.8c: Third Identified Modal Shape

4

FINITE ELEMENT MODEL

Sommario

Nel presente capitolo si mostra il lavoro svolto per la generazione di un modello agli elementi finiti della struttura in analisi. Per arrivare al modello finale, presentato nel quarto paragrafo, vari modelli di tentativo sono stati creati, con un livello di dettaglio sempre più alto. In particolare, tre modelli verranno presentati: il primo, estremamente semplice, avente l'unico scopo di delineare i valori da attribuire ai parametri che descrivono il materiale costituente il Rio Dell Overpass, è costituito da un elemento trave longitudinale rappresentate l'impalcato del ponte e altri due elementi travi verticali rappresentati le pile. Col secondo modello comincia lo studio vero e proprio delle ipotesi più adatte alla rappresentazione del sistema, particolarmente approfondito è l'analisi del comportamento trasversale del ponte e la ricerca della tipologia d'elemento che meglio riproduce il comportamento del ponte stesso. Nel terzo ed ultimo modello l'impalcato è costituito da elementi bidimensionali.

Ognuno dei sopraddetti modelli è considerato ragionevole quando i parametri modali che lo caratterizzano sono sufficientemente vicini a quelli individuati nel capitolo precedente.

Una volta che le caratteristiche dinamiche del modello agli elementi finiti siano soddisfacentemente vicine, comincia la fase di calibrazione che per questo lavoro è stata operata attraverso un algoritmo genetico. Tale fase rappresenta l'anello di congiunzione tra il lavoro portato a termine nell'identificazione strutturale e quello di modellazione della struttura e stabilisce le basi per la creazione dell'ultimo modello agli elementi finti, destinato a rappresentare l'attuale comportamento della struttura.

4.1 Introduction

The linear-elastic analysis of continuous body if formulated in terms of displacements leads to a system of partial differential equations. In the following will be briefly recalled the finite element method for a body with linear elastic behavior and assuming small displacements.

The closed form solution of the linear elasticity problem is possible only in some well defined cases. The finite element method is a numerical technique able to give an approximate solution to the problem under consideration, and , in general, to any problem defined by partial differential equations. The basis of the approach is replacing the differential problem with an algebraic one, and then solve the simplified new problem. Essentially, the finite element method permits the description of the behavior of an infinite degrees of freedom system through a finite set of parameters, that are the nodal characteristics.

To present the main idea of the method, let consider the surface of function $u(x,y)$, in figure 4.1, representing the unknown solution of a partial differential equation of the second order:

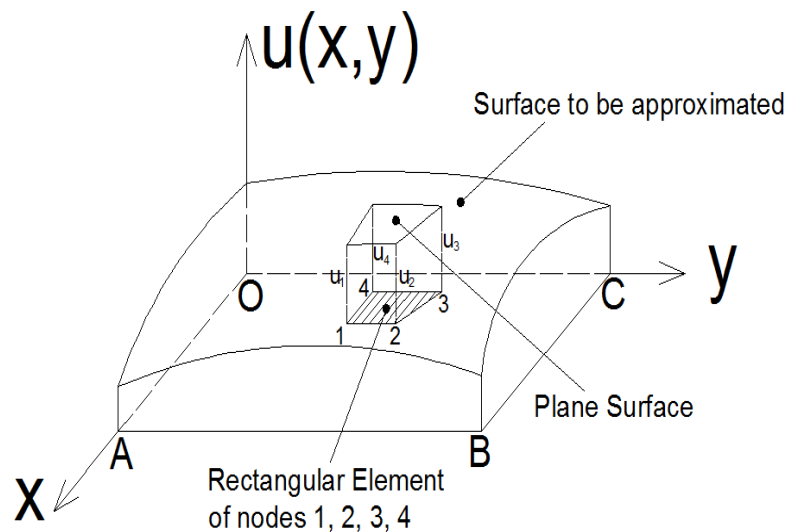


Figure 4.1: Approximation of Function $u(x,y)$ by Means of Interpolant Functions

The domain of the function is represented by the rectangle of corners OABC. Such a domain can be subdivided into a finite number of smaller sub-regions, called *elements*. In figure 4.1, for example, is indicated only one rectangular element. The vertices of the elements are denominated *nodes*. By discretizing the domain into N rectangular element, on each element the function $u(x, y)$ can be approximated through the following linear polynomial:

$$u^e(x, y) = a_1 + a_2x + a_3y + a_4xy \quad (4.1)$$

By means of the 4.1, the surface $u(x, y)$ may be approximated by a set of surfaces, each one defined correspondently to an element. The values u_1, u_2, u_3, u_4 of the function $u(x, y)$ at nodes 1, 2, 3, 4 respectively, are the nodal parameters, and are the unknown of the problem solvable by the finite element method. In place of the plane elements, one could have used curved elements, in this case the number of the polynomial coefficients would have increased, leading to an increase of the number of unknowns too. Surely, the function $u(x, y)$ would be better approximated, but the computational effort would increase.

No matter what is the approximation level, for each element, the internal points behavior t is represented by a sum of the kind shown by equation 4.2:

$$u(x, y) \cong \sum_{i=1}^n N_i u_i \quad (4.2)$$

where $N_i = N_i(x, y)$ is the *shape function* correspondent to the i -th node, and the unknowns $q_i = u_i$ are what we called *nodal parameters*.

Briefly, the finite element method, in its displacement formulation, is developed in the following six steps:

1. structure discretization;
2. evaluation of the element stiffness matrix and of the nodal forces vector;
3. element stiffness matrix and nodal forces vector assembly;
4. imposition of the boundary conditions;
5. solution of the resulting algebraic system of equations;
6. computation of the secondary characteristics, such as deformation and internal foces, from the gained nodal parameters.

4.2 Formulation of the Displacement-Based Finite Element Method

In this paragraph will be presented the finite element method procedure applied in the area of linear analysis of solids and structures. Indeed, this is where the numerical technique was applied and obtained its original thrust of development. Nowadays, many types of linear analyses of structures can be performed in a routine manner by using standard computer programs.

In the following, the displacement-based formulation method will be introduced: at first, the governing finite element equations will be evaluated and then the method convergence properties will be discussed. Finally, since the displacement-based formulation is not preferred for certain analysis, the use of mixed formulation will be introduced, in which, in addition to the displacements, other parameters are introduced as unknowns.

The displacement-based finite element method can be considered as an extension of the displacement method of analysis of beam and truss structures, for which the basic steps of the analysis are recalled next:

1. idealization of the total structure as a set of beam and truss elements interconnected at structural joints;
2. identification of the unknowns joint displacements that completely define the displacement response of the structural idealization;
3. formulation of the equilibrium equations corresponding to the unknown joint displacements and solution of the equations;
4. calculation of the internal element stress distribution;
5. interpretation of results, based on the assumptions used.

The solutions gained through displacement and finite element methods have a major difference: in the displacement method the exact element stiffness matrices (exact within the beam theory) could be evaluated. In fact, the stiffness properties of a beam element are physically the beam end forces corresponding to unit element end displacement. The named forces can be computed by solving the

partial differential equations of the equilibrium of the element, once the appropriate boundary conditions are applied. In these differential equations the three requirements of the exact solution are fulfilled, i.e. the stress equilibrium, the compatibility and the constitutive requirements are defined, therefore the exact element internal displacements and stiffness matrices can be computed. On the contrary, by using finite element technique, paired with Galerkin method, it is necessary to introduce some trial functions. This approach will lead to the “exact” solution only when such trial functions are the exact element internal displacements, otherwise, approximate stiffness coefficients will be obtained. Indeed, when applying the finite element method, the exact displacement functions are unknown, therefore, in using the variational approach one is obliged to employ trial function that approximate the actual displacements. As a result, the equilibrium equations are not satisfied in general, but the error can be reduced by increasing the mesh refinement.

It is worth to recall that the general formulation of the displacement-based finite element method is based on the use of the principle of displacements, equivalent to the use of either Galerkin or Ritz methods, where the last mentioned approach consists in minimizing the total potential energy of the system to find the equilibrium equations.

4.2.1 General Derivation of Finite Element Equilibrium Equations

Consider the equilibrium of a general three-dimensional body (figure 4.2), fixed in a reference coordinate system OXYZ. On the body surface area, the system is supported on Γ_u with prescribed displacements $\bar{\mathbf{u}}$ and subjected to surface tractions $\bar{\mathbf{t}}$ on the surface area Γ_t . Moreover, the forces per unit volume \mathbf{f}^B and concentrated load \mathbf{R}_C^i (I denotes the point of load application) are also applied to the body:

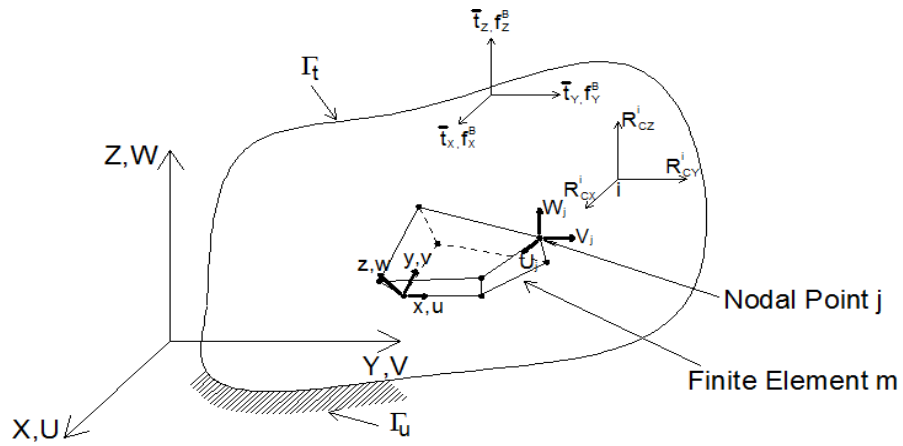


Figure 4.2: General Three-Dimensional Body with an 8-node Three Dimensional element

In general, the externally applied forces have three components corresponding to X, Y, Z coordinate axes:

$$\mathbf{f}^B = \begin{bmatrix} f_X^B \\ f_Y^B \\ f_Z^B \end{bmatrix}; \quad \bar{\mathbf{t}} = \begin{bmatrix} \bar{t}_X \\ \bar{t}_Y \\ \bar{t}_Z \end{bmatrix}; \quad \mathbf{R}_C^i = \begin{bmatrix} R_{CX}^i \\ R_{CY}^i \\ R_{CZ}^i \end{bmatrix}; \quad (4.3)$$

The displacements of the nody from the unloaded configuration are measured in the coordinate system OXYZ and are collected in the vector \mathbf{U} :

$$\mathbf{U} = \begin{bmatrix} U \\ V \\ Z \end{bmatrix} \quad (4.4)$$

and $\bar{\mathbf{U}}$ on the surface area Γ_u . The strain corresponding to \mathbf{U} are:

$$\begin{aligned} \boldsymbol{\varepsilon}^T &= [\varepsilon_X \quad \varepsilon_Y \quad \varepsilon_Z \quad \gamma_{XY} \quad \gamma_{XZ} \quad \gamma_{YZ}] = \\ &= \left[\frac{\partial U}{\partial X} \quad \frac{\partial V}{\partial Y} \quad \frac{\partial W}{\partial Z} \quad \frac{\partial U}{\partial Y} + \frac{\partial V}{\partial X} \quad \frac{\partial U}{\partial Z} + \frac{\partial W}{\partial X} \quad \frac{\partial V}{\partial Z} + \frac{\partial W}{\partial Y} \right] \end{aligned} \quad (4.5)$$

while the stresses corresponding to $\boldsymbol{\varepsilon}$ are:

$$\boldsymbol{\sigma}^T = [\sigma_X \quad \sigma_Y \quad \sigma_Z \quad \tau_{XY} \quad \tau_{XZ} \quad \tau_{YZ}] \quad (4.6)$$

where $\boldsymbol{\sigma} = \mathbf{C}\boldsymbol{\varepsilon} + \bar{\boldsymbol{\sigma}}$ where \mathbf{C} is the material matrix and $\bar{\boldsymbol{\sigma}}$ denotes the given initial stresses.

The problem we want to solve is the following: given the geometry of the body, the applied loads, the boundary conditions on Γ_u , the constitutive law and the initial stresses $\bar{\boldsymbol{\sigma}}$, calculate the displacement \mathbf{U} of the system and the corresponding strains $\boldsymbol{\varepsilon}$ and stresses $\boldsymbol{\sigma}$. In the problem solution proposed herein, linear analysis assumptions will be considered:

1. displacements infinitesimally small so that equation 4.5 is valid and the equilibrium of the body can be evaluated with respect to the undeformed configuration;
2. the material matrix \mathbf{C} does not depend on stress state.

4.2.1.1 The Principle of Virtual Displacements

It constitutes the basis of the displacement-based formulation for the finite element method. The principle states that the equilibrium of the body in figure 4.3 requires that for any compatible small virtual displacements imposed on the body in its state of equilibrium, the total internal virtual work is equal to the total external virtual work:

$$\int_V \hat{\boldsymbol{\varepsilon}}^T \boldsymbol{\sigma} dV = \int_V \hat{\mathbf{U}}^T \mathbf{f}^B dV + \int_{\Gamma_t} \hat{\mathbf{U}}^T \mathbf{t} dS + \sum_i \hat{\mathbf{U}}^{iT} \mathbf{R}_C^i \quad (4.7)$$

where the $\hat{\mathbf{U}}$ are the virtual displacements and the $\hat{\boldsymbol{\varepsilon}}$ are the corresponding virtual strains. It is important to note that the adjective ‘virtual’ denotes displacements and strains totally independent from the actual displacements and used with the only aim to evaluate the integral equilibrium equations. To clarify how the principle of virtual displacements can be used, assume to have been given a continuous displacement field that satisfies the boundary conditions on Γ_u and that is believed being the exact solution displacement field of the body. Therefore, it is possible to evaluate $\boldsymbol{\sigma}$ and $\boldsymbol{\varepsilon}$. The stresses vector $\boldsymbol{\sigma}$ will list the correct stresses if and only if the equation 4.7 holds for any arbitrary virtual displacements $\hat{\mathbf{U}}$ that are continuous and that satisfy the prescribed displacement on Γ_u . Meaning that if we can individuate a virtual displacement $\hat{\mathbf{U}}$ for which the 4.7 is not satisfied, then this proves that $\boldsymbol{\sigma}$ is not the correct stress vector, and hence the given displacement field is not the exact solution displacement field. Furthermore, the principle of virtual displacements can be directly related to the principle of stationarity of the total potential energy of the system. For a linear elastic continuum body with zero initial stresses, as the one presented in figure 4.2, the total potential energy can be expressed as in 4.8:

$$\Pi = \frac{1}{2} \int_V \boldsymbol{\varepsilon}^T \mathbf{C} \boldsymbol{\varepsilon} dV - \int_V \mathbf{U}^T \mathbf{f}^B dV - \int_{\Gamma_t} \bar{\mathbf{U}}^T \mathbf{t} dS - \sum_i \mathbf{U}^{iT} \mathbf{R}_C^i \quad (4.8)$$

The abovementioned principle states that of all of the configurations that a body can assume, under the action of the applied load, the equilibrium state is individuated by the configuration for which the total potential energy Π is stationary. Therefore, evaluating $\delta\Pi$, and make it vanishing, we find again equation 4.7:

$$\begin{aligned}\delta\Pi &= \int_V \delta\boldsymbol{\varepsilon}^T \mathbf{C} \boldsymbol{\varepsilon} dV - \int_V \delta\mathbf{U}^T \mathbf{f}^B dV - \int_{\Gamma_t} \delta\bar{\mathbf{U}}^T \bar{\mathbf{t}} dS - \sum_i \delta\mathbf{U}^{iT} \mathbf{R}_C^i \\ \Rightarrow \int_V \delta\boldsymbol{\varepsilon}^T \mathbf{C} \boldsymbol{\varepsilon} dV &= \int_V \delta\mathbf{U}^T \mathbf{f}^B dV + \int_{\Gamma_t} \delta\bar{\mathbf{U}}^T \bar{\mathbf{t}} dS + \sum_i \delta\mathbf{U}^{iT} \mathbf{R}_C^i\end{aligned}\quad (4.9)$$

Summarizing, by applying the principle of virtual work the following fundamental requirements are fulfilled:

1. equilibrium holds because the principle of virtual displacements is an expression of equilibrium;
2. compatibility holds because the displacements field \mathbf{U} is continuous and satisfies the displacement boundary conditions;
3. the constitutive law holds because the stresses $\boldsymbol{\sigma}$ have been calculated using the constitutive relationships from the strains $\boldsymbol{\varepsilon}$.

4.2.1.2 Finite Element Equations

So far it has always been assumed that the body of reference is properly supported. Nonetheless, in formulating the finite element equations, it results more convenient to assume to remove the supports and replace them with the correct reactions. In this case, the space Γ_u is zero, and the space Γ_t is identified with all of the body surface S . The first step in applying the finite element technique is discretized the body under consideration in n discrete finite elements interconnected at nodal points on the element boundaries. For each element, a convenient reference system xyz is then chosen, and the displacements within each element are assumed to be a function of the displacement at the N finite element nodal points. Therefore, for an element m it can be written that:

$$\mathbf{u}^m(x, y, z) = \mathcal{N}^m(x, y, z) \tilde{\mathbf{U}} \quad (4.10)$$

where \mathcal{N}^m is the shape functions matrix referred to element m , and $\tilde{\mathbf{U}}$ is a vector of the three global displacement components U_i, V_i, W_i at all nodal points. In figure 4.2, a typical finite element of the assemblage is shown, such an 8-node three-dimensional element is called brick. The body must be thought subdivided in many bricks put together in order to cover the entire domain, without leaving any gap. Of course, depending on the characteristics of the body under analysis, the shape of the elements can be very different: it is possible to handle with 1-, 2- or 3-dimensional elements, the number of the nodes for elements can vary, according to the kind of formulation chosen, moreover, for 2- and 3-dimensional elements, also the shape can vary. Starting from the definition given in 4.10, it is possible to define the element strains:

$$\boldsymbol{\varepsilon}^m(x, y, z) = \mathbf{D}\mathcal{N}^m(x, y, z) \tilde{\mathbf{U}} = \mathbf{B}^m \tilde{\mathbf{U}} \quad (4.11)$$

where it has been introduced the compatibility matrix \mathbf{D} and the strain-displacement matrix \mathbf{B}^m referred to the m element.

By constitutive equations, the stresses in finite element can be defined according to equation 4.12:

$$\boldsymbol{\sigma}^m(x, y, z) = \mathbf{C}\mathbf{B}^m \tilde{\mathbf{U}} + \bar{\boldsymbol{\sigma}}^m \quad (4.12)$$

Now we have all the ingredients to derive the equilibrium equations that correspond to the nodal point displacements of the set of finite elements. First of all, let rewrite the virtual displacement formula 4.11 as a sum of integrations over the volume and areas of all finite elements:

$$\sum_m \int_{V^m} \hat{\boldsymbol{\varepsilon}}^{mT} \boldsymbol{\sigma}^m dV^m = \sum_m \int_{V^m} \hat{\mathbf{u}}^{mT} \mathbf{f}^{Bm} dV^m + \sum_m \int_{S_1^m, \dots, S_q^m} \bar{\hat{\mathbf{u}}}^{mT} \bar{\mathbf{t}}^m dS^m + \sum_i \hat{\mathbf{u}}^{iT} \mathbf{R}_C^i \quad (4.13)$$

where $m=1, \dots, n$, and S denote element surfaces S_1^m, \dots, S_q^m part of the body surface S . It is important to note that in the use of principle of virtual displacements the same assumptions for the virtual displacements and strains are employed, in order to obtain a symmetric stiffness matrix:

$$\begin{aligned} \hat{\mathbf{u}}^m(x, y, z) &= \mathcal{N}^m(x, y, z) \hat{\mathbf{U}} \\ \hat{\boldsymbol{\varepsilon}}^m(x, y, z) &= \mathbf{B}^m(x, y, z) \hat{\mathbf{U}} \end{aligned} \quad (4.14)$$

By plugging the 4.14 into 4.13, equation 4.15 is obtained:

$$\begin{aligned} \hat{\mathbf{U}}^T \left[\sum_m \int_{V^m} \mathbf{B}^{mT} \mathbf{C}^m \mathbf{B}^m dV^m \right] \tilde{\mathbf{U}} &= \hat{\mathbf{U}}^T \left[\left\{ \sum_m \int_{V^m} \mathcal{N}^{mT} \mathbf{f}^{Bm} dV^m \right\} + \right. \\ &+ \left. \left\{ \sum_m \int_{S_1^m, \dots, S_q^m} \mathcal{N}^{mT} \bar{\mathbf{t}}^m dS^m \right\} + \right. \\ &\left. - \left\{ \sum_m \int_{V^m} \mathbf{B}^{mT} \bar{\boldsymbol{\sigma}}^m dV^m \right\} + \mathbf{R}_C \right] \end{aligned} \quad (4.15)$$

To obtain the equations for the unknown nodal point displacements from equation 4.15, it is necessary to apply the principle of virtual displacement n times by imposing unit virtual displacements in turn for all components of $\hat{\mathbf{U}}$, so that the result is:

$$\mathbf{KU} = \mathbf{R} \quad (4.16)$$

where

$$\begin{aligned} \mathbf{K} &= \sum_m \int_{V^m} \mathbf{B}^{mT} \mathbf{C}^m \mathbf{B}^m dV^m = \sum_m \mathbf{K}^m && \text{stiffness matrix} \\ \mathbf{R} &= \mathbf{R}_B + \mathbf{R}_S - \mathbf{R}_I + \mathbf{R}_C && \text{load vector} \\ \mathbf{R}_B &= \sum_m \int_{V^m} \mathcal{N}^{mT} \mathbf{f}^{Bm} dV^m = \sum_m \mathbf{R}_B^m && \text{element body forces} \\ \mathbf{R}_S &= \sum_m \int_{S_i^m, \dots, S_q^m} \mathcal{N}^{mT} \bar{\mathbf{t}}^m dS^m = \sum_m \mathbf{R}_S^m && \text{element surface forces} \\ \mathbf{R}_I &= \sum_m \int_{V^m} \mathbf{B}^{mT} \boldsymbol{\sigma}^m dV^m = \sum_m \mathbf{R}_I^m && \text{element initial stresses} \end{aligned} \quad (4.17)$$

Equation 4.14 is obtained by an operation called of assembly performed on the elements stiffness matrices and load vectors: for example, to obtain the total body stiffness matrix \mathbf{K} , it is necessary to expand the element stiffness matrix to the body size and then directly add the resulting \mathbf{K}^m matrices.

The method is completed by applying the boundary conditions and solving the resulting system of equations 4.16. From the determined displacements is then possible retrieving the secondary quantities, as deformations, stresses and internal forces.

4.2.2 Finite Element Formulation for Euler-Bernoulli Beams

The Euler-Bernoulli beam theory is appropriate for slender beams, for which the deformations can be considered small. Let consider an Euler-Bernoulli beam subjected to a uniform distributed load over its total length:

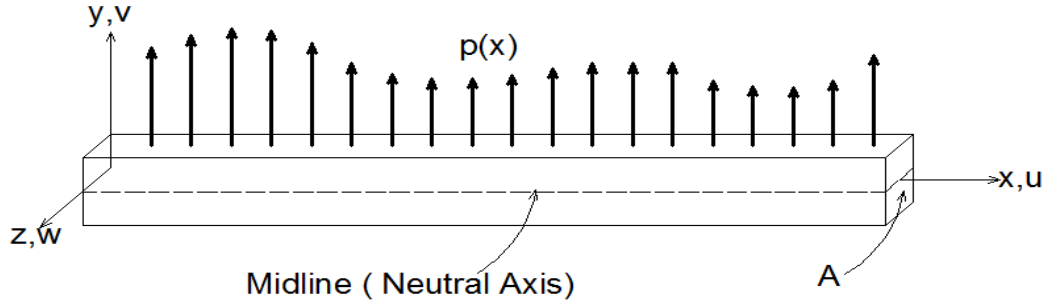


Figure 4.3: Euler-Bernoulli Beam Subjected to Uniform Distributed Load

By combining compatibility, Hooke's Law and equilibrium, it is possible to get the well known equation representing the bending behavior of the beam. Moreover, imposing the boundary conditions, finally one can write the strong form of the problem:

$$(S) \left\{ \begin{array}{ll} \frac{d^2}{dx^2} \left(EI \frac{d^2 v}{dx^2} \right) - p(x) = 0 & \text{in } \Omega \\ v = \bar{v} & \text{on } \Gamma_u \text{ Displacement} \\ \frac{dv}{dx} = \bar{\theta} & \text{on } \Gamma_\theta \text{ Angle} \\ EI \frac{d^2 v}{dx^2} = \bar{M} & \text{on } \Gamma_M \text{ Bending Moment} \\ -EI \frac{d^3 v}{dx^3} = \bar{S} & \text{on } \Gamma_S \text{ Shear Force} \end{array} \right. \quad (4.18)$$

To apply the finite element formulation, it is now necessary to multiply the first, the fourth and the fifth equations of the 4.18 by w and then integrate over the domain:

$$\begin{aligned}
& \int_0^1 w[(EIv'')'-p(x)]dx = 0 \\
& [w'(EIv''-\bar{M})]_{\Gamma_M} = 0 \\
& [w(-EIv'''-\bar{S})]_{\Gamma_S} = 0
\end{aligned} \tag{4.19}$$

Then, integrating by part the first of the 4.19, it is possible to arrive at the weak form:

$$(W) \left\{ \begin{aligned}
& \text{Find } v \in S \text{ such that} \\
& \int_0^1 w''EI v'' dx = \int_0^1 w p(x) v'' dx + [w'\bar{M}]_{\Gamma_M} + [w\bar{S}]_{\Gamma_S} \quad \forall w \in S^0 \\
& S = \{v \mid v \in C^1, v = \bar{v} \text{ on } \Gamma_u, v' = \bar{\theta} \text{ on } \Gamma_\theta\} \\
& S^0 = \{w \mid w \in C^1, w = 0 \text{ on } \Gamma_u, w' = 0 \text{ on } \Gamma_\theta\}
\end{aligned} \right. \tag{4.20}$$

The space C^1 is the set of continuous functions with continuous first derivative. It can be observed that the first term of the 4.20 is symmetric in w and v , that will lead to a symmetric stiffness matrix.

The next step consists in discretize the space domain:

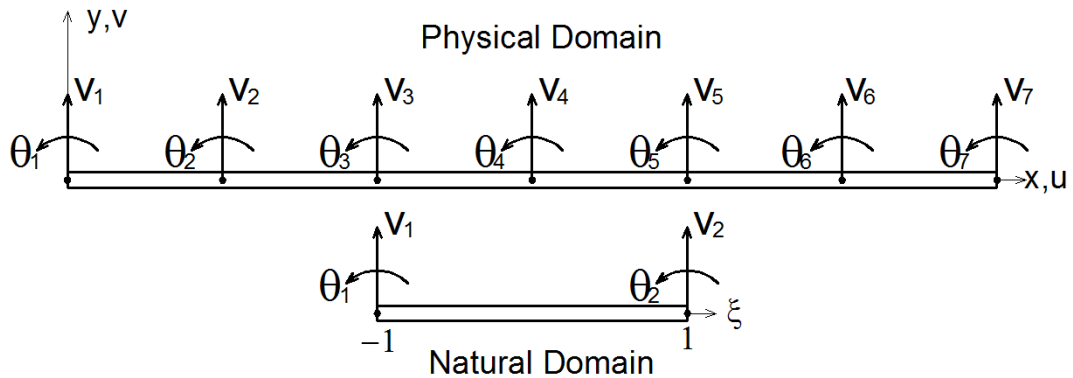


Figure 4.4: Space Discretization

For this particular case, the Hermite functions are employed as shape functions: they are cubic functions whose expression is given in 4.21:

$$\begin{aligned}
H_I &= a_I + b_I \xi + c_I \xi^2 + d_I \xi^3 \\
H_1 &= \frac{1}{4}(1-\xi)^2(2+\xi) \\
H_2 &= \frac{1}{4}(1-\xi)^2(1+\xi) \\
H_3 &= \frac{1}{4}(1+\xi)^2(2-\xi) \\
H_4 &= \frac{1}{4}(1+\xi)^2(\xi-1)
\end{aligned} \tag{4.21}$$

Through the 4.21, the displacement is approximated by:

$$\begin{aligned}
v^e(\xi) &= H_1 v_1 + H_2 \theta_1 + H_3 v_2 + H_4 \theta_2 = \\
&= H_1 v_1 + H_2 \left(\frac{dv}{d\xi} \right)_1 + H_3 v_2 + H_4 \left(\frac{dv}{d\xi} \right)_2
\end{aligned} \tag{4.22}$$

and from coordinate transformation:

$$\begin{aligned}
x &= \frac{1-\xi}{2} x_1^e + \frac{1+\xi}{2} x_2^e \\
dx &= \frac{l^e}{2} d\xi \Rightarrow \frac{dv}{d\xi} = \frac{l^e}{2} \frac{dv}{dx}
\end{aligned} \tag{4.23}$$

Applying the Galerkin's method:

$$\begin{aligned}
v^e &= H^e d^e \\
w^e &= H^e w^e
\end{aligned} \tag{4.24}$$

where :

$$d^T = [v_1 \quad \theta_1 \quad v_2 \quad \theta_2]$$

Once computed the derivative of $v(x)$ and substituted everything back into the 4.20, finally we obtain the discrete problem where the stiffness matrix K is obtained by assembling the element stiffness matrices given by 4.25:

$$\mathbf{K}^e = \frac{EI}{(l^e)^3} \begin{bmatrix} 12 & 6l^e & -12 & 6l^e \\ 6l^e & 4(l^e)^2 & -6l^e & 2(l^e)^2 \\ -12 & -6l^e & 12 & -6l^e \\ 6l^e & 2(l^e)^2 & -6l^e & 4(l^e)^2 \end{bmatrix} \quad (4.25)$$

while the force vector, assuming constant distributed force, is collected once assembled the element force vectors given by the 4.26:

$$\mathbf{f}^e = \frac{pl^e}{2} \begin{bmatrix} 1 \\ l^e/6 \\ 1 \\ l^e/6 \end{bmatrix} \quad (4.26)$$

4.2.3 Finite Element Formulation for Plates and Shells

A plate is a three dimensional body with one dimension much smaller than the other two, and the curvature of the plate mid-surface in the reference configuration equal to zero. On the other hand, a shell is a three dimensional body with one of the dimension much smaller than the other two, but with non-zero curvature of the plate mid-surface in the current configuration. Therefore, as can be easily understood, plates and shells are special case of 3D solids. Nonetheless, the use of the plate/shell elements is preferable when the thickness of the system is negligible compared to the other dimensions. In this case full 3D numerical treatment is costly and leads to serious ill-conditioning problems. Moreover, the plate/shell theory should be employed only to system subjected to very smooth loading. Nonetheless, if we are interested in global behavior, local details may be neglected. Table 4.1 gives a guideline for the theory to use depending on the geometrical and behavioral characteristics of the system under analysis:

	<i>Thick</i>	<i>Thin</i>	<i>Very Thin</i>
<i>L/t</i>	From 5 to 10	From 10 to 100	Greater than 100
<i>Characteristics</i>	With transverse shear deformation	Without Transverse Shear Deformation	Geometrically Non-Linear
<i>Plate Theory</i>	Reissner-Mindlin	Kirchhoff-Love	Von Karman
<i>Beam Theory</i>	Timoshenko in 2D	Euler Bernoulli in 2D	

Table 4.1: Different Plate Theories

4.2.3.1 Kirchhoff Plate

The Kirchhoff-Love theory is the plate/shell theory corresponding to the Euler-Bernoulli theory for the beams. In fact, the key assumptions of this theory are the following:

1. geometrically linear systems: small strains and deformations;
2. linear elastic material (Hooke's Law can be employed);
3. plane normal to the plate mid-surface in the undeformed configuration remains normal to that plane in the deformed shape. This implies that the transverse shear strains with respect to the z-axis are null:

$$\gamma_{xz}=0; \gamma_{yz} = 0$$

4. the dilatation ϵ_z is negligible;
5. the displacement along the plate thickness are much smaller than the thickness itself, therefore, the in-plane forces are neglected, leading to the the following simplifications:

$$u = u(x, y, 0) = 0$$

$$v = v(x, y, 0) = 0$$

$$w = w(x, y, 0)$$

Figure 4.5 represents the stress configuration of a plate treated through Kirchhoff-Love theory:

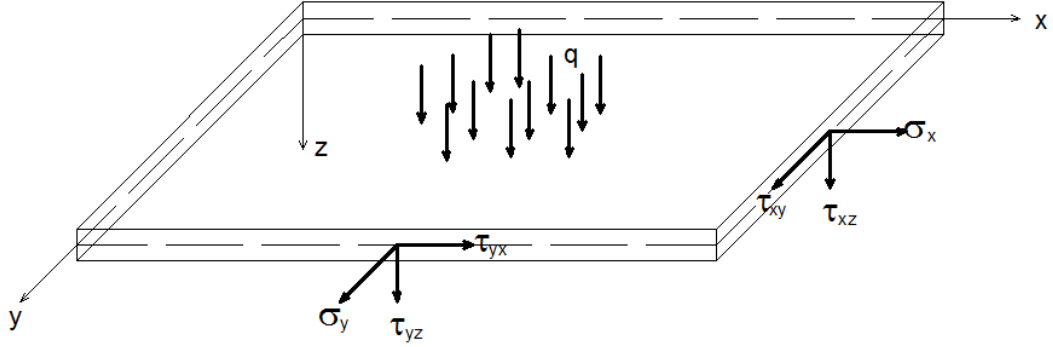


Figure 4.5: Stress Configuration for the Kirchhoff-Love Theory

From the Kirchhoff assumptions theory derive the following expressions:

$$\begin{aligned} u &= z \frac{\partial w}{\partial x} \\ v &= z \frac{\partial w}{\partial y} \end{aligned} \quad (4.27)$$

Once define the curvature of the plate according to equation 4.28:

$$\mathbf{k}^T = [\mathbf{k}_x \quad \mathbf{k}_y \quad \mathbf{k}_z] = \begin{bmatrix} \frac{\partial^2 w}{\partial x^2} & \frac{\partial^2 w}{\partial y^2} & 2 \frac{\partial^2 w}{\partial x \partial y} \end{bmatrix} \quad (4.28)$$

in-plane strain-displacement equations become:

$$[\varepsilon_x \quad \varepsilon_y \quad \gamma_z] = -z[\mathbf{k}_x \quad \mathbf{k}_y \quad \mathbf{k}_z] \quad (4.29)$$

and assuming plane-stress conditions, the constitutive equations are:

$$\begin{bmatrix} \sigma_x \\ \sigma_y \\ \tau_{xy} \end{bmatrix} = \frac{E}{1-\nu^2} \begin{bmatrix} 1 & \nu & 0 \\ \nu & 1 & 0 \\ 0 & 0 & \frac{1-\nu}{2} \end{bmatrix} \begin{bmatrix} \varepsilon_x \\ \varepsilon_y \\ \gamma_{xy} \end{bmatrix} = -\frac{Ez}{1-\nu^2} \begin{bmatrix} 1 & \nu & 0 \\ \nu & 1 & 0 \\ 0 & 0 & \frac{1-\nu}{2} \end{bmatrix} \begin{bmatrix} \mathbf{k}_x \\ \mathbf{k}_y \\ \mathbf{k}_{xy} \end{bmatrix} \quad (4.30)$$

From the stresses definition, via static equivalence, the moments can be retrieved, and then, the equilibrium equations are:

$$\begin{aligned}\frac{\partial M_x}{\partial x} + \frac{\partial M_{xy}}{\partial y} - Q_x &= 0 \\ \frac{\partial M_{xy}}{\partial x} + \frac{\partial M_y}{\partial y} - Q_y &= 0 \\ \frac{\partial Q_x}{\partial x} + \frac{\partial Q_y}{\partial y} + p &= 0\end{aligned}\tag{4.31}$$

It is easy to observe that the shear forces Q can be defined as function of the moment M , by plugging the results into the third of the 4.31, a biharmonic equation is obtained:

$$\frac{Eh^3}{12(1-\nu^2)} \left(\frac{\partial^4 w}{\partial x^4} + 2 \frac{\partial^4 w}{\partial x^2 \partial y^2} + \frac{\partial^4 w}{\partial y^4} \right) = p\tag{4.32}$$

Now, let consider the a 3-node triangular element (with three degrees of freedom per node), the displacement $w(x, y)$ can be approximated as:

$$\begin{aligned}w(x, y) = a_1 + a_2x + a_3y + a_4x^2 + a_5xy + \\ + a_6y^2 + a_7x^3 + a_8(x^2y + y^2x) + a_9y^3\end{aligned}\tag{4.33}$$

and the nodal displacement vector can be then defined as:

$$\begin{aligned}\mathbf{d} &= \overline{\mathbf{X}} \mathbf{a} \\ \text{where} \\ \mathbf{d}^T &= [w_1 \quad (w_x)_1 \quad (w_y)_1 \quad w_2 \quad (w_x)_2 \quad (w_y)_2 \quad w_3 \quad (w_x)_3 \quad (w_y)_3] \\ \mathbf{X}^T &= [1 \quad x \quad y \quad x^2 \quad xy \quad y^2 \quad x^3 \quad x^2y + y^2x \quad y^3] \\ \mathbf{a}^T &= [a_1 \quad a_2 \quad a_3 \quad a_4 \quad a_5 \quad a_6 \quad a_7 \quad a_8 \quad a_9]\end{aligned}\tag{4.34}$$

and finally the stiffness matrix is easily evaluable.

4.2.3.21 Reissner-Mindlin Plate

The computation of the stiffness matrix for the Reissner-Mindlin formulation is instead a little more complicated. In fact, for this theory the transverse shear deformation is not neglected, leading to the problem of shear locking. Essentially this phenomenon leads to a non-convergent solution when the traditional computation of the stiffness matrix is employed. To avoid such a problem, once defined the degrees of freedom of the element, that for a 4-node quadrilateral element with three degrees of freedom per node are:

$$\begin{aligned} w^e &= N_i(\xi, \eta) w_i \\ \theta_x^e &= N_i(\xi, \eta) (\theta_x)_i \\ \theta_y^e &= N_i(\xi, \eta) (\theta_y)_i \end{aligned} \quad (4.35)$$

it is possible to construct the stiffness matrix in the following way:

$$\mathbf{K}^e = \mathbf{K}_b^e + \mathbf{K}_S^e = \frac{h^3}{12} \int_{\Omega^e} \mathbf{B}_b^T \mathbf{D}_b \mathbf{B}_b \, d\Omega + \kappa h \int_{\Omega^e} \mathbf{B}_S^T \mathbf{D}_S \mathbf{B}_S \, d\Omega \quad (4.36)$$

where the first term represents the exact integration, performed according the 2×2 Gauss Quadrature technique, while the second term is obtained through a reduced integration performed following the 1-point Gauss Quadrature. It is the introduction of this second term that avoids shear locking.

4.2.3 Modal Analysis

Modal analysis is used to determine the vibration modes of a structure, that are useful tools to understand the behavior of a structure. In the following, the results shown are those obtained via the usual modal analysis, i.e. with the analysis that determines the undamped free-vibration modal parameters of the system. The aim of a standard modal analysis is that of calculate the mode shapes and frequencies of the structure under analysis.

Let consider an undamped system of N degrees of freedom, with no force applied. System 4.37 represents the set of equations of motion that give the dynamical behavior of the system:

$$[\mathbf{m}]\{\ddot{\mathbf{u}}\} + [\mathbf{k}]\{\mathbf{u}\} = \{\mathbf{0}\} \quad (4.37)$$

where $[\mathbf{m}]$ is the mass matrix of the system, $[\mathbf{k}]$ its stiffness matrix, and $\{\mathbf{u}\}$ the vector of displacements. Now, set $\{\mathbf{u}(t)\}$ as

$$\{\mathbf{u}\} = \{\boldsymbol{\phi}\}g(t) \quad (4.38)$$

where $\{\boldsymbol{\phi}\}$ is a $N \times 1$ vector, and plug 4.38 into the equation of motion:

$$\begin{aligned} \ddot{g}(t)[\mathbf{m}]\{\boldsymbol{\phi}\} + g(t)[\mathbf{k}]\{\boldsymbol{\phi}\} &= \{\mathbf{0}\} \\ \Rightarrow \frac{[\mathbf{k}]\{\boldsymbol{\phi}\}}{[\mathbf{m}]\{\boldsymbol{\phi}\}} &= -\frac{\ddot{g}(t)}{g(t)} = \omega^2 \end{aligned} \quad (4.39)$$

where it has been introduced the constant ω^2 . The 4.39 leads to a system of two equations, in which the first represents an eigenvalues problem, while the second gives the equation of harmonic motion:

$$\begin{cases} ([\mathbf{k}] - \omega^2[\mathbf{m}])\{\boldsymbol{\phi}\} = 0 \\ \ddot{g}(t) + \omega^2g(t) = 0 \end{cases} \quad (4.40)$$

The modal analysis the first equation of 4.40 by setting equal to zero the determinant of the matrix into round brackets: the positive square roots of the eigenvalues represent the so called natural frequencies of the system, while the corresponding eigenvectors represent its modal shapes. From the natural frequency it is easy to get the cyclic frequencies f and the modal periods:

$$\begin{cases} f = \frac{\omega}{2\pi} \\ T = \frac{1}{f} \end{cases} \quad (4.41)$$

Obviously, once solved, the eigenvalue problem in equation 4.40 gives as many natural frequencies as the number of degrees of freedom. Conventionally, modes are ordered with respect to the frequencies: the smallest modal frequency represents the first mode, the biggest modal frequency represents the N-th mode. By combining the modal shape, one gets the deformed configuration of the system. The modal superposition is possible only because the system under analysis is linear. It is important to underline that this superposition does not occur by a simple sum of the various terms, but it can be thought as a weighted sum: the first modes count more than the last, meaning that the first modes give a larger contribute to the overall deformation of the system than the last. Because of this consideration, the majority of the computational programs allows the user to choose to compute only some modes, i.e. the ones identified by small values of natural frequencies.

Let come back to the solution of the eigenvalue problem in 4.4, it can be demonstrated that:

$$\begin{aligned} \{\phi\}^T [\mathbf{m}] \{\phi\} &= \delta_{rs} M_r \\ \{\phi\}^T [\mathbf{k}] \{\phi\} &= \delta_{rs} K_r \end{aligned} \quad (4.42)$$

The 4.42 represents the orthogonality property of natural modes, and allows to drastically simplify the problem to solve. In fact, due to this property, the mass and stiffness matrices are transformed into diagonal matrices. Therefore, the system of N equations in N unknowns linearly dependent becomes a system of N equations with N unknowns linearly independent: every equation represents the equation of motion of a single degree of freedom system, very easy to solve.

4.2.3.1 Verification Example: Modal Analysis of a Beam via STRAUS7 and SAP2000

In order to prove the equivalence of the two programs, in the following a simple problem is solved with both Straus7 and SAP2000. Results are compared to the exact ones, obtained via analytical solution.

The problem considered is that of a concrete undamped cantilever beam in free-vibration 96 inches long. The material properties given to the system are the following:

Young Modulus (E): 3,600 kip/in²

Mass per Volume (m): 2.3 × 10⁻⁷ kip-sec²/in⁴

while the cross section characteristics are:

b = 12 in

d = 18 in

A = 216 in²

I_y = 5,832 in⁴

I_z = 2,592 in⁴

With these values, the first three modes for a cantilever beam, derived from the solution of the equation of motion, are given by the following expressions:

$$\begin{aligned}\omega_1 &= 1.875^2 \sqrt{\frac{EI}{\bar{m}L^4}} \\ \omega_2 &= 4.694^2 \sqrt{\frac{EI}{\bar{m}L^4}} \\ \omega_3 &= 7.855^2 \sqrt{\frac{EI}{\bar{m}L^4}}\end{aligned}\tag{4.43}$$

where:

I is the moment of inertia with respect either to the weak (z) and strong (y) axis

\bar{m} is the mass per unit length ($\bar{m} = m \times A$)

Plugging the values of the parameters just defined, the first six modes are characterized by the natural frequencies and periods given in table 4.2:

Mode	Expression	Frequency [rad/sec]	Frequency [Hz]	Periods [sec]
1	$\omega_1 = 1.875^2 \sqrt{\frac{EI_z}{\bar{m}L^4}}$	165.32481	26.3122608	0.038005
2	$\omega_2 = 1.875^2 \sqrt{\frac{EI_y}{\bar{m}L^4}}$	247.987216	39.4683912	0.025337
3	$\omega_3 = 4.694^2 \sqrt{\frac{EI_z}{\bar{m}L^4}}$	1036.14768	164.9080254	0.006064
4	$\omega_4 = 4.694^2 \sqrt{\frac{EI_y}{\bar{m}L^4}}$	1554.22152	247.3620381	0.004043
5	$\omega_5 = 7.855^2 \sqrt{\frac{EI_z}{\bar{m}L^4}}$	2901.53536	461.7936957	0.002165
6	$\omega_6 = 7.855^2 \sqrt{\frac{EI_y}{\bar{m}L^4}}$	4352.30305	692.6905435	0.001444

Table 4.2: Modal Parameters for a cantilever beam computed analytically

The same problem is then solved with the two design program. It is important to note that the solution presented in table 4.2 take into account only the bending modes, therefore, in order to get results close to the analytical ones, it is necessary to not consider the shear deformation and the axial and torque contribute. In SAP2000 the first assumption is obtained by setting equal to zero the shear areas, while the second is respected by canceling out the torsion coefficient and ignoring both the axial translation and the rotation with respect to the longitudinal direction. In order to get results resembling the analytical ones in STRAUS7, it is necessary to cancel out the terms of shear area and inertia, to fix the rotation around the x-axis and the translation along the same axis, and impose consistent the mass distribution, operation set by default in SAP2000.

In table 4.3 are presented the results got from both programs by using a model consisting in 96 line elements, each one 1 inch long:

Mode	SAP2000		STRAUS7	
	<i>Freq. [Hz]</i>	<i>Period [sec]</i>	<i>Freq. [Hz]</i>	<i>Period [sec]</i>
1	26.314	0.038	26.536	0.038
2	39.471	0.025	39.654	0.025
3	164.89	0.006	163.381	0.006
4	247.33	0.004	239.074	0.004
5	461.63	0.002	445.178	0.002
6	692.45	0.001	632.683	0.002

Table 4.3: Comparison between results of SAP2000 and STRAUS7

It is apparent that the solution obtained with the two programs is really similar; nonetheless, it can be observed that results obtained with SAP2000 are closer to the analytical ones. Then, the last mentioned program will be used to build the final model, although the results got via STRAUS7 can be considered reliable.

4.3 Finite Element Models

4.3.1 First Model: the Beam Model

This model is considerable as a benchmark for the definition of some fundamental characteristics of the system. One of the main topic to explore is the definition of the material characteristics. In fact, the Rio Dell Overpass plans available (Appendix A) give some indication that have to be considered erroneous: the compressive strength of the concrete used is set equal to 12 psf, that is a value too low for a structure such as that analyzed.

The model here proposed is composed by a unique longitudinal beam representing the deck, and two vertical beams representing the piers. The objective is finding the concrete characteristics such that the lowest modal frequencies are appreciably close to the ones individuated in the structural identification via OKID/ERA. It is well known that the modal frequencies depend on the mass and on the stiffness of the system, therefore, if the choice of the material parameters is correct, the first modal characteristics will be close to the structural ones.

Appreciable results are obtained by choosing the following values for the materials:

Compressive Strength:	4 ksi
Young Modulus E:	4,490.369 ksi
Poisson Coefficient ν :	0.2
Shear Modulus G:	1,870.987 ksi
Density ρ :	$2.695 \cdot 10^{-7} \text{ lb/ft}^3$

The deck is modeled with a unique beam element with the section shown by figure 4.6:

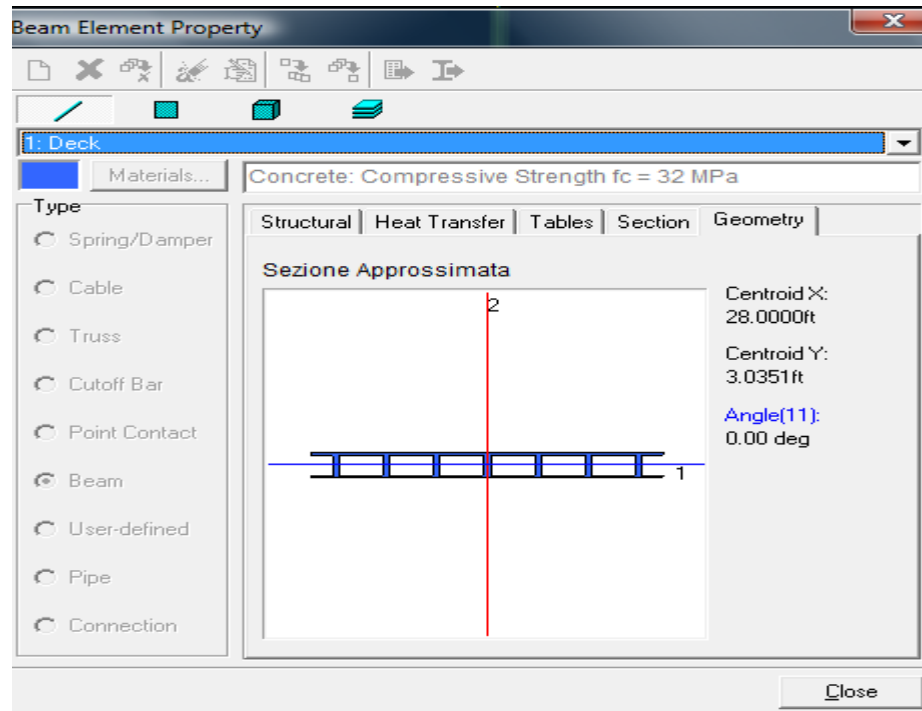


Figure 4.6: Deck Section of Model One

The boundary conditions for the deck are here simplified by fixing all of the degrees of freedom at both extremes of the deck-beam.

On the other hand, the piers are modeled with two types of sections: the top pier, 10 ft high, is modeled with a beam whose round section has a radius of 3.5 ft, while the radius of the bottom section is of 2.5 ft.

Table 4.4 shows the first six modal frequencies obtained by solving the model via Natural Frequencies Solver. The choice of the material properties results satisfied from the comparison of these results to the ones shown in previous chapter. In fact, the first six modes are sufficiently close to those identified with OKID/ERA. Figure 4.7 shows the first three modal shapes in the normal and solid views .

Mode	Frequency [rad/sec]	Frequency [Hz]	Period [sec]
1	20.1564585	3.208	0.312
2	23.3922989	3.723	0.269
3	27.2690242	4.340	0.230
4	36.0152182	5.732	0.174
5	40.0992886	6.382	0.157
6	50.6361904	8.059	0.124

Table 4.4: Six Modal Frequencies Obtained with the First FEM

By maintaining the characteristics just defined, the model is improved by modifying the boundary conditions of the deck. Once created a proper coordinated system, turned of 39° with respect to the Y axis, a translational spring, with the stiffness calculated via Makris method, is introduced along the x direction of the new system. Practically, now the deck cannot traslate neither in the vertical nor in the longitudinal direction, nor can rotate around any axis, but the transverse motion is restrained by the springs. The introduction of the spring leads to results even closer to the ones identified, as can be observed in table 4.5:

Mode	Frequency [rad/sec]	Frequency [Hz]	Period [sec]
1	23.12	3.68	0.27
2	26.83	4.27	0.23
3	30.47	4.85	0.21
4	31.73	5.05	0.20
5	41.09	6.54	0.15
6	42.73	6.80	0.15

Table 4.5: Six Modal Frequencies Obtained with the First FEM with the addition of the springs to the deck extremes

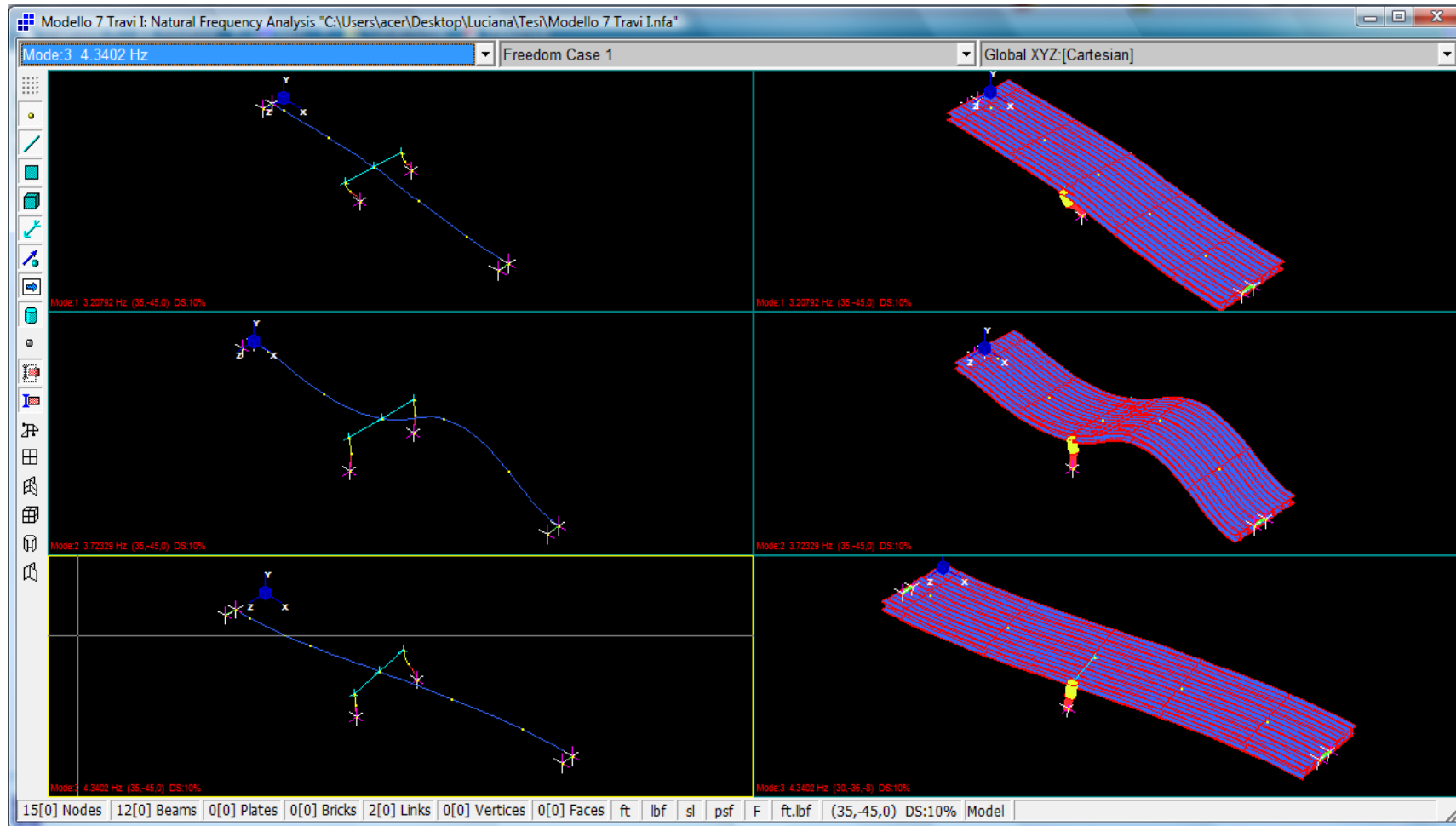


Figure 4.7: First, Second and Third Modal Shapes of the First Model

4.3.2 Second Model: the Grid Model

Through this model it is possible to begin exploring the behavior of the structure. In fact, in the model presented in this section there are all of the elements present in the actual system.

A grid model is chosen to permit the rotational inertia of the deck about the longitudinal axis, skew and deep beam effects and intermediate diaphragms to be directly incorporated. Each superstructure girder is modeled as a series of longitudinal members with the flanges assumed effective out to one-half the distance to the adjacent girder. The exterior girder elements are assumed to use the entire overhang but not the sidewalk or barrier rail. Transverse diaphragms are also modeled as beams with effective flanges. However, a similar model is not adequate for incorporating the transverse stiffness, since an intersecting series of beams would not capture the shear stiffness. Therefore, plane stress elements representing the deck are used to fill between the intersecting beams.

In Straus⁷ 'beam' is a generic name for a group of one-dimensional or line elements. These elements are all connected between two nodes at their ends and the single dimension is length. In its most general form the beam element can carry axial force, shear force, bending moment and torque. The active degrees of freedom for a beam element depend on the beam type and the stiffness it provides: a conventional beam can be characterized by stiffness against all of the solicitations. The beam elements are used to model the girders of the deck, the diaphragms, the abutments, the bent and the piers.

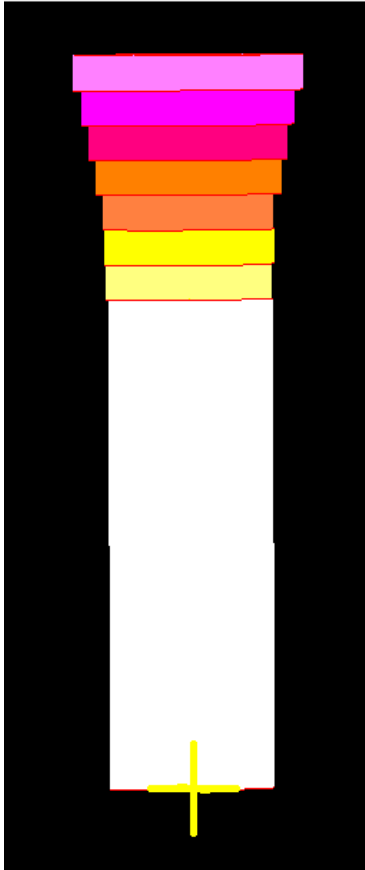


Fig. 4.8: Tapered Pier

Two issues have to be solved: the first is that of the boundary conditions. The study of the frequency content presented in the second chapter has proved that the piers move as a rigid body with the soil of the foundations, therefore, the basis of the piers can be fixed without any risk of oversimplification of the structural behavior. The piers itself are modeled with a series of beams, whose cross section is increasing from the 11th feet from the ground until the deck, as shown in figure 4.8. On the other hand, it has been underlined the necessity of considering a more specific model for the representation of the interaction between the soil and the abutments. This interaction is represented by means of transversal springs whose reaction is directed along a line skewed of 39° with respect to the longitudinal axis of the system. Practically, a new coordinate system needs to be defined; in particular, for this model a the new coordinate system has the y-axis directed along the 39°

skewed line, and the springs are defined in this new reference system, in the y direction, as can be observed in figure 4.9. The translational stiffness is 1.043×10^7 lbf/ft, that is the value resulting from the application of Makris method:

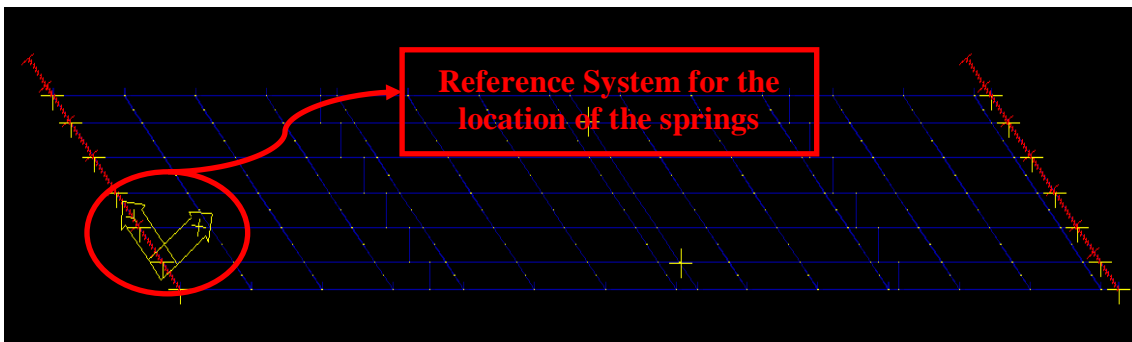


Figure. 4.9: Abutment Boundary Conditions, New Reference System

The second problem that needs to be solved is how to model the deck. In fact, in the existent structure this element consists in a unique piece cast in place. That means the system is characterized by a strong stiffness both in longitudinal and in transverse direction. By modeling the deck by means of seven longitudinal girders, only the stiffness along x-axis can be reproduced, but not that in the z-axis direction (figures 4.10):

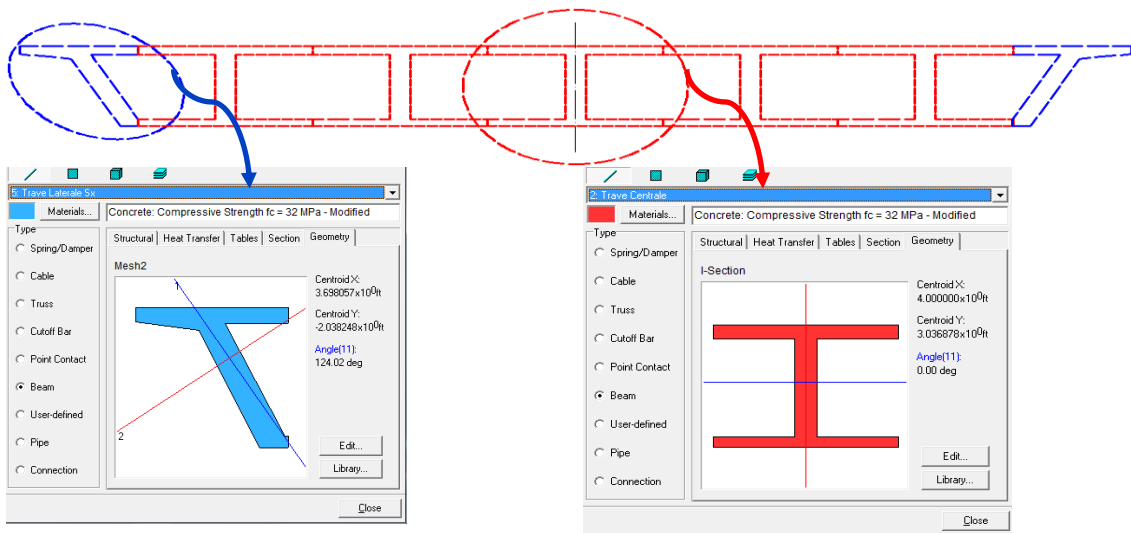


Fig. 4.10a: Lateral Girder Cross Section Fig. 4.10b: Central Girder Cross Section

The actual problem is finding the best element that gives transverse stiffness, without modifying the response of the structure. A number of experiments is developed, the first being the use of plates elements in order to model the transverse connections. In STRAUS7 plate is a generic name for a group of two-dimensional surface elements. The surface elements include the three and six node triangular elements, and four, eight and nine node quadrilateral elements. In particular, for this model two types of plate elements are tested. The first is the plane stress eight node plate element. A plane stress analysis assumes a thin two-dimensional sheet of material. All stresses are in the plane and the stress through the thickness is zero. The only active degrees of freedom are those associated with displacement in the XY plane, as shown in figure 4.11.

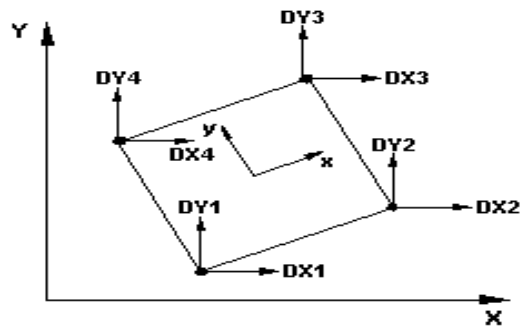


Figure 4.11: Active Degrees of Freedom in the in the Plane Strees Plate Elelement

The second is the plate/shell eight node element, the most general type of plate element in that it is a three-dimensional membrane and bending element (figure 4.12) . It is the only plate element that permits out of plane displacements associated with bending behavior.

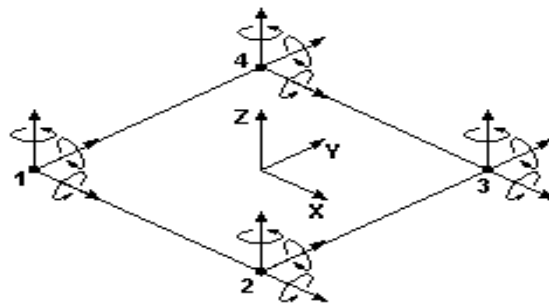


Figure 4.12: Membrane and Bending Actions in the Plate/shell Element

Results obtained with the first kind of element are shown in figure 4.13 and table 4.6:

Mode	Frequency [rad/sec]	Frequency [Hz]	Period [sec]
1	17.1531	2.73	0.366
2	21.0487	3.35	0.299
3	21.9283	3.49	0.287
4	24.2531	3.86	0.259
5	29.4681	4.69	0.213
6	31.4159	5	0.200

Table 4.6: Modal Parameters Resulting from the Model with Plane Stress Plates giving the Transverse Stiffness to the Deck

while table 4.7 and figure 4.14 show what results from the model in which plate/shell elements are used:

Mode	Frequency [rad/sec]	Frequency [Hz]	Period [sec]
1	17.1531	2.73	0.366
2	20.8602	3.32	0.301
3	21.6142	3.44	0.291
4	23.8761	3.8	0.263
5	25.9496	4.13	0.242
6	31.3531	4.99	0.200

Table 4.7: Modal Parameters Resulting from the Model with Plate/Shell elements giving the Transverse Stiffness to the Deck

From comparison between figures 4.13 and 4.14, it can be observed that the use of plate/shell elements gives more reasonable modal shapes, nevertheless, the natural frequencies are too low. In fact, the introduction of such elements in the system add some structural modes that represent a local deformation of the plates itself rather than the global behavior of all of the structure.

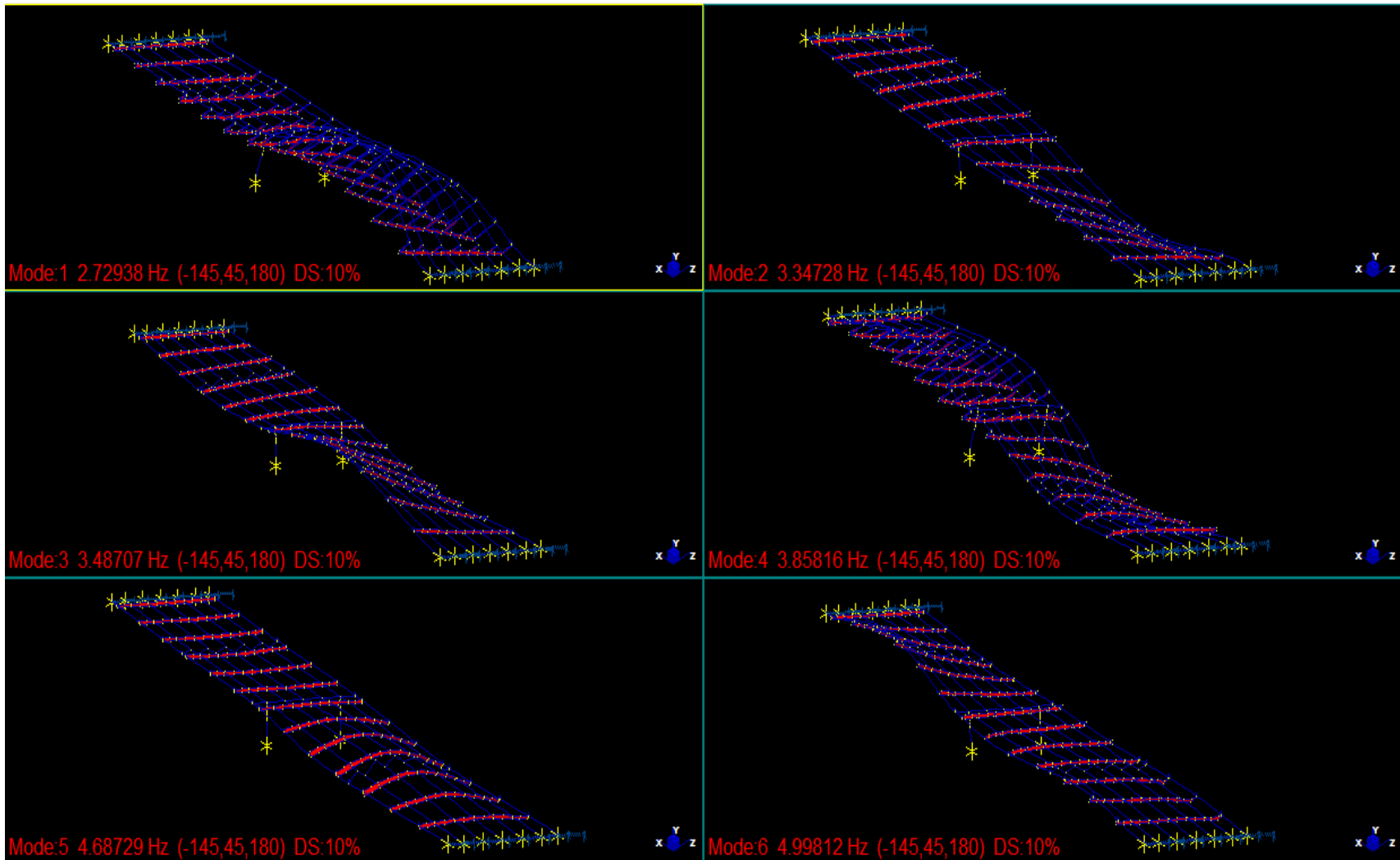


Fig. 4.13: Modal Shapes Resulting from the Second Model in Which the Transverse Stiffness is given by Plane Stress Elements

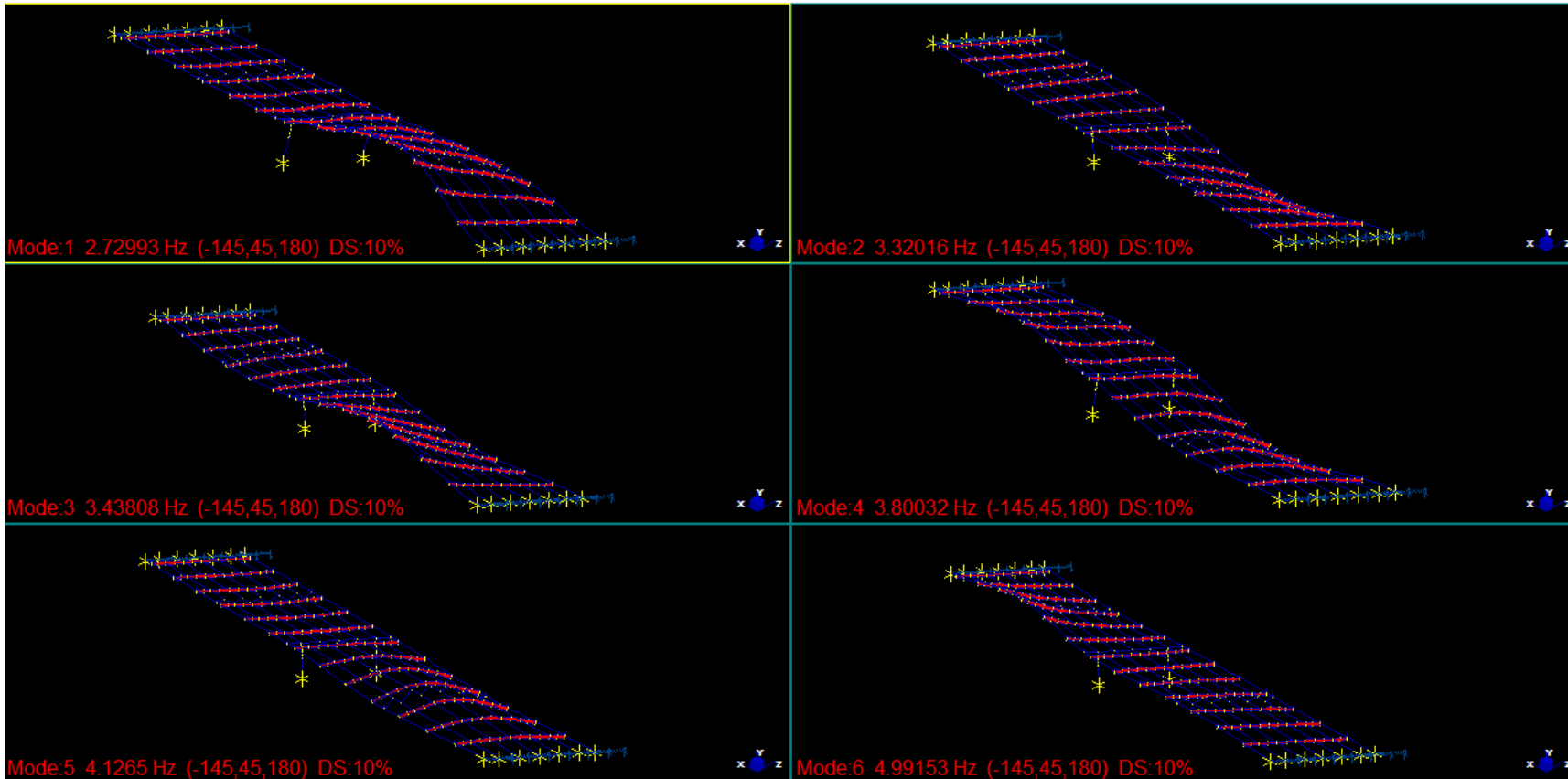


Fig. 4.14: Modal Shapes Resulting from the Second Model in Which the Transverse Stiffness is given by Plate/Shell Elements

Therefore, even though the values of the modal parameters obtained are appreciable, another solution has to be inspected. In place of the plates are chosen some beams with the section given in figure 4.15:

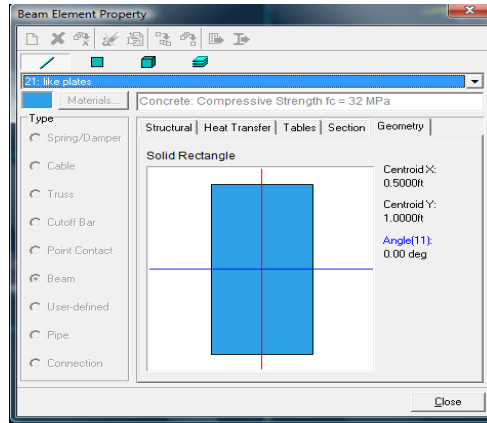


Fig. 4.15: Transverse Element Cross Section

With this approach the results obtained are given in table 4.8 and in figure 4.16:

Mode	Frequency [rad/sec]	Frequency [Hz]	Period [sec]
1	17.7814	2.83	0.353
2	20.9858	3.34	0.299
3	21.8655	3.48	0.287
4	25.3841	4.04	0.248
5	27.269	4.34	0.230
6	31.6044	5.03	0.199

Table 4.8: Modal Parameters Resulting from the Second Model with Beams giving the Transverse Stiffness to the Deck

The overall stiffness is increased compared to the one observed with the previous models, nonetheless, the results obtained are still not sufficiently closed to the values gained in the structural identification of chapter 3. The aim is increasing the transverse stiffness of the deck.

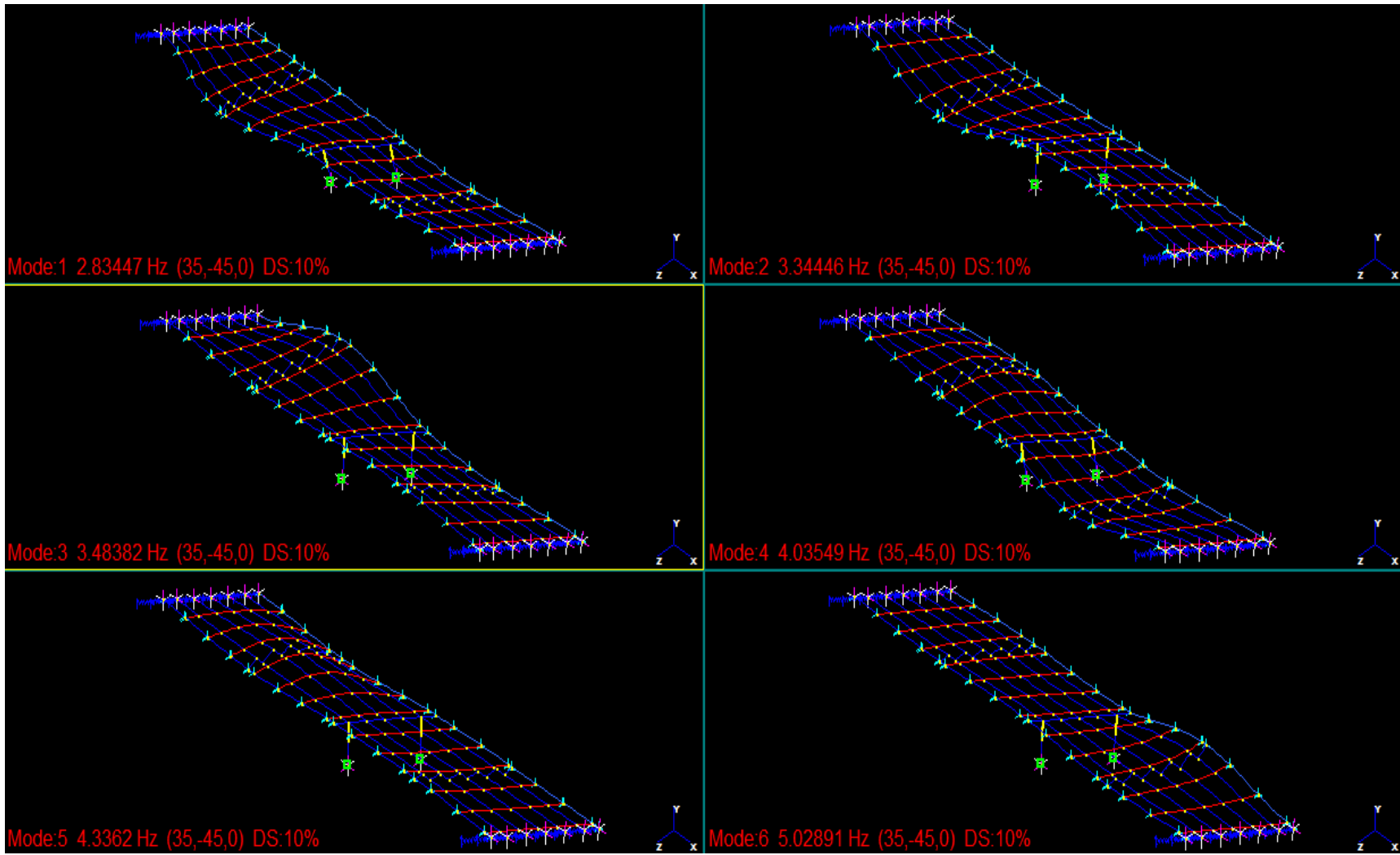


Fig. 4.16: Modal Shapes Resulting from the Second Model in Which the Transverse Stiffness is given by Beams

In the next model the transverse beams are substituted with rigid links. These elements provides an infinitely stiff connection between two nodes and constraints on the nodal rotation such that there is no relative rotation between the connected nodes. A typical example of the use of a rigid link in one of the global planes, is the modeling of rigid diaphragms for the analysis of floor slabs. The modal parameters got with this system are presented in table 4.9:

Mode	Frequency [rad/sec]	Frequency [Hz]	Period [sec]
1	22.054	3.51	0.285
2	27.7088	4.41	0.227
3	34.1805	5.44	0.184
4	39.2071	6.24	0.160
5	62.9575	10.02	0.100
6	66.2876	10.55	0.095

Table 4.9: Modal Parameters Resulting from the Second Model with Rigid Links giving the Transverse Stiffness to the Deck

while figure 4.17 represents the modal shapes of this new model. It is clear that this solution gets closer to the expected values. However, the gap between the fourth and the fifth natural frequencies, united to the comparison of the natural frequencies identified with OKID/ERA, suggests that this model still does not catch sufficiently well the actual behavior of the structures.

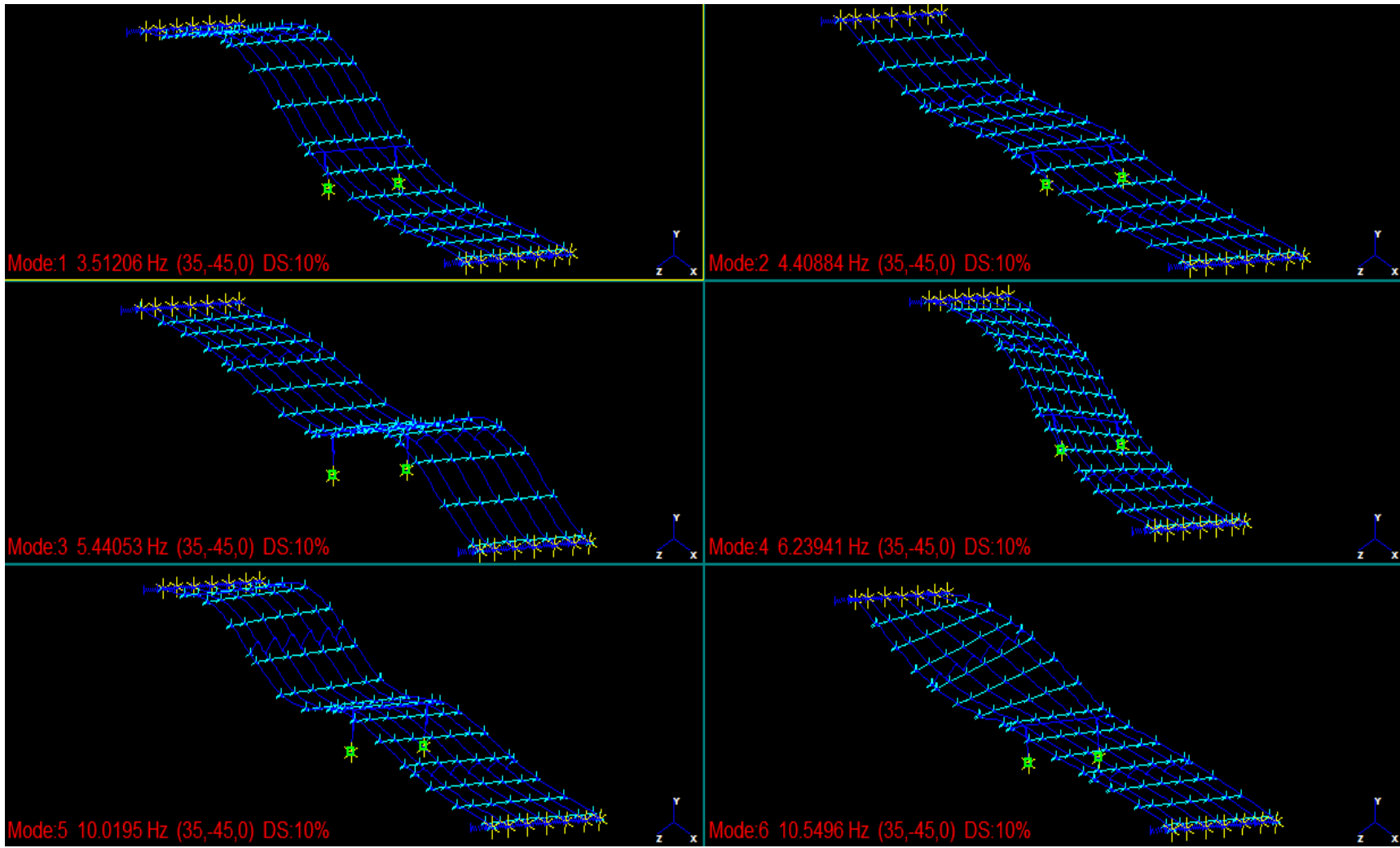


Fig. 4.17: Modal Shapes Resulting from the Second Model in Which the Transverse Stiffness is given by Rigid Links

Until now, it has been neglected the fact that the deck is constituted by pre-tensioned concrete. STRAUS7 allows to apply an axial load to the beam as a pre tension force. The specified pre tension force is applied as two equal and opposite forces on the ends of the beam element, but the jack force will not be recovered as an axial force in the beam element at the end of the solution. In the model a positive pre tension value is applied, this generates a tensile axial force in the fully fixed girders. As said at the beginning, the modal analysis solves the problem of an undamped free-vibration system; thus, the action of the pre-tension forces does not affect directly the analysis, but it changes the initial conditions. The jack forces will generates an initial displacement to the elements to which they are applied, then the modal parameters will change, as actually is observed in table 4.10:

Mode	Frequency [rad/sec]	Frequency [Hz]	Period [sec]
1	18.4097	2.93	0.341
2	21.1115	3.36	0.298
3	29.531	4.7	0.213
4	31.9186	5.08	0.197
5	40.4009	6.43	0.156
6	50.1398	7.98	0.125

Table 4.10: Modal Parameters Resulting from the Second Model with Pre-Tensioned Girders

Finally, the modal parameters obtained with this model are sufficiently closed to those previously identified. Anyway, some of the modal shapes are not reasonable, as observable in figure 4.18.

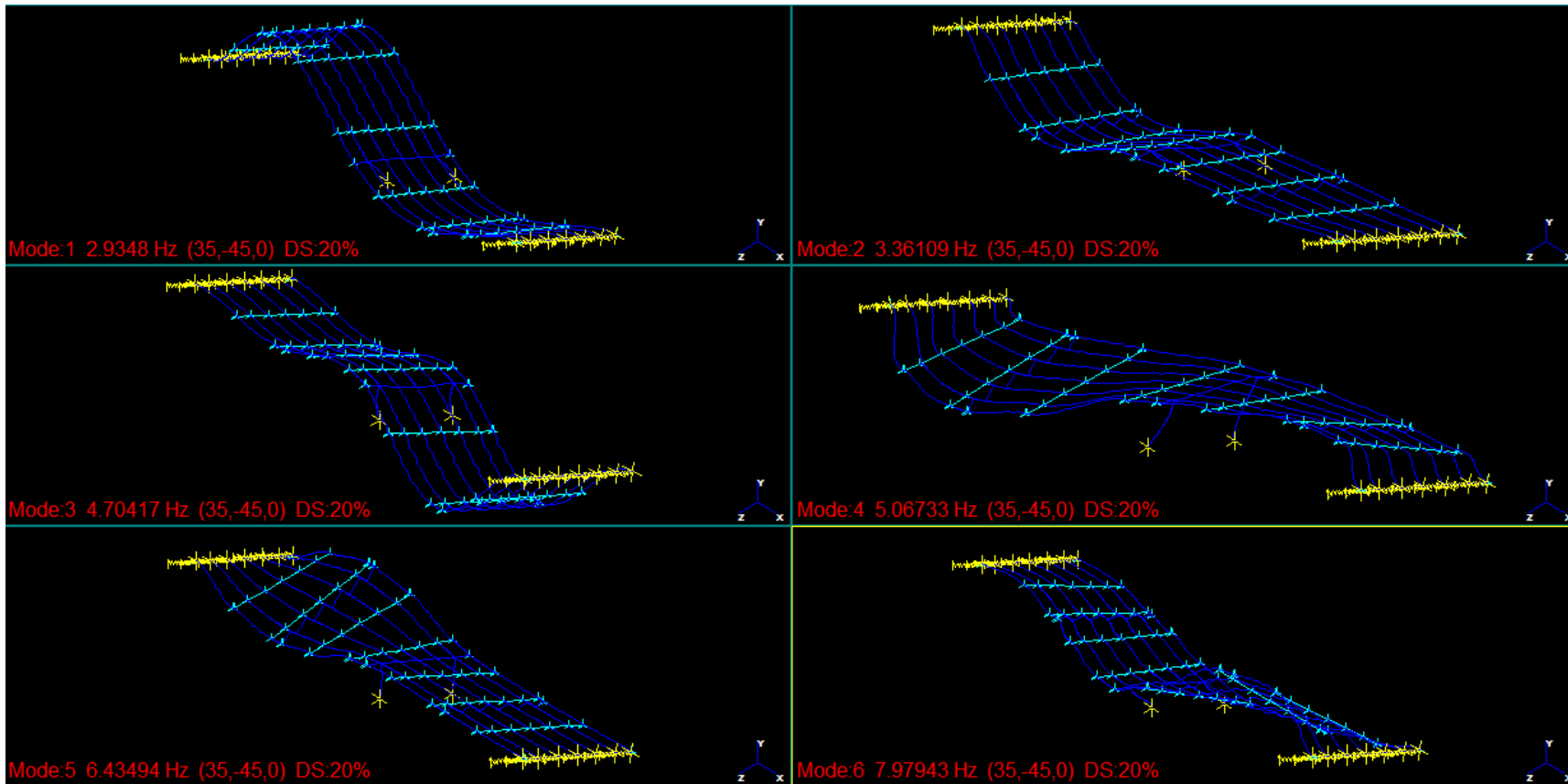


Fig. 4.18: Modal Shapes Resulting from the Second Model by adding a pre-tended cable in the seven deck girders

4.3.3 Third Model: Shell Model

4.3.3.1 The Shell Element in SAP2000

The Shell Element is a three or four node formulation that combines separate membrane and plate-bending behavior. Actually, the homogeneous shell combines independent membrane and plate behaviors, that are coupled when the element is non-planar. In this kind of element all six degrees of freedom are activated at each corner: the element is capable of supporting both forces and moments.

The membrane behavior is defined by an isoparametric formulation, that takes into account the translational in-plane components and a drilling rotational stiffness component in the direction normal to the plane of the element. On the other hand, plate-bending behavior includes two-way, out of plane, plate rotational stiffness components and a translational stiffness component in the direction normal to the plane of the element. The user can choose between the shell-thin and shell-thick formulations: the first neglects the transverse shearing deformation, according to Kirchhoff-Love theory, while the second includes those effects, being developed according to Reissner-Mindlin theory. Shearing deformations are important for elements whose thickness is greater than about one-tenth to one-fifth of the span, as also close to bending-stress concentrations, that can occur near sudden changes in thickness or support conditions.

The shell elements used in the generation of the third model have quadrilateral shape, defined by four nodes, as shown in figure 4.19:

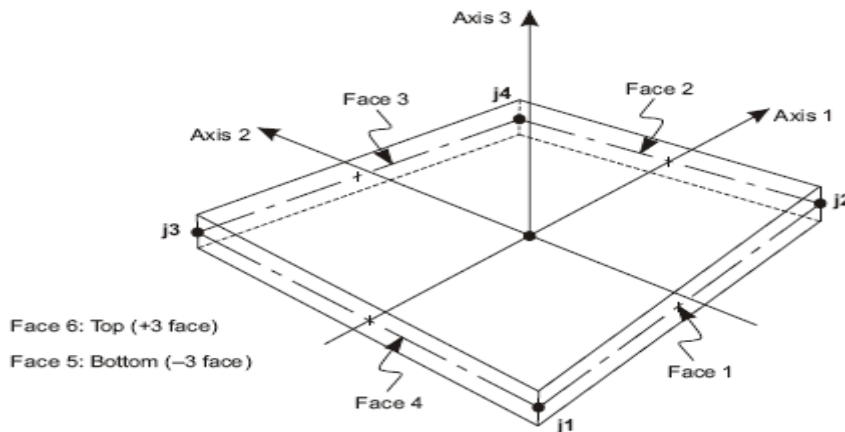


Figure. 4.19: Four-node Quadrilateral Shell Element

where joints j_1 and j_4 serve as corners of the reference surface of the shell element. In particular, for the homogeneous shell, the reference surface is the mid-surface of the element. In the SAP2000 Analysis Reference Manual is explicitly stated that the best results with the quadrilateral element may be obtained by locating the joints according to well defined geometrical conditions: the inside angle at each corner must be in the range of 45° to 135° , the ratio of the longer distance between midpoints of opposite sides to the shorter such distance should be less than four.

Each shell element has its own local coordinate system used to define all kind of assignments on it, such as material properties, loads, etc. The axes of the local system are denoted with 1, 2 and 3: the 1 and 2 axes lie in the plane of the element with an orientation specified by the user, the 3-axis is normal to the other two. The 1-2-3 coordinate system is generally different than the global X-Y-Z coordinate system. By default, the local 3-2 plane is taken parallel to the Z axis; the local 2 axis is taken to have an upward sense (+Z), unless the element is horizontal, in which case the 2 axis is taken along the global +Y direction; the 1-axis lies in the X-Y plane (Figure 4.20):

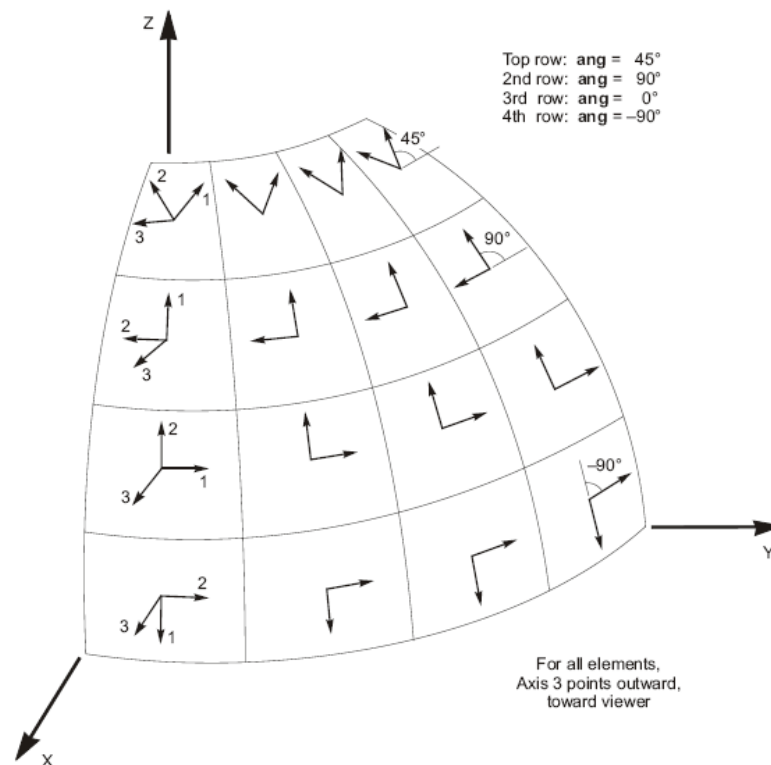


Figure 4.20: Element System with Respect to the Global Coordinate System

In defining the element section properties, the user has to decide what value give to the membrane (th) and bending (thb) thicknesses. Usually, the two values are maintained identical, and the user can vary the computed section properties by operating on the property modifiers.

Finally, the shell element stress resultants are the forces and the moments that result from integrating the stress over the element thickness as follows:

$$\begin{aligned}
 F_{11} &= \int_{-th/2}^{th/2} \sigma_{11} dx & M_{11} &= \int_{-thb/2}^{thb/2} \sigma_{11} \cdot x dx & V_{13} &= \int_{-thb/2}^{thb/2} \sigma_{13} dx \\
 F_{22} &= \int_{-th/2}^{th/2} \sigma_{22} dx & M_{22} &= \int_{-thb/2}^{thb/2} \sigma_{22} \cdot x dx & V_{23} &= \int_{-thb/2}^{thb/2} \sigma_{23} dx \\
 F_{12} &= \int_{-th/2}^{th/2} \sigma_{12} dx & M_{12} &= \int_{-thb/2}^{thb/2} \sigma_{12} \cdot x dx & &
 \end{aligned} \tag{4.44}$$

The 4.44 are forces and moment per unit of in-plane length. For the thick-plane formulation of the homogeneous shell the shear stresses are computed directly from the shearing deformation, while for the thin plate homogeneous shell the V_{12} and V_{23} are determined from the equilibrium equations 4.45:

$$\begin{aligned}
 V_{13} &= -\frac{dM_{11}}{dx_1} - \frac{dM_{12}}{dx_2} \\
 V_{23} &= -\frac{dM_{12}}{dx_1} - \frac{dM_{22}}{dx_2}
 \end{aligned} \tag{4.45}$$

where x_1 and x_2 are the coordinates parallel to the local axis 1 and 2. Stresses acting on a positive face are oriented in the positive direction of the element local axes. Stresses acting on a negative face are oriented in the negative direction of the element local axes (figure 4.21):

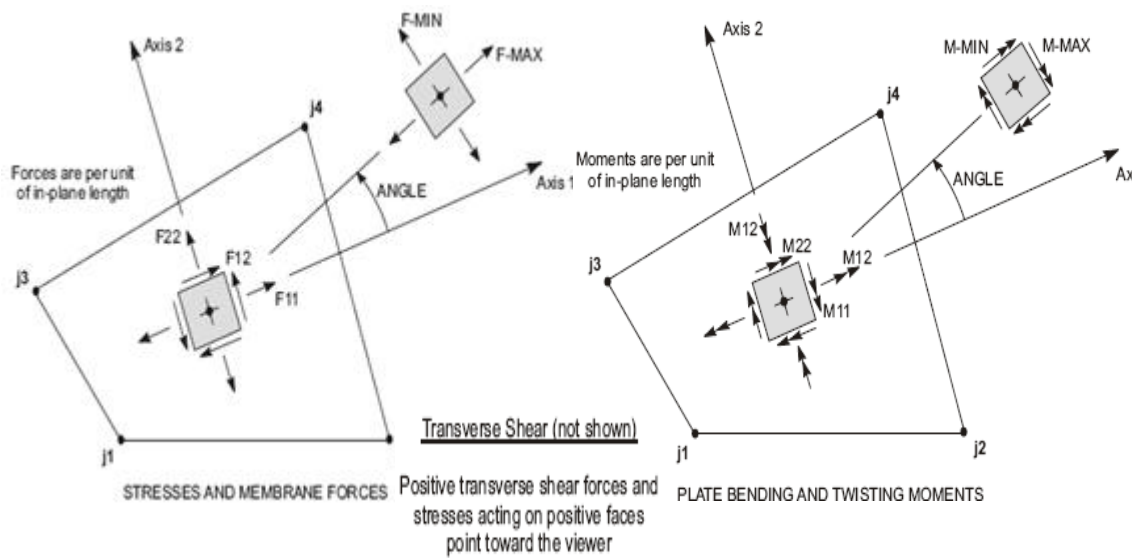


Figure 4.21: Shell Element Internal Resultants Forces and Moments

Stresses are reports for homogeneous shells at the top and bottom surfaces, and are linear in between. Stresses and internal forces are evaluated at the standard Gauss integration points of the element and extrapolated to the joints.

4.3.3.2 Thick-Shell Elements Model

Maintaining the same material properties as the ones employed for the previous models, the new generated system is built by using thick-shell elements for the deck, diaphragms and abutments and beams elements for the piers and the bent representations. The boundary conditions remain those identified above: the basis of piers have the translational and rotational degrees of freedom restrained in all of the three directions; to apply the boundary conditions at the basis of the abutments a proper new coordinate system is introduced, in which the y-axis denotes the direction parallel to a line skewed of 39° with respect to the global X-axis. The basis of the abutments cannot either translate in the longitudinal and vertical direction or rotate with respect to any of the global axis, while in the y-axis direction, springs characterized by 869.1667 kips/in stiffness restrain the translational motion.

The first experiments are focused on understanding the contribute to the global behavior of the diaphragms. The same model is analyzed with and without the diaphragms, and in table 4.11 are presented the results:

Mode	<i>Model with Diaphragms</i>		<i>Model Without Diaphragms</i>	
	Freq. [Hz]	Period [sec]	Freq. [Hz]	Period [sec]
1	2.905	0.344	2.934	0.341
2	3.557	0.281	3.576	0.280
3	4.628	0.216	4.683	0.214
4	6.390	0.156	6.400	0.156
5	8.279	0.121	8.274	0.121
6	8.617	0.116	8.635	0.116

Table 4.11: Comparison between model with and without Diaphragms Representations

As can be observed from the table above, the presence of the diaphragms does not affects greatly the overall behavior of the structure. Therefore, they can be neglected in the generation of the finite element model, gaining a simpler system. Indeed, introducing less elements in the model decreases the computational request and offers a system simpler to calibrate, since with less variables to handle with.

Figures 4.22 show the first height modal shapes obtained for the model without diaphragms.

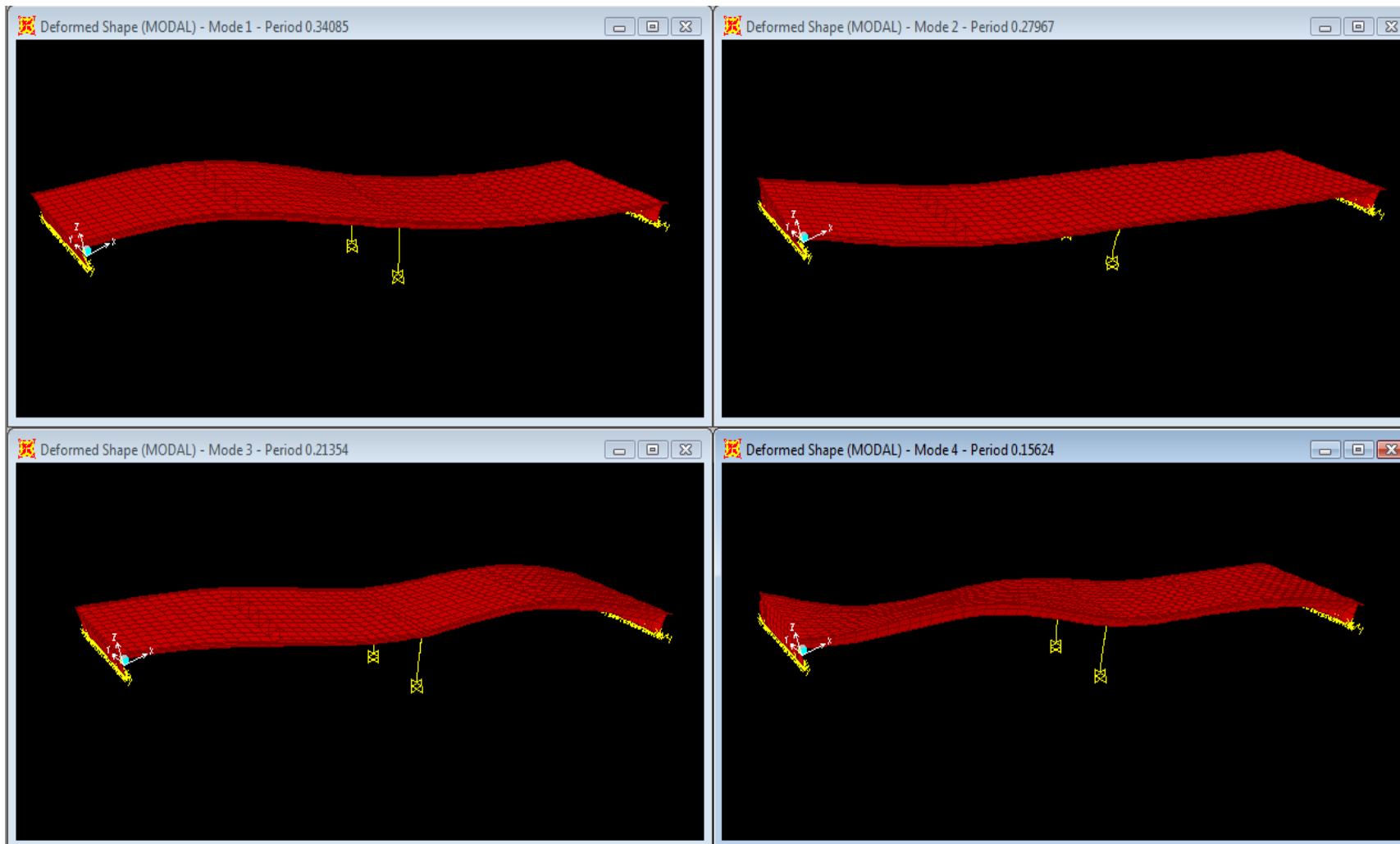


Figure 4.22a: First, Second, Third and Fourth Modal Shapes for the Shell Model without Diaphragms

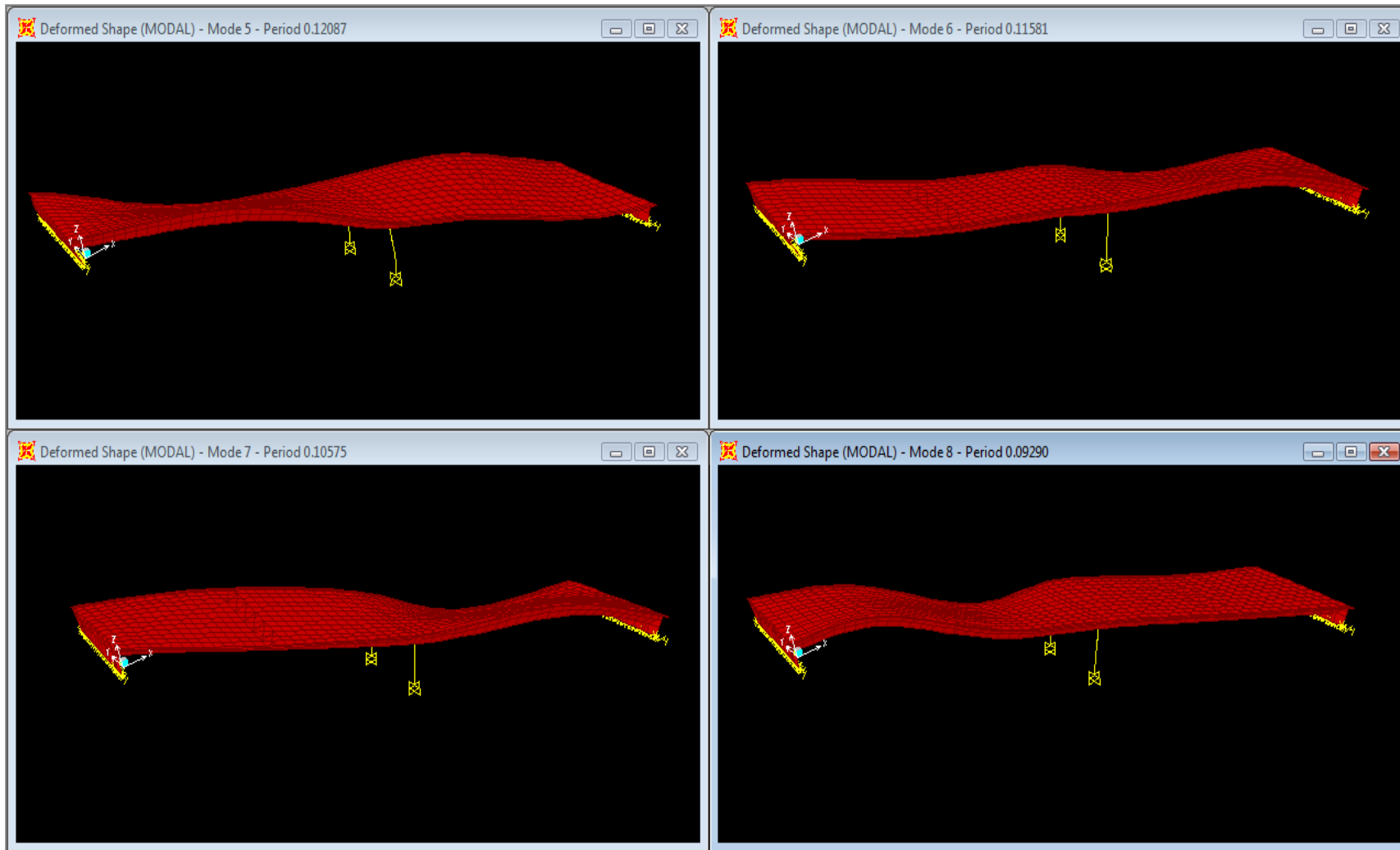


Figure 4.22b: Fifth, Sixth, Seventh and Eighth Modal Shapes for the Shell Model without Diaphragms

4.3.3.3 Thin-Shell Elements Model

The new trial model is identical to the previous one, but the shell elements used are now the thin-shell elements, i.e. the ones formulated according to Kirchhoff-Love theory. In table 4.12 are presented the modal parameters obtained:

Mode	Freq. [Hz]	Period [sec]
1	3.356	0.298
2	4.606	0.217
3	5.200	0.192
4	6.802	0.147
5	7.256	0.138
6	9.079	0.110
7	10.498	0.095
8	11.848	0.084

Table 4.12: Modal Frequencies and Periods for Thin-Shells Model

It is certainly worth to highlight the fact that the values detected are finally sufficiently close to those identified in chapter 3, therefore the model here obtained is ready to be calibrated. Figures 4.23 show the first eight modal shapes of the structure. The first five modes are compared with the modal shapes obtained in the identification via OKID/ERA to underline once again the reasonability of the results.

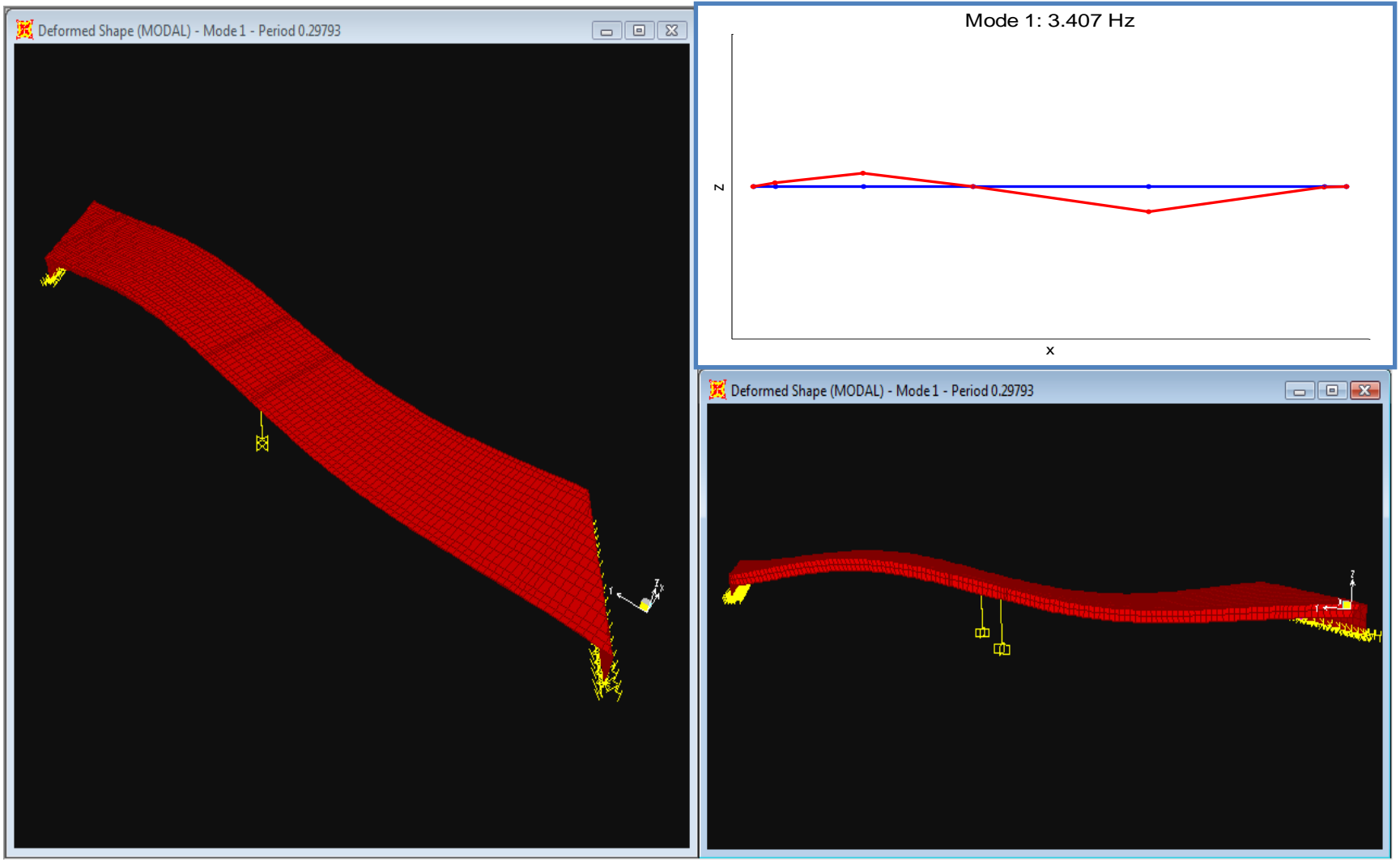


Figure 4.23a: First Mode Shape for the Model to Be Calibrated

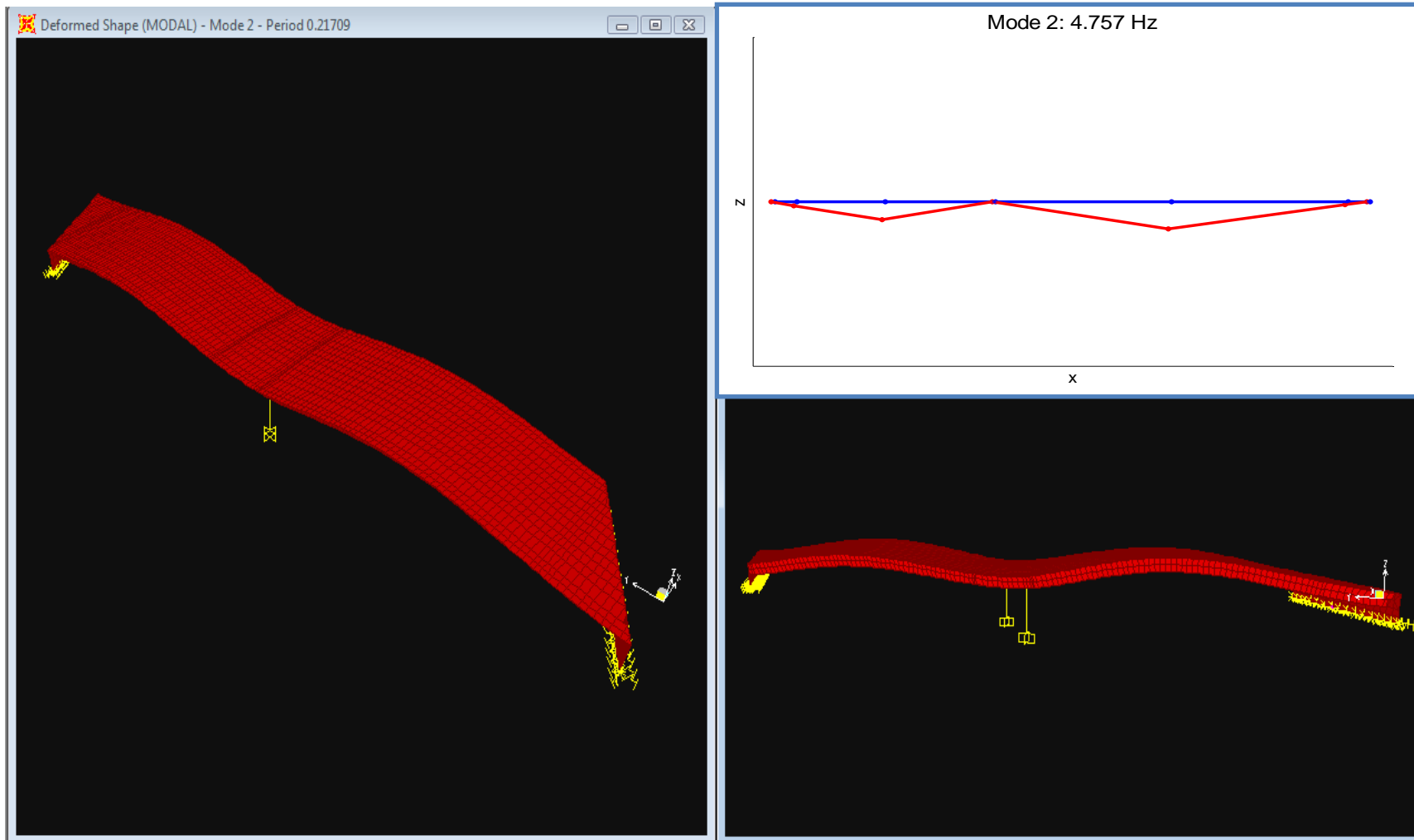


Figure 4.23b: Second Mode Shape for the Model to Be Calibrated

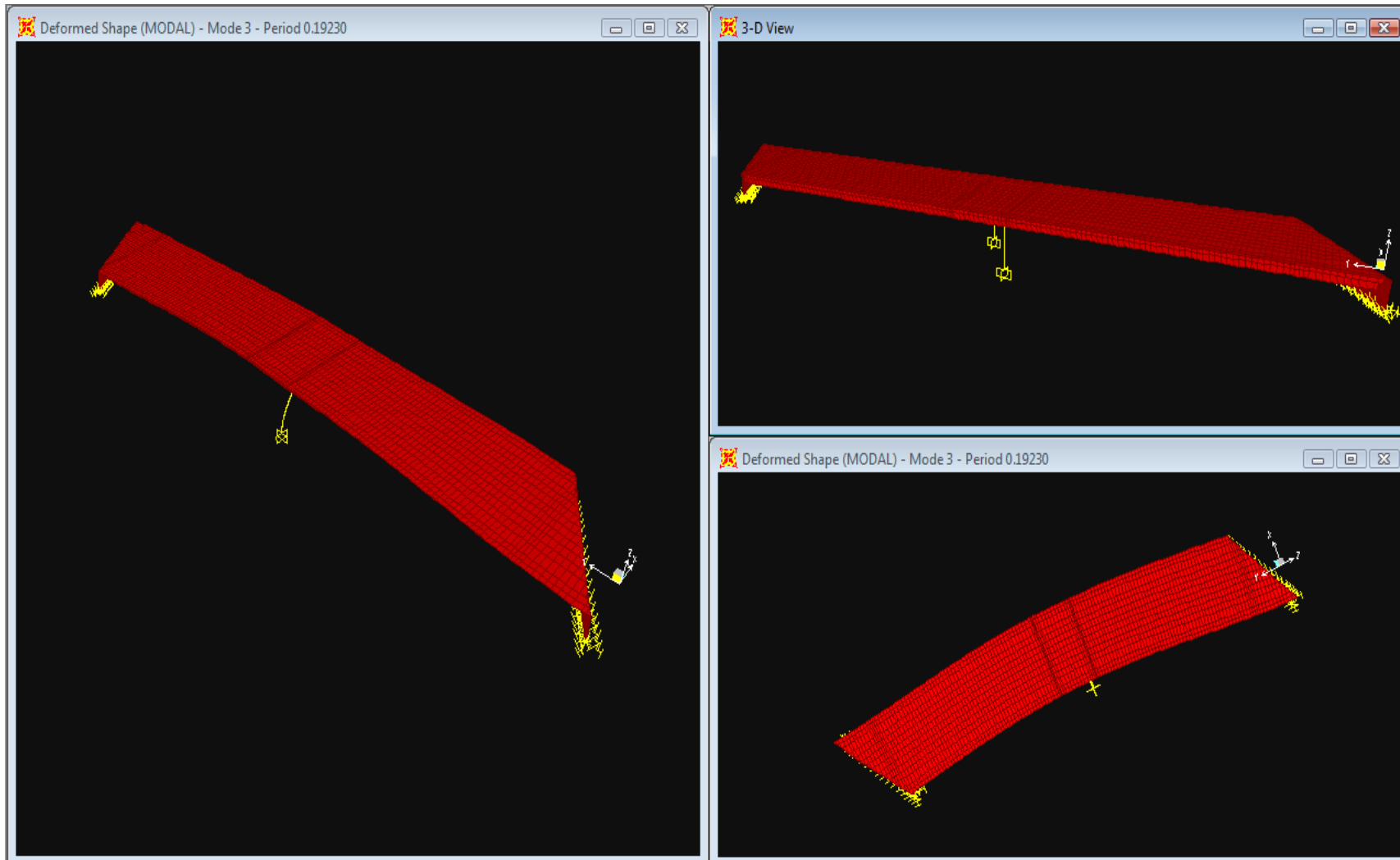


Figure 4.23c: Third Mode Shape for the Model to Be Calibrated

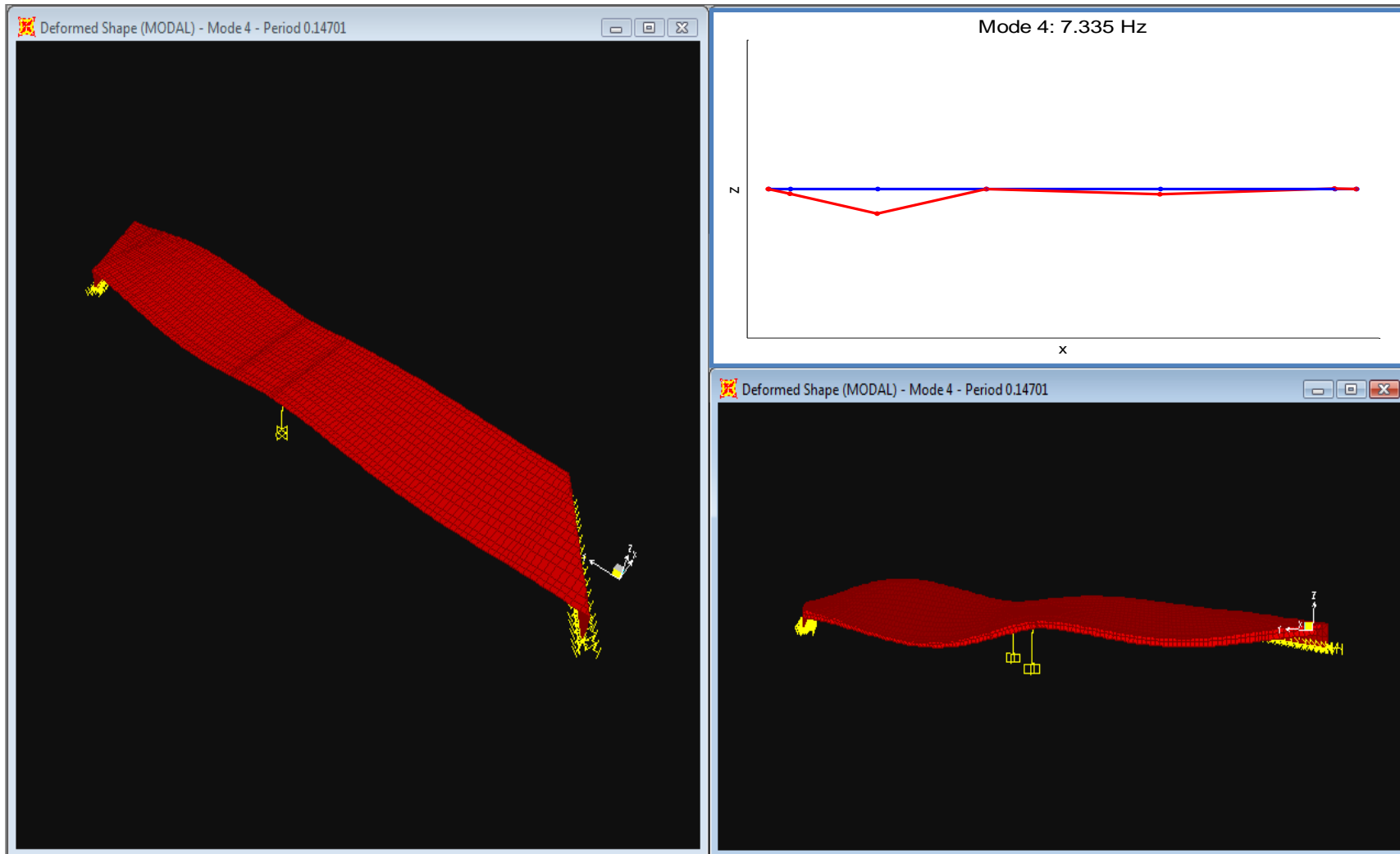


Figure 4.23d: Fourth Mode Shape for the Model to Be Calibrated

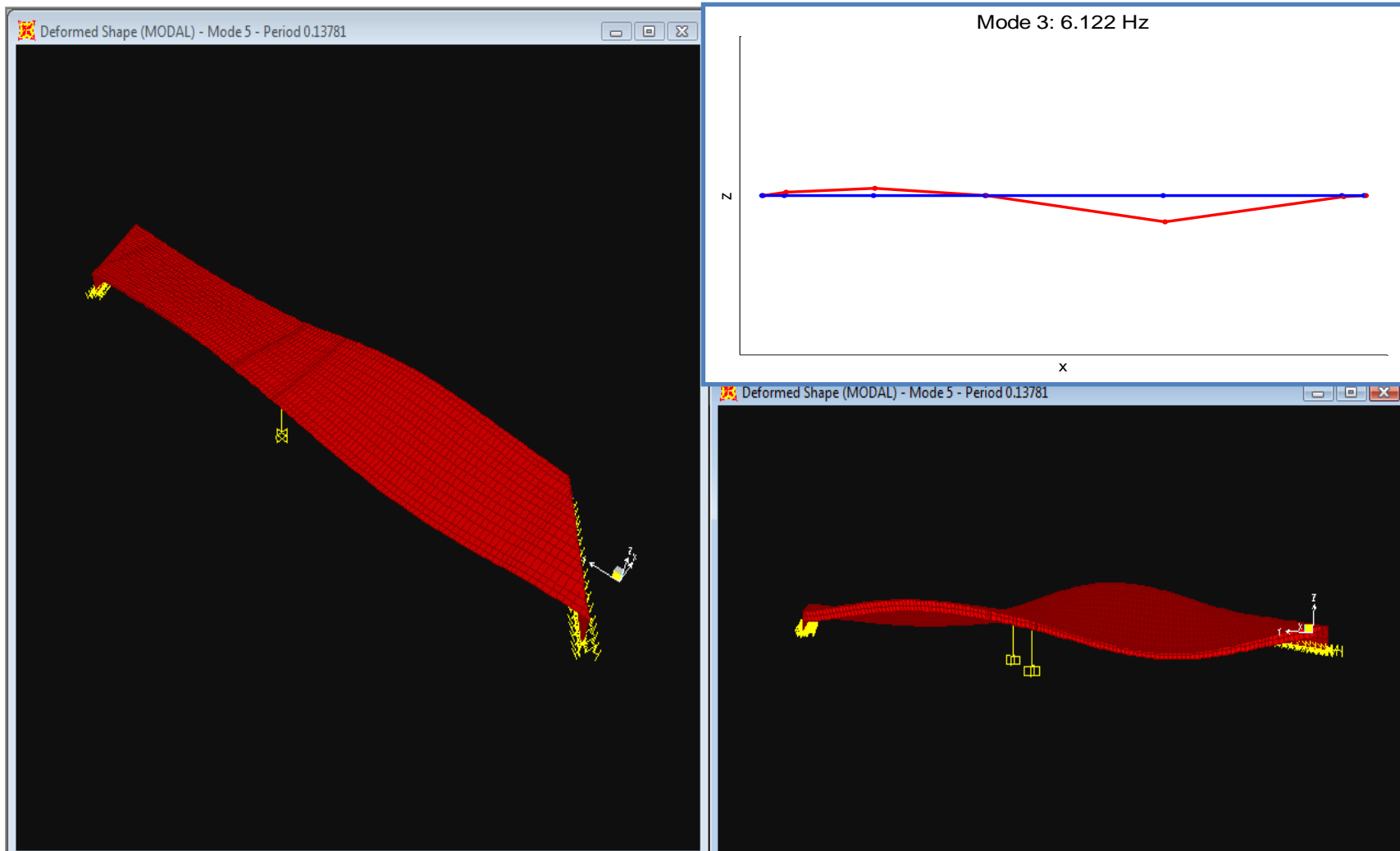


Figure 4.23e: Fifth Mode Shape for the Model to Be Calibr

4.4 Model Calibration

In Chapter 3, the modal characteristics of the Painter Street Overpass have been obtained through the OKID algorithm. The results obtained are now used to optimize the FEM model defined in the first paragraphs of this chapter. The objective is that of minimize the error given by the sum of the difference of the modal frequencies obtained by OKID (our threshold) and the ones obtained through the SAP model. This result is achieved by varying three parameters through a genetic algorithm, until the best combination is found. Obviously, the best combination of the three parameters is the one that minimizes the error. The parameters chosen are the mass and stiffness coefficients and the Young's modulus of the concrete, since these are the factors the mostly affect the modal characteristics of any system.

4.4.1 Genetic Algorithm (GA)

In order to understand how a genetic algorithm works, it is useful to remind some basics of Biology. Every organism has a set of rules describing how it is built up. These rules are encoded in the genes of an organism, and connected into strings called chromosomes. Each gene represents a specific trait of the organism, and the settings of the genes are known as the organism's genotype. The physical expression of the genotype is the phenotype. When two organisms mate they share their genes, in a processes usually referred to as recombination. Sometimes, a gene may be mutated. Occasionally the mutation will affect the phenotype, as well. Genetic Algorithms are stochastic global search methods that mimic the metaphor of natural biological evaluation, being based on the principles of Darwinian theory of survival of the fittest.

Before someone can use a GA to solve a problem, it is necessary to find a way to encode any potential solution of the problem. This could be done through a string of real number or, more typically, a binary bit string. In the following, the bit string will be

referred to as a chromosome. At the beginning of a run of a genetic algorithm, a large number of random chromosome is created. Each new chromosome will represent a solution to the problem, once it is decoded. Assuming a population of N chromosomes, the following steps are repeated until a solution is found:

1. Test the validity of the chromosome in solving the problem, and assign a fitting score to the chromosome.
2. Select two members from the current population: higher the fitting score, higher is the probability of the chromosome to be selected.
3. Depending on the crossover rate, crossover the bits from each chosen chromosome at a randomly chosen point. The crossover rate is the chance that two chromosomes will swap their bits. A good crossover rate value is around 0.7.
4. Depending on the mutation rate, step through the chosen chromosomes bits and flip. The mutation rate is the chance that a bit within a chromosome will be flipped. In binary encoded genes, the mutation rate has usually very low values, as 0.001. Then, whenever a chromosome is chosen from the population, the algorithm first checks to see if crossover should be applied, then, the algorithm iterates down the length of each chromosome mutating the bits if applicable.
5. Repeat from step 2 to 3 resulting in a new population of N chromosomes.

4.4.2 The Code used in the Optimization Process

In calibrating the model, a GA coded by Prof. David L. Carroll is used. In the following will be briefly explained how it works. The copyright by which the code is subjected does not authorize me to show the code in appendix. Then, I will not give any details on how it has been built, but I will only explain the main phases of which it is compound.

The code initializes a random sample of individuals with different parameters to be optimized using the genetic algorithm approach. As mentioned in the introduction, I have chosen to vary three parameters: mass coefficient (a_M), stiffness coefficient (a_K) and Young's modulus of the concrete (E). For what concerns a_M and a_K , the range of variation of these two coefficients has been evaluated according to the Rayleigh approach. Through previous process, the modal frequencies of the model have been obtained. Fixed the first two natural frequencies, it is possible to get the value of a_M and a_K by solving for the unknow parameters the following system of equations:

$$\begin{Bmatrix} \zeta_1 \\ \zeta_2 \end{Bmatrix} = \begin{bmatrix} 1/2\omega_1 & \omega_1/2 \\ 1/2\omega_2 & \omega_2/2 \end{bmatrix} \begin{Bmatrix} a_M \\ a_K \end{Bmatrix} \quad (4.46)$$

The minimum values of a_M and a_K are calculated by fixing the ζ_i 's equal to 0.01, while the maximum values are obtained by setting the damping ratios equal to 0.1. The ranhges of the three parameters are shown in the table 4.13:

	parmin	parmax
Mass Coefficient	0.2077	2.0768
Stiffness Coefficient	0.0005	0.0047
Young's Modulus	3000 ksi	8000 ksi

Table 4.13: Range of Parameters used for the Calibration of the linear FEM

The next step is the one of the evaluation of the population: once the chromosomes are generated, the fitness score is them assigned, and the best individual is established. This peocedure is acted on each member of the population. It is now necessary to create some space where locate and mantaine multiple solutions. This is obtaiend through the niching method. In particular, the Goldberg’s multidimensional phenotypic sharing scheme with a triangular sharing function is implemented in the code.

It is time to select the better of two possible parents for mating. The selection scheme used is tournament selection with a shuffling technique. Follows the crossover step. The program allows you to choose between two options: single point crossover at a random chromosome point, and unform crossover between randomly selected pair. Then, mutation is perfomed on the children generation. A jump mutation will be performed if a random number is less than 0.05, random creep mutation will be used if a different number is less than 0.1. Finally a new generation is run consisting in writing the child array back into parent array, while checking if the best individual was replicated. The last mentioned check is called elitism.

The procedure explained will continue until either the user stop the debugging of the code because the error is reasonably minimized, or the maximum number of iterations is reached, i.e. 100 generations have been performed.

Parameter Summary

Population Size	7	Crossover Rate	0.5
Number of Children	2	Mutation Rate	0.05
Niching	Yes	Creep Mutation Rate	0.1
Selection Strategy	Tournament	Elitism	yes

Table 4.14: Parameters Used in the Genetic Algorithm

4.4.2.1 Tournament Selection with a Shuffling Technique

There are several techniques by which a mating pool for reproduction can be created. The one used in the code is the tournament selection method. Also called the ranking method, selection probabilities are calculated normally and successive pairs of individuals are drawn using roulette wheel selection. Practically, the last mentioned method selects parents according to a spin of a weighted roulette wheel. The roulette wheel is weighted according to string fitness values. A high-fit string will have more area assigned to it on the wheel and hence, a higher probability of ending up as the choice when the biased roulette wheel is spun.

After drawing a pair, the string with the highest fitness is declared the winner and is inserted into the mating pool, and another pair is drawn. The process continues until the mating pool is full.

4.4.2.2 Single Point and Uniform Crossover

When single point Crossover is applied, one crossover point is selected, binary string from beginning of chromosome to the crossover point is copied from one parent, the rest is copied from the second parent, as well explained by figure 4.24:

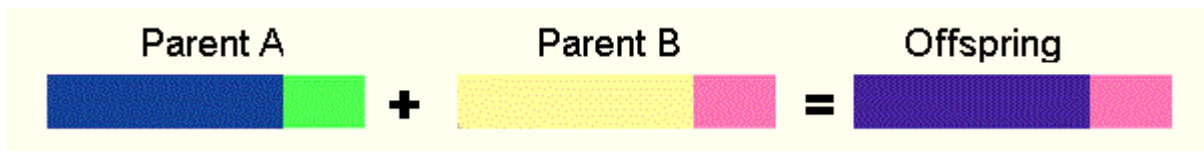


Figure 4.24: Graphical Explanation of Single Point Crossover

When Uniform crossover is performed, bits are randomly copied from the first or from the second parent, as shown in figure 4.25:

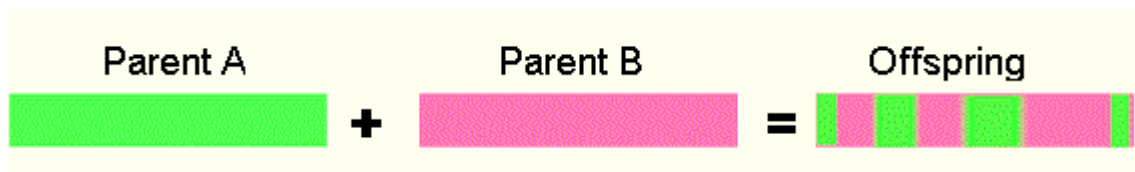


Figure 4.25: Graphical Explanation of Uniform Crossover

4.4.2.3 Jump and Creep Mutation

There are two types of mutation operators: the standard jump mutation and the creep mutation. The first one acts on the chromosome (referred to as genotype in the introductory explanation of GA's), while the second one acts on the decoded individual (the phenotype in the biological parallelism). The mutation probabilities have to be low; otherwise disruption of promising schemes may result.

5

CONCLUSIONS

The thesis describes a dynamically-based technique to detect and locate damage and illustrates the performance in the case of the Rio Dell – Hwy 101/Painter Street Overpass. The method discussed, conceptually simple and practically tractable, aims to retrieve an high fidelity finite element model whose response can be compared to that of the actual structure. The final objective is comprehending whether the structure has been damaged during a strong seismic event and, possibly, detect the location of the eventual damage. The approach is developed in five steps:

1. From the study of previous papers, the main characteristics of the system are individuated. In particular, from the analysis of the frequency content of the acceleration time histories recorded during three seismic events, natural frequency values of reference and boundary conditions to apply to the finite element model were evaluated.
2. Through the employment of a two-stage system identification methodology (OKID/ERA) the characterization of dynamic properties of the Painter Street Overpass has been performed by identifying its natural frequencies, damping ratios, and mode shapes, using three ambient vibration data sets recorded through the acceleration monitoring system. First, a first-order state-space model of the structural system is identified using only the available input-output measurement data and then, such a model is converted to a second-order mass, damping and stiffness model. Some of the advantages that is worth to restated are that the technique does not require any numerical manipulation (integration, differentiation, filtering) of the recorded data and that it does not impose any limitation on the nature and type of structural damping and on the coupling of the vibrational modes. For the structure under consideration, six modal frequencies were identified: 3.407 Hz, 4.757 Hz, 5.541 Hz, 6.122 Hz, 7.335 Hz, 8.106 Hz. Moreover, plots of the corresponding modal shapes were plotted,

although those may only represent a reference for the actual structural modal shape.

Results obtained through this step are considered quite reliable, although some issues had to be solved, as it was discussed in detail in the body of the thesis. First of all, the available time histories are too short. Indeed, researches have demonstrated that for the OKID/ERA to be effective, records covering a time of more than 60 seconds are necessary. Instead, the data available refer to records at most 60 second long. Moreover, the only data having these characteristics had been strongly corrupted by noise, maybe consequently to the high energy generated during the seismic event. The second problem that had to be faced was the location of the sensors, that does not permit the visualization of the torsional natural modes, that anyway are not negligible for this kind of structure. A further assessment on the robustness of the identification results had to await, therefore, the finite element model analysis validation.

3. Using the modal parameter estimates identified as thresholds, a linear finite element model has been generated. After some trials, the model considered more accurate in resembling the modal parameters thresholds was selected to be that in which deck and abutments are constituted by shell elements, formulated according to the Kirchhoff theory. The first six natural frequencies computed with this model were found to be equal to 3.356 Hz, 4.606 Hz, 5.200 Hz, 6.802 Hz, 7.256 Hz, 9.079 Hz. The finite element model has been then calibrated by means of a genetic algorithm in order to retrieve the same modes individuated in the previous structural identification. The parameters chosen to be modified were the Young's modulus of the concrete, the mass and the damping ration of the system. The initial value for the damping ratio was computed via Rayleigh approach.
4. The final step should be that of modifying the calibrated FEM by inserting some non linear elements. Such elements have to be placed in the most stressed areas, that may be detected by means of an approach similar to the push-over analysis. The technique employable may be that of applying excitation of increasing intensity, until an area of the system overcomes the elastic-limit

behavior. It is reasonable to suppose that these areas would experience a big deformation during a particularly strong earthquake. Therefore, for this zones it is inappropriate a linear model, that does not allow to appreciate the real response of the structure. However, this analysis has to be enfaced from the beginning, topics that would be properly explored would be those of which elements to use to model the non-linearities of the system, and how to detect the zones that need to be modeled as non-linear.

5. Once all of the material is collected, we have a powerful tool able to resemble the structural response of the real system. By comparing the model response to the actual one, we are immediately capable of assume whether the structure has suffered damage. Moreover, individuating the zones where the structural response differs significantly with respect to the model reponse, it is possible to simplify the detection of the damage, addressing the inspections in those areas.

Therefore, a potentially important limitation in the strategy derives from the difficulties that can be incurred in the structural identification simulated via OKID/ERA. However, most of the difficulties can be circumvented in comparing the identification results with the findings assessed through the finite element model analysis. In conclusion, the technique engaged offers a valid alternative to the traditional methods of damage detection. Some of the advantages that is worth to restate are the generality with respect to the type of structures that it applies to, the fact that can operate with a small set of data and finally that the OKID/ERA structural identification is computed strictly from the measured data. To utterly complete the analysis, the non-linear finite element model should be created, and experimental validation should be performed.

BIBLIOGRAPHY

- [1] Bathe, K.J. 1996. *Finite Element Procedures*. Prentice Hall

- [2] Babu, S.C. *Development of Tailored Preform Processing Technology for Net-Shape Manufacturing of Large Monolithic Structures*, Ph. D. Thesis, Graduate School University of Missouri, Columbia

- [3] Bernal, D. and Gunes, B. 2004. “ Flexibility Based Approach for Damage Characterization: Benchmark Application”, *Journal of Engineering Mechanics*, ASCE, Vol. 130, No. 1

- [4] Bernal, D. “Flexibility-based Damage Localization from Stochastic Realization Results”, *Journal of Engineering Mechanics*, ASCE, Vol 132, No. 6, pp. 651-658

- [5] Bernal, D. 2002. “Load Vectors for Damage Localization”, *Journal of Engineering Mechanics*, ASCE, Vol. 128, No.1, pp. 7-14.

- [6] Bernal, D. “Extracting Flexibility Matrices from State-Space Realizations”, *COST F3 Conference*, Madrid, Spain, Vol. 1., pp. 127-135

- [7] Caicedo, J.M., Dutta, A.K., Zarate, B.A. 2006, “System Identification and Model Updating of the Bill Emerson Memorial Bridge”, *Proceeding of IV World Conference on Structural Control and Monitoring*, San Diego

- [8] Chopra, A.K., 2001. *Dynamics of Structures*, Prentice-Hall

- [9] Goel, R.K. and Chopra, A.K., ‘Seismic Response Study of the US 101/Painter Street Overpass Using Strong Motion Records’, *SMIP94 Seminar Proceedings*

- [10] Goldberg, D.E. 1989. "Genetic Algorithms in Search, Optimization and Machine Learning". *Reading, MA: Addison-Wesley*, pp. 28–33.
- [11] Hong, A.L., Betti, R. "Identification of Dynamic Models of a Building Structure Using Multiple Earthquake Records", *Journal of the International Association for Structural Control and Monitoring*, Vol. 16, No. 2, pp. 178-199
- [12] Juang, J.N. and Pappa, R.S. 1985. "An Eigensystem Realization Algorithm for Modal Parameters Identification and Model Reduction." *Journal of Guidance Control and Dynamics*, Vol.8, No.5, pp. 620-627
- [13] Lus, H., Betti, R. and Longman, R.W. 1999 'Identification of Linear Structural Systems Using Earthquake-Induced Vibration Data', *Earthquake Engineering and Structural Dynamics*, Vol. 28, pp. 1449-1467
- [14] Lus, H. 2001. *Control Theory Based System Identification*. Ph. D. Thesis, Columbia University, New York.
- [15] Lus, H., Betti, R. and Longman, R.W. 2002 'Obtaining Refined First Order Predictive Models of Linear Structural Systems', *Earthquake Engineering and Structural Dynamics*, 31, pp. 1413-1440
- [16] Lus, H., Betti, R., Yu, J. and M. De Angelis. "Investigation of a System Identification Methodology in the Context of the ASCE Benchmark Problem.", *Journal of Engineering Mechanics*, Benchmark Issue, ASCE
- [17] Lus, H., De Angelis, M. and Betti R. 2002. "A New Approach for Reduced Order Modeling of Mechanical System Using Vibration Measurements", submitted to *ASME Journal of Applied Mechanics*.

- [18] Mahin, S. 2005. "Future Directions in Earthquake Simulation," *Proceedings, International Conference on Advances in Experimental Structural Engineering, Int. Association of Experimental Structural Engineering, AESE*. Keynote paper, Nagoya, Japan, July 2005, 11 pp.
- [19] Pepper, D.W. and J.C. Heinrich. 1992. "THE FINITE ELEMENT METHOD: Basic Concepts and Applications." Hemisphere Publishing Corporation
- [20] Romstad, K., Maroney, B. and Chajes, M., 'Interpretation of Rio Dell Freeway Response During Six Recorded Earthquake Events', *SMIP89 Seminar Proceedings*
- [21] Romstad, K. and Maroney, B., 'Interpretation of Painter Street Overcrossing Records to Define Input Motions to the Bridge Superstructure', *SMIP90 Seminar Proceedings*
- [22] SAP2000 (2009), 'Integrated Finite Element Analysis and Design of Structures', by Computers and Structures, Inc., Berkeley, CA
- [23] Shamsabadi, A., Kapuskan, M. 'Nonlinear Seismic-Soil Abutment-Structure Interaction Analysis of Skewed Bridges'
- [24] Viola, E. *Fondamenti di Analisi Matriciale delle Strutture*, Pitagora Editrice, Bologna
- [25] Yu, J. 2004. *Identification of Structural System with Limited Set of Instrumentation*, Ph. D. Thesis, Columbia University, New York

- [26] Waisman, H. 2009 *Finite Element Analysis II Notes from Class of Finite*.
Columbia University, New York
- [27] Zhang, J., Makris, N. 2002. “Kinematic Response Functions and Dynamic
Stiffnesses of Bridge Embankments”, *Earthquake Engineering and Structural
Dynamics*, Vol. 31, No. 11, pp. 1933-1966

APPENDIX A

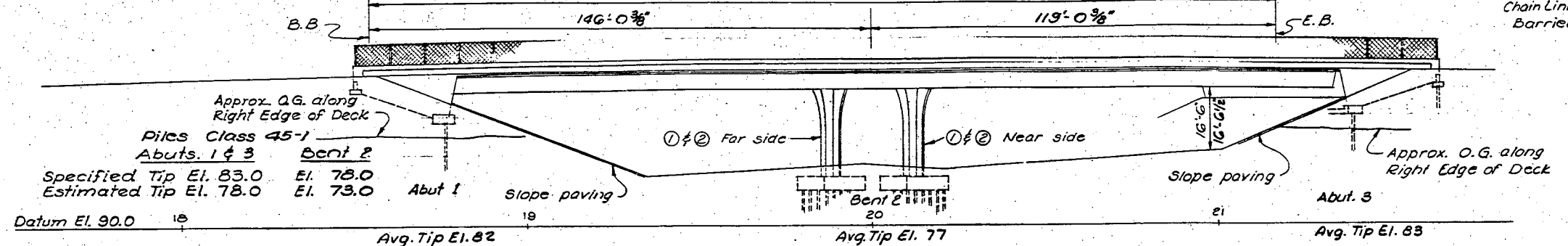
Rio Dell – Hwy 101/Painter Street Overpass Plans

REGISTERED CIVIL ENGINEER NUMBER 9013
 ASSISTANT STATE HIGHWAY ENGINEER
 DATE APR. 19 November 19, 1976



PROFILE GRADE
No Scale

Distances measured along Painter Street
265'-0 3/4"

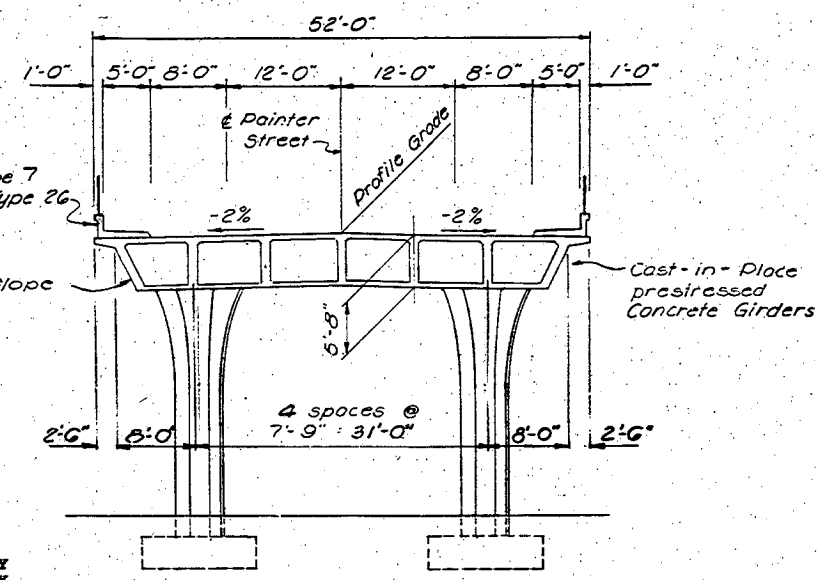


ELEVATION
Scale: 1" = 20'-0"

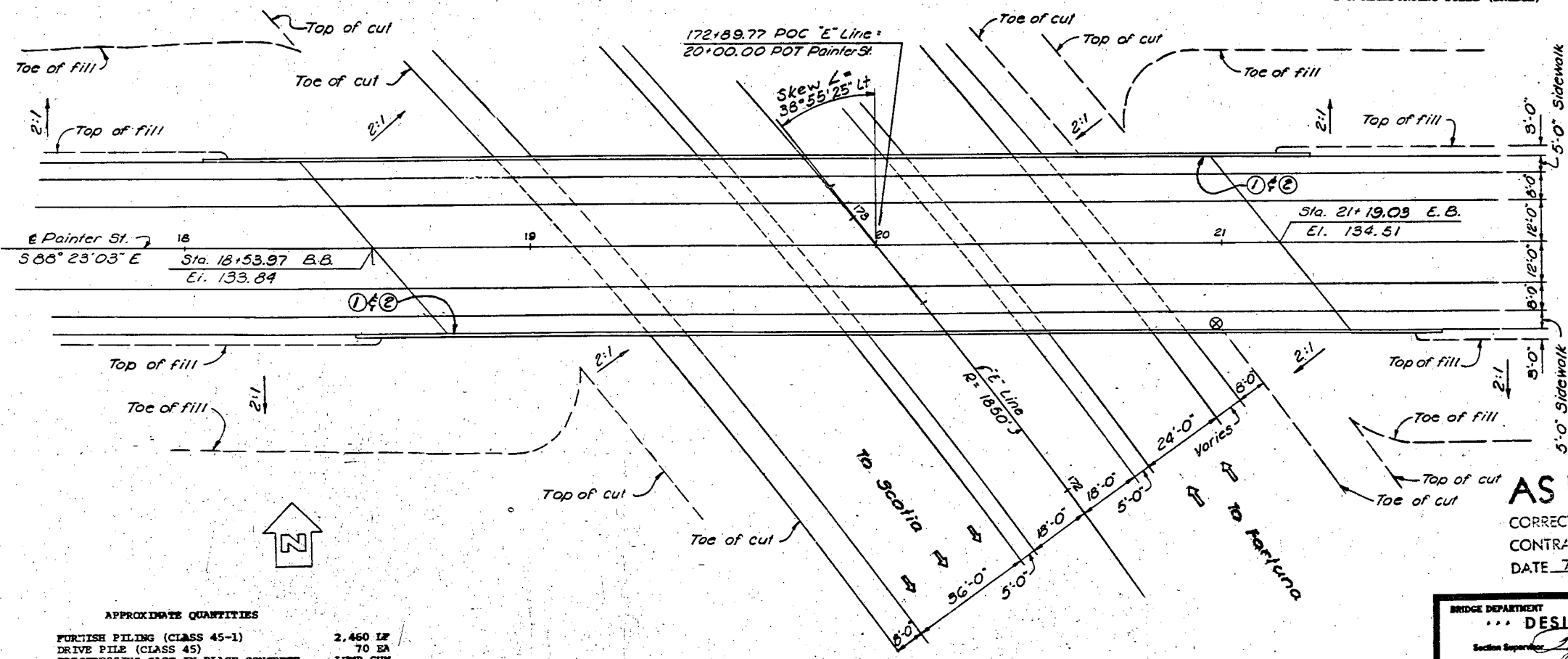
Class 45-1 12" Prestressed Piles

FINAL PAY QUANTITIES

STRUCTURE EXCAVATION (BRIDGE)	340 CY
STRUCTURE BACKFILL (BRIDGE)	175 CY
STRUCTURE CONCRETE, BRIDGE FOOTING	88 CY
STRUCTURE CONCRETE, BRIDGE	230 CY
CAST-IN-PLACE PRESTRESSED CONCRETE (GRADE 35-50)	1,025 CY
BAR REINFORCING STEEL (BRIDGE)	225,000 LB



TYPICAL SECTION
Scale: 1" = 10'-0"



PLAN
Scale: 1" = 20'-0"

INDEX TO PLANS

Sheet No.	Title
1	General Plan
2	Deck Contours
3	Foundation Plans
4	Abutment Details
5	Bent 2 Details
6	Typical Section
7	Girder Layout
8	Simple Beam Wingwall Details
9	Slope Paving Details - Full Slope
10	Log of Test Borings

STANDARD PLANS DATED JANUARY, 1973

A62-BB	EXCAVATION AND BACKFILL BRIDGE-LIMITS OF PAYMENT
B0-1	BRIDGE DETAILS (GENERAL & ABUTMENT)
B0-3	BRIDGE DETAILS (WALLS)
B0-5	BRIDGE DETAILS (DECKS)
B2-1	PILE DETAILS - CLASS 45-1 & CLASS 45-2
B7-1	BOX GIRDER DETAILS
B8-5	CAST-IN-PLACE PRESTRESSED GIRDER DETAILS
B11-52	CHAIN LINK RAILING TYPE 7
B11-54	BARRIER RAILING TYPE 26

AS BUILT

CORRECTIONS BY I.A. Schroeder
 CONTRACT NO. 01-061224
 DATE 7-23-76 R.T. 4-1-77

APPROXIMATE QUANTITIES

FURNISH PILING (CLASS 45-1)	2,460 LP
DRIVE PILE (CLASS 45)	70 EA
PRESTRESSING CAST-IN-PLACE CONCRETE	1,025 CY
WATERSTOP	35 LP
STRIP WATERSTOP	60 LP
8" PERFORATED STEEL PIPE UNDERDRAIN (.064" THICK)	116 LP
CLASS 1 PERMEABLE MATERIAL (BRIDGE)	30 CY
8" CORRUGATED STEEL PIPE DOWNDRAIN (.064" THICK)	92 LP
SLOPE PAVING (CONCRETE)	69 CY
CHAIN LINK RAILING (TYPE 7)	635 LP

AS BUILT PLANS
Contract No. 01-061224

- ⊗ Point of minimum vertical clearance.
 - ① Point "Bridge No. 4-236" year constructed.
 - ② Point "Painter Street Overcrossing".
- FOR GENERAL NOTES SEE "Deck Contours" sheet

BRIDGE DEPARTMENT
DESIGN SECTION 6

Section Supervisor: P.W. Olson 10-73
Project Designer: P.W. Olson 10-73

DESIGN	By Nelson 3/70	Checked P.W. Olson
DETAILS	By W.L. Gray 2-69	Checked P.W. Olson
LAYOUT	By Nelson 3/70	Checked P.W. Olson
QUANTITIES	By R.B.R. 11/73	Checked R.B.R.
SPECIFICATIONS	By R.B.R. 11/73	Checked R.B.R.

Approval Recommended by: [Signature] District Engineer
Checked by: [Signature] District Engineer

STATE OF CALIFORNIA
DEPARTMENT OF TRANSPORTATION

PAINTER STREET OVERCROSSING
LOCATED IN THE CITY OF RIO DELL IN HUMBOLDT COUNTY

GENERAL PLAN


BRIDGE NO.	4-236	POST MILE	53.2	DRAWING NO.	09236-1	SHEET	1
------------	-------	-----------	------	-------------	---------	-------	---

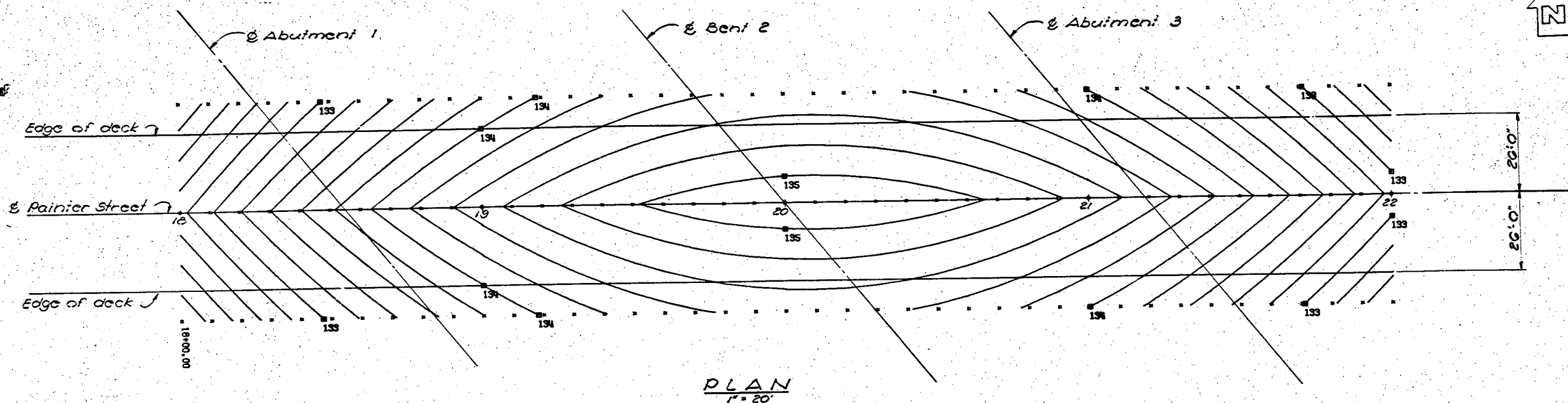
WO 061221
CU 01201

Revised print bearing earlier revision dates

REVISION DATES (PRELIMINARY STAGE ONLY)

NO.	DATE	DESCRIPTION
1	7/27/76	AS BUILT


 DATE APPROVED November 19, 1973

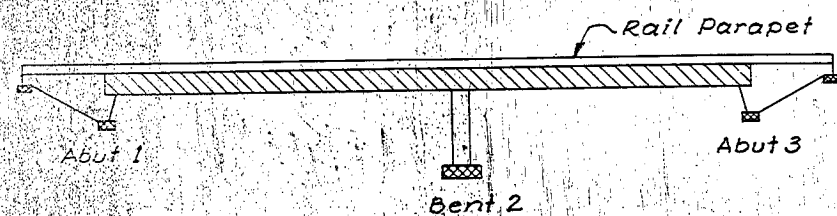


□ = indicates even foot contours.
 X = 10' intervals
 Contours do not include camber.


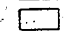

GENERAL NOTES
 DESIGN: A.A.S.H.O. dated 1973 with revisions and as supplemented by BRIDGE PLANNING AND DESIGN MANUAL.

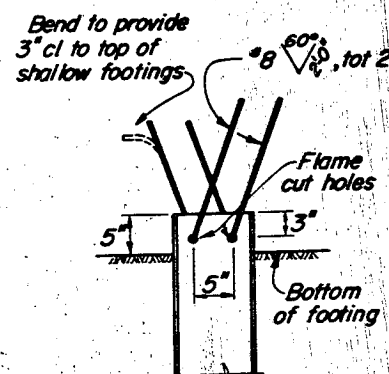
LIVE LOADING: HS20-44 and alternative
 REINFORCED CONCRETE: $f_s = 24,000$ psi, except
 = 20,000 PSI in transverse deck slabs and stirrups
 $f_c = 1,300$ psi, except
 = 1,200 psi in transverse deck slabs
 $n = 10$

PRESTRESSING NOTES
 $P_{jack} = 11,690$ kips total at jacking ends. $A_s = \frac{P_{jack}}{0.75 f_s}$
 Total number of girders = 7
 CONCRETE: $f_c = 3500$ psi @ 28 days; $f_{ci} = 3500$ psi @ time of stressing
 GENERAL: *1. Design is based on $u = 0.25$ and $k = 0.0002$. For girders on horizontal curved alignment $(k+k') = \frac{P_{jack}}{A_s}$ where k' is a modification factor which considers the effect of such curvature on friction
 P_{jack} specified at the jacking ends includes friction losses and provision for 25,000 psi loss in stress
 2. Tendons to be jacked to $0.75 f_s$ and anchored at an equivalent anchor set = $5/8"$.



PAY LIMITS OF CONCRETE

-  Cast-in-place Prestressed Concrete
-  Structure Concrete, Bridge
-  Structure Concrete, Bridge Footing



STEEL PILE ANCHOR

 Standard Plan Sheet No.
 Detail No.

NO AS BUILT CORRECTION
AS BUILT
 CORRECTIONS BY I.A. Schroeder
 CONTRACT NO. 01-061224
 DATE 8-03-76 R.T. 4-1-77

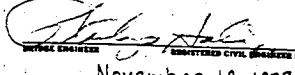
BRIDGE DEPARTMENT DESIGN SECTION 6		STATE OF CALIFORNIA DEPARTMENT OF TRANSPORTATION	
Project Engineer: P. W. Olson		PAINTER STREET OVERCROSSING	
DESIGN: By: W. J. Olson		DECK CONTOURS	
DETAILS: By: P. W. Olson		BRIDGE NO. 4-230	
QUANTITIES: By: P. W. Olson		POST MILE 53.2	
Checked: R. Green		DRAWING NO. 2	
SHEET 2		DRAWING NO. 2	

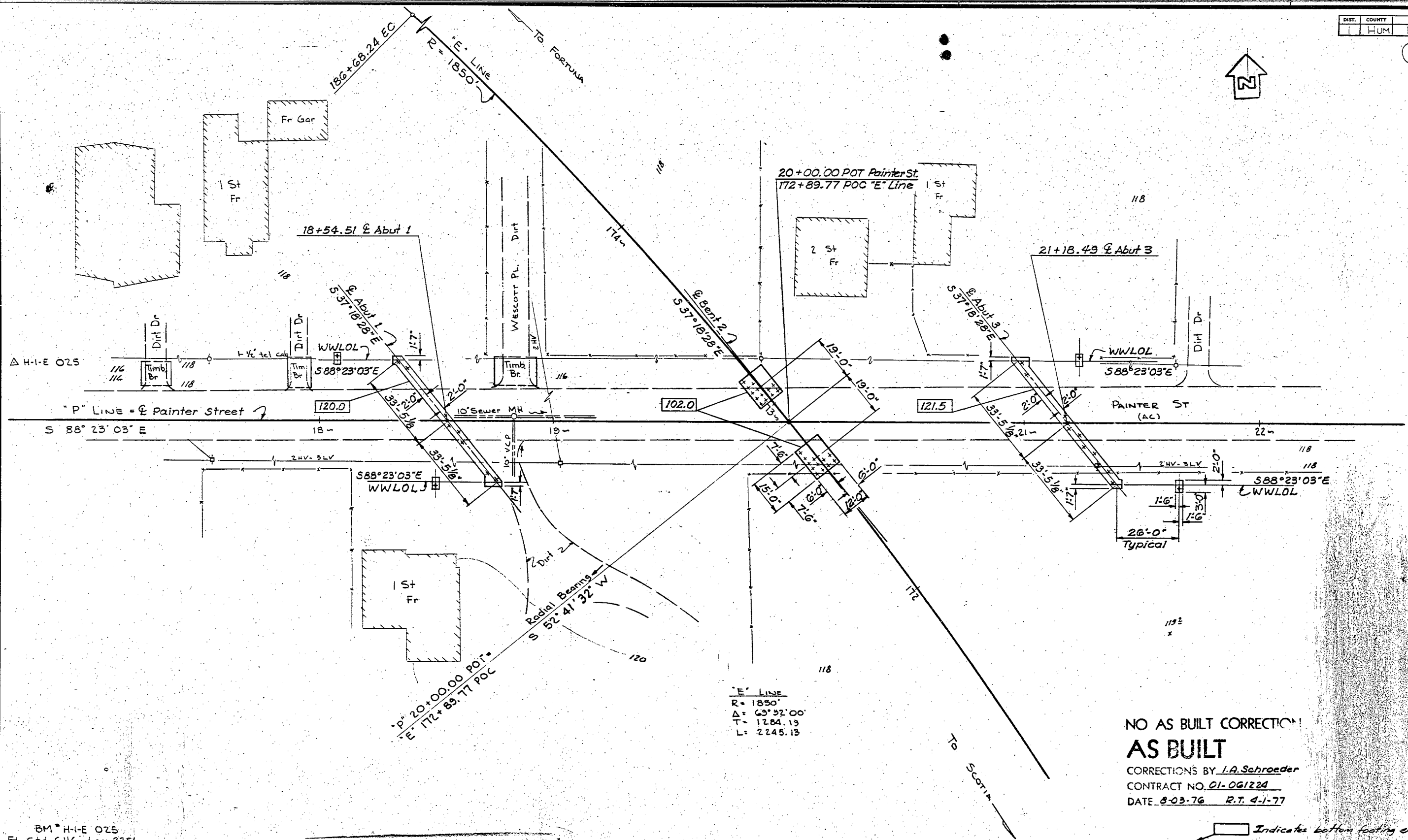
AS BUILT PLANS
 Contract No. 01-061224

WO
CU

Disregard prints bearing earlier revision dates

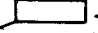
REVISION DATES	PRELIMINARY STAGE ONLY


 REGISTERED CIVIL ENGINEER NO. 1207
 DATE APPROVED November 19, 1973



'E' LINE
 R = 1850'
 Δ = 63° 32' 00"
 T = 1284.13
 L = 2245.13

NO AS BUILT CORRECTIONS!
AS BUILT
 CORRECTIONS BY I.A. Schroeder
 CONTRACT NO. 01-061224
 DATE 8-03-76 R.T. 4-1-77

 Indicates bottom footing elevation

BM H-I-E 025
 Fd. Sta. CHC disc 225'
 Lf. 'E' 175+45
 El. 118.80

NOTE: 2-FT CONTOURS

AS BUILT PLANS
 Contract No. 01-061224
 Date Completed
 Document No. 1000-2617

SCALE 1" = 20'
 LEVEL DATUM: MSL
 FOR ALIGNMENT TIES SEE PR-4236-4
 CONTOURS AS OF OCTOBER 1968
 SITE PLAN FROM DISTRICT DATA
 SURVEY BY: EGD DATE 10-68
 DRAWN BY: RBB DATE 11-68
 TRACED BY: RDR DATE 11-68

BRIDGE DEPARTMENT DESIGN SECTION	
Project Engineer	<u>P.N. Clavin</u>
DESIGN	By <u>Wehner 3/70</u> Checked <u>P.N. Clavin</u>
DETAILS	By <u>R.Green 4/70</u> Checked <u>P.N. Clavin</u>
QUANTITIES	By <u>S. Shimura 4/73</u> Checked <u>R.Green</u>

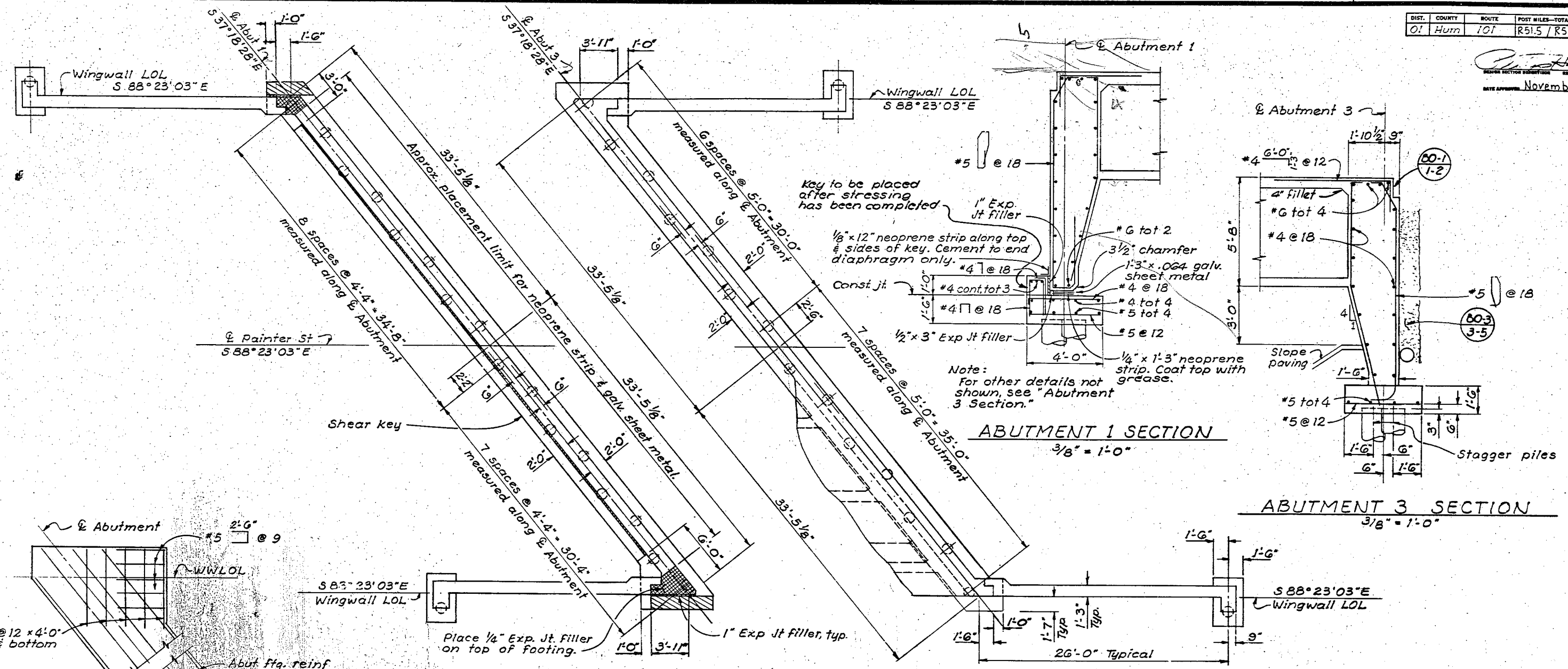
STATE OF CALIFORNIA DEPARTMENT OF TRANSPORTATION	
PAINTER STREET OVERCROSSING	
FOUNDATION PLAN	
BRIDGE NO. <u>4-236</u>	POST MILE <u>53.2</u>
DRAWING NO. <u> </u>	SHEET <u>3</u> OF <u>3</u>

WO 061221
 CU 01201

Disregard prints bearing earlier revision dates
 REVISION DATES (PRELIMINARY STAGE ONLY)

PR-4236-1

DATE APPROVED: November 14, 1973



Key to be placed after stressing has been completed

1" Exp. Jt filler

1/8" x 12" neoprene strip along top & sides of key. Cement to end diaphragm only.

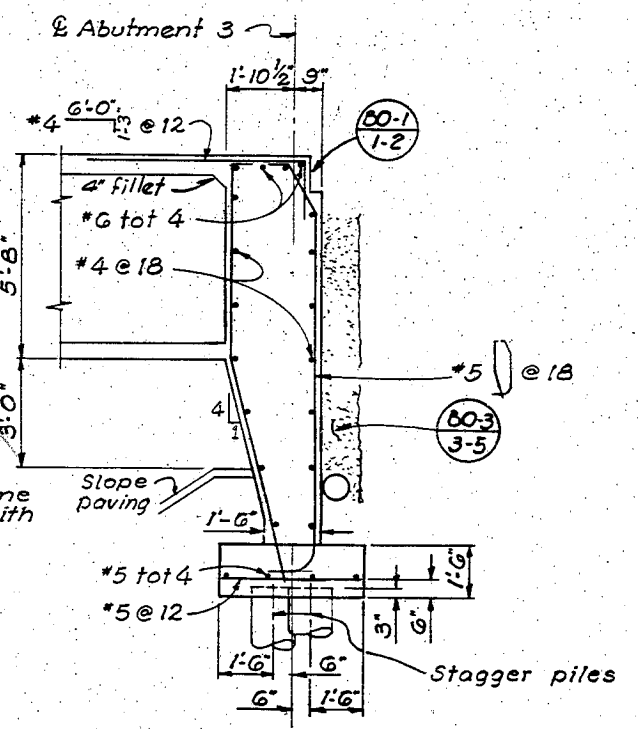
Const. jt.

7 spaces @ 5'-0" = 35'-0" measured along @ Abutment

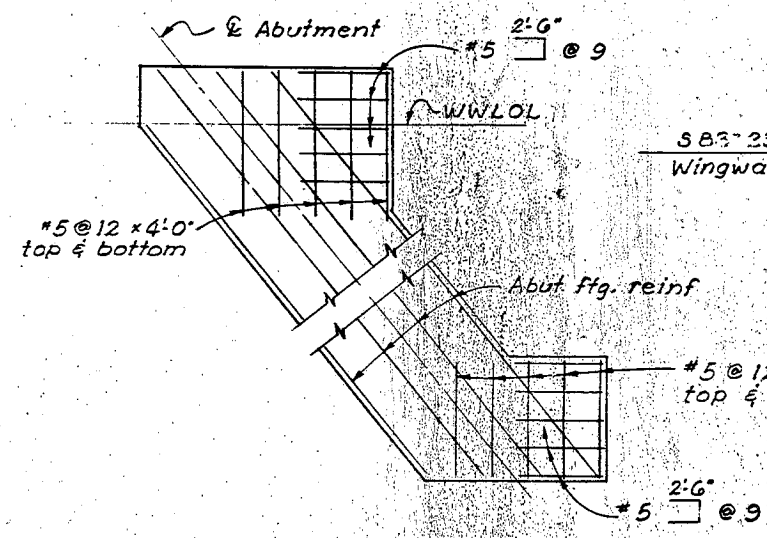
3/8" = 1'-0"

Note: For other details not shown, see "Abutment 3 Section."

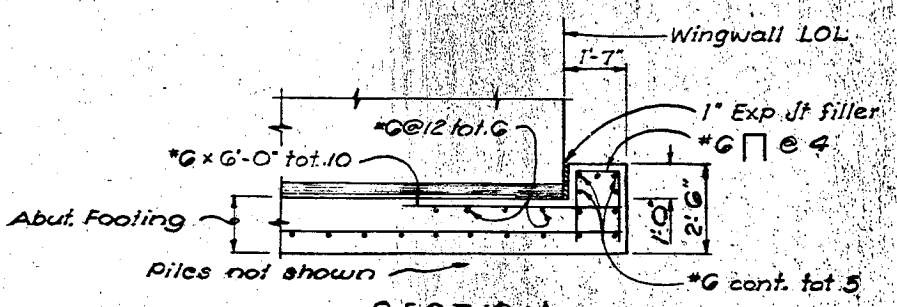
ABUTMENT 1 SECTION
3/8" = 1'-0"



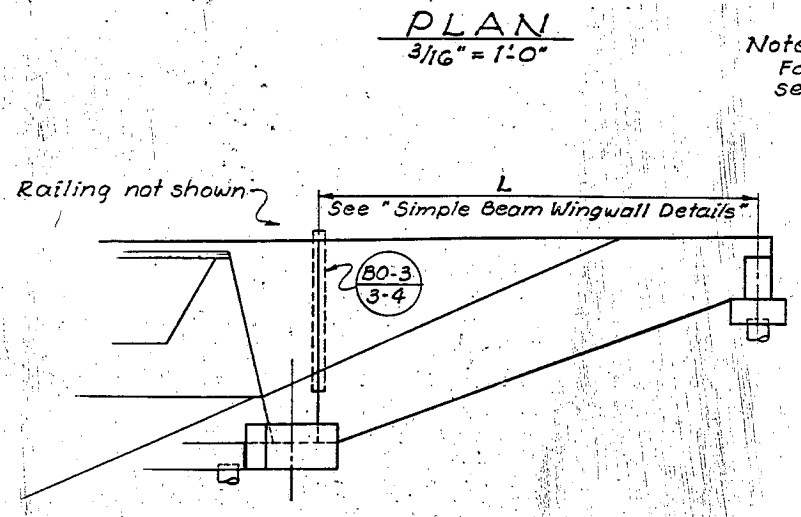
ABUTMENT 3 SECTION
3/8" = 1'-0"



FOOTING CORNER DETAIL
3/8" = 1'-0"



SECTION SHEAR KEY DETAIL
3/8" = 1'-0"

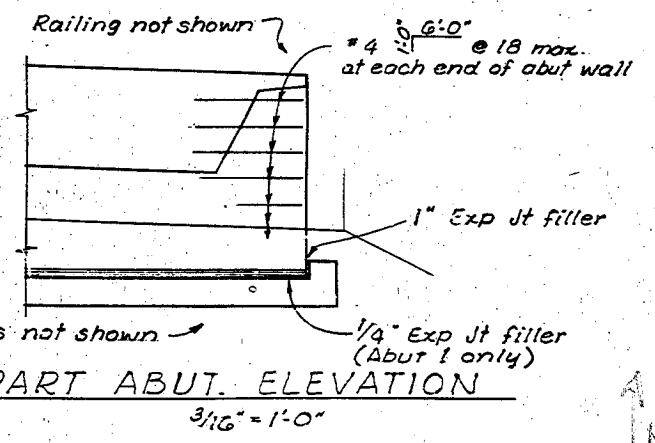


WINGWALL ELEVATION
3/16" = 1'-0"

Note: For Abutment corners and Wingwall details, see "Simple Beam Wingwall Details" sheet.

NO AS BUILT CORRECTION
AS BUILT

CORRECTIONS BY I.A. Schroeder
CONTRACT NO. 01-061224
DATE 3-03-76 R.T. 4-1-77



PART ABUT. ELEVATION
3/16" = 1'-0"

AS BUILT PLANS
Contract No. 01-061224

BRIDGE DEPARTMENT DESIGN SECTION 6		STATE OF CALIFORNIA DEPARTMENT OF TRANSPORTATION	
Project Engineer: PNOlson	DESIGN: W Helmer 3/70	PAINTER STREET OVERCROSSING	
DETAILS: R Green 3/70	Checked: PNOlson	ABUTMENT DETAILS	
QUANTITIES: D. Chinn 7/73	Checked: R Green	BRIDGE NO. 4-23G	POST MILE 53.2
		DRAWING NO.	SHEET 4 OF 10

WO
CU

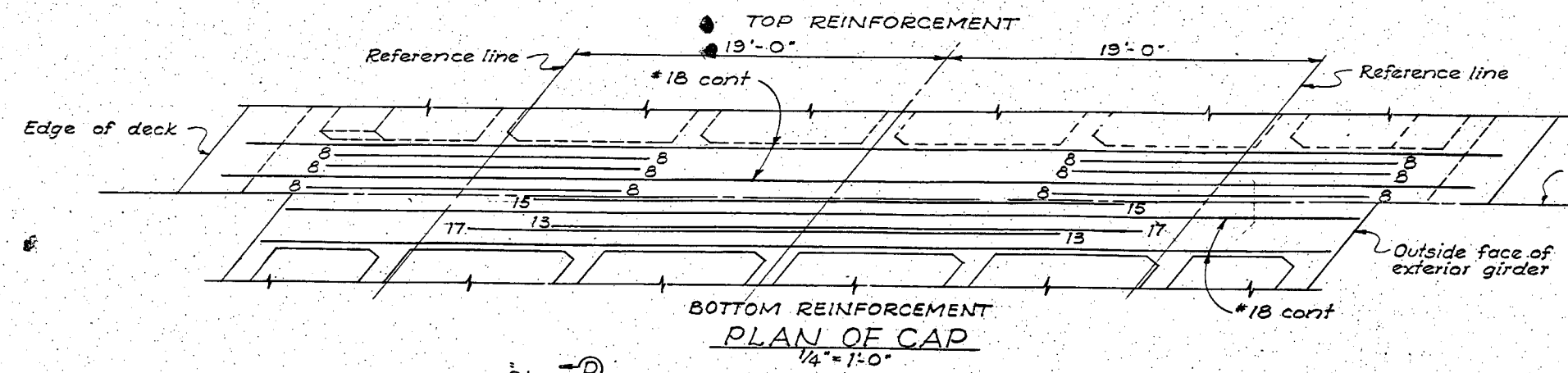
Revised prints bearing earlier revision dates.

REVISION DATES (PRELIMINARY STAGE ONLY)

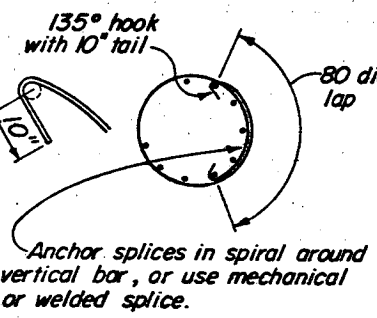
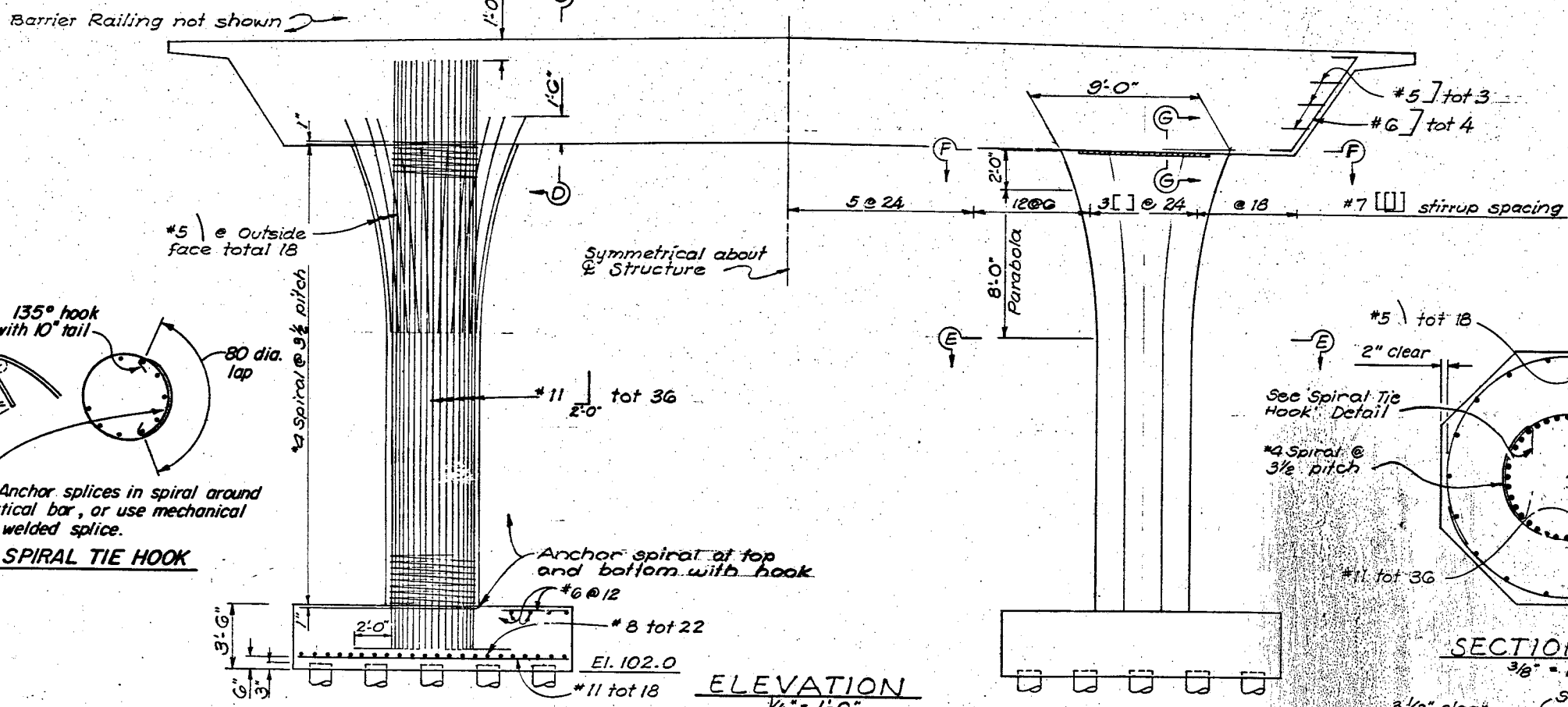
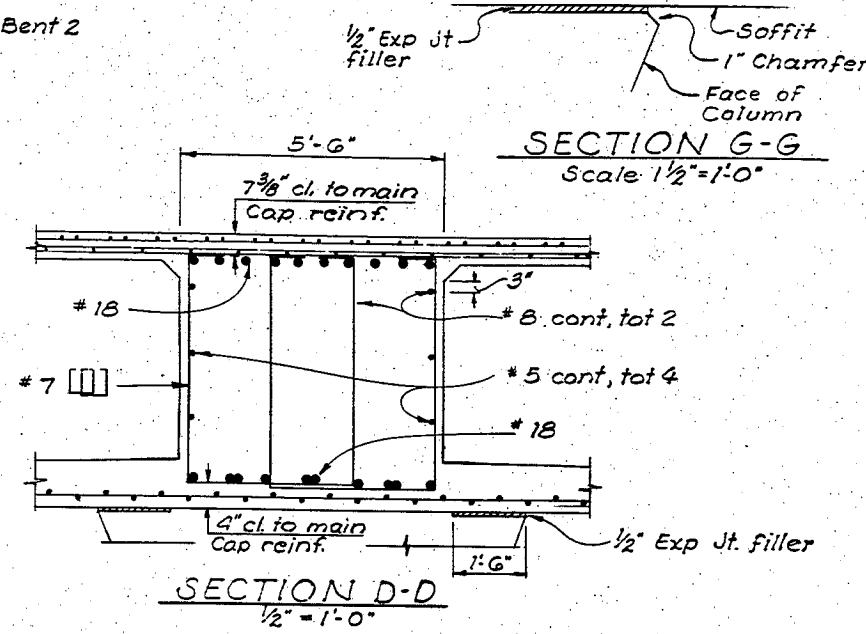
DIST.	COUNTY	ROUTE	POST MILES-TOTAL PROJECT	SHEET	TOTAL SHEETS
01	Hum	101	R5.5/R53.9	133	150

DATE APPROVED: November 19, 1913

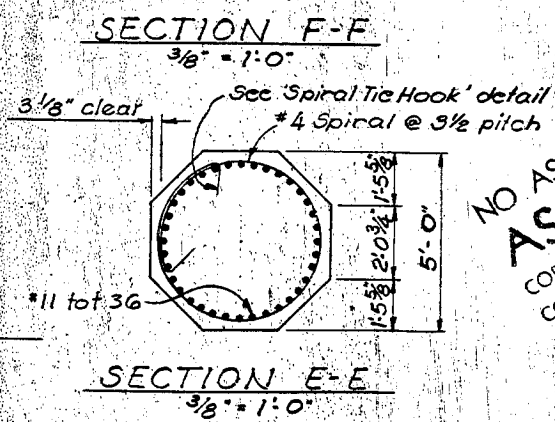
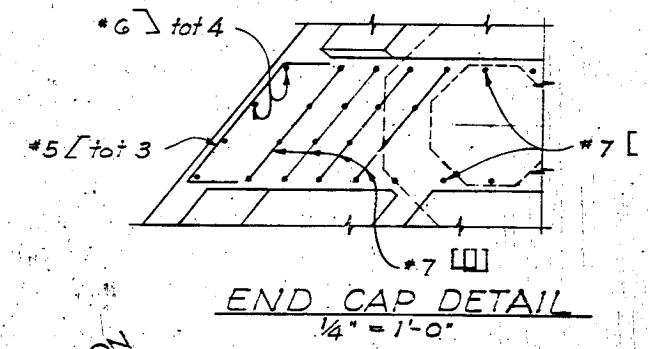
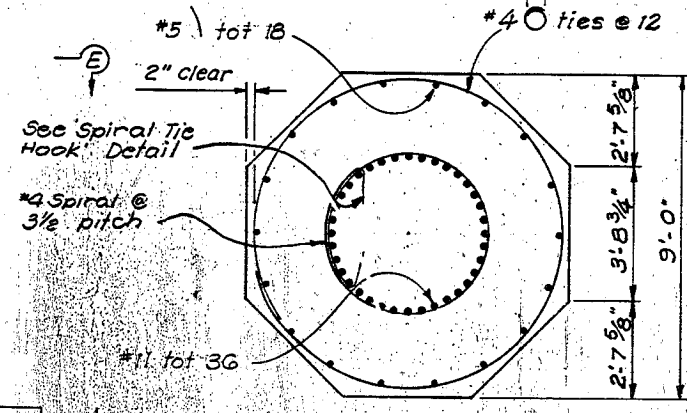
Note
All reinforcement #18 unless noted otherwise.
Numbers at ends of bars indicate distance in feet from Reference line for top reinforcement and from E Structure for bottom reinforcement.



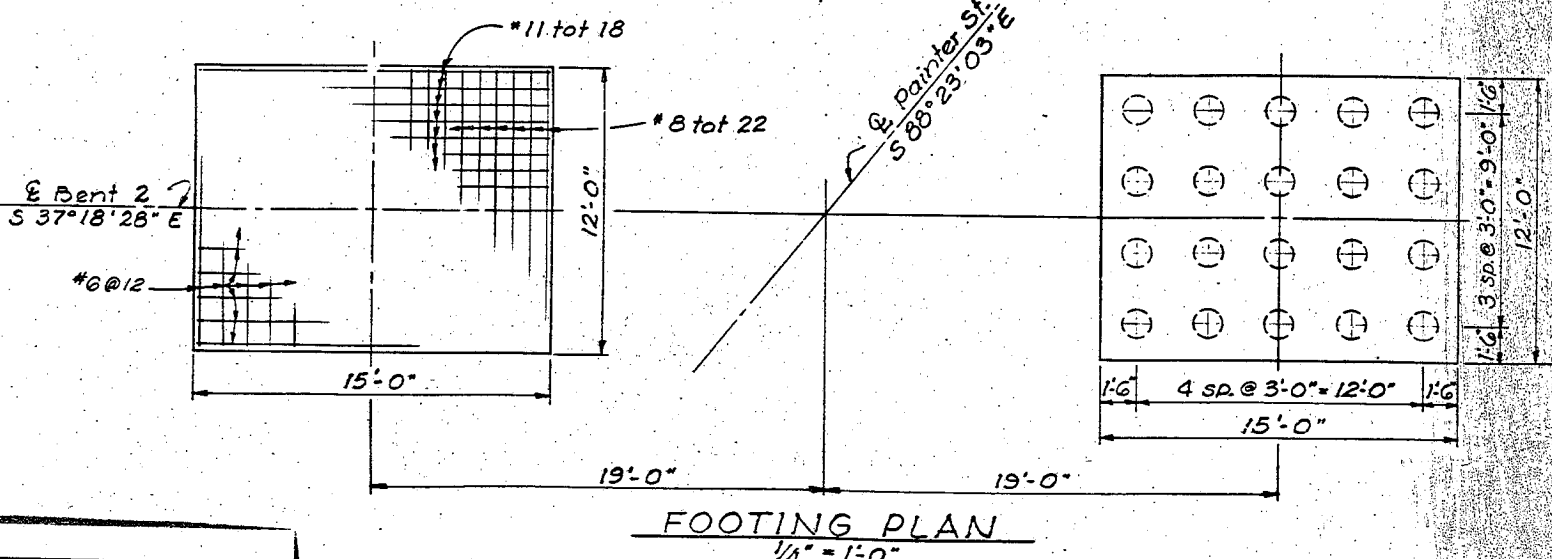
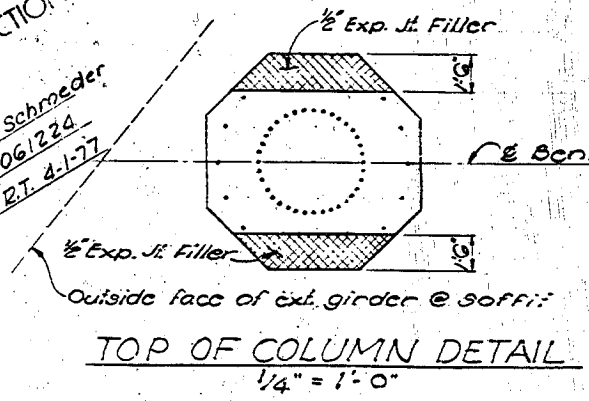
Reinforcement symmetrical about E Bent 2
S 37° 18' 28" E



Anchor splices in spiral around vertical bar, or use mechanical or welded splice.



NO AS BUILT CORRECTION
AS BUILT
CORRECTIONS BY L.A. Schneider
CONTRACT NO. 01-061224
DATE 8-03-76 ET. 4-1-77



BRIDGE DEPARTMENT		DESIGN SECTION 6	
Project Engineer	PN Olson	Checked	PN Olson
DESIGN	By Helmer 370	Checked	PN Olson
DETAILS	By R Green 4170	Checked	PN Olson
QUANTITIES	By R Green 4170	Checked	PN Olson

STATE OF CALIFORNIA DEPARTMENT OF TRANSPORTATION			
PAINTER STREET OVERCROSSING			
BENT 2 DETAILS			
BRIDGE NO.	4-236	POST MILE	53.2
DRAWING NO.	5	SHEET	10

AS BUILT PLANS
Contract No. 01-061224

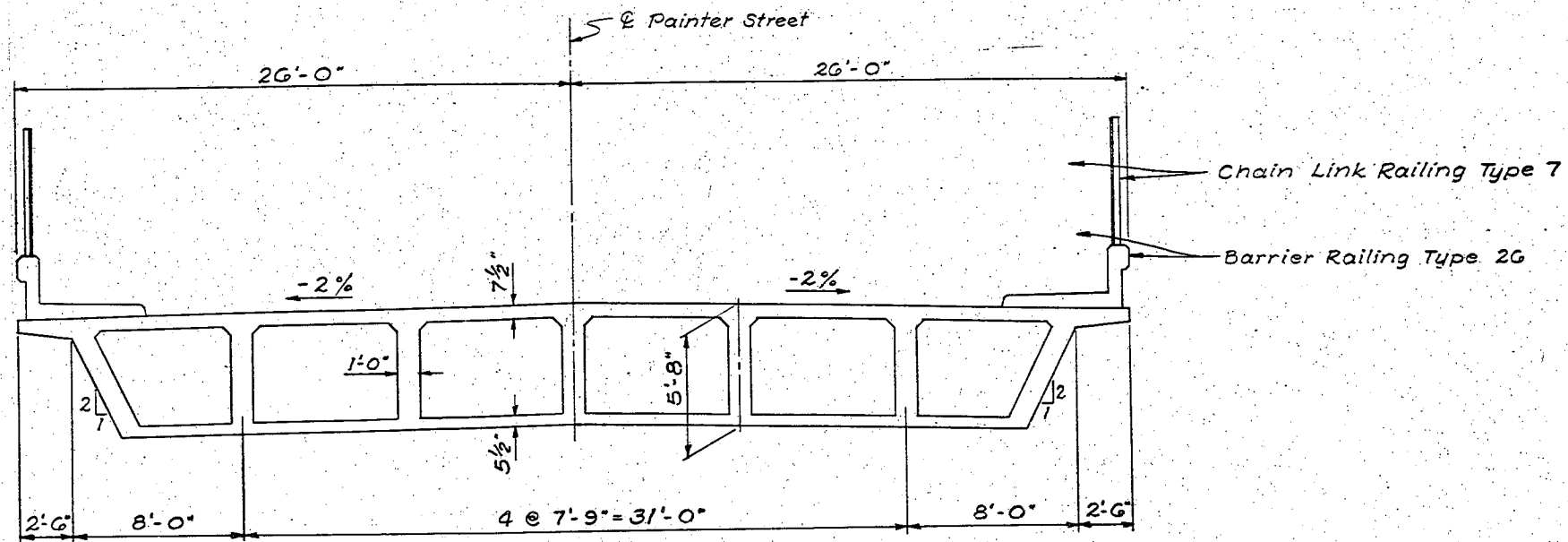
WO CU

Disregard prints bearing earlier revision dates

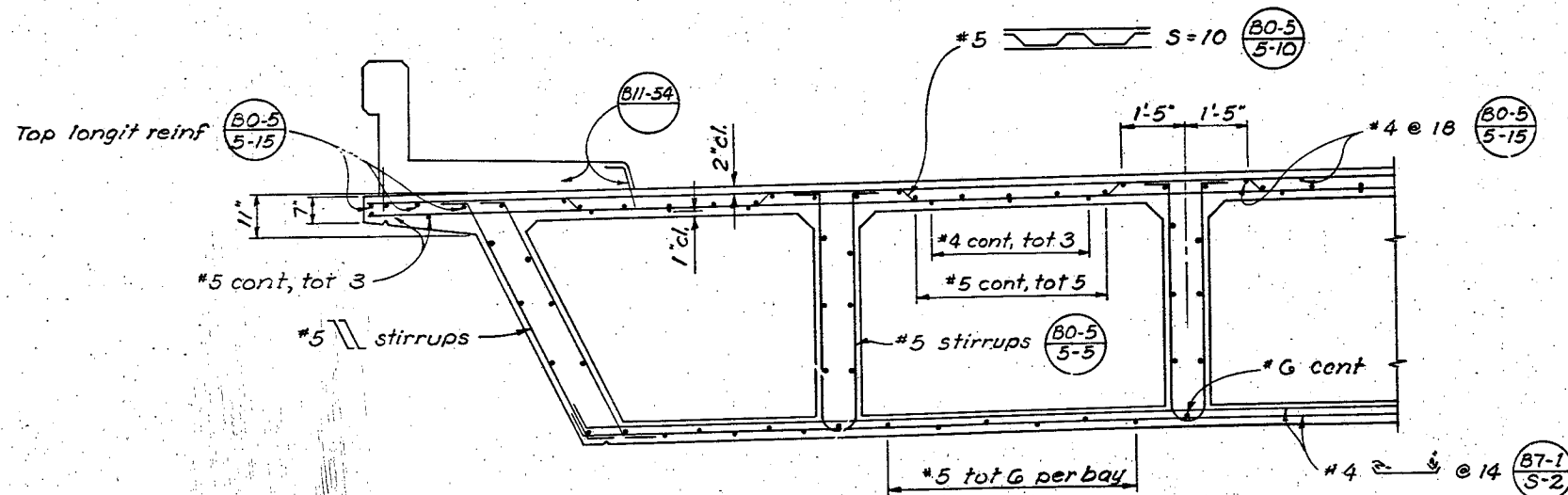
REVISION DATES (PRELIMINARY STAGE ONLY)

DIST.	COUNTY	ROUTE	POST MILES-TOTAL PROJECT	SHEET NO.	TOTAL SHEETS
01	Hum	101	R51.5/R53.9	134	150

DESIGN SECTION SUPERVISOR
 REGISTERED CIVIL ENGINEER NO. 1287
 DATE APPROVED November 19, 1973



TYPICAL SECTION
 Scale 1/4" = 1'-0"



PART-SECTION (B7-1/B-1)
 Scale 1/2" = 1'-0"

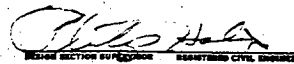
NO AS BUILT CORRECTION!
AS BUILT
 CORRECTIONS BY I.A. Schroeder
 CONTRACT NO. 01-061224
 DATE 8-05-76 RT. 4-1-77

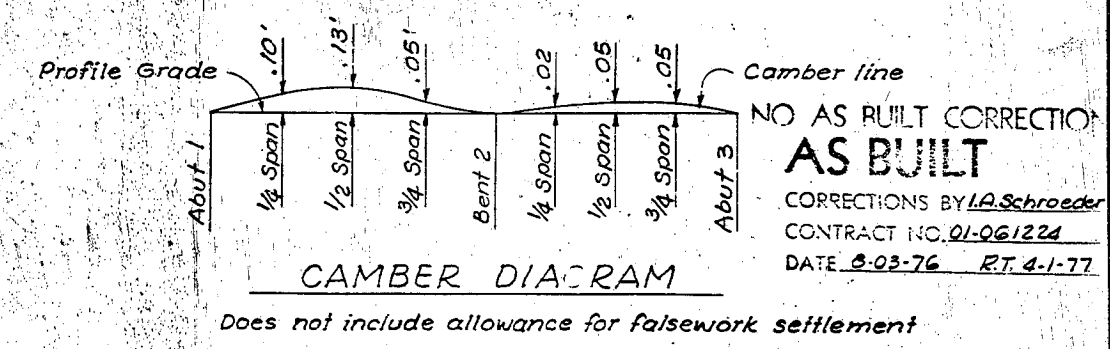
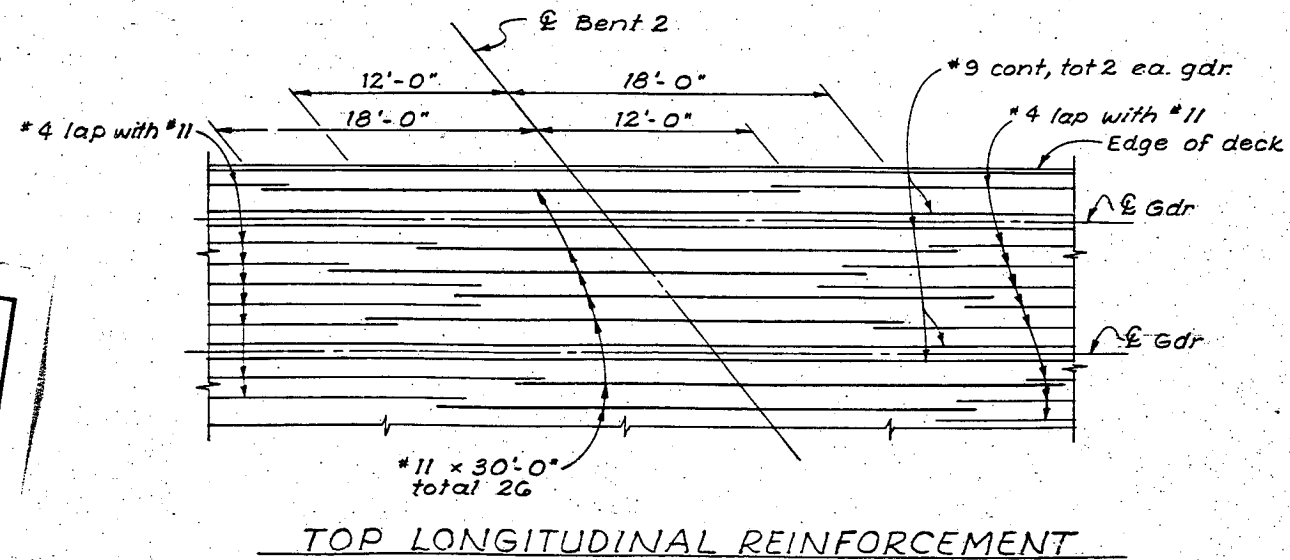
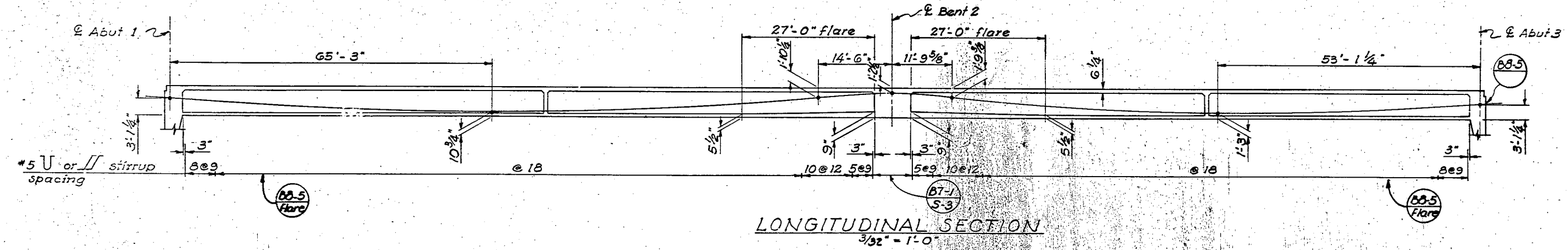
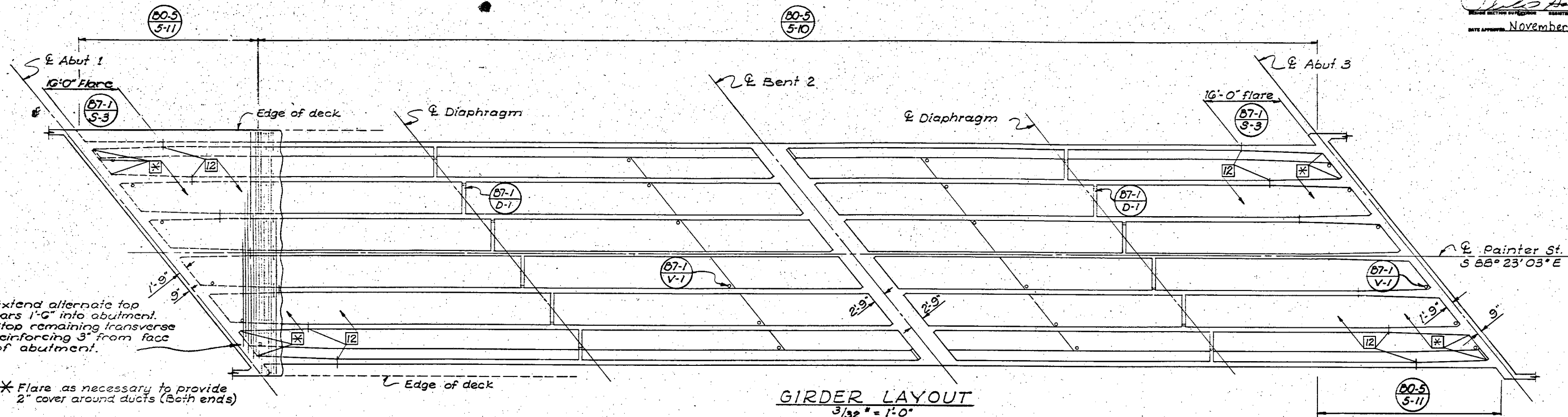
AS BUILT PLANS
 Contract No. 01-061224
 Date Completed
 Document No. 1000-2612

BRIDGE DEPARTMENT DESIGN SECTION 6		STATE OF CALIFORNIA DEPARTMENT OF TRANSPORTATION	
Project Engineer: P. Olson		PAINTER STREET OVERCROSSING	
DESIGN: By: Wehner, Checked: P. Olson		TYPICAL SECTION	
DETAILS: By: R. Green, Checked: P. Olson		BRIDGE NO. 4-236	POST MILE 53.2
QUANTITIES: By: Chimera, Checked: R. Green		DRAWING NO. 6	SHEET 10
REVISIONS: DATE		(PRELIMINARY STAGE ONLY)	

ORIGINAL SCALE 0 1 2 3 4 WO 111

DIST.	COUNTY	ROUTE	POST MILES—TOTAL PROJECT	SHEET NO.	TOTAL SHEETS
01	Hum	101	R51.5/R53.4	135	150


 REGISTERED CIVIL ENGINEER NO. 12407
 DATE APPROVED: November 19, 1973



AS BUILT PLANS
 Contract No. 01-061224
 Date Completed _____
 Document No. 10002617

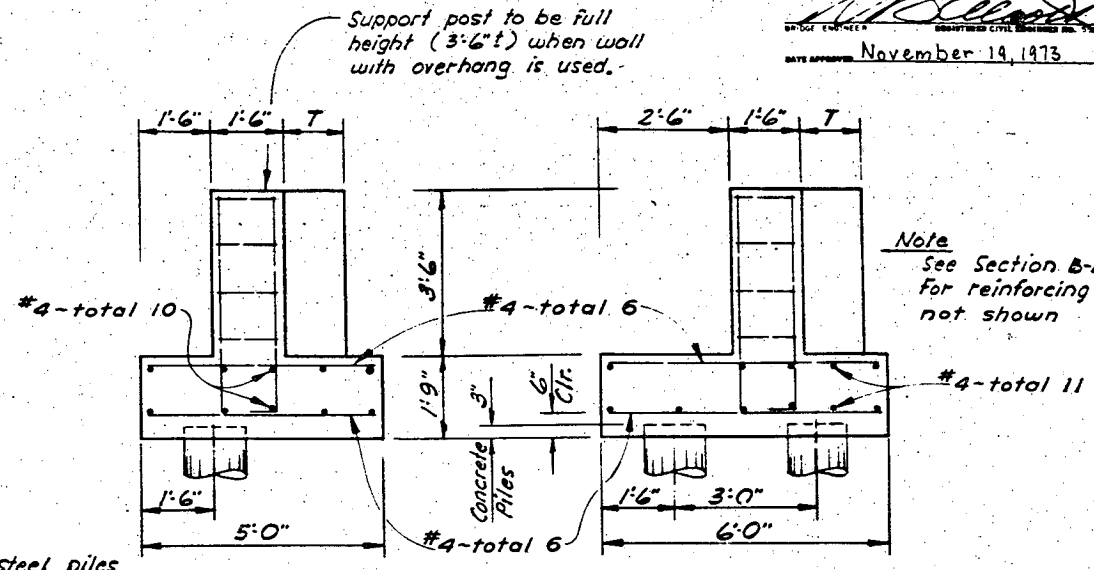
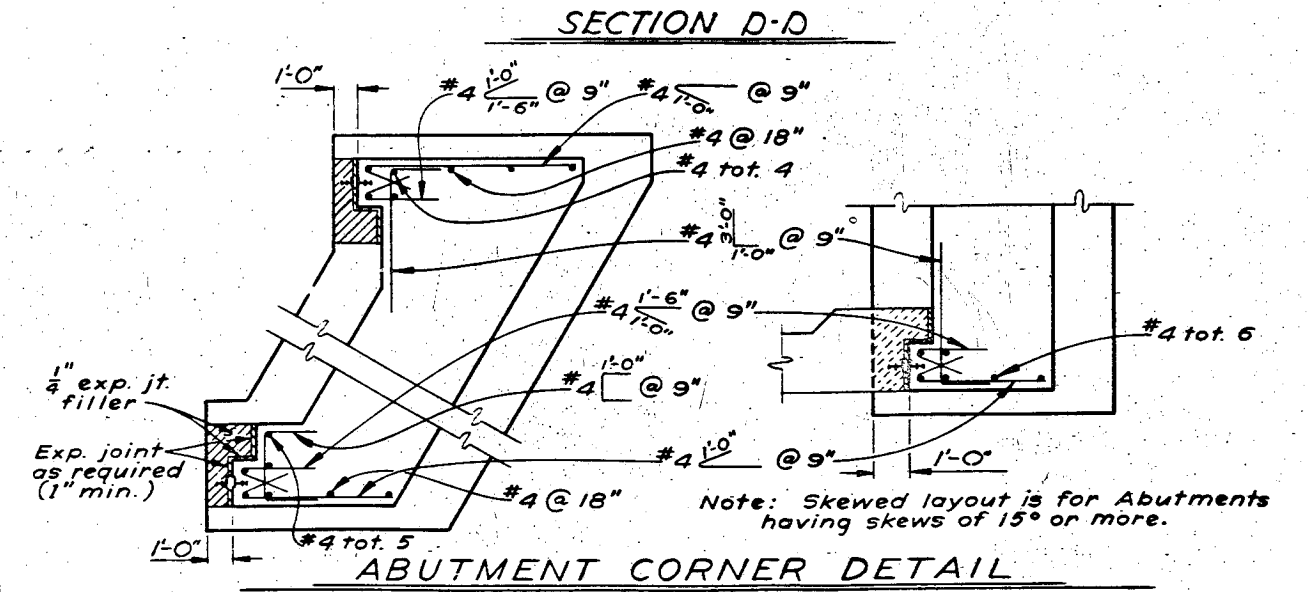
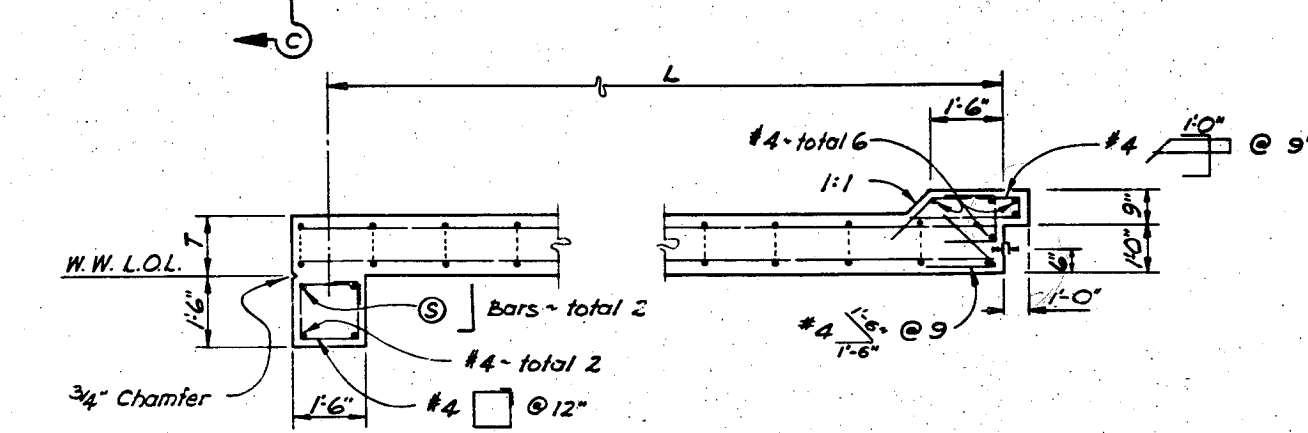
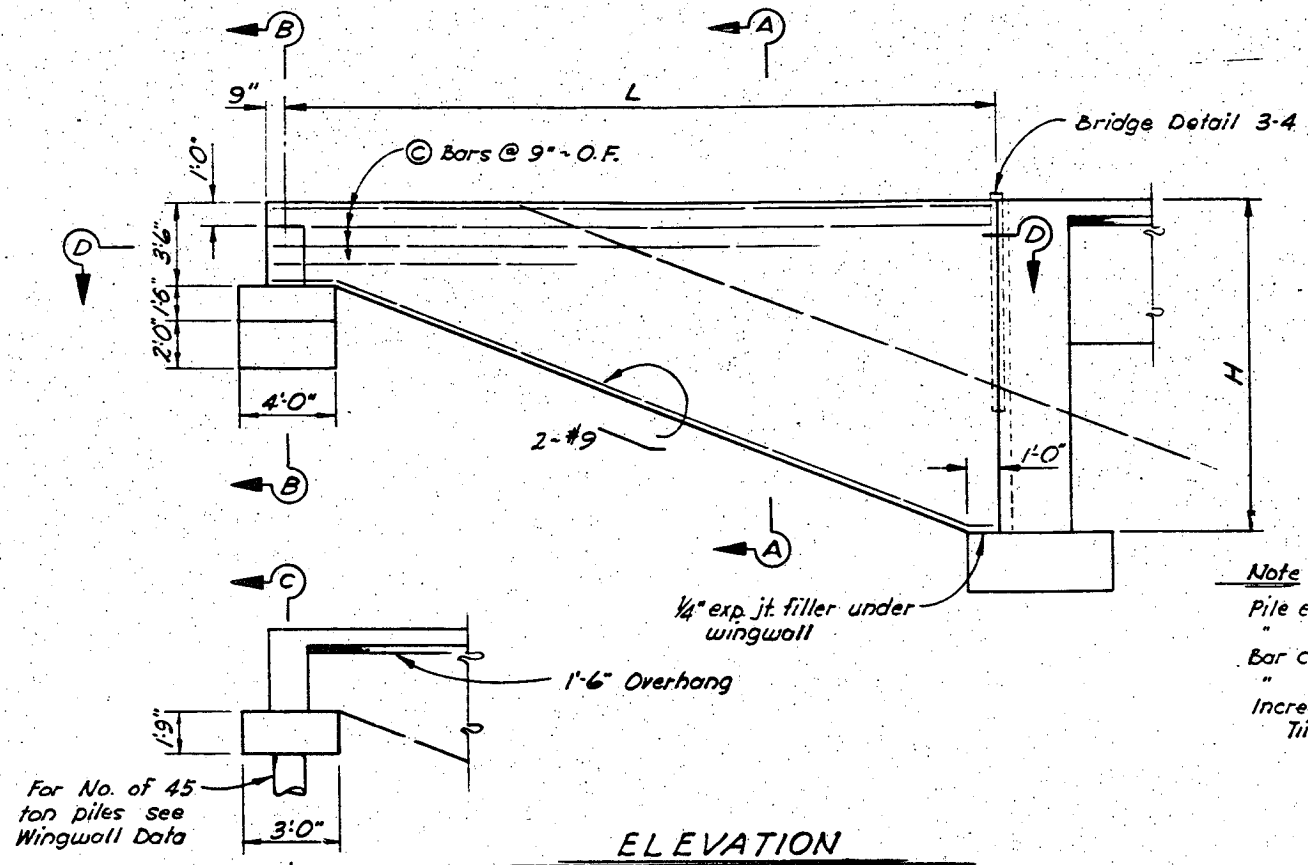
BRIDGE DEPARTMENT DESIGN SECTION 6		STATE OF CALIFORNIA DEPARTMENT OF TRANSPORTATION	
Project Engineer: <i>P. H. H. H.</i>		PAINTER STREET OVERCROSSING	
DESIGN by <i>K. H. H. H.</i> Checked <i>P. H. H. H.</i>		GIRDER LAYOUT	
DETAILS by <i>R. Green 3/70</i> Checked <i>P. H. H. H.</i>		BRIDGE NO. 4-236	
QUANTITIES by <i>J. O. H. H. 9/73</i> Checked <i>R. Green</i>		POST MILE 53.2	
REVISION DATES		DRAWING NO.	
(PRELIMINARY STAGE ONLY)		SHEET 7 OF 10	

WO CU

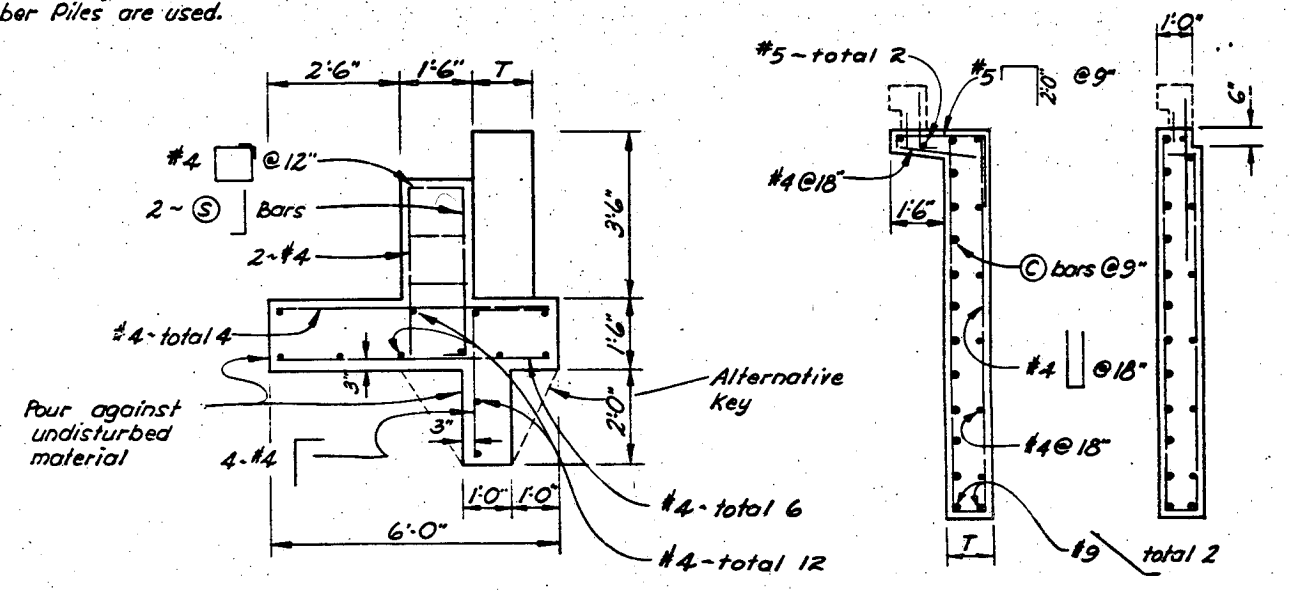
Discard prints bearing earlier revision dates

DATE APPROVED: November 14, 1973

WINGWALL DATA				
L (ft)	H (ft)	T	# Bars	No Piles
20	10	1'-0"	7	1
	11	1'-0"	7	1
	12	1'-0"	7	1
	13	1'-0"	7	1
22	14	1'-0"	8	1
	10	1'-0"	8	1
	11	1'-0"	8	1
	12	1'-0"	8	1
24	13	1'-0"	8	1
	14	1'-0"	8	1
	10	1'-0"	8	1
	11	1'-0"	8	1
26	12	1'-3"	8	1
	13	1'-3"	8	1
	14	1'-3"	8	2
	10	1'-3"	8	1
28	11	1'-3"	8	1
	12	1'-3"	9	2
	13	1'-3"	9	2
	14	1'-3"	9	2
30	10	1'-3"	9	1
	11	1'-3"	9	1
	12	1'-3"	9	2
	13	1'-3"	9	2
32	14	1'-6"	9	2
	10	1'-3"	9	1
	11	1'-6"	9	2
	12	1'-6"	9	2
34	13	1'-6"	9	2
	14	1'-6"	10	2
	10	1'-6"	9	1
	11	1'-6"	9	2
36	12	1'-6"	9	2
	13	1'-6"	10	2
	14	1'-6"	10	2
	38	10	1'-6"	10
11		1'-6"	10	2
12		1'-6"	10	2
13		1'-6"	10	2
40	14	1'-9"	10	2
	10	1'-6"	10	2
	11	1'-6"	10	2
	12	1'-9"	10	2
	13	1'-9"	10	2
	14	1'-9"	10	2



Note
 Pile embedment = 5" for steel piles
 = 6" for timber piles
 Bar clearance = 6" for Steel Piles
 " " = 9" for Timber Piles
 Increase footing depth to 2'-0" if
 Timber Piles are used.



Note: When superstructure is prestressed,
 the wingwall must be placed after stress-
 ing is completed. Backfill material
 inside of walls must be placed prior to
 placing backfill outside of walls.

1'-6" OVERHANG NO OVERHANG
 SECTION A-A

AS BUILT PLANS
 Contract No. 01-061224
 Date Completed _____
 Document No. 1000-261

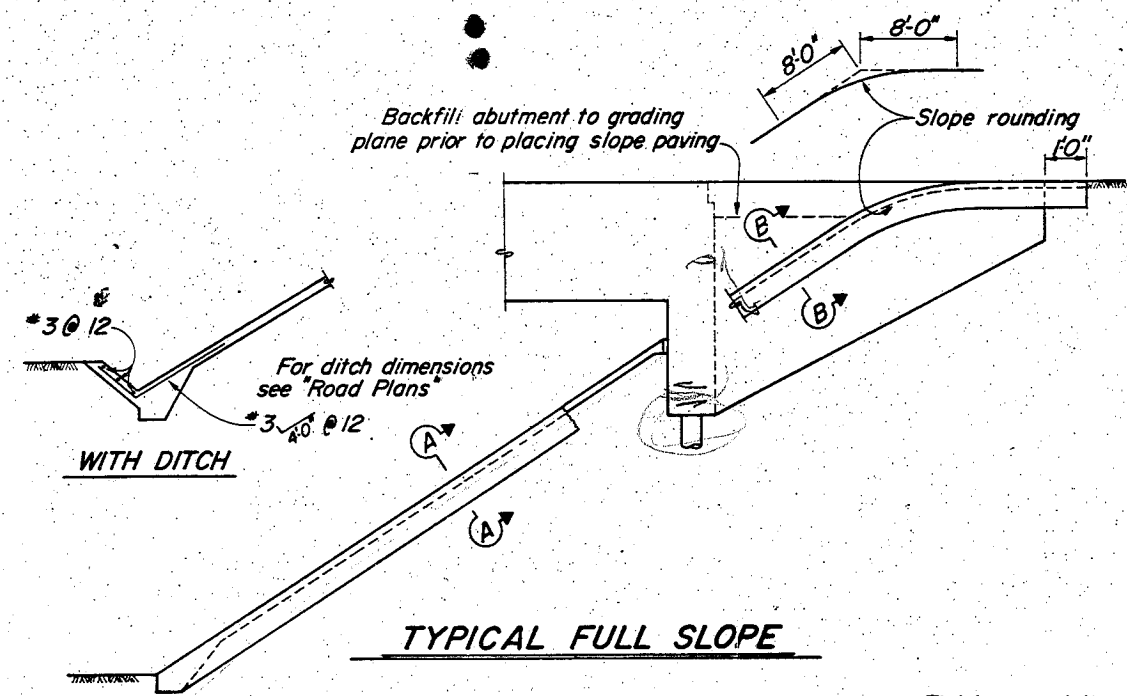
NO AS BUILT CORRECTION
AS BUILT
 CORRECTIONS BY I.A. Schroeder
 CONTRACT NO. 01-061224
 DATE 8-03-76 R.T. 4-1-77

STATE OF CALIFORNIA		XS-4-25	
6/71 DEPARTMENT OF TRANSPORTATION			
PAINTER STREET OVERCROSSING			
SIMPLE BEAM WINGWALL DETAILS			
BRIDGE NO. 4-23G	POST MILE 53.2	DRAWING NO.	SHEET 8 OF 10
REVISION DATES (PRELIMINARY STAGE ONLY)			

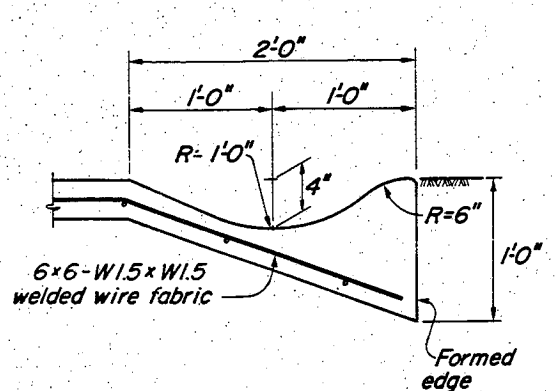
WO
CU

Discard prints bearing earlier revision dates

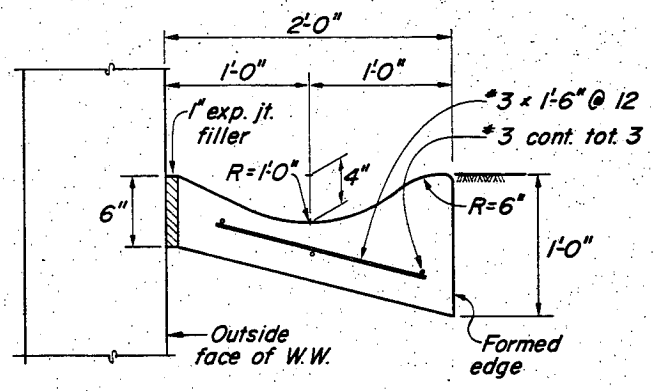
BRIDGE ENGINEER
 REGISTERED CIVIL ENGINEER 5585
 DATE APPROVED November 19, 1973



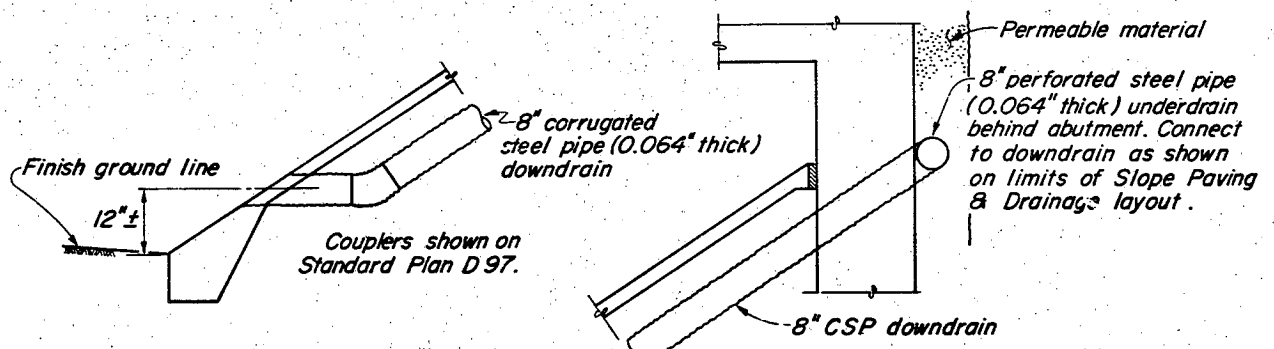
TYPICAL FULL SLOPE



SECTION A-A

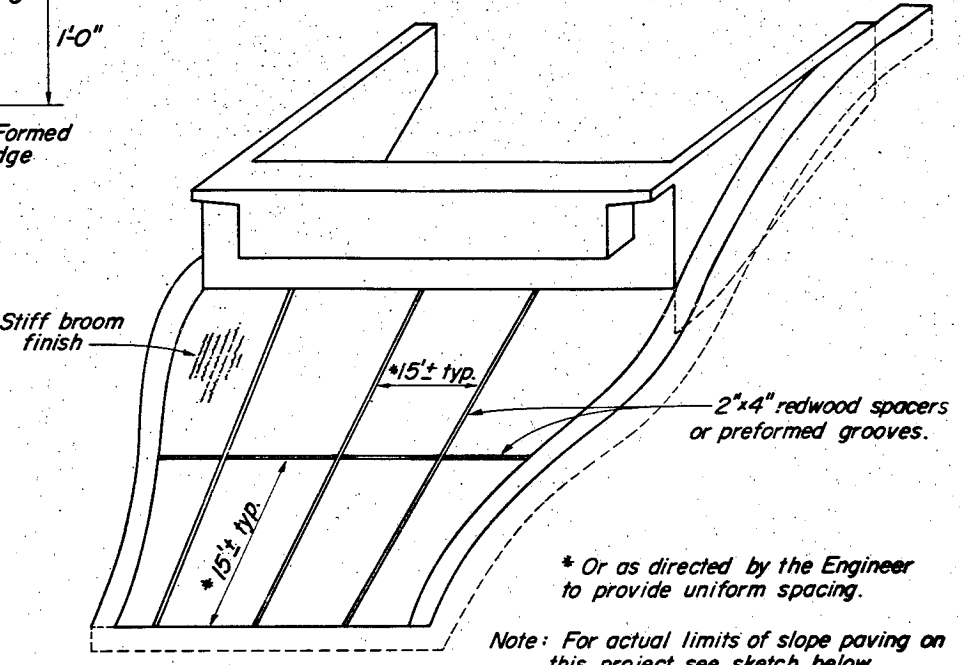


SECTION B-B



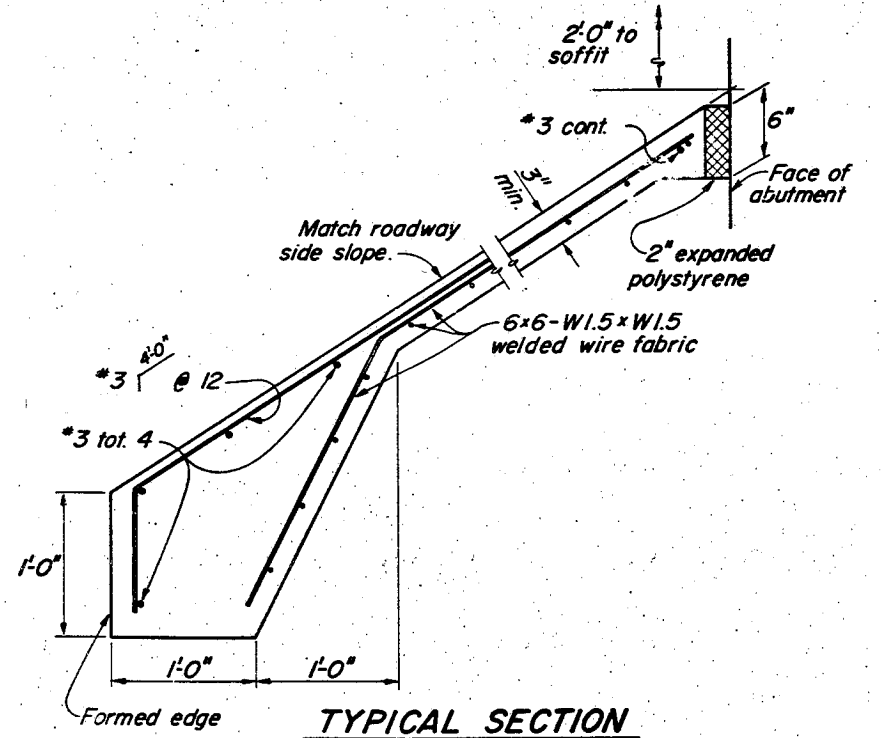
TYPICAL-NO CURB

TYPICAL-DRAIN CONNECTION

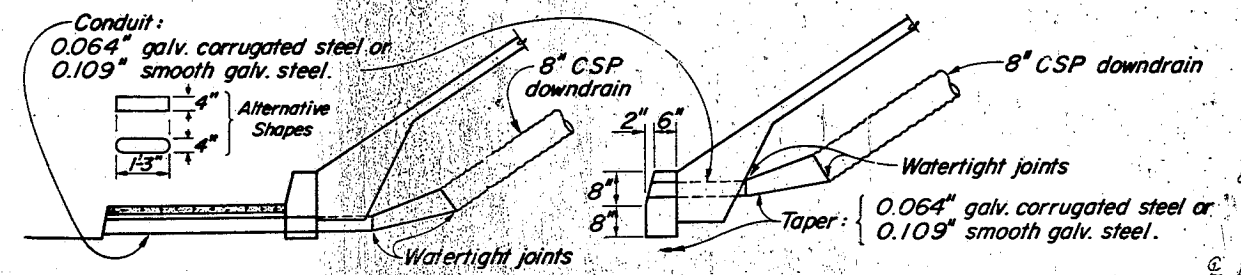


PICTORIAL VIEW OF TYPICAL INSTALLATION

* Or as directed by the Engineer to provide uniform spacing.
 Note: For actual limits of slope paving on this project see sketch below.



TYPICAL SECTION

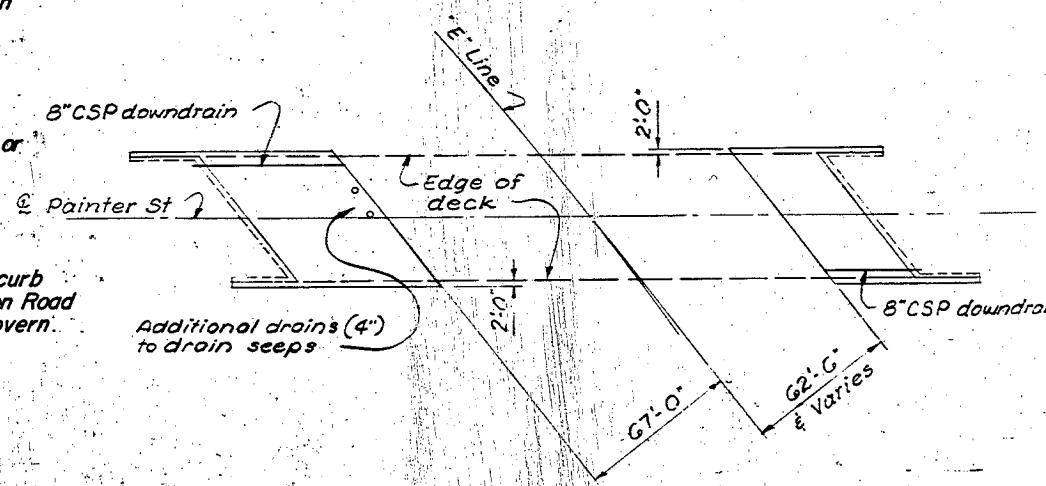


TYPICAL WITH SIDEWALK

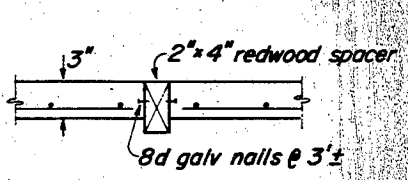
TYPICAL WITH CURB

DRAINAGE DETAILS

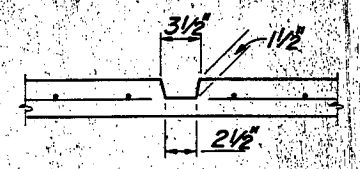
Note: In case of conflict between curb details shown here and those on Road Plans, the Road Plans shall govern.



LIMITS OF SLOPE PAVING & DRAINAGE LAYOUT
 Scale 1" = 40'



SPACER DETAIL



PREFORMED GROOVE

AS BUILT PLANS
 Contract No. 01-061224
 Date Completed _____
 Document No. 1000-2617

AS BUILT
 CORRECTED BY I.A. Schroeder
 CONTRACT NO. 01-061224
 DATE 8-03-76 RT. 4-1-77

STATE OF CALIFORNIA		XS-22-11	
10/72 DEPARTMENT OF TRANSPORTATION			
PAINTER STREET OVERCROSSING			
SLOPE PAVING DETAILS - FULL SLOPE			
BRIDGE NO. 4-23G	POST MILE 53.2	DRAWING NO.	SHEET 9 OF 10
REVISION DATES			
DISCARD PRINT BEARING EARLIER REVISION DATES			

WO
 CU

APPENDIX B: Lists of results form OKID/ERA application

In the following pages are presented some examples of the results obtained by running the OKID/ERA algorithms as given by MATLAB. It is worth to remember that these are only the final trials performed. In order to individuate the values of the parameters such as the model order or the number of Markov parameters to evaluate a year of experiments has been performed.

For each set of data, in addition to the tables of the results, at the beginning the plots that serve as tools for the choice of the abovementioned parameters are shown.

B.1 RESULTS WITH TRINIDAD SET OF DATA (p=73; SVs=558; Order=118)

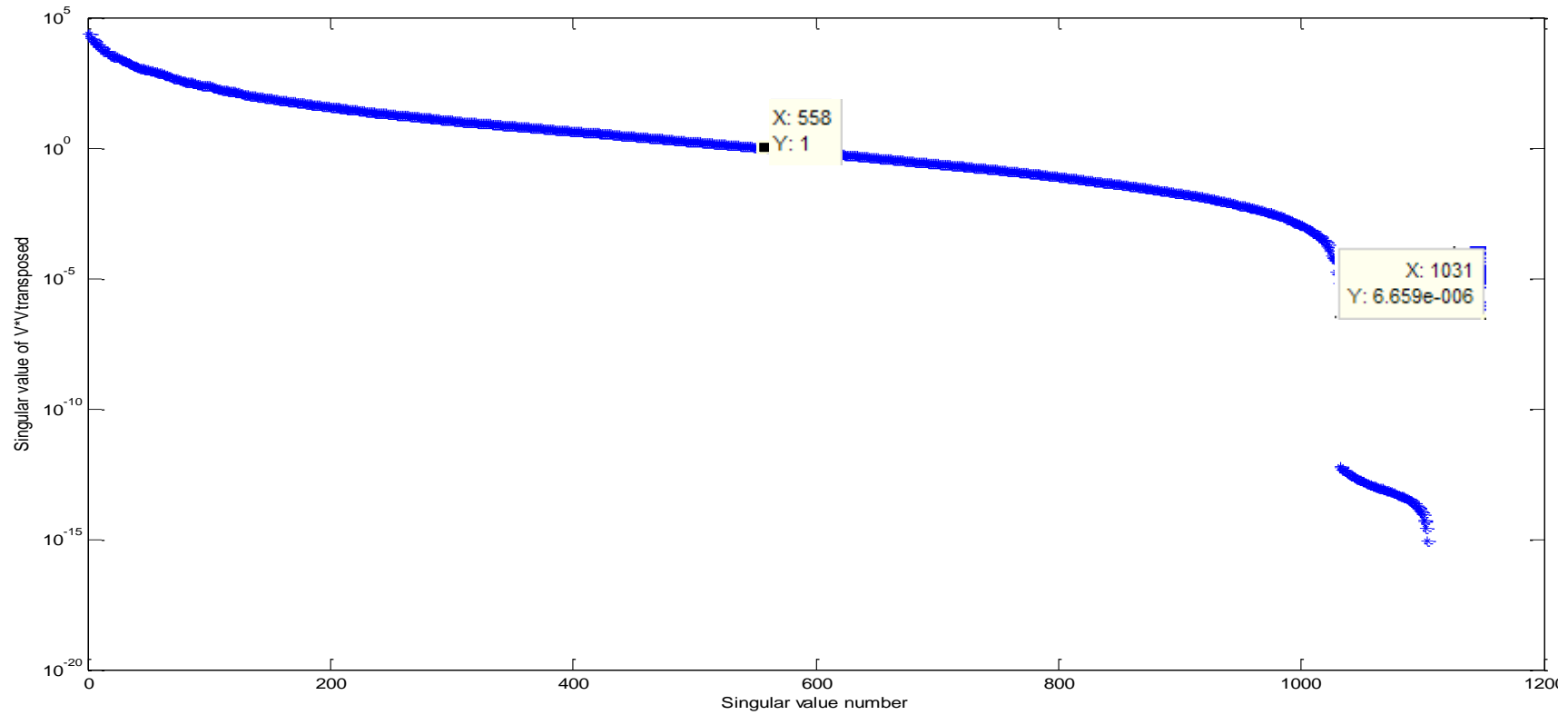


Fig. B.1: Singular values for V^*VT

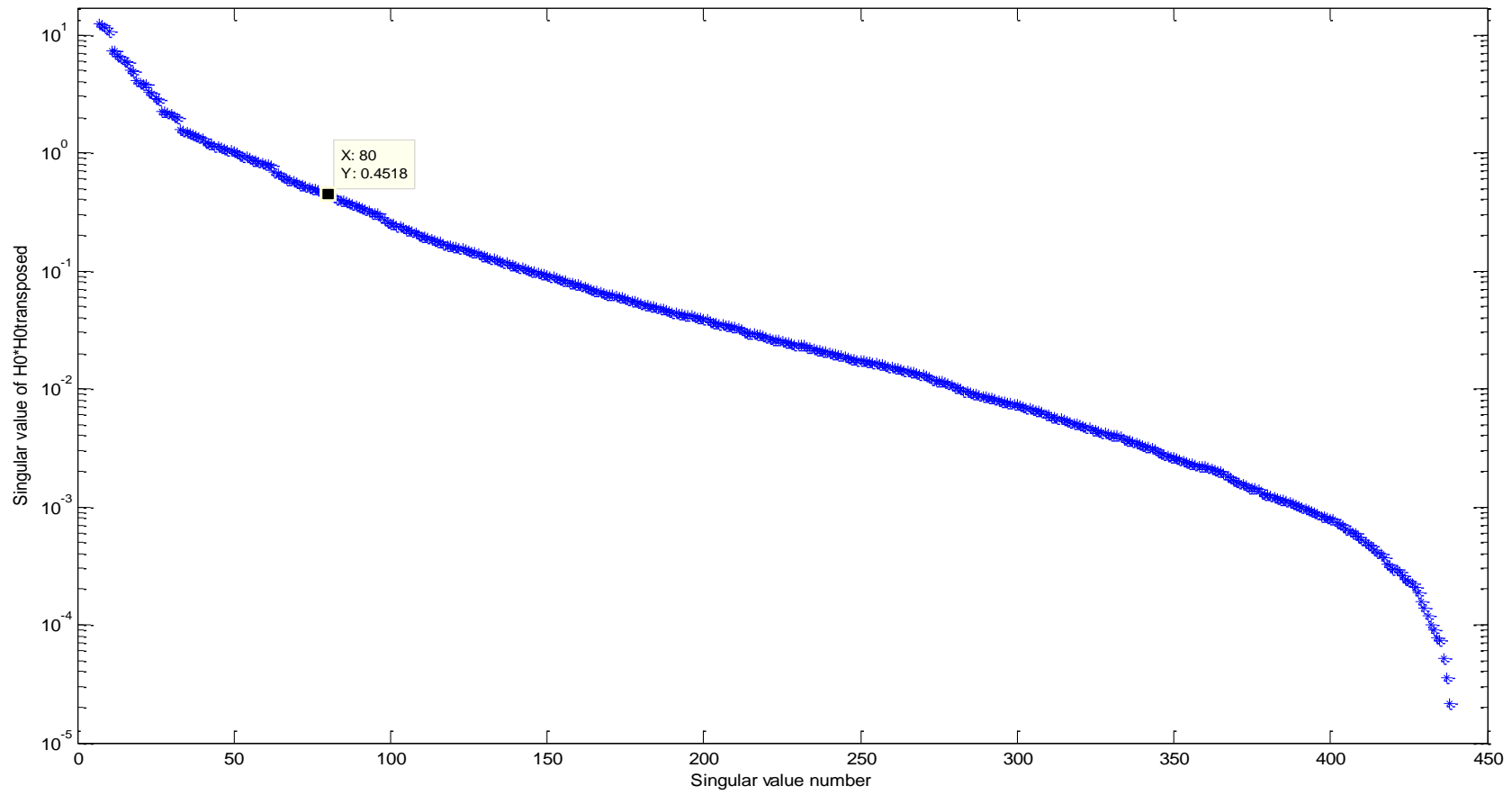


Fig. B.2: Singular values for $H(0) \cdot H(0)$

Trial 1 [1:44 47:118]

Initial system			Optimized System		
Freq. (rad/sec.)	Freq. (Hz.)	Modal Damp.	Freq. (rad/sec.)	Freq. (Hz.)	Modal Damp.
1.6263e+000	2.5884e-001	3.6907e-001	2.6058e+000	4.1472e-001	4.2060e-001
4.7061e+000	7.4901e-001	3.7313e-001	7.5703e+000	1.2049e+000	7.5171e-001
1.1856e+001	1.8869e+000	5.5772e-001	1.2560e+001	1.9990e+000	5.3972e-001
1.3401e+001	2.1328e+000	9.2760e-002	1.5859e+001	2.5241e+000	2.1812e-001
1.7727e+001	2.8213e+000	8.1885e-002	1.8125e+001	2.8847e+000	6.0329e-002
2.0257e+001	3.2239e+000	2.9910e-002	2.0286e+001	3.2286e+000	1.9448e-002
2.1658e+001	3.4469e+000	2.2515e-002	2.1642e+001	3.4444e+000	2.6521e-002
2.4984e+001	3.9763e+000	4.3300e-002	2.5182e+001	4.0078e+000	9.7377e-002
2.7531e+001	4.3818e+000	4.9645e-002	2.6712e+001	4.2513e+000	6.1321e-002
2.8120e+001	4.4754e+000	1.6275e-002	2.8149e+001	4.4800e+000	7.1672e-003
2.9516e+001	4.6976e+000	8.5542e-002	2.9431e+001	4.6841e+000	1.6886e-001
2.9642e+001	4.7176e+000	1.5335e-002	2.9679e+001	4.7235e+000	9.8254e-003
3.0303e+001	4.8229e+000	5.9044e-003	3.0243e+001	4.8133e+000	5.8856e-003
3.3073e+001	5.2637e+000	3.2569e-002	3.3081e+001	5.2650e+000	2.9936e-002
3.3372e+001	5.3114e+000	1.5867e-002	3.3137e+001	5.2739e+000	1.0760e-001
3.3497e+001	5.3311e+000	1.1295e-001	3.3468e+001	5.3266e+000	9.4189e-003
3.6314e+001	5.7796e+000	1.7623e-002	3.6351e+001	5.7855e+000	6.6280e-003
3.6891e+001	5.8714e+000	3.3015e-002	3.7129e+001	5.9092e+000	4.6429e-002
3.9082e+001	6.2201e+000	5.1165e-003	3.9091e+001	6.2216e+000	3.2229e-006
4.0058e+001	6.3754e+000	9.9622e-003	3.9996e+001	6.3656e+000	1.0220e-002
4.1467e+001	6.5997e+000	6.4068e-002	4.0703e+001	6.4781e+000	4.9319e-002
4.3496e+001	6.9225e+000	1.9734e-002	4.3359e+001	6.9007e+000	5.4895e-003

4.6318e+001	7.3717e+000	5.1364e-002	4.6015e+001	7.3236e+000	7.6645e-002
4.6434e+001	7.3901e+000	7.9941e-003	4.6321e+001	7.3722e+000	2.0581e-003
4.8100e+001	7.6554e+000	8.2914e-003	4.7873e+001	7.6192e+000	2.4424e-003
4.9427e+001	7.8666e+000	1.1212e-002	4.9567e+001	7.8888e+000	5.7130e-004
5.0203e+001	7.9901e+000	2.2032e-002	5.0214e+001	7.9918e+000	2.4542e-002
5.2047e+001	8.2835e+000	1.9103e-002	5.1569e+001	8.2075e+000	4.8701e-002
5.4758e+001	8.7150e+000	2.5912e-002	5.4177e+001	8.6226e+000	8.4222e-001
5.5890e+001	8.8951e+000	7.9595e-003	5.5018e+001	8.7564e+000	4.5129e-002
5.7131e+001	9.0927e+000	2.4412e-002	5.5763e+001	8.8750e+000	1.0971e-002
5.8015e+001	9.2334e+000	1.3332e-002	5.7501e+001	9.1515e+000	3.0537e-002
6.0999e+001	9.7082e+000	1.7913e-002	5.8254e+001	9.2714e+000	1.2162e-002
6.1199e+001	9.7401e+000	3.7580e-002	6.0711e+001	9.6625e+000	4.4475e-002
6.2750e+001	9.9870e+000	1.5351e-002	6.1363e+001	9.7662e+000	2.1369e-002
6.7443e+001	1.0734e+001	3.0588e-002	6.3299e+001	1.0074e+001	1.2369e-002
6.7789e+001	1.0789e+001	1.3959e-002	6.7789e+001	1.0789e+001	9.4429e-003
7.1043e+001	1.1307e+001	2.0156e-002	6.8267e+001	1.0865e+001	8.3844e-002
7.2079e+001	1.1472e+001	2.9356e-002	7.1376e+001	1.1360e+001	2.1415e-002
7.4499e+001	1.1857e+001	8.0286e-003	7.2213e+001	1.1493e+001	4.9406e-002
7.6746e+001	1.2215e+001	1.7319e-002	7.4376e+001	1.1837e+001	6.4884e-004
7.9699e+001	1.2684e+001	9.3028e-003	7.5883e+001	1.2077e+001	5.6523e-002
8.3011e+001	1.3212e+001	1.0057e-002	7.9553e+001	1.2661e+001	1.4436e-002
8.5069e+001	1.3539e+001	6.5968e-003	8.2277e+001	1.3095e+001	2.7892e-002
8.9790e+001	1.4290e+001	1.4264e-002	8.6289e+001	1.3733e+001	1.5340e-002
9.0898e+001	1.4467e+001	1.3026e-002	8.8162e+001	1.4031e+001	6.4267e-001
9.5189e+001	1.5150e+001	1.4247e-002	8.8874e+001	1.4145e+001	7.6426e-003
9.5808e+001	1.5248e+001	3.0645e-001	8.9872e+001	1.4304e+001	1.2424e-002
1.0145e+002	1.6146e+001	2.1199e-002	9.4318e+001	1.5011e+001	2.7337e-001

1.0485e+002	1.6688e+001	4.8218e-002	9.5828e+001	1.5251e+001	2.0454e-001
1.0511e+002	1.6729e+001	7.7829e-003	9.6136e+001	1.5300e+001	2.8424e-001
1.1139e+002	1.7728e+001	1.1076e-002	1.0423e+002	1.6589e+001	1.1026e-002
1.1826e+002	1.8822e+001	8.6634e-003	1.0721e+002	1.7064e+001	1.8604e-001
1.2287e+002	1.9555e+001	9.2927e-003	1.1765e+002	1.8724e+001	1.0581e-002
1.2683e+002	2.0186e+001	2.0321e-002	1.2191e+002	1.9403e+001	4.8224e-002
1.2978e+002	2.0655e+001	1.6972e-002	1.2301e+002	1.9578e+001	8.4338e-003
1.3566e+002	2.1591e+001	1.0347e-002	1.3192e+002	2.0995e+001	4.7602e-002
1.4465e+002	2.3022e+001	5.5555e-003	1.4131e+002	2.2490e+001	1.0286e-001

Trial 2 [3:18 23:26 31:38 41,42 47:64 67:70 73:96 99:102 105,106 109:116]

Initial system			Optimized System		
Freq. (rad/sec.)	Freq. (Hz.)	Modal Damp.	Freq. (rad/sec.)	Freq. (Hz.)	Modal Damp.
-----	-----	-----	-----	-----	-----
4.7473e+000	7.5556e-001	3.9221e-001	1.1169e+001	1.7777e+000	8.9534e-001
1.3378e+001	2.1292e+000	7.5845e-002	1.5839e+001	2.5209e+000	3.0048e-001
1.7570e+001	2.7964e+000	6.8863e-002	1.8092e+001	2.8794e+000	4.3880e-002
2.0266e+001	3.2254e+000	3.0802e-002	2.0321e+001	3.2342e+000	1.5604e-002
2.1645e+001	3.4449e+000	2.2599e-002	2.1606e+001	3.4387e+000	2.7348e-002
2.4904e+001	3.9636e+000	4.5418e-002	2.6623e+001	4.2372e+000	1.7133e-001
2.7662e+001	4.4025e+000	5.7244e-002	2.8322e+001	4.5077e+000	2.3830e-002
2.8119e+001	4.4753e+000	1.5463e-002	2.9058e+001	4.6247e+000	3.8038e-002
3.0307e+001	4.8235e+000	5.8146e-003	3.0240e+001	4.8128e+000	4.4399e-003
3.2964e+001	5.2464e+000	3.3896e-002	3.1433e+001	5.0028e+000	3.6139e-001
3.6317e+001	5.7800e+000	1.6504e-002	3.3217e+001	5.2867e+000	4.9706e-002

3.6945e+001	5.8800e+000	3.5688e-002	3.6385e+001	5.7909e+000	2.8394e-003
3.9084e+001	6.2203e+000	4.8967e-003	3.6535e+001	5.8148e+000	4.7654e-001
4.0087e+001	6.3801e+000	1.0225e-002	3.7588e+001	5.9823e+000	3.8758e-002
4.3487e+001	6.9211e+000	2.1150e-002	3.9004e+001	6.2076e+000	3.1716e-003
4.6449e+001	7.3926e+000	7.3787e-003	4.0097e+001	6.3816e+000	4.6588e-003
4.8072e+001	7.6509e+000	8.3162e-003	4.2510e+001	6.7656e+000	4.5193e-001
4.9397e+001	7.8618e+000	1.1618e-002	4.3321e+001	6.8948e+000	1.0937e-002
5.0033e+001	7.9631e+000	2.2055e-002	4.6359e+001	7.3783e+000	2.9973e-003
5.2032e+001	8.2812e+000	1.9898e-002	4.7727e+001	7.5960e+000	1.1785e-002
5.4779e+001	8.7183e+000	2.7163e-002	4.9580e+001	7.8909e+000	5.8299e-004
5.5904e+001	8.8974e+000	7.8455e-003	4.9624e+001	7.8978e+000	3.6814e-002
5.7009e+001	9.0732e+000	2.6841e-002	4.9659e+001	7.9034e+000	5.1055e-002
5.7989e+001	9.2293e+000	1.2687e-002	5.4403e+001	8.6586e+000	2.5283e-002
6.1312e+001	9.7580e+000	3.5228e-002	5.6826e+001	9.0442e+000	1.1148e-001
6.2775e+001	9.9909e+000	1.5344e-002	5.6878e+001	9.0524e+000	2.6547e-002
6.7777e+001	1.0787e+001	1.3800e-002	5.8165e+001	9.2573e+000	5.6554e-003
7.1063e+001	1.1310e+001	1.9700e-002	5.9587e+001	9.4835e+000	5.9118e-002
7.2158e+001	1.1484e+001	3.2008e-002	6.3547e+001	1.0114e+001	1.7722e-002
7.4498e+001	1.1857e+001	8.5387e-003	6.7172e+001	1.0691e+001	5.2492e-003
7.6739e+001	1.2213e+001	1.8222e-002	6.9823e+001	1.1113e+001	5.6867e-002
7.9709e+001	1.2686e+001	9.3905e-003	7.0397e+001	1.1204e+001	4.7528e-002
8.3048e+001	1.3217e+001	9.5898e-003	7.4437e+001	1.1847e+001	2.3772e-007
8.5078e+001	1.3541e+001	6.5836e-003	7.4981e+001	1.1934e+001	8.2081e-002
8.9798e+001	1.4292e+001	1.4353e-002	7.9490e+001	1.2651e+001	4.7888e-002
9.0872e+001	1.4463e+001	1.2419e-002	8.0695e+001	1.2843e+001	4.7562e-001
9.5125e+001	1.5140e+001	1.3381e-002	8.3577e+001	1.3302e+001	6.8219e-002
1.0153e+002	1.6159e+001	2.0986e-002	8.5831e+001	1.3660e+001	7.1186e-003

1.0514e+002	1.6733e+001	7.9979e-003	8.8710e+001	1.4119e+001	9.6586e-003
1.1137e+002	1.7726e+001	1.0775e-002	9.5921e+001	1.5266e+001	1.0901e-001
1.2276e+002	1.9539e+001	9.7529e-003	9.8276e+001	1.5641e+001	1.5034e-001
1.2615e+002	2.0078e+001	1.9833e-002	1.0115e+002	1.6099e+001	9.6357e-002
1.2957e+002	2.0622e+001	1.4214e-002	1.2348e+002	1.9653e+001	7.4481e-003
1.3548e+002	2.1563e+001	1.1375e-002	1.2554e+002	1.9980e+001	5.9235e-003
1.4462e+002	2.3017e+001	6.0174e-003	1.2570e+002	2.0006e+001	1.7682e-001

Trial 3

[7:18 23,24 31:36 41,42 47,48 51:56 59:64 67:70 73:84 87:90 93:96 99:102 105,106 109:114]

Initial system			Optimized System		
Freq. (rad/sec.)	Freq. (Hz.)	Modal Damp.	Freq. (rad/sec.)	Freq. (Hz.)	Modal Damp.
-----	-----	-----	-----	-----	-----
1.7570e+001	2.7964e+000	6.8863e-002	1.8444e+001	2.9355e+000	6.3660e-002
2.0266e+001	3.2254e+000	3.0802e-002	2.0083e+001	3.1962e+000	1.6100e-002
2.1645e+001	3.4449e+000	2.2599e-002	2.1609e+001	3.4392e+000	2.4809e-002
2.4904e+001	3.9636e+000	4.5418e-002	2.7477e+001	4.3731e+000	1.6959e-001
2.7662e+001	4.4025e+000	5.7244e-002	2.8040e+001	4.4626e+000	8.8817e-002
2.8119e+001	4.4753e+000	1.5463e-002	2.8253e+001	4.4966e+000	3.8024e-003
2.8996e+001	4.6149e+000	1.1522e-001	2.9674e+001	4.7227e+000	1.5229e-002
2.9638e+001	4.7170e+000	1.5459e-002	3.0240e+001	4.8129e+000	7.3529e-003
3.0307e+001	4.8235e+000	5.8146e-003	3.2577e+001	5.1848e+000	1.6932e-001
3.6317e+001	5.7800e+000	1.6504e-002	3.6410e+001	5.7948e+000	6.7056e-004
3.6945e+001	5.8800e+000	3.5688e-002	3.7129e+001	5.9092e+000	3.7252e-002
3.9084e+001	6.2203e+000	4.8967e-003	3.9330e+001	6.2596e+000	3.2706e-003
4.3487e+001	6.9211e+000	2.1150e-002	4.3157e+001	6.8686e+000	9.2474e-003

4.6449e+001	7.3926e+000	7.3787e-003	4.6704e+001	7.4332e+000	5.1736e-003
4.9397e+001	7.8618e+000	1.1618e-002	4.8336e+001	7.6929e+000	6.1775e-002
5.0033e+001	7.9631e+000	2.2055e-002	4.9624e+001	7.8978e+000	3.2352e-003
5.2032e+001	8.2812e+000	1.9898e-002	4.9958e+001	7.9510e+000	4.9651e-001
5.5904e+001	8.8974e+000	7.8455e-003	5.0143e+001	7.9805e+000	4.9024e-002
5.7009e+001	9.0732e+000	2.6841e-002	5.4691e+001	8.7043e+000	9.9956e-002
5.7989e+001	9.2293e+000	1.2687e-002	5.6775e+001	9.0360e+000	2.7037e-002
6.1312e+001	9.7580e+000	3.5228e-002	5.7744e+001	9.1903e+000	4.6406e-002
6.2775e+001	9.9909e+000	1.5344e-002	5.9643e+001	9.4925e+000	6.7745e-001
6.7777e+001	1.0787e+001	1.3800e-002	6.0605e+001	9.6456e+000	4.0323e-001
7.1063e+001	1.1310e+001	1.9700e-002	6.3082e+001	1.0040e+001	6.9475e-002
7.2158e+001	1.1484e+001	3.2008e-002	6.4674e+001	1.0293e+001	2.8875e-002
7.4498e+001	1.1857e+001	8.5387e-003	6.7253e+001	1.0704e+001	5.4506e-003
7.6739e+001	1.2213e+001	1.8222e-002	7.0144e+001	1.1164e+001	7.7205e-002
7.9709e+001	1.2686e+001	9.3905e-003	7.1668e+001	1.1406e+001	6.5793e-002
8.5078e+001	1.3541e+001	6.5836e-003	7.4263e+001	1.1819e+001	1.2358e-003
8.9798e+001	1.4292e+001	1.4353e-002	7.5873e+001	1.2076e+001	1.4797e-001
9.5125e+001	1.5140e+001	1.3381e-002	7.9990e+001	1.2731e+001	1.7269e-002
1.0153e+002	1.6159e+001	2.0986e-002	8.5135e+001	1.3550e+001	2.2719e-001
1.0514e+002	1.6733e+001	7.9979e-003	8.5879e+001	1.3668e+001	4.0211e-006
1.1137e+002	1.7726e+001	1.0775e-002	8.9175e+001	1.4193e+001	6.9763e-003
1.2276e+002	1.9539e+001	9.7529e-003	9.6316e+001	1.5329e+001	2.2181e-001
1.2615e+002	2.0078e+001	1.9833e-002	1.2036e+002	1.9156e+001	3.3001e-001
1.2957e+002	2.0622e+001	1.4214e-002	1.2335e+002	1.9631e+001	1.1502e-002
1.3548e+002	2.1563e+001	1.1375e-002	1.4255e+002	2.2687e+001	2.4417e-001

Trial 4

[7:12 15,16 19:22 33:36 41,42 47,48 51:54 59:64 67,68 75:84 87:90 93,94 101,102 111,112]

Initial system			Optimized System		
Freq. (rad/sec.)	Freq. (Hz.)	Modal Damp.	Freq. (rad/sec.)	Freq. (Hz.)	Modal Damp.
1.7570e+001	2.7964e+000	6.8863e-002	1.8504e+001	2.9451e+000	8.8683e-002
2.0266e+001	3.2254e+000	3.0802e-002	2.0131e+001	3.2039e+000	3.4906e-002
2.1645e+001	3.4449e+000	2.2599e-002	2.1593e+001	3.4366e+000	2.3138e-002
2.7662e+001	4.4025e+000	5.7244e-002	2.9187e+001	4.6453e+000	8.9185e-002
2.8996e+001	4.6149e+000	1.1522e-001	3.0375e+001	4.8343e+000	3.1868e-002
2.9638e+001	4.7170e+000	1.5459e-002	3.0474e+001	4.8500e+000	3.0055e-001
3.6945e+001	5.8800e+000	3.5688e-002	3.0646e+001	4.8775e+000	5.0832e-002
3.9084e+001	6.2203e+000	4.8967e-003	3.5208e+001	5.6035e+000	3.0291e-001
4.3487e+001	6.9211e+000	2.1150e-002	3.7379e+001	5.9491e+000	1.9663e-002
4.6449e+001	7.3926e+000	7.3787e-003	3.9181e+001	6.2359e+000	2.5368e-003
4.9397e+001	7.8618e+000	1.1618e-002	4.3422e+001	6.9108e+000	1.0491e-002
5.0033e+001	7.9631e+000	2.2055e-002	4.6469e+001	7.3957e+000	5.9603e-003
5.5904e+001	8.8974e+000	7.8455e-003	4.8615e+001	7.7373e+000	5.1824e-002
5.7009e+001	9.0732e+000	2.6841e-002	4.9543e+001	7.8851e+000	5.9421e-003
5.7989e+001	9.2293e+000	1.2687e-002	5.4741e+001	8.7124e+000	5.0218e-002
6.1312e+001	9.7580e+000	3.5228e-002	5.6450e+001	8.9843e+000	5.2490e-002
7.1063e+001	1.1310e+001	1.9700e-002	5.7123e+001	9.0914e+000	4.1464e-002
7.2158e+001	1.1484e+001	3.2008e-002	6.0763e+001	9.6708e+000	8.7532e-002
7.4498e+001	1.1857e+001	8.5387e-003	7.1512e+001	1.1381e+001	4.5699e-002
7.6739e+001	1.2213e+001	1.8222e-002	7.2086e+001	1.1473e+001	1.1011e-001
7.9709e+001	1.2686e+001	9.3905e-003	7.2572e+001	1.1550e+001	6.9410e-002

8.5078e+001	1.3541e+001	6.5836e-003	7.4451e+001	1.1849e+001	8.7279e-007
8.9798e+001	1.4292e+001	1.4353e-002	7.9333e+001	1.2626e+001	4.1323e-002
9.5125e+001	1.5140e+001	1.3381e-002	8.6285e+001	1.3733e+001	5.4043e-002
1.1137e+002	1.7726e+001	1.0775e-002	9.4550e+001	1.5048e+001	2.7614e-001
1.2957e+002	2.0622e+001	1.4214e-002	9.5766e+001	1.5242e+001	5.6629e-001

Trial 5

[7:12 15,16 19,20 33,34 41,42 47,48 51:54 59:64 67,68 75:84 89,90 93,94]

Initial system			Optimized System		
Freq. (rad/sec.)	Freq. (Hz.)	Modal Damp.	Freq. (rad/sec.)	Freq. (Hz.)	Modal Damp.
-----	-----	-----	-----	-----	-----
1.7570e+001	2.7964e+000	6.8863e-002	2.0277e+001	3.2272e+000	2.6171e-002
2.0266e+001	3.2254e+000	3.0802e-002	2.1152e+001	3.3664e+000	1.5980e-001
2.1645e+001	3.4449e+000	2.2599e-002	2.1621e+001	3.4411e+000	2.6324e-002
2.7662e+001	4.4025e+000	5.7244e-002	3.0438e+001	4.8444e+000	4.2599e-002
2.8996e+001	4.6149e+000	1.1522e-001	3.0654e+001	4.8787e+000	7.6071e-002
3.6945e+001	5.8800e+000	3.5688e-002	3.4755e+001	5.5314e+000	1.7209e-001
4.3487e+001	6.9211e+000	2.1150e-002	3.8395e+001	6.1107e+000	2.1140e-002
4.6449e+001	7.3926e+000	7.3787e-003	3.8424e+001	6.1154e+000	2.6216e-001
4.9397e+001	7.8618e+000	1.1618e-002	4.0941e+001	6.5160e+000	3.4530e-001
5.0033e+001	7.9631e+000	2.2055e-002	4.2144e+001	6.7074e+000	3.1772e-001
5.5904e+001	8.8974e+000	7.8455e-003	4.3641e+001	6.9457e+000	1.2425e-002
5.7009e+001	9.0732e+000	2.6841e-002	4.4911e+001	7.1479e+000	1.3987e-001
5.7989e+001	9.2293e+000	1.2687e-002	4.5323e+001	7.2134e+000	1.3878e-001
6.1312e+001	9.7580e+000	3.5228e-002	4.6331e+001	7.3737e+000	7.8671e-007
7.1063e+001	1.1310e+001	1.9700e-002	4.6583e+001	7.4139e+000	1.5003e-001

7.2158e+001	1.1484e+001	3.2008e-002	4.8628e+001	7.7393e+000	5.0487e-001
7.4498e+001	1.1857e+001	8.5387e-003	5.0033e+001	7.9630e+000	4.4739e-002
7.6739e+001	1.2213e+001	1.8222e-002	5.0302e+001	8.0057e+000	5.3524e-002
7.9709e+001	1.2686e+001	9.3905e-003	5.8327e+001	9.2831e+000	3.0636e-001
8.9798e+001	1.4292e+001	1.4353e-002	7.4941e+001	1.1927e+001	1.0597e-001
9.5125e+001	1.5140e+001	1.3381e-002	7.8842e+001	1.2548e+001	1.4756e-001

Trial 6

[7:12 15,16 19,20 33,34 41,42 59:64 75,76 79:82 89,90 93,94]

Initial system			Optimized System		
Freq. (rad/sec.)	Freq. (Hz.)	Modal Damp.	Freq. (rad/sec.)	Freq. (Hz.)	Modal Damp.
-----	-----	-----	-----	-----	-----
1.7570e+001	2.7964e+000	6.8863e-002	1.8404e+001	2.9291e+000	6.7082e-002
2.0266e+001	3.2254e+000	3.0802e-002	2.0449e+001	3.2545e+000	2.6261e-001
2.1645e+001	3.4449e+000	2.2599e-002	2.1615e+001	3.4402e+000	2.7120e-002
2.7662e+001	4.4025e+000	5.7244e-002	2.3892e+001	3.8025e+000	4.9212e-001
2.8996e+001	4.6149e+000	1.1522e-001	3.0157e+001	4.7997e+000	1.8908e-001
3.6945e+001	5.8800e+000	3.5688e-002	3.0219e+001	4.8096e+000	9.5402e-002
4.3487e+001	6.9211e+000	2.1150e-002	3.0979e+001	4.9305e+000	2.2761e-002
5.5904e+001	8.8974e+000	7.8455e-003	3.5427e+001	5.6383e+000	2.6823e-001
5.7009e+001	9.0732e+000	2.6841e-002	3.7455e+001	5.9612e+000	2.7615e-001
5.7989e+001	9.2293e+000	1.2687e-002	3.7984e+001	6.0453e+000	1.7835e-002
7.1063e+001	1.1310e+001	1.9700e-002	3.8899e+001	6.1909e+000	6.3622e-002
7.4498e+001	1.1857e+001	8.5387e-003	4.2772e+001	6.8074e+000	1.4706e-001
7.6739e+001	1.2213e+001	1.8222e-002	4.3242e+001	6.8822e+000	2.3528e-001
8.9798e+001	1.4292e+001	1.4353e-002	4.5953e+001	7.3136e+000	3.4588e-002

9.5125e+001 1.5140e+001 1.3381e-002 4.7622e+001 7.5792e+000 7.2827e-003

Trial 7 [7,8 11,12 19,20 33,34 41,42 63,64 75,76 79,80 89,90 93,94]

Initial system			Optimized System		
Freq. (rad/sec.)	Freq. (Hz.)	Modal Damp.	Freq. (rad/sec.)	Freq. (Hz.)	Modal Damp.
-----	-----	-----	-----	-----	-----
1.7570e+001	2.7964e+000	6.8863e-002	1.7997e+001	2.8642e+000	7.9247e-002
2.1645e+001	3.4449e+000	2.2599e-002	2.1613e+001	3.4398e+000	2.1975e-002
2.8996e+001	4.6149e+000	1.1522e-001	2.7982e+001	4.4535e+000	7.5723e-002
3.6945e+001	5.8800e+000	3.5688e-002	3.7488e+001	5.9664e+000	3.2766e-002
4.3487e+001	6.9211e+000	2.1150e-002	4.3622e+001	6.9427e+000	2.2688e-002
5.7989e+001	9.2293e+000	1.2687e-002	5.7898e+001	9.2148e+000	1.4495e-002
7.1063e+001	1.1310e+001	1.9700e-002	7.0442e+001	1.1211e+001	9.4549e-008
7.4498e+001	1.1857e+001	8.5387e-003	7.4765e+001	1.1899e+001	2.0392e-002
8.9798e+001	1.4292e+001	1.4353e-002	9.0378e+001	1.4384e+001	1.1309e-001
9.5125e+001	1.5140e+001	1.3381e-002	9.0531e+001	1.4408e+001	7.5376e-002

Trial 8 [7,8 11,12 19,20 33,34 41,42 63,64 79,80 89,90 93,94]

Initial system			Optimized System		
Freq. (rad/sec.)	Freq. (Hz.)	Modal Damp.	Freq. (rad/sec.)	Freq. (Hz.)	Modal Damp.
-----	-----	-----	-----	-----	-----
1.7570e+001	2.7964e+000	6.8863e-002	1.9085e+001	3.0374e+000	1.2008e-001
2.1645e+001	3.4449e+000	2.2599e-002	2.1574e+001	3.4336e+000	2.1130e-002
2.8996e+001	4.6149e+000	1.1522e-001	3.0451e+001	4.8465e+000	4.9062e-002
3.6945e+001	5.8800e+000	3.5688e-002	3.0480e+001	4.8510e+000	2.3941e-001
4.3487e+001	6.9211e+000	2.1150e-002	3.6161e+001	5.7553e+000	9.8805e-002

5.7989e+001	9.2293e+000	1.2687e-002	3.6743e+001	5.8479e+000	7.8058e-002
7.4498e+001	1.1857e+001	8.5387e-003	3.7763e+001	6.0102e+000	3.9831e-003
8.9798e+001	1.4292e+001	1.4353e-002	3.9216e+001	6.2415e+000	7.7344e-002
9.5125e+001	1.5140e+001	1.3381e-002	4.5980e+001	7.3180e+000	3.6677e-002

Trial 9 [7,8 11,12 19,20 41,42 63,64 79,80 89,90 93,94]

Initial system			Optimized System		
Freq. (rad/sec.)	Freq. (Hz.)	Modal Damp.	Freq. (rad/sec.)	Freq. (Hz.)	Modal Damp.
-----	-----	-----	-----	-----	-----
1.7570e+001	2.7964e+000	6.8863e-002	1.8969e+001	3.0190e+000	1.2305e-001
2.1645e+001	3.4449e+000	2.2599e-002	2.1574e+001	3.4336e+000	1.9912e-002
2.8996e+001	4.6149e+000	1.1522e-001	2.8908e+001	4.6009e+000	4.4667e-001
4.3487e+001	6.9211e+000	2.1150e-002	3.0248e+001	4.8141e+000	1.6940e-001
5.7989e+001	9.2293e+000	1.2687e-002	3.0617e+001	4.8729e+000	4.8925e-002
7.4498e+001	1.1857e+001	8.5387e-003	3.2769e+001	5.2154e+000	1.2026e-001
8.9798e+001	1.4292e+001	1.4353e-002	3.8250e+001	6.0877e+000	2.7360e-002
9.5125e+001	1.5140e+001	1.3381e-002	4.5991e+001	7.3198e+000	3.8030e-002

Trial 10 [7,8 11,12 41,42 63,64 79,80 89,90 93,94]

Initial system			Optimized System		
Freq. (rad/sec.)	Freq. (Hz.)	Modal Damp.	Freq. (rad/sec.)	Freq. (Hz.)	Modal Damp.
-----	-----	-----	-----	-----	-----
1.7570e+001	2.7964e+000	6.8863e-002	1.9414e+001	3.0898e+000	1.2924e-001
2.1645e+001	3.4449e+000	2.2599e-002	2.1455e+001	3.4147e+000	2.0257e-002
4.3487e+001	6.9211e+000	2.1150e-002	2.9094e+001	4.6305e+000	1.1777e-001
5.7989e+001	9.2293e+000	1.2687e-002	3.0978e+001	4.9303e+000	7.3875e-002

7.4498e+001	1.1857e+001	8.5387e-003	3.1131e+001	4.9546e+000	1.4208e-001
8.9798e+001	1.4292e+001	1.4353e-002	3.8118e+001	6.0666e+000	2.9782e-002
9.5125e+001	1.5140e+001	1.3381e-002	4.5972e+001	7.3166e+000	3.6968e-002

Trial 11 [7,8 11,12 41,42 63,64 89,90 93,94]

Initial system			Optimized System		
Freq. (rad/sec.)	Freq. (Hz.)	Modal Damp.	Freq. (rad/sec.)	Freq. (Hz.)	Modal Damp.
-----	-----	-----	-----	-----	-----
1.7570e+001	2.7964e+000	6.8863e-002	2.0169e+001	3.2099e+000	5.8809e-002
2.1645e+001	3.4449e+000	2.2599e-002	2.1389e+001	3.4042e+000	2.8521e-002
4.3487e+001	6.9211e+000	2.1150e-002	3.0181e+001	4.8035e+000	3.6279e-002
5.7989e+001	9.2293e+000	1.2687e-002	3.4432e+001	5.4800e+000	1.9504e-001
8.9798e+001	1.4292e+001	1.4353e-002	3.8340e+001	6.1020e+000	3.0813e-002
9.5125e+001	1.5140e+001	1.3381e-002	4.6030e+001	7.3260e+000	3.6044e-002

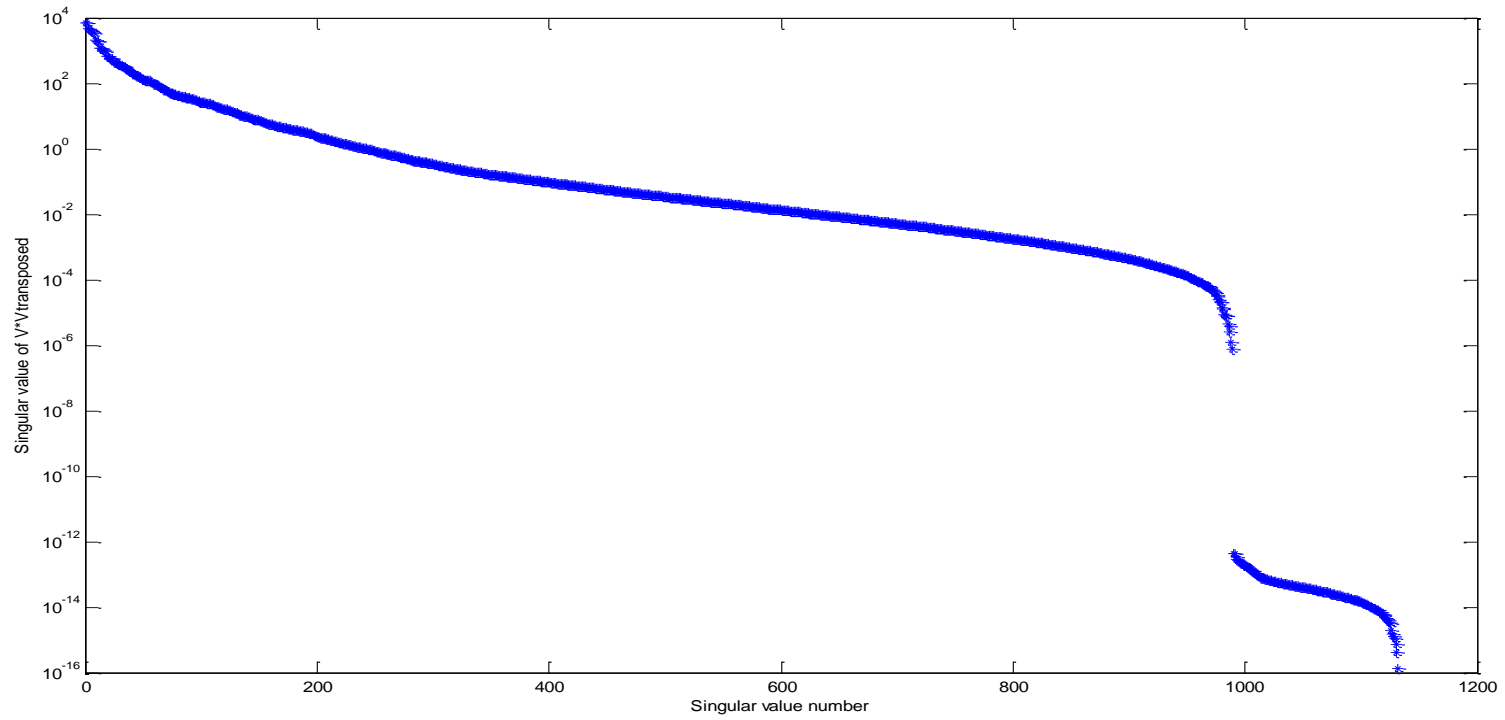
Trial 12 [7,8 11,12 41,42 89,90 93,94]

Initial system			Optimized System		
Freq. (rad/sec.)	Freq. (Hz.)	Modal Damp.	Freq. (rad/sec.)	Freq. (Hz.)	Modal Damp.
-----	-----	-----	-----	-----	-----
1.7570e+001	2.7964e+000	6.8863e-002	2.0441e+001	3.2532e+000	7.6041e-002
2.1645e+001	3.4449e+000	2.2599e-002	2.1384e+001	3.4034e+000	2.7716e-002
4.3487e+001	6.9211e+000	2.1150e-002	2.9984e+001	4.7722e+000	4.6498e-002
8.9798e+001	1.4292e+001	1.4353e-002	3.8457e+001	6.1205e+000	3.1055e-002
9.5125e+001	1.5140e+001	1.3381e-002	4.6038e+001	7.3271e+000	3.3881e-002

Trial 13 [11,12 41,42 89,90 93,94]

Initial system			Optimized System		
Freq. (rad/sec.)	Freq. (Hz.)	Modal Damp.	Freq. (rad/sec.)	Freq. (Hz.)	Modal Damp.
-----	-----	-----	-----	-----	-----
2.1645e+001	3.4449e+000	2.2599e-002	2.1409e+001	3.4074e+000	2.6201e-002
4.3487e+001	6.9211e+000	2.1150e-002	2.9891e+001	4.7572e+000	5.5308e-002
8.9798e+001	1.4292e+001	1.4353e-002	3.8469e+001	6.1225e+000	3.2199e-002
9.5125e+001	1.5140e+001	1.3381e-002	4.6088e+001	7.3351e+000	3.3733e-002

B.2 RESULTS WITH RIO DELL SET OF DATA ($p=75$; $SVs=138$; $Order=80$)



*Fig. B.3: Singular values for $V(0)*V(0)$*

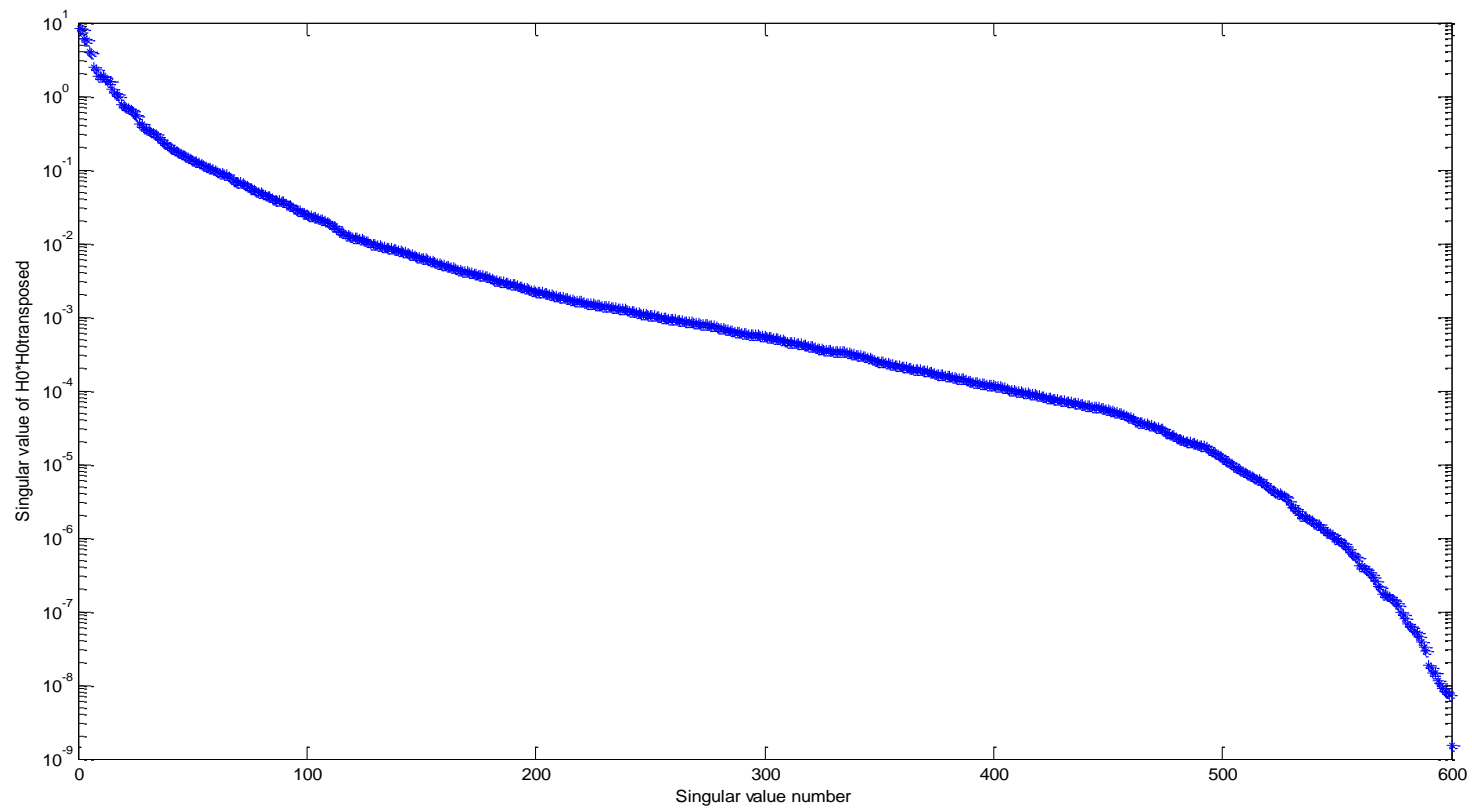


Fig. B.4: Singular values for $H(0) \cdot H(0)$

Trial 1 [9, 10, 13, 14, 19,20, 23, 24, 27, 28, 33, 34, 39, 40, 43, 44, 47:68, 77,78]

Initial system			Optimized System		
Freq. (rad/sec.)	Freq. (Hz.)	Modal Damp.	Freq. (rad/sec.)	Freq. (Hz.)	Modal Damp.
-----	-----	-----	-----	-----	-----
1.5485e+001	2.4646e+000	3.4120e-002	1.5537e+001	2.4727e+000	5.4686e-002
1.8241e+001	2.9031e+000	7.4815e-002	1.9414e+001	3.0898e+000	5.1631e-002
2.1360e+001	3.3995e+000	1.3798e-002	2.1330e+001	3.3947e+000	2.1115e-002
2.3646e+001	3.7633e+000	2.7736e-002	2.4818e+001	3.9499e+000	4.9141e-002
2.7424e+001	4.3646e+000	4.6977e-002	3.0756e+001	4.8950e+000	4.8256e-002
3.2187e+001	5.1226e+000	1.2064e-001	3.0899e+001	4.9178e+000	6.8726e-002
3.6661e+001	5.8348e+000	2.8122e-002	3.6560e+001	5.8188e+000	4.2777e-002
3.8732e+001	6.1644e+000	4.3148e-002	3.7913e+001	6.0341e+000	3.7673e-002
4.4938e+001	7.1520e+000	1.2992e-002	4.4260e+001	7.0442e+000	3.3766e-002
4.7420e+001	7.5472e+000	2.6475e-002	4.6352e+001	7.3772e+000	2.6038e-002
5.1100e+001	8.1329e+000	1.7085e-002	5.1037e+001	8.1228e+000	2.7027e-002
5.3924e+001	8.5823e+000	2.7080e-002	5.2114e+001	8.2943e+000	3.2925e-002
5.7896e+001	9.2145e+000	3.0421e-002	5.5723e+001	8.8685e+000	1.2310e-001
5.9419e+001	9.4568e+000	1.9899e-002	5.9173e+001	9.4176e+000	2.5762e-002
6.1957e+001	9.8607e+000	3.2406e-002	6.1726e+001	9.8240e+000	1.4110e-002
6.9874e+001	1.1121e+001	1.9115e-002	7.1894e+001	1.1442e+001	4.4741e-003
7.5532e+001	1.2021e+001	1.8652e-002	7.5479e+001	1.2013e+001	2.1634e-002
8.1772e+001	1.3014e+001	2.0305e-002	8.4233e+001	1.3406e+001	4.9176e-008
8.5972e+001	1.3683e+001	1.8264e-002	8.6759e+001	1.3808e+001	8.4471e-002
1.4202e+002	2.2603e+001	1.6823e-002	1.5759e+002	2.5082e+001	1.3851e-001

Trial 2 [9, 10, 13, 14, 19,20, 23, 24, 27, 28, 33, 34, 39, 40, 43, 44, 47:54, 57:64, 67, 68]

Initial system			Optimized System		
Freq. (rad/sec.)	Freq. (Hz.)	Modal Damp.	Freq. (rad/sec.)	Freq. (Hz.)	Modal Damp.
-----	-----	-----	-----	-----	-----
1.5485e+001	2.4646e+000	3.4120e-002	1.5466e+001	2.4615e+000	2.9497e-002
1.8241e+001	2.9031e+000	7.4815e-002	1.8759e+001	2.9856e+000	3.7273e-002
2.1360e+001	3.3995e+000	1.3798e-002	2.1343e+001	3.3969e+000	1.4876e-002
2.3646e+001	3.7633e+000	2.7736e-002	2.3872e+001	3.7994e+000	2.6926e-002
2.7424e+001	4.3646e+000	4.6977e-002	2.7505e+001	4.3775e+000	4.5688e-002
3.2187e+001	5.1226e+000	1.2064e-001	3.2311e+001	5.1425e+000	9.3071e-002
3.6661e+001	5.8348e+000	2.8122e-002	3.6512e+001	5.8110e+000	3.1268e-002
3.8732e+001	6.1644e+000	4.3148e-002	3.8339e+001	6.1019e+000	2.0321e-002
4.4938e+001	7.1520e+000	1.2992e-002	4.4724e+001	7.1181e+000	1.3614e-002
4.7420e+001	7.5472e+000	2.6475e-002	4.7344e+001	7.5350e+000	1.6052e-002
5.1100e+001	8.1329e+000	1.7085e-002	5.0845e+001	8.0922e+000	2.2172e-002
5.3924e+001	8.5823e+000	2.7080e-002	5.3260e+001	8.4765e+000	2.7550e-003
5.9419e+001	9.4568e+000	1.9899e-002	5.9480e+001	9.4666e+000	2.1233e-008
6.1957e+001	9.8607e+000	3.2406e-002	6.0816e+001	9.6792e+000	3.5284e-002
6.9874e+001	1.1121e+001	1.9115e-002	7.1565e+001	1.1390e+001	1.3085e-002
7.5532e+001	1.2021e+001	1.8652e-002	7.4654e+001	1.1882e+001	3.0334e-002
8.5972e+001	1.3683e+001	1.8264e-002	8.5372e+001	1.3587e+001	2.2580e-003

Trial 3 [9, 10, 13, 14, 19,20, 23, 24, 27, 28, 33, 34, 39, 40, 43, 44, 47:54, 59:64, 67, 68]

Initial system			Optimized System		
Freq. (rad/sec.)	Freq. (Hz.)	Modal Damp.	Freq. (rad/sec.)	Freq. (Hz.)	Modal Damp.
-----	-----	-----	-----	-----	-----
1.5485e+001	2.4646e+000	3.4120e-002	1.5623e+001	2.4865e+000	2.1263e-002
1.8241e+001	2.9031e+000	7.4815e-002	2.0305e+001	3.2316e+000	1.0262e-001
2.1360e+001	3.3995e+000	1.3798e-002	2.1372e+001	3.4015e+000	2.1008e-002
2.3646e+001	3.7633e+000	2.7736e-002	2.4968e+001	3.9737e+000	3.8298e-002
2.7424e+001	4.3646e+000	4.6977e-002	3.0844e+001	4.9089e+000	5.1617e-002
3.2187e+001	5.1226e+000	1.2064e-001	3.1670e+001	5.0404e+000	1.1675e-001
3.6661e+001	5.8348e+000	2.8122e-002	3.5667e+001	5.6766e+000	7.4251e-002
3.8732e+001	6.1644e+000	4.3148e-002	3.8860e+001	6.1848e+000	6.3267e-002
4.4938e+001	7.1520e+000	1.2992e-002	4.2594e+001	6.7790e+000	5.6183e-002
4.7420e+001	7.5472e+000	2.6475e-002	4.7654e+001	7.5844e+000	6.3696e-003
5.1100e+001	8.1329e+000	1.7085e-002	5.1497e+001	8.1960e+000	1.0118e-002
5.3924e+001	8.5823e+000	2.7080e-002	5.3471e+001	8.5102e+000	4.0224e-003
6.1957e+001	9.8607e+000	3.2406e-002	6.1547e+001	9.7955e+000	5.1417e-002
6.9874e+001	1.1121e+001	1.9115e-002	6.8734e+001	1.0939e+001	8.8937e-002
7.5532e+001	1.2021e+001	1.8652e-002	7.0275e+001	1.1185e+001	6.6988e-002
8.5972e+001	1.3683e+001	1.8264e-002	8.7695e+001	1.3957e+001	3.9158e-002

Trial 4 [9, 10, 19,20, 23, 24, 27, 28, 39, 40, 43, 44, 47:54, 59:64, 67, 68]

Initial system			Optimized System		
Freq. (rad/sec.)	Freq. (Hz.)	Modal Damp.	Freq. (rad/sec.)	Freq. (Hz.)	Modal Damp.
-----	-----	-----	-----	-----	-----
1.5485e+001	2.4646e+000	3.4120e-002	1.5577e+001	2.4792e+000	3.0928e-002
2.1360e+001	3.3995e+000	1.3798e-002	2.1359e+001	3.3994e+000	1.4180e-002
2.3646e+001	3.7633e+000	2.7736e-002	2.3776e+001	3.7840e+000	2.4082e-002
2.7424e+001	4.3646e+000	4.6977e-002	2.7475e+001	4.3728e+000	4.1930e-002
3.6661e+001	5.8348e+000	2.8122e-002	3.6579e+001	5.8218e+000	3.1620e-002
3.8732e+001	6.1644e+000	4.3148e-002	3.8610e+001	6.1449e+000	3.2790e-002
4.4938e+001	7.1520e+000	1.2992e-002	4.4926e+001	7.1502e+000	1.2715e-002
4.7420e+001	7.5472e+000	2.6475e-002	4.7859e+001	7.6170e+000	2.6479e-002
5.1100e+001	8.1329e+000	1.7085e-002	5.1385e+001	8.1781e+000	1.8320e-002
5.3924e+001	8.5823e+000	2.7080e-002	5.3785e+001	8.5601e+000	1.9601e-002
6.1957e+001	9.8607e+000	3.2406e-002	6.1688e+001	9.8180e+000	1.9326e-002
6.9874e+001	1.1121e+001	1.9115e-002	7.0201e+001	1.1173e+001	1.3842e-002
7.5532e+001	1.2021e+001	1.8652e-002	7.5853e+001	1.2072e+001	4.6485e-002
8.5972e+001	1.3683e+001	1.8264e-002	8.5284e+001	1.3573e+001	8.3995e-010

Trial 5 [9, 10, 19,20, 23, 24, 27, 28, 39, 40, 43, 44, 47:54, 59:64]

Initial system			Optimized System		
Freq. (rad/sec.)	Freq. (Hz.)	Modal Damp.	Freq. (rad/sec.)	Freq. (Hz.)	Modal Damp.
-----	-----	-----	-----	-----	-----
1.5485e+001	2.4646e+000	3.4120e-002	1.5636e+001	2.4886e+000	2.2363e-002
2.1360e+001	3.3995e+000	1.3798e-002	2.1351e+001	3.3981e+000	1.3150e-002
2.3646e+001	3.7633e+000	2.7736e-002	2.3764e+001	3.7822e+000	2.0457e-002
2.7424e+001	4.3646e+000	4.6977e-002	2.7338e+001	4.3509e+000	4.0491e-002
3.6661e+001	5.8348e+000	2.8122e-002	3.6657e+001	5.8342e+000	2.6934e-002

3.8732e+001	6.1644e+000	4.3148e-002	3.8622e+001	6.1468e+000	3.5712e-002
4.4938e+001	7.1520e+000	1.2992e-002	4.4966e+001	7.1565e+000	1.2543e-002
4.7420e+001	7.5472e+000	2.6475e-002	4.7681e+001	7.5886e+000	2.7364e-002
5.1100e+001	8.1329e+000	1.7085e-002	5.1686e+001	8.2261e+000	2.0405e-002
5.3924e+001	8.5823e+000	2.7080e-002	5.3538e+001	8.5209e+000	7.1043e-003
6.1957e+001	9.8607e+000	3.2406e-002	6.0817e+001	9.6793e+000	8.6536e-008
6.9874e+001	1.1121e+001	1.9115e-002	6.9615e+001	1.1080e+001	2.1988e-002
7.5532e+001	1.2021e+001	1.8652e-002	7.5112e+001	1.1954e+001	2.7410e-002

Trial 6 [9, 10, 19,20, 23, 24, 27, 28, 39, 40, 43, 44, 47:54, 61:64]

Initial system			Optimized System		
Freq. (rad/sec.)	Freq. (Hz.)	Modal Damp.	Freq. (rad/sec.)	Freq. (Hz.)	Modal Damp.
-----	-----	-----	-----	-----	-----
1.5485e+001	2.4646e+000	3.4120e-002	1.6846e+001	2.6812e+000	5.9551e-002
2.1360e+001	3.3995e+000	1.3798e-002	2.1143e+001	3.3650e+000	2.3866e-002
2.3646e+001	3.7633e+000	2.7736e-002	2.6506e+001	4.2186e+000	9.5128e-002
2.7424e+001	4.3646e+000	4.6977e-002	3.1091e+001	4.9482e+000	7.3664e-002
3.6661e+001	5.8348e+000	2.8122e-002	3.5546e+001	5.6573e+000	7.7602e-002
3.8732e+001	6.1644e+000	4.3148e-002	3.8689e+001	6.1575e+000	2.5943e-002
4.4938e+001	7.1520e+000	1.2992e-002	4.2826e+001	6.8159e+000	7.0395e-002
4.7420e+001	7.5472e+000	2.6475e-002	4.4217e+001	7.0373e+000	6.0741e-001
5.1100e+001	8.1329e+000	1.7085e-002	4.7305e+001	7.5289e+000	9.6378e-002
5.3924e+001	8.5823e+000	2.7080e-002	5.0837e+001	8.0910e+000	6.0691e-003
6.9874e+001	1.1121e+001	1.9115e-002	5.1765e+001	8.2386e+000	1.8902e-001
7.5532e+001	1.2021e+001	1.8652e-002	7.2076e+001	1.1471e+001	1.2272e-001

Trial 7 [9, 10, 19,20, 23, 24, 27, 28, 39, 40, 43, 44, 47,48, 51:54, 63, 64]

Initial system			Optimized System		
Freq. (rad/sec.)	Freq. (Hz.)	Modal Damp.	Freq. (rad/sec.)	Freq. (Hz.)	Modal Damp.
-----	-----	-----	-----	-----	-----
1.5485e+001	2.4646e+000	3.4120e-002	1.6239e+001	2.5845e+000	4.4439e-002
2.1360e+001	3.3995e+000	1.3798e-002	2.1243e+001	3.3809e+000	2.5512e-002
2.3646e+001	3.7633e+000	2.7736e-002	2.6062e+001	4.1479e+000	1.2055e-001
2.7424e+001	4.3646e+000	4.6977e-002	3.1303e+001	4.9820e+000	7.3972e-002
3.6661e+001	5.8348e+000	2.8122e-002	3.2926e+001	5.2404e+000	8.6678e-002
3.8732e+001	6.1644e+000	4.3148e-002	3.8781e+001	6.1722e+000	2.7948e-002
4.4938e+001	7.1520e+000	1.2992e-002	4.4196e+001	7.0340e+000	5.5618e-002
5.1100e+001	8.1329e+000	1.7085e-002	5.0154e+001	7.9823e+000	1.2031e-003
5.3924e+001	8.5823e+000	2.7080e-002	5.2979e+001	8.4319e+000	6.7218e-002
7.5532e+001	1.2021e+001	1.8652e-002	7.0440e+001	1.1211e+001	1.9538e-001

Trial 8 [9, 10, 19,20, 23, 24, 27, 28, 39, 40, 43, 44, 47,48, 51:54]

Initial system			Optimized System		
Freq. (rad/sec.)	Freq. (Hz.)	Modal Damp.	Freq. (rad/sec.)	Freq. (Hz.)	Modal Damp.
-----	-----	-----	-----	-----	-----
1.5485e+001	2.4646e+000	3.4120e-002	1.6278e+001	2.5908e+000	4.4399e-002
2.1360e+001	3.3995e+000	1.3798e-002	2.1261e+001	3.3838e+000	2.6192e-002
2.3646e+001	3.7633e+000	2.7736e-002	2.6004e+001	4.1387e+000	1.4297e-001
2.7424e+001	4.3646e+000	4.6977e-002	3.1136e+001	4.9554e+000	5.6108e-002
3.6661e+001	5.8348e+000	2.8122e-002	3.6573e+001	5.8207e+000	4.2684e-002
3.8732e+001	6.1644e+000	4.3148e-002	3.8505e+001	6.1282e+000	3.4822e-002
4.4938e+001	7.1520e+000	1.2992e-002	4.4233e+001	7.0399e+000	7.2897e-002
5.1100e+001	8.1329e+000	1.7085e-002	4.8486e+001	7.7167e+000	2.0329e-001
5.3924e+001	8.5823e+000	2.7080e-002	5.0892e+001	8.0997e+000	1.4619e-002

Trial 9 [9, 10, 19,20, 27, 28, 39, 40, 43, 44, 47,48, 53,54]

Initial system			Optimized System		
Freq. (rad/sec.)	Freq. (Hz.)	Modal Damp.	Freq. (rad/sec.)	Freq. (Hz.)	Modal Damp.
-----	-----	-----	-----	-----	-----
1.5485e+001	2.4646e+000	3.4120e-002	2.1230e+001	3.3788e+000	2.6582e-002
2.1360e+001	3.3995e+000	1.3798e-002	2.1471e+001	3.4172e+000	2.3208e-001
2.7424e+001	4.3646e+000	4.6977e-002	3.0741e+001	4.8926e+000	5.1421e-002
3.6661e+001	5.8348e+000	2.8122e-002	3.6074e+001	5.7413e+000	3.9962e-002
3.8732e+001	6.1644e+000	4.3148e-002	3.6743e+001	5.8478e+000	3.5309e-002
4.4938e+001	7.1520e+000	1.2992e-002	4.4467e+001	7.0772e+000	4.1803e-002
5.3924e+001	8.5823e+000	2.7080e-002	5.0883e+001	8.0983e+000	1.4875e-001

Trial 10 [9, 10, 27, 28, 39, 40, 43, 44, 47,48, 53,54]

Initial system			Optimized System		
Freq. (rad/sec.)	Freq. (Hz.)	Modal Damp.	Freq. (rad/sec.)	Freq. (Hz.)	Modal Damp.
-----	-----	-----	-----	-----	-----
1.5485e+001	2.4646e+000	3.4120e-002	2.1439e+001	3.4121e+000	2.7751e-002
2.7424e+001	4.3646e+000	4.6977e-002	2.2571e+001	3.5923e+000	1.5866e-001
3.6661e+001	5.8348e+000	2.8122e-002	3.0548e+001	4.8619e+000	6.0050e-002
3.8732e+001	6.1644e+000	4.3148e-002	3.6199e+001	5.7613e+000	4.0232e-002
4.4938e+001	7.1520e+000	1.2992e-002	4.5003e+001	7.1624e+000	6.9605e-002
5.3924e+001	8.5823e+000	2.7080e-002	4.9681e+001	7.9070e+000	1.2711e-001

Trial 11 [9, 10, 39, 40, 43, 44, 47,48, 53,54]

Initial system			Optimized System		
Freq. (rad/sec.)	Freq. (Hz.)	Modal Damp.	Freq. (rad/sec.)	Freq. (Hz.)	Modal Damp.
-----	-----	-----	-----	-----	-----
1.5485e+001	2.4646e+000	3.4120e-002	2.1439e+001	3.4121e+000	2.7751e-002

2.7424e+001	4.3646e+000	4.6977e-002	2.2571e+001	3.5923e+000	1.5866e-001
3.6661e+001	5.8348e+000	2.8122e-002	3.0548e+001	4.8619e+000	6.0050e-002
3.8732e+001	6.1644e+000	4.3148e-002	3.6199e+001	5.7613e+000	4.0232e-002
4.4938e+001	7.1520e+000	1.2992e-002	4.5003e+001	7.1624e+000	6.9605e-002
5.3924e+001	8.5823e+000	2.7080e-002	4.9681e+001	7.9070e+000	1.2711e-001

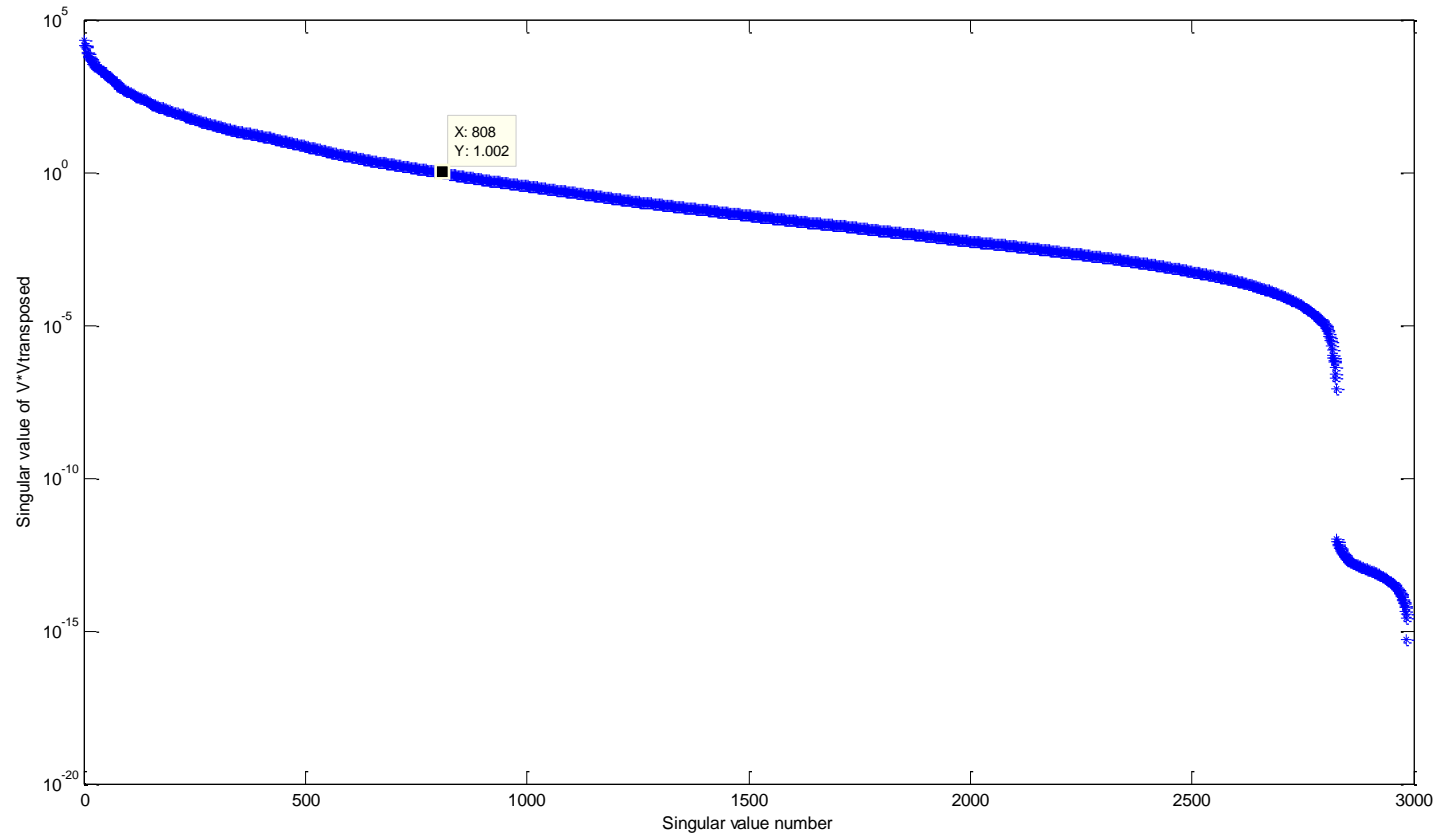
Trial 11 [9, 10, 39, 40, 43, 44, 53,54]

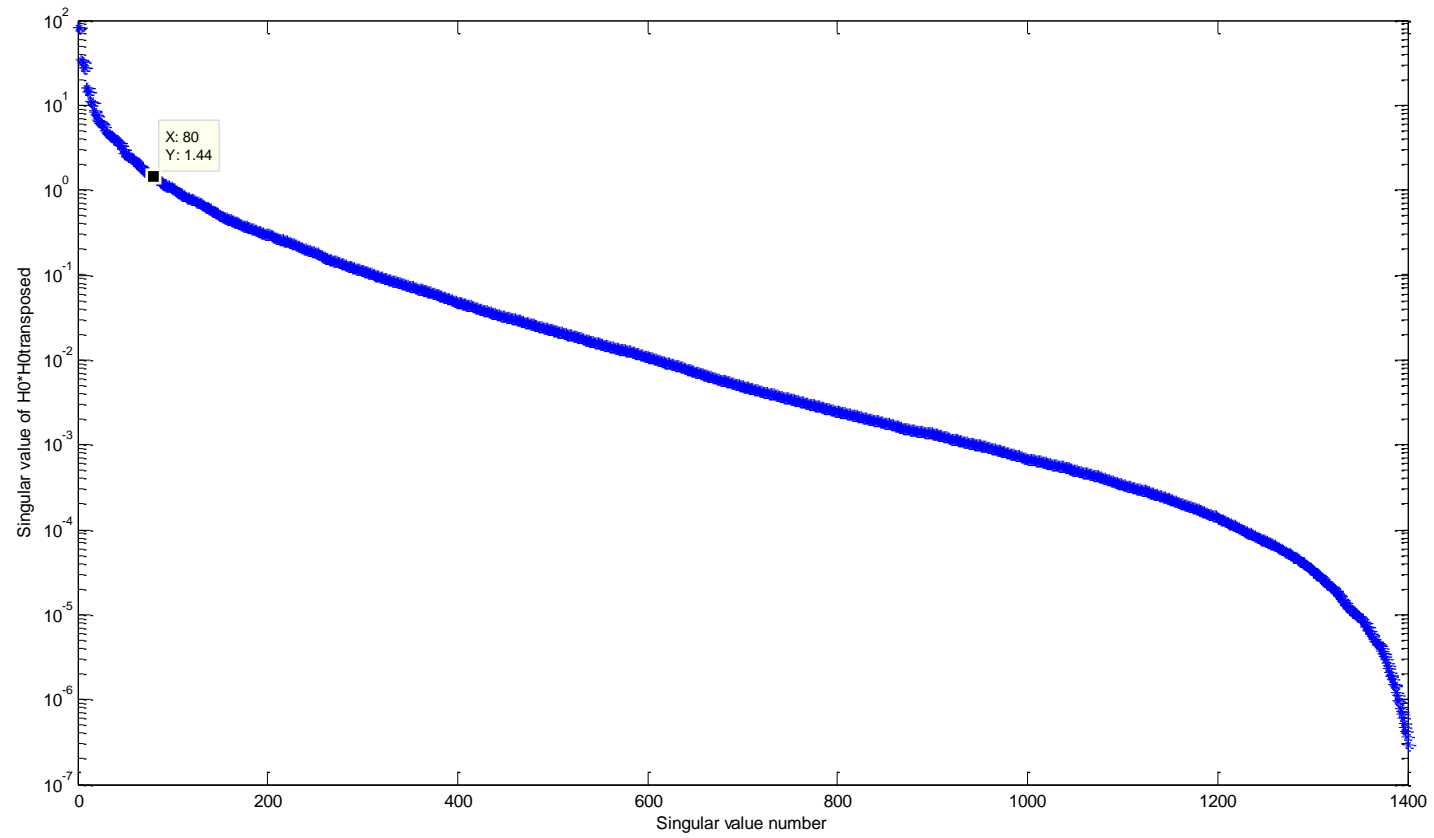
Initial system			Optimized System		
Freq. (rad/sec.)	Freq. (Hz.)	Modal Damp.	Freq. (rad/sec.)	Freq. (Hz.)	Modal Damp.
-----	-----	-----	-----	-----	-----
1.5485e+001	2.4646e+000	3.4120e-002	2.1022e+001	3.3458e+000	1.5205e-001
3.6661e+001	5.8348e+000	2.8122e-002	3.2537e+001	5.1783e+000	7.1218e-002
3.8732e+001	6.1644e+000	4.3148e-002	3.3271e+001	5.2952e+000	9.4628e-002
4.4938e+001	7.1520e+000	1.2992e-002	4.3699e+001	6.9549e+000	1.8980e-001
5.3924e+001	8.5823e+000	2.7080e-002	4.4301e+001	7.0508e+000	1.1114e-001

Trial 12 [9, 10, 39, 40, 43, 44, 53,54]

Initial system			Optimized System		
Freq. (rad/sec.)	Freq. (Hz.)	Modal Damp.	Freq. (rad/sec.)	Freq. (Hz.)	Modal Damp.
-----	-----	-----	-----	-----	-----
1.5485e+001	2.4646e+000	3.4120e-002	1.6273e+001	2.5900e+000	6.2947e-002
3.6661e+001	5.8348e+000	2.8122e-002	3.3606e+001	5.3485e+000	5.0274e-002
3.8732e+001	6.1644e+000	4.3148e-002	3.6016e+001	5.7322e+000	6.2522e-002
5.3924e+001	8.5823e+000	2.7080e-002	5.0935e+001	8.1065e+000	7.9887e-002

B.2 RESULTS WITH PETROLIA SET OF DATA ($p=175$; $SVs=808$; $Order=60$)





Trial 1 [1:60]

Initial system			Optimized System		
Freq. (rad/sec.)	Freq. (Hz.)	Modal Damp.	Freq. (rad/sec.)	Freq. (Hz.)	Modal Damp.
-----	-----	-----	-----	-----	-----
6.9353e+000	1.1038e+000	5.6086e-002	9.2548e+000	1.4729e+000	3.0020e-001
1.8148e+001	2.8883e+000	1.5603e-002	1.7644e+001	2.8082e+000	2.9897e-002
1.9760e+001	3.1449e+000	1.5360e-002	1.9465e+001	3.0979e+000	2.1087e-002
1.9991e+001	3.1817e+000	1.9110e-002	1.9472e+001	3.0991e+000	1.9407e-002
2.0938e+001	3.3323e+000	2.0711e-003	2.0981e+001	3.3392e+000	9.0668e-003
2.1385e+001	3.4036e+000	4.8990e-002	2.1836e+001	3.4753e+000	1.4526e-001
2.2321e+001	3.5525e+000	2.3044e-003	2.2311e+001	3.5509e+000	1.0134e-003
2.3104e+001	3.6771e+000	1.9240e-002	2.3538e+001	3.7462e+000	8.6241e-002
2.4709e+001	3.9326e+000	1.2646e-001	2.5516e+001	4.0610e+000	1.5234e-001
2.5414e+001	4.0448e+000	1.8564e-002	2.5673e+001	4.0860e+000	1.0068e-002
2.5787e+001	4.1042e+000	9.8213e-003	2.6153e+001	4.1624e+000	7.3381e-002
2.8535e+001	4.5415e+000	1.1329e-002	2.8530e+001	4.5406e+000	2.8076e-002
2.9025e+001	4.6194e+000	2.0734e-003	2.8795e+001	4.5828e+000	2.6178e-002
3.1064e+001	4.9440e+000	2.7908e-002	3.1314e+001	4.9837e+000	2.1373e-003
3.1250e+001	4.9736e+000	1.5404e-003	3.1983e+001	5.0903e+000	1.0582e-001
3.4476e+001	5.4870e+000	6.3636e-003	3.4496e+001	5.4902e+000	1.1312e-002
3.5364e+001	5.6284e+000	2.0560e-003	3.5477e+001	5.6463e+000	5.0645e-003
3.7125e+001	5.9086e+000	5.5037e-003	3.7209e+001	5.9221e+000	3.3839e-003
3.9373e+001	6.2664e+000	7.5132e-003	3.8907e+001	6.1922e+000	3.8878e-002

4.1175e+001	6.5533e+000	8.5331e-003	4.1849e+001	6.6604e+000	1.8441e-002
4.3166e+001	6.8701e+000	8.3983e-003	4.2992e+001	6.8425e+000	1.5266e-002
4.4573e+001	7.0941e+000	9.4450e-003	4.4844e+001	7.1371e+000	3.1770e-002
4.6631e+001	7.4216e+000	1.6864e-002	4.6247e+001	7.3605e+000	9.3361e-002
6.0867e+001	9.6873e+000	4.9209e-003	5.6281e+001	8.9573e+000	1.4244e-001
6.4579e+001	1.0278e+001	1.4039e-002	5.9816e+001	9.5200e+000	3.2651e-002
8.5269e+001	1.3571e+001	9.6588e-004	8.5821e+001	1.3659e+001	3.9098e-003
8.7656e+001	1.3951e+001	4.1815e-003	8.7054e+001	1.3855e+001	8.8677e-002
9.7607e+001	1.5535e+001	3.0128e-003	9.7762e+001	1.5559e+001	1.4758e-002
1.1530e+002	1.8351e+001	2.3276e-003	1.2166e+002	1.9363e+001	6.7112e-002
1.2969e+002	2.0640e+001	7.7809e-003	1.2433e+002	1.9788e+001	1.2575e-001

Trial 2 [3:10 13:16 19:46 49:58]

Initial system			Optimized System		
Freq. (rad/sec.)	Freq. (Hz.)	Modal Damp.	Freq. (rad/sec.)	Freq. (Hz.)	Modal Damp.
-----	-----	-----	-----	-----	-----
1.8148e+001	2.8883e+000	1.5603e-002	1.7749e+001	2.8249e+000	2.9654e-002
1.9760e+001	3.1449e+000	1.5360e-002	1.9441e+001	3.0942e+000	2.6070e-002
1.9991e+001	3.1817e+000	1.9110e-002	1.9829e+001	3.1559e+000	1.2503e-001
2.0938e+001	3.3323e+000	2.0711e-003	2.0991e+001	3.3408e+000	1.6057e-004
2.2321e+001	3.5525e+000	2.3044e-003	2.2329e+001	3.5538e+000	2.5049e-003

2.3104e+001	3.6771e+000	1.9240e-002	2.4885e+001	3.9605e+000	1.4440e-001
2.5414e+001	4.0448e+000	1.8564e-002	2.4933e+001	3.9681e+000	1.3736e-001
2.5787e+001	4.1042e+000	9.8213e-003	2.5822e+001	4.1097e+000	2.6097e-001
2.8535e+001	4.5415e+000	1.1329e-002	2.8349e+001	4.5119e+000	2.8460e-002
2.9025e+001	4.6194e+000	2.0734e-003	2.8407e+001	4.5211e+000	2.0358e-002
3.1064e+001	4.9440e+000	2.7908e-002	3.1286e+001	4.9793e+000	1.8835e-003
3.1250e+001	4.9736e+000	1.5404e-003	3.2037e+001	5.0988e+000	9.3975e-002
3.4476e+001	5.4870e+000	6.3636e-003	3.4523e+001	5.4945e+000	1.9720e-002
3.5364e+001	5.6284e+000	2.0560e-003	3.5556e+001	5.6590e+000	6.6215e-003
3.7125e+001	5.9086e+000	5.5037e-003	3.7154e+001	5.9132e+000	1.7772e-003
3.9373e+001	6.2664e+000	7.5132e-003	3.8772e+001	6.1707e+000	6.8483e-002
4.1175e+001	6.5533e+000	8.5331e-003	4.1546e+001	6.6122e+000	1.4829e-001
4.3166e+001	6.8701e+000	8.3983e-003	4.1979e+001	6.6812e+000	1.8738e-002
4.4573e+001	7.0941e+000	9.4450e-003	4.2972e+001	6.8393e+000	1.6393e-002
4.6631e+001	7.4216e+000	1.6864e-002	4.3586e+001	6.9369e+000	6.2656e-001
6.4579e+001	1.0278e+001	1.4039e-002	4.4250e+001	7.0425e+000	4.9178e-002
8.5269e+001	1.3571e+001	9.6588e-004	5.3525e+001	8.5187e+000	4.0421e-001
8.7656e+001	1.3951e+001	4.1815e-003	7.3114e+001	1.1636e+001	9.8264e-001
9.7607e+001	1.5535e+001	3.0128e-003	8.6327e+001	1.3739e+001	2.6188e-002

1.1530e+002 1.8351e+001 2.3276e-003 9.7104e+001 1.5455e+001 3.5024e-002

Trial 3 [3:8 13,14 19,20 23:44 49,50 55:58]

Initial system			Optimized System		
Freq. (rad/sec.)	Freq. (Hz.)	Modal Damp.	Freq. (rad/sec.)	Freq. (Hz.)	Modal Damp.
-----	-----	-----	-----	-----	-----
1.8148e+001	2.8883e+000	1.5603e-002	1.7468e+001	2.7801e+000	6.3648e-002
1.9760e+001	3.1449e+000	1.5360e-002	2.0039e+001	3.1894e+000	6.0075e-002
1.9991e+001	3.1817e+000	1.9110e-002	2.0567e+001	3.2733e+000	3.7310e-002
2.2321e+001	3.5525e+000	2.3044e-003	2.2307e+001	3.5502e+000	2.6619e-003
2.5414e+001	4.0448e+000	1.8564e-002	2.4071e+001	3.8310e+000	1.4676e-001
2.8535e+001	4.5415e+000	1.1329e-002	2.5507e+001	4.0596e+000	9.9576e-001
2.9025e+001	4.6194e+000	2.0734e-003	2.8317e+001	4.5068e+000	3.8444e-002
3.1064e+001	4.9440e+000	2.7908e-002	2.8661e+001	4.5616e+000	2.4639e-002
3.1250e+001	4.9736e+000	1.5404e-003	2.9501e+001	4.6953e+000	7.8576e-002
3.4476e+001	5.4870e+000	6.3636e-003	3.1289e+001	4.9797e+000	1.5686e-003
3.5364e+001	5.6284e+000	2.0560e-003	3.4450e+001	5.4829e+000	1.6560e-002
3.7125e+001	5.9086e+000	5.5037e-003	3.5561e+001	5.6597e+000	4.4209e-003
3.9373e+001	6.2664e+000	7.5132e-003	3.7207e+001	5.9217e+000	1.9098e-003
4.1175e+001	6.5533e+000	8.5331e-003	3.9702e+001	6.3188e+000	3.7974e-002

4.3166e+001	6.8701e+000	8.3983e-003	4.0510e+001	6.4473e+000	1.4869e-001
4.4573e+001	7.0941e+000	9.4450e-003	4.2306e+001	6.7332e+000	1.3758e-002
6.4579e+001	1.0278e+001	1.4039e-002	4.5086e+001	7.1756e+000	4.6804e-002
9.7607e+001	1.5535e+001	3.0128e-003	6.2337e+001	9.9212e+000	1.0560e-001
1.1530e+002	1.8351e+001	2.3276e-003	9.7248e+001	1.5477e+001	2.4271e-002

Trial 4 [3:8 13,14 19,20 25:44 49,50 55:58]

Initial system			Optimized System		
Freq. (rad/sec.)	Freq. (Hz.)	Modal Damp.	Freq. (rad/sec.)	Freq. (Hz.)	Modal Damp.
-----	-----	-----	-----	-----	-----
1.8148e+001	2.8883e+000	1.5603e-002	1.7145e+001	2.7288e+000	8.1201e-002
1.9760e+001	3.1449e+000	1.5360e-002	2.0131e+001	3.2040e+000	5.5808e-002
1.9991e+001	3.1817e+000	1.9110e-002	2.0453e+001	3.2552e+000	3.8699e-002
2.2321e+001	3.5525e+000	2.3044e-003	2.2279e+001	3.5457e+000	5.0515e-003
2.5414e+001	4.0448e+000	1.8564e-002	2.3423e+001	3.7279e+000	1.4967e-001
2.9025e+001	4.6194e+000	2.0734e-003	2.8198e+001	4.4879e+000	2.6111e-002
3.1064e+001	4.9440e+000	2.7908e-002	2.8625e+001	4.5558e+000	9.9959e-001
3.1250e+001	4.9736e+000	1.5404e-003	2.9125e+001	4.6354e+000	5.7161e-002
3.4476e+001	5.4870e+000	6.3636e-003	3.1340e+001	4.9879e+000	2.7646e-003

3.5364e+001	5.6284e+000	2.0560e-003	3.4580e+001	5.5036e+000	2.3787e-002
3.7125e+001	5.9086e+000	5.5037e-003	3.5547e+001	5.6575e+000	3.0306e-003
3.9373e+001	6.2664e+000	7.5132e-003	3.7188e+001	5.9187e+000	2.0490e-003
4.1175e+001	6.5533e+000	8.5331e-003	4.0041e+001	6.3727e+000	5.0010e-002
4.3166e+001	6.8701e+000	8.3983e-003	4.1644e+001	6.6278e+000	1.8006e-001
4.4573e+001	7.0941e+000	9.4450e-003	4.1737e+001	6.6427e+000	2.9883e-002
6.4579e+001	1.0278e+001	1.4039e-002	4.4890e+001	7.1444e+000	3.9301e-002
9.7607e+001	1.5535e+001	3.0128e-003	5.1182e+001	8.1459e+000	4.8314e-001
1.1530e+002	1.8351e+001	2.3276e-003	9.6894e+001	1.5421e+001	3.2188e-002

Trial 5 [3:8 13,14,19,20,25,26 29:40 43,44,49,50,57,58]

Initial system			Optimized System		
Freq. (rad/sec.)	Freq. (Hz.)	Modal Damp.	Freq. (rad/sec.)	Freq. (Hz.)	Modal Damp.
-----	-----	-----	-----	-----	-----
1.8148e+001	2.8883e+000	1.5603e-002	1.7787e+001	2.8309e+000	6.0163e-002
1.9760e+001	3.1449e+000	1.5360e-002	2.0194e+001	3.2140e+000	4.8213e-002
1.9991e+001	3.1817e+000	1.9110e-002	2.0572e+001	3.2741e+000	3.2011e-002
2.2321e+001	3.5525e+000	2.3044e-003	2.2308e+001	3.5505e+000	4.1052e-003
2.5414e+001	4.0448e+000	1.8564e-002	2.5753e+001	4.0988e+000	9.7398e-002
2.9025e+001	4.6194e+000	2.0734e-003	2.8670e+001	4.5630e+000	1.0980e-002

3.1250e+001	4.9736e+000	1.5404e-003	3.1246e+001	4.9730e+000	1.4528e-003
3.4476e+001	5.4870e+000	6.3636e-003	3.4630e+001	5.5115e+000	2.4057e-002
3.5364e+001	5.6284e+000	2.0560e-003	3.5424e+001	5.6379e+000	2.5094e-003
3.7125e+001	5.9086e+000	5.5037e-003	3.7244e+001	5.9276e+000	7.3685e-003
3.9373e+001	6.2664e+000	7.5132e-003	3.9485e+001	6.2842e+000	1.7415e-002
4.1175e+001	6.5533e+000	8.5331e-003	4.2374e+001	6.7440e+000	7.4879e-002
4.4573e+001	7.0941e+000	9.4450e-003	4.4806e+001	7.1310e+000	5.6629e-002
6.4579e+001	1.0278e+001	1.4039e-002	6.3024e+001	1.0031e+001	9.5102e-002
1.1530e+002	1.8351e+001	2.3276e-003	1.1707e+002	1.8633e+001	7.4366e-001

Trial 6 [3:8 13,14,19,20,25,26 29:40 43,44,49,50]

Initial system			Optimized System		
Freq. (rad/sec.)	Freq. (Hz.)	Modal Damp.	Freq. (rad/sec.)	Freq. (Hz.)	Modal Damp.
-----	-----	-----	-----	-----	-----
1.8148e+001	2.8883e+000	1.5603e-002	1.7039e+001	2.7118e+000	1.4087e-001
1.9760e+001	3.1449e+000	1.5360e-002	2.0342e+001	3.2375e+000	5.6258e-002
1.9991e+001	3.1817e+000	1.9110e-002	2.0624e+001	3.2825e+000	3.2574e-002
2.2321e+001	3.5525e+000	2.3044e-003	2.2252e+001	3.5415e+000	1.0479e-002
2.5414e+001	4.0448e+000	1.8564e-002	2.5917e+001	4.1249e+000	1.0726e-001
2.9025e+001	4.6194e+000	2.0734e-003	2.8064e+001	4.4665e+000	2.4637e-002
3.1250e+001	4.9736e+000	1.5404e-003	3.1243e+001	4.9724e+000	1.2855e-003

3.4476e+001	5.4870e+000	6.3636e-003	3.4587e+001	5.5047e+000	3.6748e-001
3.5364e+001	5.6284e+000	2.0560e-003	3.4716e+001	5.5253e+000	3.1003e-002
3.7125e+001	5.9086e+000	5.5037e-003	3.5414e+001	5.6363e+000	5.5764e-003
3.9373e+001	6.2664e+000	7.5132e-003	3.7196e+001	5.9200e+000	5.5441e-003
4.1175e+001	6.5533e+000	8.5331e-003	3.9601e+001	6.3027e+000	3.5687e-002
4.4573e+001	7.0941e+000	9.4450e-003	4.5367e+001	7.2204e+000	6.1224e-002
6.4579e+001	1.0278e+001	1.4039e-002	5.7354e+001	9.1281e+000	2.5082e-001

Trial 7 [3:8 13,14,19,20,25,26 29:40 43,44,49,50]

Initial system			Optimized System		
Freq. (rad/sec.)	Freq. (Hz.)	Modal Damp.	Freq. (rad/sec.)	Freq. (Hz.)	Modal Damp.
-----	-----	-----	-----	-----	-----
1.8148e+001	2.8883e+000	1.5603e-002	1.7428e+001	2.7738e+000	1.0266e-001
1.9760e+001	3.1449e+000	1.5360e-002	2.0284e+001	3.2283e+000	5.3079e-002
1.9991e+001	3.1817e+000	1.9110e-002	2.0699e+001	3.2944e+000	3.4973e-002
2.2321e+001	3.5525e+000	2.3044e-003	2.2284e+001	3.5466e+000	7.0680e-003
2.5414e+001	4.0448e+000	1.8564e-002	2.6274e+001	4.1817e+000	1.0542e-001
2.9025e+001	4.6194e+000	2.0734e-003	2.8256e+001	4.4972e+000	1.8769e-002
3.1250e+001	4.9736e+000	1.5404e-003	3.0207e+001	4.8076e+000	1.9096e-001
3.5364e+001	5.6284e+000	2.0560e-003	3.1240e+001	4.9719e+000	2.6059e-003

3.7125e+001	5.9086e+000	5.5037e-003	3.4911e+001	5.5562e+000	1.8937e-002
3.9373e+001	6.2664e+000	7.5132e-003	3.6068e+001	5.7404e+000	7.1827e-002
4.1175e+001	6.5533e+000	8.5331e-003	3.6919e+001	5.8758e+000	2.0090e-002
4.4573e+001	7.0941e+000	9.4450e-003	4.5493e+001	7.2404e+000	5.8593e-002

Trial 8 [3:8 13,14,19,20, 29:40 43,44,49,50]

Initial system			Optimized System		
Freq. (rad/sec.)	Freq. (Hz.)	Modal Damp.	Freq. (rad/sec.)	Freq. (Hz.)	Modal Damp.
-----	-----	-----	-----	-----	-----
1.8148e+001	2.8883e+000	1.5603e-002	1.7453e+001	2.7778e+000	1.2658e-001
1.9760e+001	3.1449e+000	1.5360e-002	2.0279e+001	3.2274e+000	5.1063e-002
1.9991e+001	3.1817e+000	1.9110e-002	2.0657e+001	3.2876e+000	3.5161e-002
2.2321e+001	3.5525e+000	2.3044e-003	2.2296e+001	3.5484e+000	6.2903e-003
2.5414e+001	4.0448e+000	1.8564e-002	2.5970e+001	4.1333e+000	1.1122e-001
2.9025e+001	4.6194e+000	2.0734e-003	2.8403e+001	4.5204e+000	1.7227e-002
3.5364e+001	5.6284e+000	2.0560e-003	3.0235e+001	4.8120e+000	2.0319e-001
3.7125e+001	5.9086e+000	5.5037e-003	3.4846e+001	5.5459e+000	1.5942e-002
3.9373e+001	6.2664e+000	7.5132e-003	3.6398e+001	5.7929e+000	7.3737e-002
4.1175e+001	6.5533e+000	8.5331e-003	3.6885e+001	5.8705e+000	2.4054e-002
4.4573e+001	7.0941e+000	9.4450e-003	4.5476e+001	7.2377e+000	6.1123e-002

Trial 9 [3:8 13,14,19,20,25,26 35:40 43,44]

Initial system			Optimized System		
Freq. (rad/sec.)	Freq. (Hz.)	Modal Damp.	Freq. (rad/sec.)	Freq. (Hz.)	Modal Damp.
-----	-----	-----	-----	-----	-----
1.8148e+001	2.8883e+000	1.5603e-002	1.7496e+001	2.7845e+000	1.2224e-001
1.9760e+001	3.1449e+000	1.5360e-002	2.0262e+001	3.2248e+000	5.2801e-002
1.9991e+001	3.1817e+000	1.9110e-002	2.0738e+001	3.3006e+000	3.4778e-002
2.2321e+001	3.5525e+000	2.3044e-003	2.2297e+001	3.5487e+000	5.0833e-003
2.5414e+001	4.0448e+000	1.8564e-002	2.5816e+001	4.1087e+000	1.2197e-001
2.9025e+001	4.6194e+000	2.0734e-003	2.8520e+001	4.5391e+000	1.5162e-002
3.7125e+001	5.9086e+000	5.5037e-003	2.9925e+001	4.7627e+000	2.2625e-001
3.9373e+001	6.2664e+000	7.5132e-003	3.5779e+001	5.6945e+000	8.3466e-002
4.1175e+001	6.5533e+000	8.5331e-003	3.6134e+001	5.7509e+000	3.5667e-002
4.4573e+001	7.0941e+000	9.4450e-003	4.5460e+001	7.2352e+000	6.1322e-002

Trial 10 [3:8 13,14,19,20,25,26 37:40 43,44]

Initial system			Optimized System		
Freq. (rad/sec.)	Freq. (Hz.)	Modal Damp.	Freq. (rad/sec.)	Freq. (Hz.)	Modal Damp.
-----	-----	-----	-----	-----	-----
1.8148e+001	2.8883e+000	1.5603e-002	1.7490e+001	2.7836e+000	2.7954e-001
1.9760e+001	3.1449e+000	1.5360e-002	2.0457e+001	3.2558e+000	5.6474e-002
1.9991e+001	3.1817e+000	1.9110e-002	2.0769e+001	3.3055e+000	2.9059e-002
2.2321e+001	3.5525e+000	2.3044e-003	2.2214e+001	3.5354e+000	1.7531e-002
2.5414e+001	4.0448e+000	1.8564e-002	2.6160e+001	4.1635e+000	9.2974e-002
2.9025e+001	4.6194e+000	2.0734e-003	2.8096e+001	4.4716e+000	2.3330e-002
3.9373e+001	6.2664e+000	7.5132e-003	3.4304e+001	5.4597e+000	8.5201e-002
4.1175e+001	6.5533e+000	8.5331e-003	3.4624e+001	5.5106e+000	6.3036e-002
4.4573e+001	7.0941e+000	9.4450e-003	4.4488e+001	7.0805e+000	1.0582e-001

Trial 11 [5:8 13,14,19,20,25,26 37:40 43,44]

Initial system			Optimized System		
Freq. (rad/sec.)	Freq. (Hz.)	Modal Damp.	Freq. (rad/sec.)	Freq. (Hz.)	Modal Damp.
-----	-----	-----	-----	-----	-----
1.9760e+001	3.1449e+000	1.5360e-002	1.9762e+001	3.1451e+000	1.5173e-001
1.9991e+001	3.1817e+000	1.9110e-002	2.1017e+001	3.3450e+000	2.9479e-002
2.2321e+001	3.5525e+000	2.3044e-003	2.1690e+001	3.4521e+000	1.0161e-001
2.5414e+001	4.0448e+000	1.8564e-002	2.5931e+001	4.1270e+000	1.4095e-001
2.9025e+001	4.6194e+000	2.0734e-003	2.8001e+001	4.4564e+000	2.0295e-002
3.9373e+001	6.2664e+000	7.5132e-003	3.4805e+001	5.5394e+000	5.6791e-002
4.1175e+001	6.5533e+000	8.5331e-003	3.4875e+001	5.5505e+000	7.4821e-002
4.4573e+001	7.0941e+000	9.4450e-003	4.0226e+001	6.4022e+000	1.8444e-001

Trial 12 [5:8 13,14,19,20,25,26 37:40]

Initial system			Optimized System		
Freq. (rad/sec.)	Freq. (Hz.)	Modal Damp.	Freq. (rad/sec.)	Freq. (Hz.)	Modal Damp.
-----	-----	-----	-----	-----	-----
1.9760e+001	3.1449e+000	1.5360e-002	2.0243e+001	3.2218e+000	5.7276e-002
1.9991e+001	3.1817e+000	1.9110e-002	2.0852e+001	3.3188e+000	3.0146e-002

2.2321e+001	3.5525e+000	2.3044e-003	2.2321e+001	3.5525e+000	5.3411e-003
2.5414e+001	4.0448e+000	1.8564e-002	2.6081e+001	4.1509e+000	9.2861e-002
2.9025e+001	4.6194e+000	2.0734e-003	2.8754e+001	4.5763e+000	1.7053e-002
3.9373e+001	6.2664e+000	7.5132e-003	3.6093e+001	5.7444e+000	1.0475e-001
4.1175e+001	6.5533e+000	8.5331e-003	3.7378e+001	5.9490e+000	1.2272e-001

Trial 13 [5:8 13,14,19,20,25,26 37:40]

Initial system			Optimized System		
Freq. (rad/sec.)	Freq. (Hz.)	Modal Damp.	Freq. (rad/sec.)	Freq. (Hz.)	Modal Damp.
-----	-----	-----	-----	-----	-----
1.9760e+001	3.1449e+000	1.5360e-002	2.0101e+001	3.1993e+000	8.2397e-002
1.9991e+001	3.1817e+000	1.9110e-002	2.0825e+001	3.3145e+000	3.7055e-002
2.5414e+001	4.0448e+000	1.8564e-002	2.5680e+001	4.0871e+000	1.0395e-001
2.9025e+001	4.6194e+000	2.0734e-003	2.8603e+001	4.5523e+000	1.3970e-001
3.9373e+001	6.2664e+000	7.5132e-003	2.9542e+001	4.7018e+000	8.4413e-002